Mechanisms and Machine Science

Volume 9

Series Editor

Marco Ceccarelli

For further volumes:
http://www.springer.com/series/8779

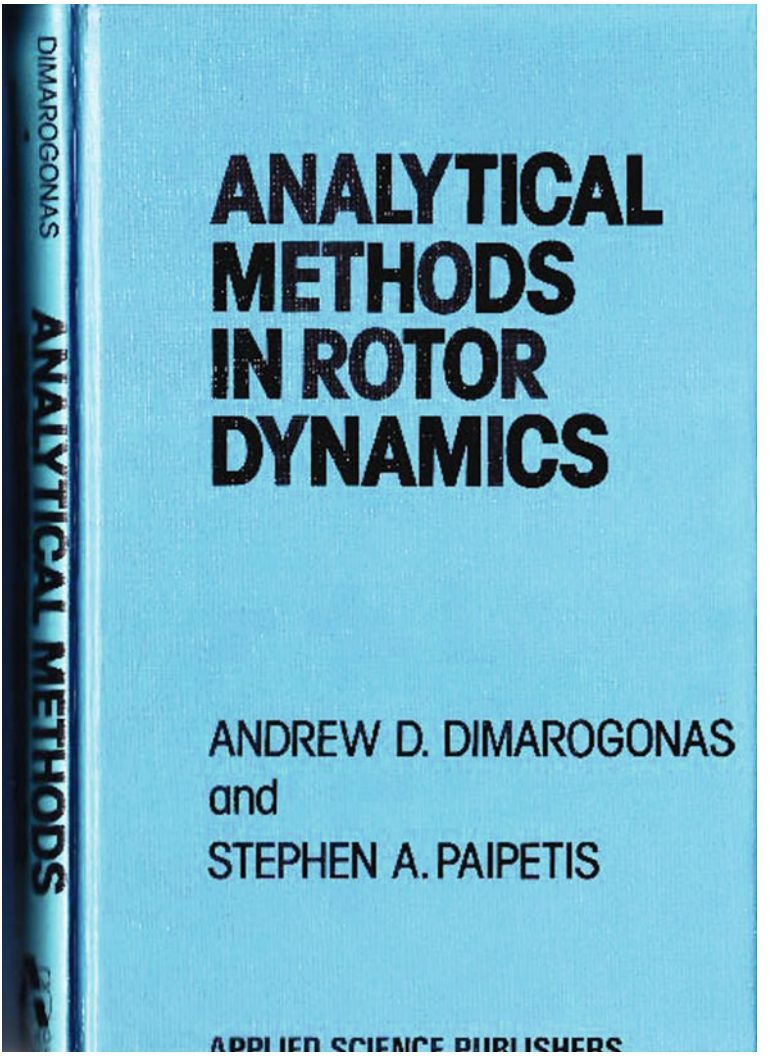
DIMAROGONAS
ANALYTICAL METHODS
ANALYTICAL METHODS IN ROTOR DYNAMICS
ANDREW D. DIMAROGONAS
and
STEPHEN A. PAIPETIS
APPLIED SCIENCE PUBLISHERS

Andrew D. Dimarogonas
Stefanos A. Paipetis · Thomas G. Chondros

Analytical Methods in Rotor Dynamics

Second Edition

Springer

Andrew D. Dimarogonas (1938–2000)

Stefanos A. Paipetis
Thomas G. Chondros
Mechanical Engineering and Aeronautics
University of Patras
Patras
Greece

ISSN 2211-0984 ISSN 2211-0992 (electronic)
ISBN 978-94-007-5904-6 ISBN 978-94-007-5905-3 (eBook)
DOI 10.1007/978-94-007-5905-3
Springer Dordrecht Heidelberg New York London

Library of Congress Control Number: 2012954538

Printed on acid-free paper

Springer is part of Springer Science+Business Media (www.springer.com)

Preface to the Revised Edition

When this book first appeared, in 1983, it soon went out of print, and on several occasions the authors were approached with photocopy requests. After almost 30 years, it seems to have turned out in a collector's item, and a few accidentally found copies were sold at enormous prices. Meanwhile, the first of the authors (ADD) passed away in 2000, leaving behind a tremendous work in science and engineering, especially in the target area of the book, and the second of the authors (SAP) jointly with the first of the revising authors (ThGC), paying a tribute to his memory, decided to proceed with an updated edition of it. SPRINGER agreed to handle the project, and the result produced by several months of hard work is now visible.

In this second edition, the various chapters were revised and updated to a different extent. There was not much to add to the first chapters, which contained fundamental knowledge or general theory of analytical methods (Chaps. 1–4). However, extended revisions along with substantial additions, reflecting the progress achieved during the last three decades in the area of each of the remaining (Chaps. 5–8), were carried out, especially on the dynamics of cracked rotors, and its use on the identification of cracks and their depth and orientation as well as on their influence on the dynamic stability and life expectancy of rotating elements and even stationary structures. Finally, what is new is the introduction of variational methods, which, being quite a bulk of material, it was not thought wise to have them squeezed in the existing chapters, therefore, two new (Chaps. 9–10) dealing with variational applications in prismatic bars and rods and turbine rotors respectively.

S. A. Paipetis
Th. G. Chondros

Preface

The design and construction of rotating machinery operating at supercritical speeds was, in the 1920s, an event of revolutionary importance for the then new branch of dynamics known as rotor dynamics. Out of the treatment of a number of new problems thus created, such as dynamic balancing, accelerating through critical speeds, effects of material damping, and the mechanical behaviour of the various types of bearings, along with the influence of all these factors on the stability of the rotatoiy motion, an individual discipline was in fact born. These problems were exhaustively treated in the classical monographs by Dimentberg and Tondl (Chap. 1, Refs. I and 2, respectively), while particular aspects are even included in standard vibration textbooks.

In the 1960s, another revolution occurred: in less than a decade, imposed by operational and economic needs, an increase in the power of turbomachinery by one order of magnitude took place. This was achieved by means of advanced design methods, aided by fast digital computers and modern optimization techniques. The new situation demanded higher and faster rotors, operating above the second and sometimes the third critical speed, as is the case with steam or gas turbines and aircraft engines. Inevitably, a whole class of new problems were created: increased power concentration entails considerable interaction between the dynamic behavior of rotors on the one hand and the associated thermal and/or fluid flow fields on the other. The dynamic analysis of complex rotor forms became a necessity, while the importance of approximate methods for dynamic analysis was stressed, because of their capability to provide both straightforward solutions and means of checking computer results based on complicated algorithms. Finally, the appearance of fracture mechanics in the last two decades, as another new branch of applied mechanics, provided the analytical tools for the investigation of cracks on the dynamic behavior of rotors. The importance of this latter development becomes evident if one bears in mind that the new philosophy of design to the limit renders complete control over such phenomena as low- or high-cycle fatigue, dynamic failure, etc., to an absolute necessity.

The scope of this book is based on these new developments. It was found that no topics related to the well-known classical problems needed to be included, but

the book rather deals exclusively with modern high-power turbomachinery. Therefore the material included has been arranged in the following manner.

In Chap. 1, the problem of the approximate evaluation of the flexural eigenfrequencies of rotors is investigated. The procedure based on Dunkerley's rule for the determination of the lowest eigenfrequency of a lumped-mass, multi-degree-of-freedom elastic shaft is examined along with its extension to higher modes. This procedure generally provides lower bounds for the eigenfrequencies, but its accuracy can be increased at will by means of the root-squaring process, as suggested by Graeffe and Lobachevsky, applicable both to undamped and damped systems.

Extension to continuous systems is considered and also an integral equation formulation of the eigenvalue problem, providing upper and lower bounds for the eigenvalues, which by means of an iterative process can be brought as close as desired.

Chapter 2 deals with the effects of variable elasticity in rotating machinery. Such effects occur with a large variety of mechanical, electrical, etc., systems, in the present case, for geometrical and/or mechanical reasons. Systems with variable elasticity are governed by differential equations with periodic coefficients of the Mathieu-Hill type and exhibit important stability problems. In this chapter, analytical tools for the treatment of these kinds of equations are given, including the classical Floquet theory, a matrix method of solution, solution by transition into an equivalent integral equation and the BWK procedure.

Chapter 3 presents the main mathematical models used in rotor dynamic analysis. The one disk-flexible rotor model, called Jeffcott or de Laval rotor, can be used to derive qualitative features, since it lends itself to analytical treatment. For realistic rotor forms, a discrete finite element model is presented, applicable to very complicated rotor geometries, yet leading to a manageable system of equations for linear or nonlinear analysis.

Chapter 4 deals with flow-induced vibration of rotors and in particular with the most important case, known as 'steam whirl', often appearing in large steam turbines. Vibration of rotors in fluid annuli is also discussed.

In Chap. 5 rotor instabilities are investigated, resulting from friction heating, a phenomenon known as the 'Newkirk effect'. The interaction between vibration characteristics and heat generation leads to a nonlinear feedback system exhibiting either stable or unstable behavior.

The problem of cracked rotor dynamics is discussed in Chap. 6. Open cracks lead to linear systems, while closing cracks lead to nonlinear ones. Analytical solutions are obtained, which can be used to monitor crack propagation or to identify cracks in service.

The question of crack detection from dynamic measurements is further extended and discussed in Chap. 7. A general stiffness matrix for cracked structural members is introduced, to model the respective dynamic system. The change in dynamic response is analytically evaluated for simple systems and by means of approximate methods for more complicated ones.

Chapter 8 deals with the inverse problem to the one encountered in Chap. 5, e.g., the heat generated by the vibration of rotating shafts. The corresponding mechanisms are associated with internal damping and plastic deformation. This phenomenon has been identified recently as the cause of large-scale failures of power equipment, with electrical disturbances being the cause of the rotor vibration.

Finally, the authors wish to express their sincere appreciation to Geoffrey and Dorothy Holister for their help and advice in preparing the final manuscript for publication.

A. D. Dimarogonas
S. A. Paipetis

Contents

Chapter 1
Approximate Evaluation of Eigenfrequencies

Abstract Approximate evaluation of rotors flexural eigenfrequencies is investigated in Chap. 1. However, the formulation is similar for torsional vibrations of shafts or even vibrations of elastic systems in general. The Dunkerley's rule for the determination of lowest eigenfrequency of a lumped-mass, multi-degree-of-freedom elastic shaft is applied along with its extension to higher modes. This procedure generally provides lower bounds for the eigenfrequencies, but its accuracy can be increased at will by means of the root-squaring process, as suggested by Graeffe and Lobachevsky, applicable both to undamped and damped systems. Extension to continuous systems is considered too, and an integral equation formulation of the eigenvalue problem, providing upper and lower bounds for the eigenvalues, which by means of an iterative process can be brought as close as desired. Those methods are useful for predicting bending and torsional fatigue life of rotors and shafts, and furthermore, for developing methodologies for damage detection, and the estimation of position and size of flaws and cracks in rotating machinery.

1.1 Introduction

Dynamics of rotating shafts has attracted attention a long time ago. Since the end of the nineteenth century, the theory of vibration was already extensively developed, and there was rapid progress in high-speed machinery construction, in particular to be used with locomotives and steam turbines. Whirling of shafts was anticipated by W. A. Rankine, who postulated that shaft operation above the critical speed was impossible. Extensive analytical investigations were performed by Dunkerley and Reynolds. De Laval observed and resolved experimentally most rotor dynamics problems, experimenting with steam turbines in the last quarter of the nineteenth century. The whirling problem was solved by A. Föpl, who

A. D. Dimarogonas et al., *Analytical Methods in Rotor Dynamics*,
Mechanisms and Machine Science 9, DOI: 10.1007/978-94-007-5905-3_1,

explained analytically why operation above the critical speed is possible, as experimentally demonstrated by De Laval. His analysis is sometimes erroneously credited to Jeffcott and the De Laval rotor is sometimes misnamed the "Jeffcott rotor." The early works of Rankine, Jeffcott and Stodola identified some of the fundamental aspects of the dynamics of rotating shafts [1–8].

In the 1920s the turbine industry designed machines to operate at substantially higher loads and at speeds above the lowest critical speed, and this introduced the modern rotor dynamics problems, which were treated by B. L. Newkirk and A. T. Kimball. Gyroscopic effects were introduced by A. Stodola. The influence of fluid bearings was investigated by Stodola and further quantified by B. L. Newkirk and H. D. Taylor and by A. Stodola. Vibration of shafts and beams of engineered shapes was first studied by Frahm, in particular, torsional vibration of ship main shafts [7, 8].

In the 1920 and 1930s electric power was in great demand in the United States due to the rapidly developing industry. Turbine manufacturers hired several engineers from Europe. Timoshenko, den Hartog and Myklestad were all hired by Westinghouse, while H. Poritsky, a General-Electric mathematician came from Russia [7, 8].

The classical rotor dynamic model is based on the assumption that one or more *rigid disks* (in a generalized sense e.g. also propellers, blade stages, etc.) are mounted rigidly or elastically on an *elastic shaft* which is supported on *elastic bearings*. In general, the equations of motion of these models are formulated in a *stationary* (non-rotating) reference system. For rotating *elastic structures* as disks, blades, bladed disks, etc., which are fixed rigidly or elastically on a *rigid shaft* on *rigid bearings*, the equations of motion are generally formulated in a *rotating reference system* with the additional static equation combining the external static forces on the rotating structure, and inertia forces [9, 10].

Simplified models to describe a rotor, namely a disk on a massless shaft, rigid or elastic, have been almost exclusively used for rotor stability analysis. For other aspects of rotor dynamics, such as critical speed and unbalanced response, better rotor models and methods of analysis have been devised. The one disc rotor representation can only be used for qualitative studies and for the derivation of general results. For analysis of specific machinery, one has to take into account the complicated geometry of the rotor and accurate forms of excitation, bearings and supports [5–10].

The present chapter deals with methods for the approximate determination of eigenfrequencies in rotating shafts. More specifically, the methods examined are referred to flexural vibrations; however, the formulation will be similar for torsional vibrations of shafts or even vibrations of elastic systems in general.

The flexural eigenfrequencies of shafts are affected by a large number of factors, such as [11–19]:

(1) Mechanical properties of the shaft material, including internal damping [20–23], and factors affecting them, such as operating temperature [24, 25].
(2) Geometric properties of the shaft and mass distribution: Cross-sections may be uniform or change in a continuous or even discontinuous manner, as is the case with stepped shafts. Mass may be continuously distributed along a shaft

or a shaft may bear a number of lumped masses. Secondary effects due to the form of the latter may appear, such as a gyroscopic effect with disc-like masses [26–29].

(3) Number, type and elastodynamic behaviour of bearings [30, 31].
(4) Mechanical prestressing and static loads [32–35].
(5) External damping [36].
(6) Local imperfections, such as flaws, cracks, fatigue microcracks etc., factors affecting the structural integrity of the shaft [8–16, 37–44].

To solve the general dynamic problem, the shaft is modeled as a continuous beam, properly supported, with or without lumped masses [45–48]. A rigorous solution of the problem usually requires a considerable amount of analytical and/or numerical work, depending on the complexity of the system considered. In order to save effort and provide straightforward solutions with only a minimum of analytical and computational work, approximate methods have been developed. These bypass the rigorous solution and provide results sufficiently accurate for specific applications. Such methods are generally centered about the Rayleigh principle and associated methods [49–53], on which a rather long list of references can be found in the literature.

One of these methods is the *Dunkerley procedure*, which, as will be seen in the following, is a convenient tool for the solution of the relevant problems when combined with certain algebraic methods to increase its accuracy [54–56]. It is mainly this procedure which will be covered in detail in this chapter.

1.2 Formulation of the Eigenvalue Problem

The flexural vibrations of a continuous beam obey the differential equation [7, 52]

$$EJ\frac{\partial^4 u}{\partial x^4} + 2\frac{\mathrm{d}}{\mathrm{dx}}(EJ)\frac{\partial^3 u}{\partial x^3} + \frac{\mathrm{d}^2}{\mathrm{dx}^2}(EJ)\frac{\partial^2 u}{\partial x^2} = -\rho A\frac{\partial^2 u}{\partial t^2} \tag{1.1}$$

where $u = u(x, t)$ is the vibration displacement, ρ is material density and

$$EJ = f(x) \tag{1.2}$$

is beam stiffness. Equation (1.2) copes for changes of cross-section, as well as of material properties along the x-axis. Moreover, density ρ and cross-section A may also be functions of x. By separating coordinates, a solution of the following form is obtained:

$$u = X(x)T(t) \tag{1.3}$$

where

$$X(x) = c_1 \sin\ ax + c_2 \cos\ ax + c_3 \sinh\ ax + c_4 \cosh\ ax \tag{1.4}$$

$$T(t) = \sin\left(a^2 \beta t - \varphi\right) \tag{1.5}$$

$\beta = (EI/\rho A)^{1/2}$, φ is phase angle, and a corresponds to the eigenvalues which are to be determined from the boundary conditions. The latter may account for lumped masses along the beam.

If the amount of the distributed mass of the beam is small, as compared with the lumped masses, the system can be approximated by means of a massless beam ($\rho = 0$) with finite stiffness ($EJ \neq 0$) and n concentrated masses $m_1, m_2, \ldots, m_n$. In this case, the system has n degrees of freedom and obeys the matrix equation [15].

$$\mathbf{M}\ddot{x} + \mathbf{K}x = \mathbf{F} \tag{1.6}$$

where

$\mathbf{M} = \text{diag}\ (m_1, m_2, \ldots, m_n)$, the mass matrix;

$\mathbf{K} = \left[k_{ij}\right]$, the stiffness matrix;

$\mathbf{F} = [f_1(t), f_2(t), \ldots, f_n(t)]^T$, the external force vector, which is a function of time in general.

In the presence of damping, a term $\mathbf{C}\dot{x}$ must be included in the left-hand side of Eq. (1.6), where $\mathbf{C} = \left[c_{ij}\right]$ is the damping matrix.

Equation (1.6), for free undamped vibration ($\mathbf{F} = 0$), leads to the equation

$$\left|-\omega^2 \mathbf{M} + \mathbf{K}\right| = 0 \tag{1.7}$$

which is an algebraic equation of $2n$ degree, i.e. yielding n roots for ω^2, the eigenfrequencies of the system.

1.3 Dunkerley's Procedure

Dunkerley's procedure is actually an approximate method of determining the roots of Eq. (1.7). It was introduced by Dunkerley [55] on a purely empirical basis, as a means of determining the lowest eigenfrequency of a shaft, carrying k concentrated masses. Dunkerley intuitively noticed that if the natural frequencies Ω_1, Ω_2, …, Ω_k for the continuous shaft without masses and the massless shaft carrying each mass separately were combined by the formula

$$\frac{1}{\omega_n^2} = \frac{1}{\Omega_s^2} + \frac{1}{\Omega_1^2} + \frac{1}{\Omega_2^2} + \ldots + \frac{1}{\Omega_k^2} \tag{1.8}$$

the resulting critical frequency ω_n rad/s of the shaft having any number of disks of masses agreed very closely with the system natural frequency determined experimentally. In Eq. (1.8); Ω_1 is the critical speed of shaft if considered massless and supporting only disk m_1, Ω_2 is the critical speed of shaft if considered massless and supporting only disk m_2 etc. If the mass of the shaft is to be included, and Ω_s is the

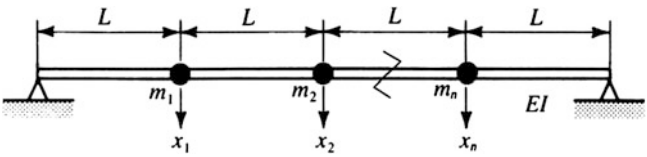

Fig. 1.1 A simply supported, massless elastic beam carrying n concentrated masses

critical speed of the shaft alone, i.e., if all disks are removed, then the term $1/\Omega_s^2$ has to be included to the right part of Eq. (1.8). Equation (1.8), known as Dunkerley's formula, was later proved by H. H. Jeffcott [7].

Consider a simply supported beam, AB as shown in Fig. 1.1, carrying masses m_k at respective positions x_k ($k = 1, 2, \ldots, n$). A unit force acting at $x = x_k$ produces a deflection f_k, which can be evaluated from the static elastic curve. If only the mass m_k at $x = x_k$ existed, the system would possess an eigenfrequency equal to

$$\Omega_k = (k_k/m_k)^{1/2} \tag{1.9}$$

where k_k is the spring constant at the position considered. According to Dunkerley, the lowest eigenfrequency ω_1 of the beam is given by

$$\frac{1}{\omega_1^2} = \sum_{k=1}^{n} \frac{1}{\Omega_k^2} \tag{1.10}$$

Equation (1.10) provides a good estimate, although somewhat low, for the fundamental flexural frequency of a massless beam carrying concentrated masses. For example, with two equal masses m equally spaced on the beam, this estimate is

$$\omega_{1D} = 5 \cdot 51135 \left(\frac{EJ}{ml^3}\right)^{1/2}$$

where l is the length of the beam, while the exact value for ω_1 is 5.692 96, i.e. ω_{1D} is lower by 3.19 % than the exact value. With three equal masses m equally spaced on the beam (Fig. 1.2), the respective values are 4.747 15 and 4.921 40, i.e. ω_{1D} is lower than ω_1 by 3.54 %.

In order to determine the principle underlying the Dunkerley procedure one has to examine Eq. (1.7), which has the following form:

$$D_n\omega^{2n} - D_{n-1}\omega^{2(n-1)} + \ldots + (-1)^{n+1}D_1\omega^2 + (-1)^n = 0 \tag{1.11a}$$

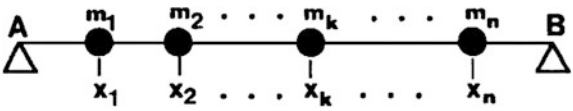

Fig. 1.2 A simply supported, massless elastic beam carrying n concentrated masses

where

$$\begin{gathered} D_1 = A_{11} + A_{12} + \ldots + A_{nn} \\ D_2 = \begin{vmatrix} A_{11} & A_{12} \\ A_{21} & A_{22} \end{vmatrix} + \ldots + \begin{vmatrix} A_{n-1,n-1} & A_{n-1,n} \\ A_{n,n-1} & A_{nn} \end{vmatrix} \\ D_3 = (\text{sum of terms } A_{ij}A_{kl}A_{mn}) \\ \vdots \\ D_n = (\text{sum of products of } nA_{ij} \text{ terms} \end{gathered} \tag{1.11b}$$

etc., and

$$A_{ij} = a_{ij}\, m_j$$

where a_{ij} are the influence coefficients, i.e. quantities expressing deflection at position j ($x = x_j$) due to unit force applied at position i. According to Maxwell's reciprocity theorem

$$a_{ij} = a_{ji} \tag{1.12}$$

From the values of the coefficients D_i (Eq. 1.11b), it is evident that D_i is of the order of A_{ij}, D_2 of A_{ij}^2, etc., and D_n is of the order of A_{ij}^n. If ω_1 is the fundamental (lowest) eigenfrequency of the system and A_{ij} are sufficiently small, terms containing powers of ω^2 higher than 1 can be neglected in Eq. (1.11a), which then assumes the form

$$D_1\omega_1^2 - 1 = 0 \tag{1.13}$$

and become equivalent to Eq. (1.9), i.e. Dunkerley's formula.

It is obvious that, under the conditions just stated, the higher harmonics of the system can be determined [17]. Indeed, if the fundamental frequency ω_1 is known, then, according to Eq. (1.11a)

$$D_n\omega_1^{2n} - D_{n-1}\omega_1^{2(n-1)} + \ldots + (-1)^{n+1}D_1\omega_1^2 + (-1)^n = 0 \tag{1.14}$$

which states that the polynomial of Eq. (1.10) has as an exact divider the binomial $\omega^2 - \omega_i^2$, which gives

$$\begin{aligned} &\omega_1^2 D_n\omega^{2(n-1)} + (\omega_1^4 D_n - \omega_1^2 D_{n-1})\omega^{2(n-2)} + (\omega_1^6 D_n - \omega_1^4 D_{n-1} + \omega_1^2 D_{n-1})\omega^{2(n-3)} \\ &+ \ldots + (\omega_1^{2n} D_n - \omega_1^{2(n-1)} D_{n-1} + \ldots + (-1)^{n+2}\omega_1^2 D_2)\omega^2 \\ &+ (\omega_1^{2n} D_n - \omega_1^{2(n-1)} D_{n-1} + \ldots + (-1)^{n+2}\omega_1^4 D_2) + (-1)^{n+1}\omega_1^2 D_1 = 0 \end{aligned} \tag{1.15}$$

Now, by virtue of Eq. (1.13), the constant term of Eq. (1.15) is equal to $(-1)^{n-1}$; hence Eq. (1.15) assumes the form of Eq. (1.11a), but the highest power of ω^2 has been reduced by 1. The coefficient of ω^2 is of the order of D_2 or A_{ij}^2 at the highest, etc. In this way, considering the smallest root ω_2^2, which corresponds to the second eigenfrequency of the system, one may neglect terms containing

Table 1.1 Dimensionless eigenfrequencies for discrete systems

$\omega(EJ/ml^3)^{1/2}$	n	Accurate	Dunkerley	Error (%)
Fundamental	2	5.69296	5.51135	−3.19
2nd mode		2.199564	22.72047	+3.29
Fundamental	3	4.49140	4.74715	−3.54
2nd mode		19.33365	18.01872	−5.93
3rd mode		39.79685	44.05223	+10.69

powers of ω^2 higher than 1. But also in the coeficient of ω^2 only the last term $(-1)^{n+2}\omega_1^2 D_2$ need be retained, and Eq. (1.15) becomes

$$\omega_1^2 \omega_2^2 D_2 = 0 \tag{1.16}$$

which provides a direct approach to the second eigenfrequency:

$$\omega_2 = 1/\omega_1 D_2 \tag{1.17}$$

By dividing the polynomial of Eq. (1.14) by $\omega^2 - \omega_i^2$ and admitting the same approximations, Eq. (1.17) may assume the following form:

$$D_n \prod_{j=1}^{n} \omega_j^2 = 1 \tag{1.18}$$

thus confirming a well-known fact from the theory of algebraic equations, i.e. that the product of all roots is equal to the constant term divided by the coefficient of the highest power of the variable.

Application of these results to a simply supported massless beam carrying n equally spaced equal masses m yields the following: The influence coefficients, as derived from the static elastic curve, are

$$a_{ij} = \frac{l^3}{6EJ} \left\{ \begin{array}{l} q_j(1-q_i)\left\{1 - q_j^2 - (1-q_i)^2\right\} (q_j < q_i) \\ q_i(1-q_j)\left\{1 - q_i^2 - (1-q_j)^2\right\} (q_j > q_i) \end{array} \right\} \tag{1.19}$$

where $q = x/l$ is a dimensionless coordinate along the axis of the beam. Now, with two equal masses, attached at $q = 1/3$ and $q = 2/3$, respectively, we have

$$D_1 = 0.032921810/(ml^3/EJ)$$
$$D_2 = 0.000063775/(ml^3/EJ)$$

Accordingly, with three equal masses attached at $q = 0.25$, $q = 0.50$ and $q = 0.75$, we have

$$D_1 = 4.438 \times 10^{-2}/(ml^3/EJ)$$
$$D_2 = 1.370 \times 10^{-4}/(ml^3/EJ)$$
$$D_3 = 0.069 \times 10^{-6}/(ml^3/EJ)$$

For both cases, exact eigenvalues, as well as the ones produced by Dunkerley's procedure, are given in Table 1.1. The error ε is expressed as

$$\varepsilon(\%) = (\omega_{acc} - \omega_{dunk}) \times 100/\omega_{acc} \tag{1.20}$$

A procedure similar to Dunkerley's, based on partial distributions of stiffness instead of mass, is expressed by Southwell's theorem (see Ref. [49], for example).

1.4 The Question of Accuracy

The sum of the roots of Eq. (1.11a) is equal to

$$\sum_{i=1}^{n} \frac{1}{\omega_i^2} = D_i \tag{1.21}$$

where, from Eq. (1.11b)

$$D_1 = \frac{1}{\Omega_1^2} + \frac{1}{\Omega_2^2} + \ldots + \frac{1}{\Omega_n^2} \tag{1.22}$$

i.e. Eq. (1.21) is the exact form of Eq. (1.10), expressing Dunkerley's principle. In the latter, the roots $\omega_2^2, \omega_3^2, \ldots, \omega_n^2$ have been omitted, obviously by assuming that their reciprocals are very small compared with ω_1^2. The same assumption must be made in order to proceed to the determination of higher eigenvalues by Dunkerley. Hence, the condition for the validity of the latter is

$$\omega_n^2 \gg \omega_{n-1}^2 \gg \ldots \gg \omega_1^2 \tag{1.23}$$

i.e. ω_1 corresponds to the fundamental eigenfrequency.

One more conclusion drawn from the comparison of Eqs. (1.10) and (1.21) is that Dunkerley's procedure provides values for the eigenfrequencies which in general are smaller than the exact ones, i.e. it provides *lower bounds* for the roots of the characteristic equation. However, in the results of Table 1.1 it should be noted that with certain higher eigenfrequencies the method yields greater values. This is due to the fact that, according to Eqs. (1.16–1.18), each higher eigenfrequency ω_k^2 is determined as a function of the lower values $\omega_1^2, \omega_2^2, \ldots, \omega_{k-1}^2$ which have been previously determined by means of the same procedure and, as they are smaller than the exact values, may produce the said effect.

Algebraic equations whose roots satisfy the condition (1.23) can, therefore, be solved in a straightforward approximate way, without lengthy computations. It is interesting to look into this fact in detail, bearing in mind that roots of characteristic equations of vibrating elastic systems without damping are always real and positive $\left(\omega_i^2\right)$.

Returning now to Eq. (1.11a), where $D_n \neq 0$ and assuming that the condition (1.23) holds, we can write

$$\left.\begin{aligned} \omega_2^2 &= \varepsilon_1 \omega_1^2 \\ \omega_3^2 &= \varepsilon_2 \omega_2^2 \\ &\vdots \\ \omega_n^2 &= \varepsilon_{n-1} \omega_{n-1}^2 \end{aligned}\right\} \tag{1.24}$$

where the quantities $\varepsilon_1, \varepsilon_2, \ldots, \varepsilon_n$ are much smaller than one. On the other hand, between the roots and the coefficients of Eq. (1.11a) the following relations hold:

$$\left.\begin{aligned} \omega_1^2 + \omega_2^2 + \ldots + \omega_n^2 &= -\tfrac{D_{n-1}}{D_N} \\ \omega_1^2\omega_2^2 + \omega_2^2\omega_3^2 + \ldots + \omega_{n-1}^2\omega_n^2 &= \tfrac{D_{n-2}}{D_N} \\ &\vdots \\ \omega_1^2\omega_2^2 \ldots \omega_n^2 &= \tfrac{1}{D_N} \end{aligned}\right\} \tag{1.25}$$

which, on the basis of Eq. (1.24), assume the form

$$\left.\begin{aligned} \omega_1^2(1 + E_1) &= -\tfrac{D_{n-1}}{D_N} \\ \omega_1^2\omega_2^2(1 + E_2) &= \tfrac{D_{n-2}}{D_N} \\ &\vdots \\ \omega_1^2\omega_2^2 \ldots \omega_n^2(1 + E_n) &= \tfrac{1}{D_N} \end{aligned}\right\} \tag{1.26}$$

where the quantities E_1, E_2,..., E_n are all much smaller than one and, without important loss of accuracy, they can be neglected, giving

$$\left.\begin{aligned} \omega_n^2 &= -\tfrac{D_{n-1}}{D_n} \\ \omega_n^2\omega_{n-1}^2(1 + E_2) &= \tfrac{D_{n-2}}{D_n} \\ &\vdots \\ \omega_1^2\omega_2^2 \ldots \omega_n^2 &= \tfrac{1}{D_n} \end{aligned}\right\} \tag{1.27a}$$

from which the following approximations to the roots of Eq. (1.11a) result:

$$\left.\begin{aligned} \omega_n^2 &= -\tfrac{D_{n-1}}{D_n} \\ \omega_{n-1}^2 &= -\tfrac{D_{n-2}}{D_{n-1}} \\ &\vdots \\ \omega_1^2 &= \tfrac{1}{D_1} \end{aligned}\right\} \tag{1.27b}$$

i.e. the roots of Eq. (1.11a) can be approximated by the roots of the following linear equations:

$$\left.\begin{aligned} D_n\omega_n^2 + D_{n-1} &= 0 \\ D_{n-1}\omega_{n-1}^2 + D_{n-2} &= 0 \\ &\vdots \\ D_1\omega_1^2 - 1 &= 0 \end{aligned}\right\} \tag{1.28}$$

It is obvious that the accuracy of the process depends on how small, as compared with one, the quantities $\varepsilon_1, \varepsilon_2, \ldots, \varepsilon_{n-1}$ in Eq. (1.24) are. For example, from the values presented in Table 1.1, $\varepsilon_1 = 0.0670$ for $n = 2$ and $\varepsilon_1 = 0.0540$, $\varepsilon_2 = 0.236$ for $n = 3$, which values have provided acceptable accuracy with Dunkerley's procedure. They also explain why the original empirical formula worked when applied to shafts.

However, there are cases where the method is not applicable, at least in its present form. Consider, for example, a massless circular plate, clamped circumferentially, carrying two equal masses m (Fig. 1.3). The static deflection w at a position defined by the polar coordinates r, θ due to a unit load at $r = b$ and $\theta = 0$ is given by the following equation [57]

$$w = \frac{\alpha^2}{16\pi D}\left[(1-x)^2(1-\xi)^2 + \left(x^2+\xi^2-2x\xi\cos\theta\right)\log\frac{x^2+\xi^2-2x\xi\cos\theta}{1+x^2\xi^2-2x\xi\cos\theta}\right] \tag{1.29}$$

where α is the radius of the plate;

$x = r/a$, $\xi = b/a$	are dimensionless coordinates;
$D = Eh^3/[12(1-\nu^2)]$,	the flexural rigidity of the plate;
h	is the thickness of the plate;
E and ν	are Young's modulus and Poisson's ratio of the plate material, respectively.

The influence coefficients are therefore

$$\alpha_{11} = 0.5625\alpha^2/16\pi D$$
$$\alpha_{12} = 0.5625\alpha^2/16\pi D$$

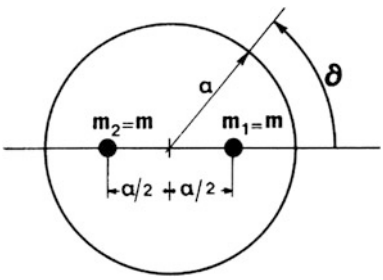

Fig. 1.3 A circumferentially clamped, massless elastic plate carrying two equal concentrated masses

and the coefficients of the frequency equation are

$$D_1 = 1.125m\alpha^2/16\pi D$$
$$D_2 = 0.3029(m\alpha^2/16\pi D)^2$$

which give the following exact solutions:

$$\omega_1 = 1.4969m\alpha^2/16\pi D$$
$$\omega_2 = 1.2138m\alpha^2/16\pi D$$

while respective values obtained by the Dunkerley procedure are

$$\omega_{D1} = (\mathrm{D}_1/\mathrm{D}_2)^{1/2} = 1.9272m\alpha^2/16\pi D \quad (\text{error} + 28.75\,\%)$$
$$\omega_{D2} = \mathrm{D}_1^{1/2} = 0.9428m\alpha^2/16\pi D \quad (\text{error} - 22.33\,\%)$$

It is obvious that the method is not applicable with the present system, where $\varepsilon_1 = 0.6575$, i.e. not much smaller than one.

1.5 The Root-Squaring Process

In order to increase the accuracy of the method, or even to make it applicable to more systems, special techniques are required, the most convenient of which is Graeffe [58] or Lobachevsky-Graeffe [59] method.

This method is based on the following principle. If, from Eq. (1.11a), a transformed equation can be derived:

$$D_n^{(m)}y^{2n} - D_{n-1}^{(m)}y^{2(n-1)} + \ldots + (-1)^{n+1}D_1^{(m)}y^2 + (-1)^n = 0 \tag{1.30}$$

whose roots $\left(y_i^2\right)$ are equal to the mth power of the respective roots (ω_i^2) of Eq. (1.11a), i.e.

$$y_i^2 = \omega_i^{2m} \quad (i = 1, 2, \ldots, n) \tag{1.31}$$

then condition (1.23) is valid more accurately for Eq. (1.30) than for Eq. (1.11a). Indeed, if y_{k-1}^2 and $y_k^2 < y_{k-1}^2$ are two consecutive roots of Eq. (1.30), we have

$$\lim \frac{y_k^2}{y_{k-1}^2} = \lim \left(\frac{\omega_k^2}{\omega_{k-1}^2}\right)^{\mathrm{m}} = 0 \quad \text{when } m \to \infty$$

This limit, however, is the quantity $\varepsilon_{\mathrm{k}-1}$, which, under these conditions, can be taken as small as necessary, provided that a suitable value for m is selected. In practice such a method works by taking the exponent m equal to a power of 2, i.e. $m = 2^p$, where p is a natural number and the process is executed in p steps. At each step, a transformed equation is obtained, whose roots are the squares of the respective roots of the transformed equation of the last step. The method is thus

called the *root-squaring process*. If some of the roots of the basic equation do not differ considerably the convergence of the method is slowed down.

The coefficients of the transformed equations can be determined as follows: The polynomial of Eq. (1.11a) can be written in the form

$$P\omega^2 = D_n\left(\omega^2 - \omega_1^2\right)\left(\omega^2 - \omega_2^2\right)\ldots\left(\omega^2 - \omega_n^2\right)$$

while

$$P\left(-\omega^2\right) = (-1)^n D_n\left(\omega^2 + \omega_1^2\right)\left(\omega^2 + \omega_2^2\right)\ldots\left(\omega^2 + \omega_n^2\right).$$

Then, equation

$$Q\left(\omega^4\right) = P\left(\omega^2\right)P\left(-\omega^2\right) = (-1)^n D_n\left(\omega^4 - \omega_1^4\right)\left(\omega^4 - \omega_2^4\right)\ldots\left(\omega^4 - \omega_n^4\right) = 0 \tag{1.32}$$

has roots equal to $\omega_1^4, \omega_2^4, \ldots, \omega_n^4$ i.e. the squares of the roots of the equation $P(\omega^2) = 0$.

Carrying out the multiplication of the polynomials

$$P\left(\omega^2\right) = D_n\omega^{2n} - D_{n-1}\omega^{2(n-1)} + \ldots + (-1)^{n-1}D_1\omega^2 + (-1)^n = 0$$
$$P\left(-\omega^2\right) = (-1)^n\left[D_n\omega^{2n} - D_{n-1}\omega^{2(n-1)} - \ldots - (-1)^{n-1}D_1\omega^2 + (-1)^n\right] = 0$$

one obtains the polynomial

$$Q\left(\omega^4\right) = D_n^{(1)}y^{2n} + D_{n-1}^{(1)}y^{2(n-1)} + \ldots + (-1)^{n-1}D_1^{(1)}y^2 + (-1)^n = 0 \tag{1.33}$$

with roots

$$y_i^2 = \omega_i^4$$

where

$$\begin{aligned} D_n^{(1)} &= D_n^2 \\ D_{n-1}^{(1)} &= D_{n-1}^2 - 2(-1)^n D_{n-2} \\ D_{n-2}^{(1)} &= D_{n-2}^2 - 2D_{n-1}D_{n-3} + 2(-1)^n D_{n-4} \\ &\vdots \\ &\text{etc.} \end{aligned}$$

or generally

$$D_k^{(i+1)} = \left[D_k^i\right]^2 + 2\sum_{s=1}^{k}(-1)^s D_{k-s}^{(i)}D_{k+s}^{(i)} \quad (k = 1, 2, \ldots, n) \tag{1.34}$$

where it is assumed that $D_s = 0$ for $s < 0$ and $s > n$. If any of the coefficients D_{k-s} or D_{k+s} is absent, it is considered to be zero.

Table 1.2 Dimensionless eigenfrequencies of Table 1.1 corrected by applying once ($p = 1$) the root-squaring process

$\omega(EJ/ml^3)^{1/2}$	n	Accurate	Dunkerley	Error (%)
Fundamental	2	5.69296	5.68659	−0.11
2nd mode		21.99564	22.02028	+0.11
Fundamental	3	4.92140	4.92799	+0.13
2nd mode		19.33365	19.13948	−1.00
3rd mode		39.79685	40.33301	+1.35

If the root-squaring process is applied p times and the roots z_i of the pth equation are determined through the linear equations

$$\begin{aligned} &D_n^{(p)} z_n^2 + D_{n-1}^{(p)} = 0 \\ &D_{n-1}^{(p)} z_{n-1}^2 + D_{n-2}^{(p)} = 0 \\ &\vdots \\ &D_1^{(p)} z_1^2 - 1 = 0 \end{aligned}$$

then the roots ω_i of the initial Eq. (1.11a) are given by

$$\omega_i = \sqrt[2p]{z_i} = \left(\frac{D_{i-1}}{D_i}\right)^{1/2p} \quad (i = 1, 2, \ldots, n) \tag{1.35}$$

It is evident that repeated application of the transformation expressed by Eq. (1.34) leads to progressively smaller values for the double products.

This remark leads to the following rule:

The root-squaring process is terminated when the coefficients of a certain transformed equation are equal to the squares of the respective coefficients of the preceding transformed equation.

Such equality is meant to be within the accuracy of computations and is due to the absence of double products.

Examples

As examples, let the simply supported beam of Fig. 1.2 and the circumferentially clamped circular plate of Fig. 1.3 be considered.

In the first case and for one application ($p = 1$), the results are presented in Table 1.2. On both occasions ($n = 2$, $n = 3$), the error has been reduced to insignificant levels, as a result of the fact that condition (1.23) was in the first place fulfilled with sufficient accuracy.

In the second case, however, such a rapid convergence of the method is not exhibited. According to the results presented in Table 1.3, the same order of accuracy as in the previous case can be obtained only by means of three successive applications of the root-squaring process.

However, it should be pointed out that

Table 1.3 Approximate dimensionless eigenfrequencies of a circumferentially clamped massless circular plate carrying two concentrated masses with repeated corrections by the root-squaring process

$\omega(16\pi D/ma^2)^{1/2}$	p	Dunkerley	Error (%)
Fundamental		0.9428	−22.33
2nd mode	0	1.9272	+28.73
Fundamental		1.1096	−8.59
2nd mode	1	1.6378	+9.41
Fundamental		1.1881	−2.12
2nd mode	2	1.5297	+2.19
Fundamental		1.2111	−0.23
2nd mode	3	1.5000	+0.21

(Accurate values $\omega_1(16\pi D/ma^2)^{1/2} = 1.4969$, $\omega_2(16\pi D/ma^2)^{1/2} = 1.2138$)

(1) the combined use of Dunkerley's procedure and Graeffe's method renders the former applicable with *any* elastic system, even with those which do not conform to condition (1.23);
(2) in the latter circumstances, the computations required are straightforward and less complex than when solving the characteristic equation by numerical means.

1.6 Application with Dissipative Systems

Assume that one or more of the masses of the system considered is subjected to viscous damping. The respective roots of the characteristic equation will then appear in pairs of complex conjugate quantities. A straightforward application of the procedures so far mentioned for their determination is not possible, as condition (1.23) is no longer valid. However, the problem can still be tackled directly, at least partially, by means of proper generalisations. Suppose that the n roots of Eq. (1.11a) can be grouped in r classes:

$$\left.\begin{array}{c} \omega_1^2, \omega_2^2, \ldots, \omega_{q_1}^2 \\ \omega_{q_1+1}^2, \omega_{q_1+2}^2, \ldots, \omega_{q_2}^2 \\ \vdots \\ \omega_{q_{r-1}+1}^2, \omega_{q_{r-1}+2}^2, \ldots, \omega_{q_r}^2 \end{array}\right\}$$

such that

$$\begin{aligned} &\omega_1^2 \le \omega_2^2 \le \ldots \le \omega_{q_1}^2 \ll \omega_{q_1+1}^2 \le \omega_{q_1+2}^2 \le \ldots \le \omega_{q_2}^2 \ll \omega_{q_{r-1}+1}^2 \le \ldots \\ &\quad \le \omega_{q_{r-1}+2}^2 \le \ldots \le \omega_{qr}^2 \end{aligned} \tag{1.36}$$

where obviously $q_1 + q_2 + \ldots + q_r = n$, i.e. the roots belonging to a lower class are much smaller than the roots belonging to a higher class. In this case, by

reasoning similar to that for the derivation of the linear Eq. (1.28) from the original Eq. (1.11a), it can be proved that the latter is approximately equivalent to the set of equations

$$\left.\begin{array}{c} D_n\omega^{2q_1} + D_{n-1}\omega^{2(q_1-1)}\ldots + D_{q1} = 0 \\ D_{q_1}\omega^{2q_2} + D_{q_1+1}\omega^{2(q_2-1)} + \ldots + D_{q_1+q_2} = 0 \\ \vdots \\ D_{q_1+q_2+\ldots+q_{p-1}}\omega^{2q_r} + D_{q_1+q_2+\ldots+q_{p-1}+1}\omega^{2(q_r+1)} + \ldots + D_{q_1+q_2+\ldots+q_r} = 0 \end{array}\right\} \tag{1.37}$$

of degree q_1, q_2,..., q_r ω^2 in respectively (only plus-signs have been used for convenience). It is obvious that, if condition (1.23) holds, $r = n$ and Eq. (1.37) are equivalent to the set of the linear *binomials* (1.28). Now, Eq. (1.37) are of much lesser degree than n and are perhaps easier to solve than the original n-degree equation. However, this procedure provides the basis for the solution of the latter, if it possesses one, two or three pairs of complex roots. With four pairs or more, the procedure becomes too complex and further methods are required.

Indeed, assuming that roots ω_m^2 and ω_{m+1}^2 are complex conjugates of the form

$$\left.\begin{array}{l} \omega_m^2 = u + iv \\ \omega_{m+1}^2 = u - iv \end{array}\right\} \tag{1.38}$$

where u and v are real, that all other roots are real and satisfy the condition

$$\omega_1^2 < \omega_2^2 < \ldots < \left|\omega_m^2\right| = \left|\omega_{m+1}^2\right| < \ldots < \omega_n^2 \tag{1.39}$$

by applying p times the root-squaring process, the equation

$$D_n^{(p)}y^n - D_{n-1}^{(p)}y^{n-1} + \ldots + D_1^{(p)}y + (-1)^n = 0 \tag{1.40}$$

is obtained, with roots

$$y_k = \left(\omega_n^2\right)^{2p} \quad (k = 1, 2, \ldots n)$$

for sufficiently large p, the real roots of Eq. (1.40) can be approximated by the $n-2$ linear equations

$$\left.\begin{array}{c} D_n^{(p)}y_n + D_{n-1}^{(p)} = 0 \\ \vdots \\ D_{m-2}^{(p)}y_{m-2} + D_{m-1}^{(p)} = 0 \\ D_{m+1}^{(p)}y_{m+1} + D_{m+2}^{(p)} = 0 \\ \vdots \\ D_1^{(p)}y_1 + (-1)^n = 0 \end{array}\right\} \tag{1.41a}$$

from which

$$\omega_k^2 = \left[D_k^{(p)}/D_{k-1}^{(p)}\right]^{1/2p} \quad (k \neq m, k \neq m+1)$$

As stated, when the root-squaring process is terminated, the double products in Eq. (1.34) tend to vanish. This is the present case with all coefficients $D_k^{(p)}$, but not $D_m^{(p)}$. This coefficient does not contain vanishing products. On the contrary, the double products assume significant values, sometimes causing the coefficient to change sign. When this occurs with the root-squaring process, it is an unmistakable sign of the *existence of complex roots*, whose position in condition (1.39) is indicated by the index m of the coefficient $D_m^{(p)}$.

Now, these complex roots must satisfy the quadratic

$$D_{m-1}^{(p)} y^2 + D_m^{(p)} y^2 + D_{m+1}^{(p)} y^2 = 0 \tag{1.41b}$$

which, along with Eq. (1.41a), provides the complete solution of the characteristic equation.

This procedure can also be applied for two or three pairs of complex roots, if sufficiently distant. However, with four such pairs and more, the improvement suggested by Brodetsky and Smeal needs to be applied. Using this, the origin of the variable x is moved by a small quantity n and then the root-squaring process is applied. All complex roots can thus be found, but the introduction of n entails considerable algebraic work, necessary for the transformation of the initial equation by means of the binomial expansion $(x' + n)^n$. The method need not be given here in detail, as it is readily available in the literature [60, 61].

1.7 Applications with Continuous Systems

Dunkerley's procedure is also applicable to continuous systems. If the influence function $\alpha(q, \xi)$ is known, i.e. the deflection at the position q due to a unit load applied at the position ξ, which can be continuous or sectionally continuous, and also the mass distribution

$$\mu(q) = \frac{dm}{dq}$$

along the beam, then the A-coefficients of Eq. (1.11b) appear in the differential form

$$dA(q, \xi) = \alpha(q, \xi) dm \tag{1.42}$$

In order to apply Dunkerley's procedure the coefficients D_k in Eq. (1.11b) must be evaluated in the following manner:

Table 1.4 Dimensionless eigenfrequencies for a simply supported uniform beam

$\omega(EJ/\mu l^4)^{1/2}$	Accurate	Dunkerley	Error (%)
Fundamental	$\pi^2 = 9.869\ 60$	9.486 52	−3.89
2nd mode	$4\pi^2 = 39.478\ 42$	38.883 43	−1.51

$$D_1 = \int_0^1 dA(q,q) \tag{1.43a}$$

$$D_2 = \int_0^1 dA(q,q) \int_0^1 dA(\xi,\xi) - \int_0^1 A(q,\xi)A(\xi,q)dq \tag{1.43b}$$

etc.

The application in a simply supported beam with uniformly distributed mass $\mu = m/l$ is straightforward. One has

$$a(q,\xi) = \frac{l^3}{6EJ} \times \left\{ \begin{array}{ll} \xi(1-q)\left[1-\xi^2-(1-q)^2\right] & (\xi < q) \\ q(1-\xi)\left[1-q^2-(1-\xi)^2\right] & (\xi > q) \end{array} \right\} \tag{1.44}$$

which, when combined with Eq. (1.42), yields

$$D_1 = 0.011\ 111\left(\mu l^4/EJ\right)$$
$$D_2 = 7.349\ \times\ 10^{-6}\left(\mu l^4/EJ\right)^2$$

These results can be obtained directly if one bears in mind the expression

$$\int_0^l x^m(1-x)^n dx = \frac{m!n!}{(m+n+1)!}$$

The first and second eigenfrequencies along with the accurate ones and the error appear in Table 1.4. It is interesting to note that one application of Graffe's method leads, for the fundamental mode, to a value

$$\left(D_1^2 - 2D_2/D_2^2\right)^{1/4} = 9.792\ 48$$

i.e. an improved value, and for the second mode to a value

$$\left(D_1^2 - 2D_2/D_2^2\right)^{1/4} = 37.668\ 54$$

which is less accurate than the first approximation. The procedure can be generalised to stepped shafts [63] or to continuous shafts carrying concentrated masses as well.

It is now expedient to consider in detail the approximate solution of the eigenvalue problem of the vibrating beam by means of its integral-equation formulation. If $\alpha(x, \xi)$ is the influence function of the beam and $P(\xi, t)$ a dynamic load

distribution, the differential deflection at the position x due to a load $P(\xi, t)\mathrm{d}\xi$ at the position ξ is

$$\mathrm{d}u = \mathrm{d}(x, \xi)P(\xi, t)\ \mathrm{d}\xi.$$

By integration over the length l of the beam, one obtains

$$u(x,t) = \int_0^l a(x,\xi)P(\xi,t)d\xi. \tag{1.45}$$

However, with freely vibrating beams the load $P(\xi,t)$ is only due to inertial forces, i.e.

$$P(\xi,t) = -m(\xi)\frac{\partial^2 u}{\partial t^2} \tag{1.46}$$

where $m(\xi)$ is the mass distribution along the beam. On the other hand, we have

$$u(\xi,t) = X(\xi)\cos(\omega t)$$

as free vibrations are harmonic, and Eq. (1.45) assumes the form

$$X(x) = \omega^2 \int_0^l a(x,\xi)m(\xi)X(\xi)d\xi. \tag{1.47}$$

By substituting [62, 63],

$$\begin{aligned} y(x) &= \sqrt{m(x)}X(x) \\ K_1(x,\xi) &= a(x,\xi)\sqrt{m(x)}\sqrt{m(\xi)}\,. \\ \lambda &= \omega^2 \end{aligned}$$

Eq. (1.47) becomes

$$y(x) = \lambda \int_0^l K_1(x,\xi)y(\xi)d\xi \tag{1.48}$$

which possesses a symmetric kernel $K_1(x, \xi)$.

Solutions of Eq. (1.48) exist for a discrete set of real and positive eigenvalues, $\lambda_1 < \lambda_2 < \ldots < \lambda_n < \ldots$, to which the eigenfunctions $y_1, y_2, \ldots, y_n, \ldots$correspond. No multiple eigenvalues exist.

The eigenfunctions are orthogonal [64], i.e.

$$\int_0^l y_n(x)y_m(x)dx = N_m\delta_{mn} \tag{1.49}$$

where δ_{mn} is Kronecker's delta, and form a complete set, on the basis of which the kernel can be expressed in the form of the series [65]

$$K_1(x,\xi) = \sum_{n=1}^{\infty} \frac{y_n(\xi) y_n(x)}{\lambda_n N_n}. \tag{1.50}$$

The lowest eigenvalue λ_i can be found from Eq. (1.50) by putting $\xi = x$ and integrating with respect to x. We then have

$$\int_0^l K_1(x,x)dx = \sum_{n=1}^{\infty} \frac{1}{\lambda_n}. \tag{1.51}$$

Now, if $\lambda_1 \ll \lambda_2 \ll \lambda_3 \ll \ldots$, i.e. a condition corresponding to (1.23), we can write

$$\frac{1}{\lambda_1} \approx \int_0^l K_1(x,x)dx = J_1 \tag{1.52}$$

which clearly provides a lower bound for the fundamental eigenfrequency and corresponds to the value from Eq. (1.43a).

In order to proceed to higher eigenvalues one must make use of a theorem [65], stating that if $\varphi_n(\xi)$ is the sequence of all eigenfunctions of a symmetric kernel $K(x, \xi)$ and λ_n the corresponding eigenvalues, then the truncated kernel

$$K^{n+1}(x,\xi) = K(x,\xi) - \sum_{m=1}^{n} \frac{y_m(x) y_m(\xi)}{\lambda_m} \tag{1.53}$$

has the eigenvalues λ_{n+1}, λ_{n+2}, … to which correspond the eigenfunctions $\varphi_{n+1}(\xi)$, $\varphi_{n+2}(\xi)$, … and no other eigenvalues or eigenfunctions. Equation (1.52) corresponds to the values from Eq. (1.43b), etc.

Finally, in order to improve the lower bound provided by Eq. (1.52), etc., and also to provide an upper bound, the mth iterated kernel $K_m(x, \xi)$, $m \geq 2$, is defined as

$$K_m(x,\xi) = \int_0^l K_{m-1}(x,\eta) K_1(\eta,\xi) d\eta \tag{1.54}$$

Moreover, we have

$$\int_0^l K_m(x,\xi) y_n(\xi) d\xi = \int_0^l K_{m-1}(x,\eta) d\eta \int_0^l K_1(x,\xi) y_n(\xi) d\xi$$

$$= \lambda_n^{-1} \int_0^l K_m(x,\eta) y_n(\eta) d\eta$$

and, by continuing

$$\int_0^l K_m(x,\xi) y_n(x) dx = \lambda_n^{-m} y_n(\xi x)$$

and the iterated kernel $K_m(x, \xi)$ can be expanded as

$$K_m(x,\xi) = \sum_{n=1}^{\infty} \frac{y_n(\xi) y_n(x)}{\lambda_n^m N_n}$$

from which it follows that

$$\sum_{n=1}^{\infty} \frac{1}{\lambda_n^m} = \int_0^l K_m(x,x)dx = J_m \tag{1.55}$$

giving Eq. (1.52) for $m = 1$. By putting

$$\left.\begin{aligned} J_m &= \tfrac{1}{\lambda_1^m}(1+\varepsilon_m) \\ J_{m-1} &= \tfrac{1}{\lambda_1^{m-1}}(1+\varepsilon_{m-1}) \end{aligned}\right\} \tag{1.56}$$

where, since $\lambda_1 < \lambda_2 < \lambda_3 \ldots$

$$0 < \varepsilon_m = \sum_{n=2}^{\infty} \left(\frac{\lambda_1}{\lambda_n}\right)^m < \varepsilon_{m-1} = \sum_{n=2}^{\infty} \left(\frac{\lambda_1}{\lambda_n}\right)^{m-1}$$

it follows that

$$\lambda_1 > \left(\frac{1}{J_m}\right)^{1/m}$$

and

$$\lambda_1 = \frac{J_{m-1}}{J_m} \frac{1+\varepsilon_m}{1+\varepsilon_{m-1}} < \frac{J_{m-1}}{J_m}$$

leading eventually to an upper and a lower bound for λ_1:

$$\left(\frac{1}{J_m}\right)^{1/m} < \lambda_1 < \frac{J_{m-1}}{J_m} \tag{1.57}$$

which are the closer the larger the value of m.

1.8 Summary and Conclusions

Dunkerley's procedure, based on a simple empirical rule for a direct approximation to the fundamental flexural eigenfrequency of vibrating shafts, can be generalized and combined with certain algebraic devices to provide approximate solutions for the eigenfrequencies corresponding to any mode for any linear vibrating elastic system. The procedure is a number of discrete components and

whose eigenfrequencies differ considerably from each other. However, by applying Graeffe's method and the root-squaring process, the accuracy of approximation can be increased at will, while the computational effort remains small. The method can also cope with vibrating masses subjected to viscous damping, in which case a respective number of complex roots results for the characteristic equation. If more than three masses are subjected to damping, the improvement suggested by Broodetsky and Smeal renders the root-squaring process applicable.

The procedure is applicable with continuous systems as well. By means of the integral equation formulation or the respective eigenvalue problem, it can be proved that upper and lower bounds are provided for the eigenvalues, and iterative processes increasing accuracy are established. Those methods are useful for predicting the bending and torsional fatigue life of rotors and shafts, and furthermore, for developing methodologies for damage detection, and the estimation of position and size of flaws and cracks in rotating machinery [66–70].

In all of the approximate procedures suggested, the necessary computations are straightforward and less complex than required for the rigorous solution of the respective problem, while any desired level of accuracy can be obtained.

References

1. Borel, L.: Vitesses Critiques des Arbres en Rotalion, Imprimerie la Concorde, Lausanne, (1954)
2. Dimentberg, F.M.: Flexural Vibrations of Rotating Shafts. Butterworths, London (1961)
3. Tondl, A.: Some Problems of Rotor Dynamics. Chapman and Hall, London (1965)
4. Gasch, R.: Selbsterregte Biegeschwingungen Rotierender Wellen, Konstruktion, **23**, 5, (1971)
5. Dynamics of rotors IUTAM symposium, Lyngby, Denmark, 1974: Springer, Berlin, 1975
6. Federn, K.: Auswuchttechnik, Springer, Berlin, (1977)
7. Dimarogonas, A.D.: Vibration for Engineers, Second Edition edn. Prentice Hall Upper Saddle River, New Jersey (1996)
8. Dimarogonas, A. D.: Vibration of cracked structures-a state of the art review. Eng. Fract. Mech. **55**(5), 831–57, (1996)
9. Dimarogonas, A. D.: A general method for stability analysis of rotating shafts. Ing. Arch. **44**, 9–20, (1975)
10. Irretier, H.: Mathematical foundations of experimental modal analysis in rotor dynamics. Mech. Syst. Signal Process. **13**(2), 183–191 (1999)
11. Papadopoulos, C. A., Dimarogonas, A. D.: Stability of cracked rotors in the coupled vibration mode. ASME J. Vib. Acoust. Stress Reliab. Des. **110**, 356–359, (1988)
12. Wauer, J.: On the dynamics of cracked rotors: A literature survey. Appl. Mech. Rev. **43**(1), 13–17, (1990)
13. Krawczuk, M., Ostachowicz, W.M.: Transverse natural vibrations of a cracked beam loaded with a constant axial force. J. Vib. Acoust. Trans. ASME **115**(4), 524–533 (1995)
14. Darpe, A.K., Gupta, K., Chawla, A.: Experimental investigations of the response of a cracked rotor to periodic axial excitation. J. Sound Vib. **260**(2), 265–286 (2003)
15. Darpe, A.K., Gupta, K., Chawla, A.: Transient response and breathing behaviour of a cracked Jeffcott rotor. J. Sound Vib. **272**(1–2), 207–243 (2004)
16. Darpe, A.K., Gupta, K., Chawla, A.: Coupled bending, longitudinal and torsional vibrations of a cracked rotor. J. Sound Vib. **269**(1–2), 33–60 (2004)

17. Chondros, T.G.: Variational formulation of a rod under torsional vibration for crack identification. Theoret. Appl. Fract. Mech. **44**, 95–104 (2005)
18. Chondros, T.G., Labeas, G.: Torsional Vibration of a cracked rod by variational formulation and numerical analysis. J. Sound Vib. **301**(3–5), 994–1006 (2007)
19. Georgantzinos, S.K., Anifantis, N.K.: An insight into the breathing mechanism of a crack in a rotating shaft. J. Sound Vib. **318**, 279–295 (2008)
20. Papadopoulos, C.A.: The strain energy release approach for modeling cracks in rotors: A state of the art review. Mech. Syst. Signal Process. **22**, 763–789 (2008)
21. Saridakis, K.M., Chasalevris, A.C., Papadopoulos, C.A., Dentsoras, A.J.: Applying neural networks, genetic algorithms and fuzzy logic for the identification of cracks in shafts by using coupled response measurements. Comput. Struct. **86**, 1318–1338 (2008)
22. Lazan, B.J.: Damping of Materials and Membranes in Structural Mechanics. Pergamon Press, Oxford (1968)
23. Paipetis, S. A.: On the motion of a linear viscoelastic oscillator, National Technical University of Athens, Scientific Yearbook, (1971)
24. Bovsunovsky, A.P.: Experimental and analytical study of the damping capacity of multilayer steels. Strength Mater. **27**(9), 516–524 (1995)
25. Panteliou, S.D., Chondros, T.G., Argyrakis, V.C., Dimarogonas, A.D.: Damping factor as an indicator of crack severity. J. Sound Vib. **241**(2), 235–245 (2001)
26. Panteliou, S., Dimarogonas, A.D.: Heat propagation on a shaft due to torsional transient vibration. Int. Commun. Heat Mass Transfer **10**(2), 111–122 (1983)
27. Panteliou, S., Aspragathos, N., Dimarogonas, A. D.: Thermal effects of rotating shafts due to electrical transients causing plastic deformation. Ingenieur Archiv. **53**, 173–179, (1983)
28. Genta, G., Tonoli, A.: A harmonic finite element for the analysis of flexural, torsional and axial rotordynamic behaviour of discs. J. Sound Vib. **196**(1), 19–43 (1996)
29. Wu, J.J.: Torsional vibration analyses of a damped shafting system using tapered shaft element. J. Sound Vib. **306**(3–5), 946–954 (2007)
30. Choi, S.T., Man, S.Y.: Dynamic analysis of geared rotor-bearing systems by the transfer matrix method. J. Mech. Des. Trans. ASME **123**(4), 562–568 (2007)
31. Xia, Z., Zheng, T., Zhang, W.: Nonlinear modeling and dynamic analysis of the rotor-bearing system. Nonlinear Dyn. **57**(4), 559–577 (2009)
32. Avramov, K. V., Borysiuk, O. V.: Nonlinear dynamics of one disk asymmetrical rotor supported by two. journal bearings. Nonlinear Dyn. **67**(2), 1201–1219, (2012)
33. Lu Y. J., Ji, L. F., Zhang, Y. F., Wu, Y., Liu, Y. Y., Yu, L.: Dynamic behaviours of the rotor non-linear system with fixed-tilting-pad journal bearings support. In: Proceedings of the Institution of Mechanical Engineers, Part J: J. Eng. Tribol. **224**(10), 1037–1047, (2010)
34. Ho, J.C., Yeo, H., Ormiston, R.A.: Investigation of rotor blade structural dynamics and modeling based on measured airloads. J. Aircr. **45**(5), 1631–1642 (2007)
35. Fusato, D., Guglieri, G., Celi, R.: Flight dynamics of an articulated rotor helicopter with an external slung load. J. Am. Helicopter Soc. **46**(1), 3–13 (2001)
36. Paipetis, S.A., Theocharis, P.S., Marchese, A.: Dynamic properties of plastically pretorsion mild steel. Materialpruefung **20**(10), 378–380 (1978)
37. Paipetis, S.A.: Dynamic properties of plastically prestressed aluminium. Materialpruefung **21**(6), 198–201 (1979)
38. Sinha, S.K.: Dynamic characteristics of a flexible bladed-rotor with Coulomb damping due to tip-rub. J. Sound Vib. **273**(4–5), 875–919 (2004)
39. Dimarogonas, A.D., Massouros, G.: Torsional vibration of a shaft with a circumferential crack. Eng. Fracture Mech. **15**, 439–444 (1981)
40. Samarin, V. K.: Possibilities of inspecting the damage of materials on the basis of the change in the frequency of natural oscillations of samples. Problemy Prochnosti **6**, 61–64, (1978)
41. Dimarogonas, A. D., Papadopoulos, A. C.: Vibration of cracked shafts in bending. J. Sound Vib. **91**(4), 583–593, (1983)
42. Papadopoulos, C. A., Dimarogonas, A. D.: Coupled longitudinal and bending vibrations of a rotating shaft with an open crack. J. Sound Vib. **117**(1), 81–93, (1987)

43. Papadopoulos, C. A., Dimarogonas, A. D.: Coupling of bending and torsional vibrations of a cracked timoshenko shaft. Ingenieur Archive (Replaced by Archive of Applied Mechanics), **57**(4), 257–66, (1987)
44. Papadopoulos, C. A., Dimarogonas, A. D.: Stability of cracked rotors in the coupled vibration mode. J. Vib. Acoust. Stress Rel. Des. **110**(3), 356–59, (1988)
45. Andrieux, S., Vare, C.: A 3D cracked beam model with unilateral contact. Application to rotors. Eur. J. Mech. A/Solids **21**, 793–810 (2002)
46. Papadopoulos, C. A.: The strain energy release approach for modelling cracks in rotors: A state of the art review, published in the special issue of mechanical systems and signal processing for crack effects in rotordynamics. **22**(4), 763–89, (2008)
47. Tong, K.N.: Theory of Mechanical Vibration. Wiley, New York (1963)
48. Meirovitch, L.: Elements of Vibration Analysis. McGraw-Hill, Tokyo (1975)
49. Bishop, R.E.D., Johnson, D.C.: The Mechanics of Vibration. Cambridge University Press, Cambridge (1979)
50. Bishop, R, E. D., Gladwell, G. M. L., Michaelson, S.: The Matrix Analysis of Vibration, Cambridge University Press, Cambridge, (1979)
51. Young, C.Y.: Random Vibration of Structures. Wiley, New York (1986)
52. Norton, M.P.: Fundamentals of Noise and Vibration Analysis for Engineers. Cambridge University Press, Cambridge (1989)
53. Centa, C.: Vibration of Structures and Machines. Springer, New York (1993)
54. Traupel, W: Thermische turbomaschinen, Springer, Berlin, (1968)
55. Fadeev, D.K., Fadeeva, V.N.: Computational Methods of Linear Algebra. Freeman and Co., San Francisco (1963)
56. Dunkerley, S.: On the whirling and vibration of shafts. Phil. Trans. Roy. Soc. A **185**, Part I, 279–360, (1894)
57. Paipetis, S.A.: A Dunkerley procedure for higher modes. Acustica **49**(1), 73–76 (1981)
58. Hidalgo, J. I., Dhingra, A. K.: High-speed balancing of rotors with overhangs: When is overhang likely to cause problems? J. Test. Eval. **34**(3), 218–223, (2006)
59. Timoshenko, S., Woinowski-Krieger, S.: Theory of Plates and Shells. McGraw-Hill Book Co., Inc., New York (1954)
60. Jacobsen, L.S., Ayre, R.S.: Engineering Vibrations. McGraw-Hill Book Co., Inc., New York (1958)
61. Demidovich, B.P., Maron, I.A.: Computational Mathematics. Mir Publishers, Moscow (1976)
62. Scarborough, J.B.: Numerical Mathematical Analysis. Johns Hopkins Press, Baltimore (1966)
63. Geipel, G.: Rechnerisches Verfahren zur Ermittlung der biegekritischen Grund-Schwingungen zweifach gelagerter Wellen, Konstruktion, **13**(5), 199–201, (1961)
64. Penny, J.E., Reed, J.R.: An integral equation approach to the fundamental frequency of vibrating beams. J. Sound Vibr. **19**(4), 393–400 (1971)
65. Rutenberg, A.: A lower bound for Dunkerley's formula in continuous elastic systems. J. Sound Vibr. **45**(2), 249–252 (1976)
66. Meirovitch, L.: Analytical Methods in Vibrations. Mc Millan Co., New York (1967)
67. Kanwal, R.P.: Linear Integral Equations. Academic Press, New York (1971)
68. Brown, F.T.: Engineering System Dynamics, 2nd edn. CRC, Taylor and Francis, London (2007)
69. Stoisser, C.M., Audebert, S.: A comprehensive theoretical, numerical and experimental approach for crack detection in power plant rotating machinery. Mech. Syst. Signal Process. **22**, 818–844 (2008)
70. Mukherjee, A., Rastogi, V., Dasgupta, A.: Extension of Lagrangian-Hamiltonian mechanics for continuous systems investigation of dynamics of a one-dimensional internally damped rotor driven through a dissipative coupling. Nonlinear Dyn. **58**(1–2), 107–127 (2009)

Chapter 2
Variable Elasticity Effects in Rotating Machinery

Abstract The effects of variable elasticity in rotating machinery occur with a large variety of mechanical, electrical, etc., systems, in the present case, geometrical and/or mechanical problems. Parameters affecting elastic behavior do not remain constant, but vary as functions of time. Systems with variable elasticity are governed by differential equations with periodic coefficients of the Mathieu-Hill type and exhibit important stability problems. In this chapter, analytical tools for the treatment of this kind of equations are given, including the classical Floquet theory, a matrix method of solution, solution by transition into an equivalent integral equation and the BWK procedure. The present analysis is useful for the solution of actual rotor problems, as, for example, in case of a transversely cracked rotor subjected to reciprocating axial forces. Axial forces can be used to control large-amplitude flexural vibrations. Flexural vibration problems can be encountered under similar formulation.

2.1 Introduction

Variable elasticity effects occur with systems in which the parameters affecting elastic behavior do not remain constant, but vary as functions of time. Equations of motion pertaining to such systems remain linear, but they possess time-dependent coefficients. Similar phenomena appear in all fields of physics and are generally associated with wave propagation in periodic media, a problem encountered as early as 1887 by Lord Rayleigh, and subsequently by other prominent physicists [1]. It was recognized that such phenomena are described by means of Hill and Mathieu differential equations. A detailed and comprehensive review on the work on waves in periodic structures was given by Brillouin [2].

A. D. Dimarogonas et al., *Analytical Methods in Rotor Dynamics*,
Mechanisms and Machine Science 9, DOI: 10.1007/978-94-007-5905-3_2,

Omitting a large number of non-mechanical phenomena mentioned in the above references, it is interesting to concentrate attention on the following vibrating mechanical systems [3–10]:

1. A rotating shaft with non-circular cross-section, i.e. non-uniform flexibility.
2. A mass suspended from a taut string with time-varying tension.
3. A pendulum with time-varying length.
4. An inverted pendulum attached to a vertically vibrating hinge.
5. The side-rod system of electric locomotives, exhibiting torsional vibrations.
6. The rotating parts of small motors, which are subject to the time-varying action of electromagnetic fields.
7. A rotating flywheel carrying radially moving masses.
8. A rotating flywheel eccentrically connected to reciprocating masses.

The list is by no means complete, but the examples are characteristic of the problems encountered.

If one of these structures is constrained to move at constant circular frequency, the respective parameters are periodic functions and under proper conditions large vibration amplitudes may develop. The reason is that, within each cycle, positive work is introduced into the system, which results in a gradually increasing amplitude, i.e. instability. This effect can be caused, for example, by a small accidental force producing an initial velocity and being enhanced, under certain conditions, by the action of gravity or static forces [3]. In Fig. 2.1, the response of a simple oscillator with a different spring constant in tension and in compression is presented. The oscillator is assumed to perform harmonic oscillations at constant circular frequency ω.

By using the analysis given in Sect. 2.2, the total energy stored in the system during the first and second half-cycles can be evaluated. This may be positive, zero or negative. The second and third cases lead to stable situations; however, the first one leads to increasing vibration amplitudes, i.e. to instability.

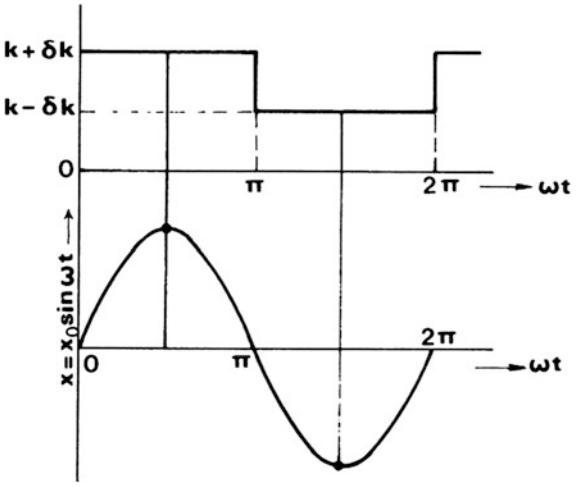

Fig. 2.1 Response of a simple oscillator with a different spring constant in tension and in compression

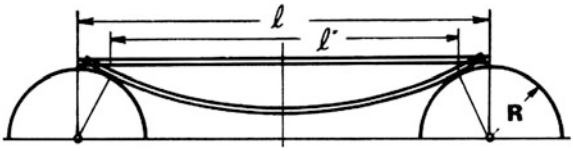

Fig. 2.2 A beam on circular supports of finite radius exhibiting periodic length variation during flexural vibration

Consider now a rotating shaft, or the more general case of a beam executing flexural vibrations. The following cases of variable elasticity can be distinguished.

2.1.1 Variable Length l

A beam resting on circular supports with finite radius undergoes periodic changes of length during flexural vibrations. This case is obviously not related to rotating machinery; however, it is an interesting example of periodic changes in elasticity (Fig. 2.2).

2.1.2 Variable Stiffness EJ

The flexural stiffness EJ may vary periodically if either elastic modulus E of the structure material or the second area moment J of the respective cross-sections or both vary accordingly. Rotor-to-stator rub often occurs in rotating machinery. Methods for detecting the rub-impact effect were developed based on the variable stiffness issue for the rotor system [11, 12]. Therefore, one can distinguish the following particular cases:

Variable elastic modulus E: Many materials, especially polymers and their composites, exhibit different elastic modulus in tension E_τ and in compression E_c [12–15]. A beam performing longitudinal vibration would exhibit a variable stiffness of ripple form, as shown in Fig. 2.1. With flexural vibration, in the presence of an axial load, a respectively oscillating neutral axis would result, giving rise to periodically varying flexural stiffness.

Variable second area moment J: The second area moment J depends on the particular form of the respective cross-sections. With circular cross-sections, J remains constant in all directions and the flexural stiffness is not affected. However, with non-circular cross-sections, for example rectangular, if the beam rotates while the direction of the load or the couple vector remains constant, a periodically varying J results. With constant rotating speed, this variation is sinusoidal. Non-circular cross-sections are produced by keyways, etc., special formations of rotors, and also by longitudinal or transverse cracks. The latter may have a considerable effect and, alternatively, their presence can be detected by the dynamic behavior of the vibrating element. A quasi-sinusoidal experimental curve

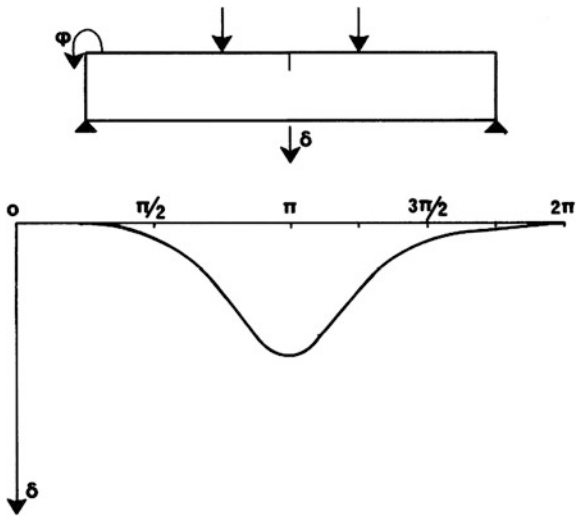

Fig. 2.3 Variation of flexural stiffness of a transversely cracked rotor

represents the periodic variation of the flexural stiffness [16] (Fig. 2.3). The simplest example of a system with periodically varying stiffness is a straight rotating shaft, whose cross-section has different principle moments of inertia. A classical example of systems with periodically varying stiffness was the drive system of an electric locomotive incorporating a coupling link for force transmission, applied during the first years of electric locomotion.

2.1.3 Variable Mass or Moment of Inertia

Such examples have already been mentioned. The case of a reciprocating engine is a very common one, by which the inertia of the piston mechanism varies periodically [17–19]. A heavy flywheel is necessary in order to maintain uniform rotating speed, a device important for all systems exhibiting variable elasticity.

In this chapter the various problems of such systems are discussed in detail, along with the respective mathematical techniques used for their treatment.

2.2 The Problem of Stability

Consider a simple oscillator, i.e. a mass m suspended from a massless spring, whose constant, however, assumes the value $k(1 + \delta)$ for tension and the value $k(1 - \delta)$ for compression. Moreover, assume that at $t = 0$, its deflection is $x = 0$ and its velocity $\dot{x} = v_0$. The *free vibration* of the system is governed by the equations

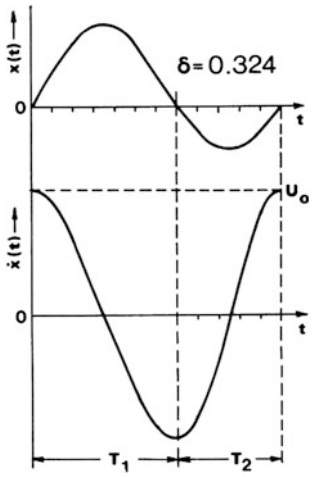

Fig. 2.4 Variation of displacement and velocity with time of a simple oscillator with a different spring constant in tension and compression

$$\left.\begin{aligned} \ddot{x} + \omega_0^2(1+\delta)x = 0 \quad & \text{for } x > 0 \ (\textit{tension}) \\ \ddot{x} + \omega_0^2(1-\delta)x = 0 \quad & \text{for } x < 0 \ (\textit{compression}) \end{aligned}\right\} \tag{2.1}$$

where $\omega_0^2 = k/m$. During the first half-cycle, the natural frequency of the system is

$$\omega_1 = \omega_0(1+\delta)^{1/2} \tag{2.2a}$$

while during the second half-cycle

$$\omega_2 = \omega_0(1-\delta)^{1/2}. \tag{2.2b}$$

The period T of a complete cycle is

$$T = T_1 + T_2 = \frac{\pi}{\omega_1} + \frac{\pi}{\omega_2} = \frac{2\pi}{\omega} \tag{2.3}$$

where ω is the circular frequency of the free vibration, which, however, is not uniform over the two half-cycles. From Eq. (2.3) we obtain

$$\frac{1}{\omega} = \frac{1}{\omega_1} + \frac{1}{\omega_2} \tag{2.4a}$$

or

$$\omega = 0.5\sqrt{\frac{k}{m}}\frac{\left(1-\delta^2\right)^{1/2}}{\left(1+\delta^2\right)^{1/2} + s\left(1-\delta^2\right)^{1/2}} \tag{2.4b}$$

In Fig. 2.4, the forms of the displacement function $x(t)$ and the velocity function $\dot{x}(t)$ are presented for $\delta = 0.324$. Amplitudes and velocities remain constant, as the system is conservative. However, the oscillation is clearly not simple harmonic, and can be analyzed as a Fourier series:

$$x(t) = a_0 + \sum_{k=1}^{\infty} (a_k \sin\, k\omega t\, + b_k \cos k\omega t) \tag{2.5}$$

Considering the odd (sine) functions, we obtain

$$a_k = \frac{2}{T}\int_0^T x(t) \sin k\omega t\, dt \tag{2.6}$$

where

$$x(t) = \left\{ \begin{array}{l} x_1 \sin \omega_1 t\ \ (0 < t < T_1) \\ x_2 \sin \omega_2 t\ \ (T_1 < t < T) \end{array} \right\} \tag{2.7}$$

As evident from Eq. (2.5), the system possesses in fact an infinite number of eigen frequencies ω, 2ω, 3ω …, multiples of the circular frequency ω of a full cycle, as defined in Eq. (2.4a).

Now, if the system is forced to oscillate at uniform circular frequency ω, stability problems may arise. The respective analysis is due to van der Pol and Strutt [3, 4] and is based on the solution of Eq. (2.1) under the proper boundary conditions. Namely, Eq. (2.1) possess the following general solutions:

$$\left. \begin{array}{l} x_1 = A_1 \sin \omega_1 t + A_2 \cos \omega_1 t \\ x_2 = B_1 \sin \omega_2 t + B_2 \cos \omega_2 t \end{array} \right\} \tag{2.8}$$

Now, considering that at the end of the first half-cycle ($t = \pi/\omega$), displacements and velocities for both solutions [Eq. (2.8)] must be equal and, moreover, that at the end of the first complete cycle ($t = 2\pi/\omega$) displacements and velocities must be λ times as large as at $t = 0$, four homogeneous linear equations result, containing the integration constants as unknowns. The condition for these equations to give solutions other than zero for the latter leads to the quadratic

$$\lambda^2 - 2q\lambda + 1 = 0 \tag{2.9}$$

giving for λ the values

$$\lambda = q \pm \sqrt{q^2 - 1} \tag{2.10}$$

where

$$q = \cos\frac{\pi\omega_1}{\omega}\cos\frac{\pi\omega_2}{\omega} - \frac{\omega_1^2 + \omega_2^2}{2\omega_1\omega_2}\sin\frac{\pi\omega_1}{\omega}\sin\frac{\pi\omega_2}{\omega} \tag{2.11a}$$

or

$$\begin{aligned} q = {} & \cos\left[\pi(1+\delta)^{\frac{1}{2}}\frac{\omega_0}{\omega}\right]\cos\left[\pi(1-\delta)^{1/2}\frac{\omega_0}{\omega}\right] - \frac{1}{2\left(1-\delta^2\right)^{\frac{1}{2}}} \\ & \times \sin\left[\pi(1+\delta)^{\frac{1}{2}}\frac{\omega_0}{\omega}\right]\sin\left[\pi(1-\delta)^{\frac{1}{2}}\frac{\omega_0}{\omega}\right] \end{aligned} \tag{2.11b}$$

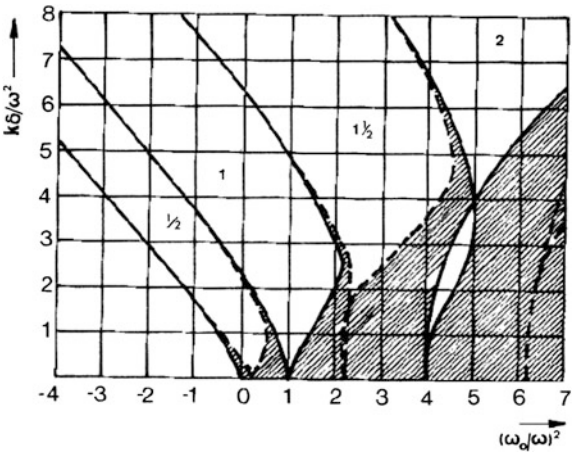

Fig. 2.5 Regions of stability and instability for a simple oscillator with a different spring constant in tension and in compression. (According to van der Pol and Strutt [3, 4])

Now, the system is stable for $q = \pm 1$, in which case $\lambda = q$, and for $|q| < 1$, when λ is complex, but its modulus equals one. Alternatively, instability occurs with $|q| > 1$. In this case, if q is positive, displacements and velocities at the end of each consecutive cycle of the spring fluctuation will increase, retaining the same sign. This means that the system vibrates at the same frequency Ω of spring fluctuation or at a multiple of it: 2Ω, 3Ω..... If q is negative, displacements and velocities will also increase at the end of each consecutive cycle of the spring fluctuation, but will have alternating sign. This means that the system vibrates at frequencies $\Omega/2$, $\Omega/3$.....

As q is a function of δ and the ratio ω_0/ω, according to Eq. (2.11b) the above conditions of stability can be plotted in the classical diagram of Fig. 2.5. The shaded regions in Fig. 2.5 correspond to stable situations ($-1 < q < 1$), blank regions to unstable ones $|q| > 1$ and full and dotted lines to $q = +1$ and $q = -1$ respectively. Details of this representation can be found in the relevant literature [2–4]. In the presence of damping, the motion is again not simple harmonic, even for the free vibration, and a solution for x must be sought in the form of Fourier series [3].

2.3 The Mathieu-Hill Equation

The general form of an equation of motion, pertaining to a system with variable elasticity, is

$$\frac{d^2x}{dt^2} + f(t)x = 0 \tag{2.12}$$

where $f(t)$ is a single-valued periodic function of fundamental period T, which can be represented by a general Fourier series of the form

$$f(t) = A_0 + \sum_{k=1}^{\infty} (A_k \cos k\omega t + B_k \sin k\omega t) \tag{2.13}$$

where $\omega = 2\pi/T$. Equation (2.12), if the function $f(t)$ has the general form (2.13), is known as *Hill's equation*. If the Fourier series (2.13) can degenerate in the simple form

$$f(t) = A_0 + A_1 \cos \omega t \tag{2.14}$$

then Eq. (2.12) is known as *Mathieu's equation*. This equation can be solved by using the tabulated Mathieu functions [16].

An important property of a system expressed by the Mathieu equation is that instabilities are exhibited for certain ranges of the parameters A_0 and A_1, i.e. if the system is displaced from the equilibrium, $x = 0$, a motion of increasing amplitude follows.

The classical method for the solution of Hill's equation, available in most textbooks [20], is as follows: Following the form (2.13) of the function $f(t)$, one can look for a similar expansion for the unknown periodic function $x(t)$:

$$x(t) = a_0 + \sum_{k=1}^{\infty} (a_k \cos k\omega t + b_k \sin\ k\omega t) \tag{2.15}$$

Equation (2.12) then leads to an infinite system of simultaneous linear homogeneous equations for the unknown coefficients a_k and b_k. In order to obtain a non-trivial solution, the corresponding infinite determinant must be zero. However, if the series of the coefficients A_k and B_k in Eq. (2.13) are absolutely converging, the latter can be easily evaluated or, alternatively, higher terms can be neglected, and the problem can be solved, by long computations in any case. The method is not very practical; however, it appears to be the only one operating with functions $f(t)$, for which no analytical expression is available, as occurs with experimentally determined forms.

Apart from Hill's method of infinite determinants, further methods have been developed for the treatment of coupled Mathieu equations [17], based on the expansion of the converging infinite determinant, which also provides a criterion for stability of the solution. Moreover, a stability criterion for the general Hill equation can be developed in a similar manner [21].

2.4 The Classical Floquet Theory

Equations of the Mathieu-Hill type can be solved by means of the Floquet theory [2, 22–25]. This theory basically deals with equations of the form

$$\dot{y} = \mathbf{A}(t)y \tag{2.16}$$

where $y = (y_1, y_2,\ldots, y_n)$ and $\mathbf{A}(t) = [a_{ij}(t)]$ is a continuous $n \times n$ matrix defined in the range $-\infty < t < \infty$. $\mathbf{A}(t)$ satisfies the relation

$$\mathbf{A}(t+T) = \mathbf{A}(t)$$

where the period T is a non-zero quantity. The complete Floquet theory, leading to the general form of solution of Eq. (2.16) can be found in the literature [24, 25]. A basic property of the solution, however, is described by the Floquet theorem stating that

For the system expressed by the matrix Eq. (2.16), *there exists a non-zero constant λ, real or complex, and at least one non-trivial solution y(t) having the property that*

$$y(t+T) = \lambda y(t)$$

The various values $\lambda_1, \lambda_2,\ldots, \lambda_m$ of the parameter λ are the distinct characteristic roots of a constant $n \times n$ matrix $\mathbf{C}$ defined by the relation

$$\mathbf{\Phi}(t+T) = \mathbf{\Phi}(t)c$$

where $\mathbf{\Phi}(t) = [\varphi_{ij}(t)]$ is a fundamental system of solutions of Eq. (2.16). The above values are called *characteristic factors or multipliers* of Eq. (2.16). The following corollary is valid:

The system (2.16) *has periodic solution of period T, if and only if there is at least one characteristic factor equal to one* [14].

The quantities $r_1, r_2,\ldots, r_m$ defined by the relations

$$\lambda_j = \exp(r_j T) \quad j = 1, 2, \ldots, m$$

are called the characteristic exponents of the system (2.16) and, according to the following theorem

There are at least m solutions of the system (2.16) *having the form*

$$x_i(t) = p_i(t)\exp(r_i t) \quad i = 1, 2, \ldots, m$$

where the functions $p_i(t)$ *are periodic with period* T.

Now, consider Hill's equation:

$$\ddot{x} + f(t)x = 0 \tag{2.12}$$

where $f(t)$ is real–valued, continuous and periodic with period T, assumed traditionally as equal to π. Let a fundamental system of solutions be $x_1(t)$ and $x_2(t)$, and

$$x_1(0) = 1 \quad \dot{x}_1(0) = 0 \quad x_2(0) = 0 \quad \dot{x}_2(0) = 1$$

whose Wronskian is equal to one. That is

$$\Phi(t) = \begin{bmatrix} x_1(t) & x_2(t) \\ \dot{x}_1(t) & \dot{x}_2(t) \end{bmatrix}$$

and

$$\mathbf{A}(t) = \begin{bmatrix} 0 & 1 \\ -f(t) & 0 \end{bmatrix}$$

when the matrix $\mathbf{C}$ is equal to

$$\mathbf{C} = \begin{bmatrix} x_1(\pi) & x_2(\pi) \\ \dot{x}_1(\pi) & \dot{x}_2(\pi) \end{bmatrix}$$

whose characteristic roots λ_1, λ_2 are roots of the equation

$$(\lambda \mathbf{I} - \mathbf{C}) = \lambda^2 - [x_1(\pi) + \dot{x}(\pi)]\lambda + 1 = 0$$

where $\lambda_1 \lambda_2 = 1$ and $\mathrm{r}_1 + \mathrm{r}_2 \equiv 0$. Hence a number r can be defined satisfying the conditions

$$\exp(ir\pi) = \lambda_1$$

and

$$\exp(-ir\pi) = \lambda_2$$

The following cases are distinguished:

1. $\lambda_1 \neq \lambda_2$, leading to two linearly independent solutions:

$$\varphi_1(t) = \exp(irt) f_1(t)$$

$$\varphi_2(t) = \exp(-irt) f_2(t)$$

   where $f_1(t)$, $f_2(t)$ are periodic with period π.
2. $\lambda_1 = \lambda_2$, leading to one non-trivial periodic solution with period π (with $\lambda_1 - \lambda_2 = 1$) or 2π (with $\lambda_1 = \lambda_2 = -1$).

In order to apply the above results, information about the matrix $\mathbf{C}$ is required, which can be derived from the conditions imposed on $\mathbf{A}(t)$, guaranteeing the existence of stable, unstable or oscillatory solutions.

Finally, for a non-homogeneous system

$$\dot{x} = A(t)x + B(t) \tag{2.17}$$

where $\mathbf{A}(t)$ and $\mathbf{B}(t)$ are periodic matrices with period T, the following theorem is valid:

For the system (2.17), *a period solution with period T exists for every* $\mathbf{B}(t)$, *if and only if the corresponding homogeneous system has no non-trivial solution of period T.*

2.5 Matrix Solution of Hill's Equation

Consider Eq. (2.12) again and two linearly independent solutions $x_1(t)$ and $x_2(t)$ in the interval $0 \leq t \leq T$. The general solution for displacement and velocity is given by the equations

$$\left.\begin{aligned} x(t) &= A_1 x_1(t) + A_2 x_2(t) \\ \dot{x}(t) &= A_1 x_1(t) + A_2 \dot{x}_2(t) \end{aligned}\right\} \tag{2.18a}$$

or in matrix form

$$\begin{bmatrix} x(t) \\ \dot{x}(t) \end{bmatrix} = \begin{bmatrix} x_1(t) & x_2(t) \\ \dot{x}_1(t) & \dot{x}_2(t) \end{bmatrix} \begin{bmatrix} A_1 \\ A_2 \end{bmatrix} \tag{2.18b}$$

The Wronskian of the two solutions $x_1(t)$ and $x_2(t)$, given by the following equation

$$W = \begin{vmatrix} x_1(t) & x_2(t) \\ \dot{x}_1(t) & \dot{x}_2(t) \end{vmatrix} = x_1(t)\dot{x}_2(t) - \dot{x}_1(t)x_2(t) \tag{2.19}$$

is constant in the interval $0 < t < T$ [21] and, since $x_1(t)$ and $x_2(t)$ are linearly independent, we have also $W \neq 0$; hence the 2×2 matrix in Eq. (2.18b) is non-singular and has the following inverse:

$$\begin{bmatrix} x_1(t) & x_2(t) \\ \dot{x}_1(t) & \dot{x}_2(t) \end{bmatrix}^{-1} = \frac{1}{W} \begin{bmatrix} \dot{x}_2(t) & -x_2(t) \\ -\dot{x}_1(t) & x_1(t) \end{bmatrix} \tag{2.20}$$

If the initial conditions are given:

$$\begin{bmatrix} x(t) \\ \dot{x}(t) \end{bmatrix}_{t=0} = \begin{bmatrix} x_0 \\ \dot{x}_0 \end{bmatrix} \tag{2.21}$$

From Eq. (2.18b) we derive

$$\begin{bmatrix} x_0 \\ \dot{x}_0 \end{bmatrix} = \begin{bmatrix} x_1(0) & x_2(0) \\ \dot{x}_1(0) & \dot{x}_2(0) \end{bmatrix} \begin{bmatrix} A_1 \\ A_2 \end{bmatrix} \tag{2.22}$$

or

$$\begin{bmatrix} A_1 \\ A_2 \end{bmatrix} = \begin{bmatrix} x_1(0) & x_2(0) \\ \dot{x}_1(0) & \dot{x}_2(0) \end{bmatrix}^{-1} \begin{bmatrix} x_0 \\ \dot{x}_0 \end{bmatrix} \tag{2.23}$$

which determines the column of arbitrary constants, and, consequently, the final solution assumes the form

$$\begin{bmatrix} x(t) \\ \dot{x}(t) \end{bmatrix} = \frac{1}{W} \begin{bmatrix} x_1(t) & x_2(t) \\ \dot{x}_1(t) & \dot{x}_2(t) \end{bmatrix} \begin{bmatrix} \dot{x}_2(0) & -x_2(0) \\ -\dot{x}_1(0) & x_1(0) \end{bmatrix} \begin{bmatrix} x_0 \\ \dot{x}_0 \end{bmatrix} \tag{2.24}$$

At the end of the first period, i.e. at $t = T$, Eq. (2.24) becomes

$$\begin{bmatrix} x(t) \\ \dot{x}(t) \end{bmatrix}_{t=T} = \mathbf{M} \begin{bmatrix} x_0 \\ \dot{x}_0 \end{bmatrix} \tag{2.25}$$

where

$$\mathbf{M} = \frac{1}{w} \begin{bmatrix} x_1(T) & x_2(T) \\ \dot{x}_1(T) & \dot{x}_2(Tt) \end{bmatrix} \begin{bmatrix} \dot{x}_2(0) & -x_2(0) \\ -\dot{x}_1(0) & x_1(0) \end{bmatrix} \tag{2.26}$$

It can be easily shown that, at the end of the nth period of $f(t)$, i.e. at $t = nT$, we have

$$\begin{bmatrix} x(t) \\ \dot{x}(t) \end{bmatrix}_{t=nT} = \mathbf{M}^n \begin{bmatrix} x_0 \\ \dot{x}_0 \end{bmatrix} \tag{2.27}$$

which provides the complete solution of Hill's equation in terms of the initial conditions, and two linearly independent solutions of Hill's equation in the fundamental interval $0 \leq t \leq T$. The nth power of the matrix $\mathbf{M}$ can be computed by means of Sylvester's theorem [26, 27]. Solutions have been given for various forms of the function $f(t)$, such as rectangular ripple, sum of step functions, exponential function, sawtooth variation, etc. [26].

2.6 Solution by Transition into an Equivalent Integral Equation

Equation (2.12), with the function $f(t)$ developable in a Maclaurin series, can be solved by means of a transition to an equivalent Volterra integral equation of the second type. Again, by using the notation of Eq. (2.21), we obtain the following form [24]:

$$x(t) = x_0\, t + x - \int_0^t (t - \tau) f(\tau) x(\tau) d\tau \tag{2.28}$$

The classical method of solution is by means of successive approxi–mations. Problems of a practical nature may appear with the determination of the iterated kernels, depending on the function f(t). Particular examples, such as for $f(t) = t^{\mathrm{n}}$ can be found in the literature [28].

2.7 The Bwk Procedure

The BWK[1] procedure, discovered while dealing with problems of wave mechanics [23, 29, 37] is suitable for the solution of Eq. (2.12) in the following manner: Let a function be considered, such that

$$u = g^{-1/2} \exp(-iS)\, S = \int_a^t G dx \tag{2.29}$$

where $G(t)$ is any given function of t. The following equation can then be derived:

$$\ddot{u} + u\left[G^2 - \frac{3}{4}\left(\frac{\dot{G}}{G}\right)^2 + \frac{1}{2}\frac{\ddot{G}}{G}\right] = 0 \tag{2.30}$$

which, when compared with Eq. (2.12), leads to the condition

$$f = G^2 - \frac{3}{4}\left(\frac{\dot{G}}{G}\right)^2 + \frac{1}{2}\frac{\ddot{G}}{G} \tag{2.31}$$

If Eq. (2.31) can be solved to a certain approximation, then the function u in Eq. (2.29) represents an approximate solution of Eq. (2.12). Moreover, in case that $\dot{G}$ and $\ddot{G}$ can be omitted in Eq. (2.31), an acceptable approximation can be obtained by taking

$$G = G_0 = [f(t)]^{1/2} \tag{2.32}$$

which is a zero–order approximation to the BWK procedure. As a particular case, with

$$G = A/(a+t)^2 \tag{2.33}$$

terms in $\dot{G}$, $\ddot{G}$ cancel out in Eq. (2.30), and a rigorous solution of Eq. (2.12) results [23].

An accurate approximation to G can be determined by means of a series

$$G = G_0 + G_1 + G_2 + \ldots \tag{2.34}$$

under the assumption that

$$\left|\dot{G}_0/G^2\right| < \varepsilon \qquad \left|\ddot{G}/G^3\right| < \varepsilon^2 \quad \varepsilon^2 \ll 1$$

[1] Named after three authors: L. Brillouin (*J. Phys.*, **7**, 1926, 353); G. Wentzel (*Z. Phys.*, *38*, 1926, 518); and E.C. Kemble (The Fundamental Principles of Quantum Mechanics, McGraw-Hill, New York, 1937).

when the successive terms would be of the order ε^2, ε^4….. By substitution in Eq. (2.30) we obtain

$$\left.\begin{aligned} G_0 &= f^{1/2} \\ 2G_0G_1 &= \tfrac{3}{4}\left(\frac{\dot{G}_0}{G_0}\right)^2 - \tfrac{1}{2}\frac{\ddot{G}_0}{G_0} \\ 2G_0G_1 + G_1^2 &= \tfrac{3}{2}\left(\frac{\dot{G}_0}{G_0}\right)^2\left(\frac{\dot{G}_1}{G_0} - \frac{\dot{G}_1}{G_0}\right) - \tfrac{1}{2}\frac{\ddot{G}_0}{G_0}\left(\frac{\ddot{G}_1}{G_0} - \frac{G_1}{G_0}\right) \end{aligned}\right\} \tag{2.35}$$

and the expansion of G would yield a first solution from Eq. (2.29). A second independent solution υ can be found either with $f > 0$, G real and positive and S real, or with $f < 0$, G and S purely imaginary and $i^{1/2}u$ real. The first case corresponds to propagating waves, the second to attenuated waves without propagation. A detailed analysis can be found in the literature [23, 37].

2.8 Vibrations of Different-Modulus Media

As an example, consider the longitudinal vibrations of a bar with uniform cross-section made of a material with a different modulus in tension and in compression [37]. The one-dimensional equation of motion is

$$\frac{\partial^2 u}{\partial t^2} = a\,\frac{\partial^2 u}{\partial x^2} \tag{2.36}$$

where $\alpha = (E/\rho)^{1/2}$, E is Young's modulus and ρ is density. Moreover

$$\alpha = \alpha_T = \left(\frac{E_T}{\rho}\right)^{\frac{1}{2}} \qquad for\,\sigma \;>\; 0\; or\; \frac{\partial u}{\partial x} \;>\; 0\,(tension)$$

$$\alpha = \alpha_C = \left(\frac{E_C}{\rho}\right)^{\frac{1}{2}} \qquad for\,\sigma \;<\; 0\; or\; \frac{\partial u}{\partial x} \;<\; 0\,(compression)$$

Assuming that the bar is initially tensioned by a force producing displacement u_0 at $x = l$ and released at $t = 0$, the initial and boundary conditions become:

$$\left.\begin{aligned} t = 0 \quad & \tfrac{\partial u}{\partial t} = 0 \quad u = \tfrac{u_0 x}{l} \\ x = 0 \quad & u = 0 \\ x = l \quad & \tfrac{\partial u}{\partial x} = 0 \end{aligned}\right\} \tag{2.37}$$

By applying separation of variables, the general solution of Eq. (2.36) can be given the following form:

$$u(x,t) = \sum_{n=1}^{x} x_n(x)T_n(t) \tag{2.38}$$

where

$$\left.\begin{aligned} X_n(x) &= A_n \sin(\omega_n x/a) + B_n \cos(\omega_n x/a) \\ T_n(t) &= C_n \sin \omega_n t + D_n \cos \omega_n t \end{aligned}\right\} \tag{2.39}$$

where the constants A_n, B_n, C_n, D_n, ω_n assume different values for tension and for compression (index c or T, respectively) and can be determined by the initial and boundary conditions. By virtue of the first boundary and the first initial condition [Eqs. (2.37), (2.38) assumes the form

$$u = \sum_{n=1}^{x} A_n sin \frac{(\omega_{Tn} x)}{a_T} \cos \omega_{Tn} t \tag{2.40}$$

and the second initial condition gives

$$\omega_{Tn} = (2n-1)\pi\alpha_T/2l \tag{2.41}$$

Moreover, we have

$$u_0 \frac{x}{l} = \sum_{n=1}^{x} A_n \sin \frac{(2n-1)}{2l} \pi x$$

leading to

$$A_n = \frac{8u_0(-1)^{n-1}}{\pi^2(2n-1)^2} \tag{2.42}$$

which gives Eq. (2.38) the following form:

$$u = \frac{8u_0}{\pi^2} \sum_{n=1}^{x} \frac{(-1)^{n-1}}{(2n-1)^2} \sin\left(\frac{2n-1}{2l}\right) \pi x \cos \frac{(2n-1)}{2l} \pi \alpha_T t \tag{2.43}$$

valid for the interval $0 \leq t \leq l/\alpha_T$, during which the bar is in the tensile state, i.e. during the first half-cycle. For the second half-cycle, when the bar enters the compressive state, the initial conditions are

$$t = \frac{1}{a_T} \qquad u = 0 \qquad \frac{\partial u}{\partial t} = -u_0 a_T / l$$

as Eq. (2.43) yields, with the same boundary conditions. From Eq. (2.36), with $a = a_c$, we have

$$u = \sum_{n=1}^{\infty} B_n \sin \frac{\omega_{cn} x}{a_c} \sin \omega_{cn} \left(t - \frac{l}{a_T}\right) \tag{2.44}$$

where

$$\omega_{cn} = \frac{2n-1}{2l}\pi\alpha_c \tag{2.45}$$

$$B_n = -\frac{8u_0 a_T}{\pi^2 \alpha_c (2n-1)^2} \tag{2.46}$$

leading eventually to the equation

$$u = \frac{8u_0}{\pi^2}\sum_{n=1}^{\infty}\frac{1}{(2n-1)^2}\sin\frac{2n-1}{2l}\pi x \sin\frac{2n-1}{2l}\pi\alpha_T\left(t - \frac{l}{a_T} - \frac{2l}{a_c}\right) \tag{2.47}$$

valid within the interval

$$\frac{l}{a_T} \le t \le \frac{l}{a_T} + \frac{2l}{a_c}$$

during which the bar is in the compressive state. The period of vibration for the bar particles is equal to

$$T = 2l\left(\frac{l}{a_T} + \frac{l}{a_c}\right)$$

or

$$T = 2l\sqrt{\rho}\frac{1+\sqrt{\frac{E_c}{E_T}}}{\sqrt{1+\frac{E_c}{E_T}}} \tag{2.48}$$

The present analysis is useful for the solution of actual rotor problems, as, for example, in the case of a transversely cracked rotor subjected to reciprocating axial forces. The problem of flexural vibrations can be encountered in a similar manner. Axial forces are very important in this case. The latter, even if not applied externally, develop during large deflections, and the problem assumes a rather complex form. An axial force can be used to control large-amplitude flexural vibrations [30, 31]. Other problems of instability including crack breathing, damping or parametric instabilities have to be treated with non-linear formulation [32–37].

References

1. Elachi, C.: Waves in active and passive periodic structures: a review. Proc. IEEE **64**, 1666–1698 (1976)
2. Brillouin, L.: Wave Propagation in Periodic Structures. Dover Publications, New York (1953)

3. Timoshenko, S.: Vibration Problems in Engineering. Van Nostrand Co., Inc., Princeton (1956)
4. Den hartog, J.P.: Mechanical Vibrations. McGraw-Hill Book Co., Inc., New York (1956)
5. Myklestad, N.O.: Fundamentals of Vibration Analysis. McGraw-Hill, New York (1956)
6. Meirovitch, L.: Analytical Methods in Vibrations. Macmillan, New York (1967)
7. Meirovitch, L.: Elements of Vibrations Analysis. McGraw-Hill, New York (1986)
8. Centa, G.: Vibration of Structures and Machines. Springer, New York (1993)
9. Kar, R., Vance, J.J.: Subsynchronous vibrations in rotating machinery—methodologies to identify potential instability. Proceedings of the ASME Turbo Expo, vol. 5, pp.719–725 (2007)
10. Muszynska, A.: Rotor-to-stationary element rub-related vibration phenomena in rotating machinery—literature survey. Shock Vib. Dig. **21**(3), 3–11 (1989)
11. Chu, F., LU, W.: Determination of the rubbing location in a multi-disk rotor system by means of dynamic stiffness identification. J. Sound Vib. **248**(2), 235–246 (2001)
12. Paolinelis, S., Paipetls, S.A., Theocaris, P.S.: Three-point bending at large deflections of beams with different moduli in tension and in compression. JTE **7**(3), 177–1781 (1979)
13. Lee, H., Neville, K.: Epoxy Resins. McGraw-Hill Book Co., Inc., New York (1967)
14. Thomson, W.J.: Vibration of slender bars with discontinuities in stiffness. J. Appl. Mech. **17**, 203–207 (1943)
15. You, L.H., Tang, Y.Y., Zhang, J.J., Zheng, C.Y.: Numerical analysis of elastic-plastic rotating disks with arbitrary variable thickness and density. Int. J. Solids. Structures **37**(52), 7809–7820 (2000)
16. Dimarogonas, A.D.: Vibration for Engineers, 2nd edn. Prentice Hall Upper Saddle River, New Jersey (1996)
17. Prentis, J.M.: Dynamics of Mechanical Systems. Ellis Horwood Ltd, Chichester (1980)
18. Eraslan, A.N., Argeso, H.: Limit angular velocities of variable thickness rotating disks. Int. J. Mech. Sci. **40**(1), 97–109 (2002)
19. Bhowmick, S., Misra, D., Nath Saha, K.: Approximate solution of limit angular speed for externally loaded rotating solid disk. Int. J. Mech. Sci. **50**(2), 163–174 (2008)
20. Whittaker, E.T., Watson, G.N.: Modern Analysis, 4th edn. Cambridge University Press, Cambridge (1927)
21. Lee, T.C.: A simplified stability criterion for the Hill equation and its applications, trans. ASME, Ser. E. J. Appl. Mech. **44**(3), 504–505 (1977)
22. Lee, T.C.: A study of coupled Mathieu equations by use of infinite determinants, trans. ASME, Ser. E, 43. J. Appl. Mech. **43**(2), 349–352 (1976)
23. Brillouin, L.: A practical method for solving Hill ‘s equation. Q. Appl. Math. **6**, 167–178 (1948)
24. Hochstadt, H.: Differential Equations. Dover Publications, New York (1964)
25. Sanchez, D.A.: Ordinary Differential Equations and Stability Theory. Dover Publications, New York (1979)
26. Pipes, L.A.: Matrix solution of equations of the Mathieu-Hill type. J. Appl. Phys. **24**(7), 902–910 (1953)
27. Kurosh, A.: Higher Algebra. Mir Publishers, Moscow (1975)
28. Chirkin, V.P.: On the solution of the differential equation $\ddot{x} + p(x)x = 0$. Prikladnaya Mekhanika. **2**(9), 119–123 (1966)
29. Brillouin, L.: The BWK approximation and Hill’s equation. Q. Appl. Math. **7**, 363–380 (1949)
30. Parameswaran, K., Varadan, T.K., Prathrap, G.: Nonlinear vibration of beams in an axial force field. J. Acoust. Soc. Am. **69**(3), 709–712 (1981)
31. Sinha, S.K., Stability of an internally damped Timoshenko rotor under dynamic axial loads. American Society of Mechanical Engineers, Design Engineering Division (Publication) DE 18-1, pp. 213–216 (1989)
32. Bolotin, V.V.: The Dynamic Stability of Elastic Systems. Holden-Day Inc. San Francisco (1964)

33. Bykhovsky, I.I.: Fundamentals of Vibration Engineering. Mir Publishers, Moscow (1972)
34. Changhe, L., Bernasconi, O., Xenophontidis, N.: A generalized approach to the dynamics of cracked shafts. J. Vib. Acous. Str. Reliab. Des. **111**, 257–263 (1989)
35. Han, Q.K., Chu, F.L.: Parametric instability of two disk-rotor with two inertia assymetries. Int. J. Struct. Stab. Dyn. **12**(2), 251–284 (2012)
36. Kanwal, R.P.: Linear Integral Equations. Academic Press, New York (1971)
37. Khachatryan, A.A.: Longitudinal vibrations of prismatic bars made of different-modulus materials. Mekhanika Tverdogo Tela **2**(5), 140–145 (1967)

Chapter 3
Mathematical Models for Rotor Dynamic Analysis

Abstract Chapter 3 presents the main mathematical models used in rotor dynamic analysis. The one disc-flexible rotor model, called Jeffcott or de Laval rotor, can be used to derive qualitative features, since it lends itself to analytical treatment. The transfer matrix is powerful to model very long and complex rotors but it is strictly limited to linear systems and has certain problems of numerical instability. Lumped mass systems lead to very tedious computations, compared with the transfer matrix method, but they can be used to describe nonlinear systems. For realistic rotor forms, a discrete finite element model is presented, applicable to very complicated rotor geometries, yet leading to a manageable system of equations for linear or non-linear analysis.

3.1 Introduction

Almost 150 years ago Rankine published his paper on 'Centrifugal whirling of shafts'. This marked the beginning of a special branch of applied mechanics dealing with the dynamics, and in particular with the stability, of rotating machinery. The ever increasing importance of the latter and the technical difficulties of extending its size and reliability have led to a considerable growth of the new discipline.

In the 1920s there were very important milestones in rotor dynamics. It was the time when higher speeds and larger machines demanded supercritical machine operation. This introduced most of the rotor stability phenomena and inspired some fundamental analyses. Newkirk studied instability problems associated with the bearing effects [1] and he identified instabilities due to dry friction [2], while Kimball [3, 4] gave basic results for internal damping in the shafts.

A. D. Dimarogonas et al., *Analytical Methods in Rotor Dynamics*,
Mechanisms and Machine Science 9, DOI: 10.1007/978-94-007-5905-3_3,

In the last few decades work on rotor stability has been concentrated on improvements of rotor and bearing description. A vast number of publications, among which, several books on the subject are now available. In classical literature, Stodola [5], in his book on steam and gas turbines, devotes a considerable portion on rotor stability while the books by Dimentberg [6], Tondl [7], Ehrich [8], Childs [9], Lalanne and Ferraris [10], and by Yamamoto and Ishida [11] are exclusively on rotor dynamics. A total of 554 references on the subject are listed in Ref. [12].[1]

Internal or ''rotating'' damping is a well-known source of potential dynamic instability of shafts operating at supercritical speeds. This kind of destabilizing damping may be present due to energy dissipation in the shaft's material or rubbing between rotating components. In some cases similar effects may also be the result of fluid flow in labyrinth seals, oil flow properties, journal bearings, etc. [13]. The Newkirk Effect, the vibration change due to thermal distortion of a rotor caused by rubbing on stationary components was studied analytically by Dimarogonas [14]. The static bow due to an arbitrary heat input was found from a convolution integral of a source bow function and a heat function. Utilizing the dynamic response of the system, the resulting dynamic bow was computed. This dynamic bow controls the generated heat and the associated heat function. The resulting model was described by a complex integral equation, consequently transformed into two nonlinear differential equations. The stability and the modes of these equations, solved with numerical methods, were studied. Three modes of the Newkirk Effect were discovered: spiralling, oscillating, and constant modes. It was found that critical speeds influence those modes only indirectly.

The influence of internal damping on the dynamic behaviour of rotating shafts has been investigated, considering the presence of nonlinearities introduced in the restoring elastic forces by the alternate tension and compression of the shaft fibres. These forces can oppose or induce shaft whirl motion affecting the rotor stability limit [15, 16].

A rotating shaft with internal damping mounted either on elastic dissipative bearings or on infinitely rigid bearings with viscoelastic suspensions affecting the stability region is investigated by Mukherjee and Montagnier [17, 18]. Comparison of viscous and hysteretic damping conditions lead to the conclusion that an appropriate material damping model is essential for an accurate prediction of these instabilities.

Tilting pad bearings have many attractive features such as high rotor-bearing stability. In predicting the stability of rotors supported by tilting pad journal bearings, it was debated whether or not the bearings should be represented with frequency dependent dynamics [19–21].

Computational fluid dynamics (CFD) have been used to model the labyrinth seal flow path and calculate rotordynamic forces. The seal influence on the rotordynamic stability, however, is a challenging task, accounting for inlet pressure, shaft whirling, and shaft rotational speed requiring relatively high computer processing power [22–26].

[1] A list of rotordynamics books can be found at www.rotordynamics.org/booklist.htm.

Several theoretical works have focused on general movements of bases, particularly in cases of seismic excitation [27, 28]. The influence of nonlinear bearings has been studied with piecewise linear coefficients using the discrete acceleration values of the El Centro earthquake [29].

In order to better understand some of the technical difficulties of rotor design and rotor operation we must turn to those laws of mechanics which determine rotor behavior. In general these laws are formulated as differential equations; i.e. relations linking to one another the derivatives (in space and time) of those variables which characterize the various phases of motion. To find the differential equations is the first step of rotor analysis. In general, no insurmountable difficulties appear at this point. Next we must study the solutions of the equations in order to obtain features of rotor behavior, and finally we have to link certain measurable properties of the solutions to the parameters of rotor design. Such properties are oscillation frequencies, amplitudes, rates of growth or decay, etc. It would be ideal to establish analytic relations between the properties and the parameters, which is the point at which difficulties begin. If one disregards the special case of ordinary linear differential equations with constant coefficients, no complete theory permitting determination of the ultimate relations required by comprehensive and rigorous analysis exists. However, numerical methods and computer codes can provide all the necessary design information without a general theory. Buckner's argument on this point is worth mentioning [30]: any differential equation has an infinite number of solutions, and a great number of them can be numerically solved by a computer, which could also extract and print out those features which interest the design engineer. But this is not enough. We cannot be satisfied with the solutions to just one equation. Any change in the design parameters means another equation. Thus, if we have m design parameters and k choices for each of them, we must consider a total of k^m parameter constellations, each constellation characterized by one differential equation (or one system of such equations). Now if n solutions for each constellation are needed, then the computer must calculate the total of nk^m solutions. If $m = 3$, $k = 4$ and $n = 50$ (none of these numbers is excessively high) then we must compute and look into 3,200 solutions. Although 3,200 solutions constitute a small computer project, which, after carried out, may not lead to any valid conclusions at all. Fortunately, in these days, there seems to be no problem for a modern computer to do the work.

It has been repeatedly happening in the past that science has dealt with a situation where a theory is missing, and where excessive cost, prohibit numerical or other experimentation on a large scale. The remedy was based on a rather simple principle: if a problem were too big for comprehensive and exact analysis try to make it smaller by simplification, but not to the point at which all features suffer a qualitative or even quantitative way, while others are deliberately dropped for the sake of simplification.

There are several examples in astronomy, physics and mechanics. In mechanics we can mention Euler's computation of the buckling load of a column under pressure. Euler simplified the differential equation of the column by 'linearization'. The simplification is good enough to predict the onset of buckling, while no

conclusion can be drawn about the size of the deflection or the energy of deformation after buckling. Another example appears in the field of aerodynamics. The rather simple theory of plane flow of an ideal fluid predicts airfoil lift correctly but fails with respect to drag.

If we describe a physical system exactly or approximately by a set of equations (e.g. differential equations), we call that set a *model* of the physical system. A model can be crude, refined or exact, depending on the quality of the equations. It is now clear what we mean by the Euler model of the buckling column. The creation of models of a finite degree of freedom enjoy the greatest use as a substitute for structures of finite degree; the finite element method in elasticity is one example, and the procedure of lumping masses for the purpose of analyzing vibrations another.

The most convenient type of model (if it can be developed at all) is the *linear* one. In this case the differential equations are linear. Homogeneous linear models, especially those described by ordinary differential equations, have a property which makes them easy to deal with. This is the feature of superposition due to which the sum of two solutions is also a solution. With ordinary differential equations the superposition principle permits a reduction of the search for all solutions; it suffices to find a finite number of them.

It is interesting to note that linear models of rotors have been introduced and applied with considerable success. The simplest linear model, namely the rigid wheel on a flexible shaft, led to the discovery of the critical speed. Linear models of a higher degree of freedom showed that a rotor can have more than one, if not infinitely more, critical speeds. By now engineers and research workers have drawn as much information from linear models as the validity of such models admits. In many cases we have reached the point where a linear model fails to predict rotor behavior. This is largely due to the non-linear characteristics of journal bearings. Today we must consider models of a high degree of freedom, where at least four of these degrees are associated with highly none linear force laws.

In the presence of non-linearities, we can no longer reduce the solutions to a finite number of models. The concept of stability, while it can be extended to characterize the behavior of solutions of non-linear equations, is not easily linked to the design parameters. Moreover, a concept ‘practical stability’ has still to be developed. It should also be noted that ‘critical speed’ is no longer well-defined for a non-linear model. Still, one can ask if it would not suffice to look for certain typical solutions and to correlate them with the design parameters [30, 31].

Most rotors have rather complicated geometries. This leads naturally to the question of the complexity of the analytical model which is to be used to investigate the rotor’s behavior in service. There is an obvious trade-off between two directions:

(a) a simple model with mist results by way of analysis, often in closed form (such features are also associated with a better qualitative understanding of the effect of the several design parameters upon the design objectives);

(b) a model with an adequate description of the properties of the rotor and the associated elements, which is often rather complicated and necessitates the use if numerical methods and lengthy machine computations, this leads to a better prediction of the behavior of the specific rotors and to more reliable numerical results, accompanied by a loss in generality and a difficulty in extracting general features of the model.

Most times, both analyses are necessary. The complexity of the model is determined from the individual features of the particular rotor in conjunction with the experience of the analyst and the scope of the analysis. For example, if the rigid body motion of a rotor has frequencies close to the rotating speed and far from the frequencies at the bending modes, a single disc description will suffice. If the rotating speed is in the vicinity of a higher bending mode, the model devised should at least be able to include that mode. A thorough discussion on the application of methods and algorithms for rotating shafts analysis is presented in [31].

3.2 The Single Disc Model

We shall begin this chapter with the simplest model of a massless elastic rotor carrying a rigid disc and revolving at a constant angular velocity as shown in Fig. 3.1, known as a de Laval rotor [31]. The disk mass is m and the mass polar moment of inertia J with respect to the axis of rotation z. If the shaft is flexible (with a lateral spring constant k) the disk is capable of movements perpendicular to its axis in the horizontal and vertical directions x and y (Fig. 3.1a), but also rotations about the three axes, such as in Fig. 3.1b. The rotation about the z axis is the steady-state motion.

To conform with practices from statics we shall describe the orientation of the disc by way of the vertical and horizontal slopes of its axis of rotation θ and φ, in

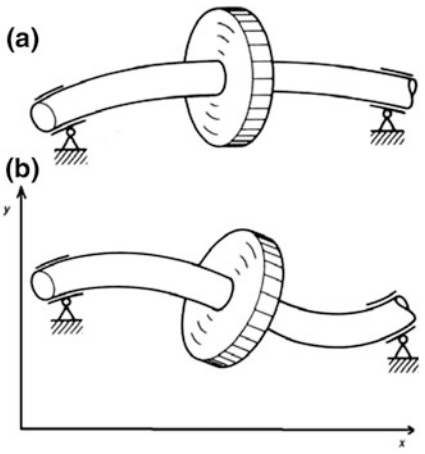

Fig. 3.1 Whirling of a de Laval rotor (from Ref. [31] by permission)

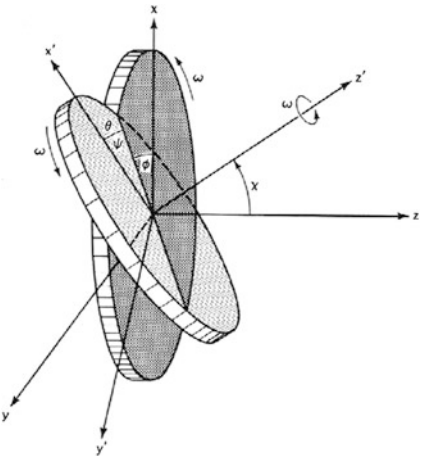

Fig. 3.2 Euler angles (from Ref. [31] by permission)

order words the angles θ and φ of the axis of rotation of the disc in respect to the planes (y, z) and (x, z) respectively (Fig. 3.2).

If the rotor has a substantial moment of inertia about its diameter and a general rigid-body motion, changing the orientation of its axis requires application of considerable moments at high speeds. This is known to change the critical speeds of high-speed rotors, rendering them functions of the rotating speed, and to generate new ones [29].

From dynamics, the position of the disk can be defined by way of the coordinates of the mass-center, plus the three *Euler angles* ϕ, χ, ψ (Fig. 3.2). The resulting equations of motion can be found at any standard textbook on advanced

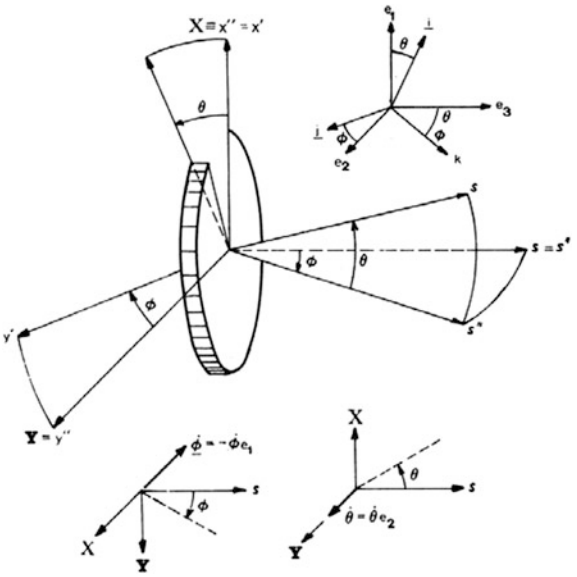

Fig. 3.3 Definition of coordinate systems for rotor motion

dynamics or mechanics. From a vibration engineering viewpoint, the Euler angle description of the motion is not a very convenient one because these angles are difficult to measure or interpret. Instead, to conform with practices from statics, we shall describe the orientation of the disk by way of the vertical and horizontal slopes of its axis rotation, θ and ϕ: in other words, the angles θ and ϕ of the axis of rotation of the disk with respect to the planes (y, s) and (x, s) respectively (Fig. 3.3).

It is known from kinematics that finite rotations do not obey the vector law of addition. However, infinitesimal rotations are commutative and can be added as vectors. Since we consider only small displacements and rotations, we can consider the angles θ and φ has no effect on the final position. Thus, we consider a coordinate system (x'', y'', s'') affixed to the disc but not rotating with it, and oriented along the principal axis of inertia of the disc. We also consider an inertial coordinate system (X, Y, s). Let the two systems coincide and rotate the system (x'', y'', s'') about the x''-axis by an angle φ to a new position (x', y', s'). Then we rotate it by an angle θ about the y'-axis to the final position (x, y, s). If the angles θ and φ change with time, the disc will have, in addition to its angular velocity of rotation Ω about the s-axis, angular velocities $\dot{\theta}$ and $\dot{\varphi}$ about the axes Y and s, respectively (Fig. 3.3).

We select the coordinate system (x, y, s) to coincide with the principal axis of inertia but not to rotate with it about the s-axis. Thus, the disc rotates in respect to this coordinate system with angular velocity Ω about the s-axis. Then, Newton's law yields

$$\mathbf{M}_G = \left(\frac{d\mathbf{H}_G}{dt}\right)_{x,y,s} + \boldsymbol{\Omega} \times \mathbf{H}_G \tag{3.1}$$

where $\mathbf{M}_G$ the moment vector about the mass is centre, G, and $\mathbf{H}_G$ is the corresponding momentum vector. If I_x, I_y, I_s are the principal moments of inertia of the disc,

$$\left.\begin{aligned} \Sigma \mathrm{M}_x &= I_x \frac{d\omega_x}{dt} - I_y \Omega_s \omega_y + I_s \Omega_y \omega_s \\ \Sigma \mathrm{M}_y &= I_y \frac{d\omega_y}{dt} - I_s \Omega_x \omega_s + I_x \Omega_s \omega_x \\ \Sigma \mathrm{M}_s &= I_s \frac{d\omega_s}{dt} - I_x \Omega_y \omega_x + I_y \Omega_x \omega_y \end{aligned}\right\} \tag{3.2}$$

where ω is the angular velocity of the disc vector.

Let $\mathbf{e}_1$, $\mathbf{e}_2$, $\mathbf{e}_3$ be the unit vectors of the coordinate system (X, Y, s) and $\mathbf{i}$, $\mathbf{j}$, $\mathbf{k}$ the unit vectors of (x, y, s). We then have

$$\omega = -\dot{\varphi}\mathbf{e}_1 + \dot{\theta}\mathbf{e}_2 \quad \boldsymbol{\Omega} = \Omega\mathbf{k} \tag{3.3}$$

We note that

$$\left.\begin{aligned} \mathrm{e}_1 &= \mathbf{i}\cos\theta + \mathbf{k}\sin\theta \\ \mathrm{e}_2 &= \mathbf{i}(\cos f + \sin\theta\sin\varphi) + \mathbf{k}\cos\theta\sin\varphi \end{aligned}\right\} \tag{3.4}$$

Thus

$$\omega = -(\dot{\varphi}\cos\theta)\mathbf{i} + \dot{\theta}(\cos\varphi + \sin\theta\cos\varphi)\mathbf{j} + \Big(\dot{\varphi}\sin\theta + \dot{\theta}\cos\theta\sin\varphi\Big)\mathbf{k}$$

We assume that $\Omega =$ constant, which means that the shaft is infinitely stiff in torsion and attached to a prime mover with infinite inertia. Moreover, in tune with the general assumptions, we assume small angles θ and φ, so that

$$\sin\theta \approx \theta \quad \cos\theta \approx 1$$

and we neglect products of θ and φ and their time derivatives to obtain

$$\left.\begin{aligned} \omega &= -\dot{\varphi}\mathrm{i} + \dot{\theta}\mathrm{j}\omega_x = -\dot{\varphi}\omega_y = \dot{\theta}\omega_s = 0 \\ \Omega &= \Omega\mathbf{k}\Omega_x = 0\Omega_y = 0\Omega_s = \Omega \end{aligned}\right\} \tag{3.5}$$

Furthermore, for a circular disk we have $I_x = J_p$, $I_x = I_y = J$ and

$$\left.\begin{aligned} -\Sigma\mathrm{M}_x &= J\ddot{\varphi} + J_p\Omega\dot{\theta} \\ +\Sigma\mathrm{M}_y &= J\ddot{\theta} - J_p\Omega\dot{\varphi} \end{aligned}\right\} \tag{3.6}$$

The centre of the disk has lateral deflections x and y with the motion restricted on the s-axis. External forces on the disc are $X(t)$, $Y(t)$, $\Theta(t)$, $\Phi(t)$ along the coordinates x, y, θ, φ respectively. Elastic forces are linearly associated with the four coordinates by way of stiffness constants $k_{ij}(i,j = x, y, \theta, \varphi)$. Application of Newton's law yields, if m is the mass of the disk

$$\left.\begin{aligned} m\ddot{x} + k_{xx}x + k_{x\theta}\theta &= X(t) \\ m\ddot{y} + k_{yy}y + k_{y\phi}\varphi &= Y(t) \\ J\ddot{\theta} + J_p\Omega\dot{\varphi} + k_{\theta\theta}\theta + k_{\theta x}x &= \Theta(t) \\ J\ddot{\varphi} - J_p\Omega\dot{\theta} + k_{\varphi\varphi}\varphi + k_{\varphi y}y &= \Phi(t) \end{aligned}\right\} \tag{3.7}$$

In the sequel, an isotropic shaft will be assumed. The problem of unequal shaft stiffness along two perpendicular lateral directions will be further explored later. Therefore, it is assumed that

$$k_{xx} = k_{yy} = k \quad k_{x\theta} = k_{y\varphi} = \lambda \quad k_{\theta\theta} = k_{\varphi\varphi} = \mu$$

Furthermore, the following complex quantities are defined:

$$\left.\begin{aligned} z &= x + iy \quad & Z &= X + iY \\ \psi &= \theta + i\varphi \quad & \Psi &= \Theta + i\Phi \end{aligned}\right\} \tag{3.8}$$

The equations of motion assume the form

$$\left.\begin{aligned} m\ddot{z} + kz + \lambda\psi &= \mathrm{Z}(t) \\ J\ddot{\psi} + i\Omega J_p\dot{\psi} + \mu\psi + \lambda z &= \Psi(t) \end{aligned}\right\} \tag{3.9}$$

A rotor-fixed coordinate system (ξ, η) is defined which rotates with the rotor at angular velocity $\boldsymbol{\Omega}$. therefore, if

$$\zeta = \xi + i\eta$$

then

$$z = \zeta \exp(i\Omega t)$$

and Eq. (3.9) become

$$\left.\begin{aligned} m\ddot{\zeta} + 2mi\Omega\dot{\zeta} + \left(k - \Omega^2 m\right)\zeta + \lambda w &= Z(t)\exp(-i\Omega t) \\ J\ddot{w} + i\Omega\left(2J + J_p\right)\dot{w} + \left(\mu - \Omega^2 J - \Omega^2 J_p\right)w + \lambda\zeta &= \Psi(t)\exp(-i\Omega t) \end{aligned}\right\} \tag{3.10}$$

where w $= u + iv$, and u and v are respective to θ and φ in the moving coordinate system representing the angles of the centerline of the rotor with the planes (η, s) and (ξ, s) respectively.

Systems of Eqs. (3.9 and 3.10) describe the motion in two different coordinate systems. The significance of using the moving coordinate system will be apparent later. In the following, the basic equations will be used to identify qualitatively some basic engineering problems in rotor dynamics.

3.2.1 Critical Speeds

Under a certain condition, the set (3.9 or 3.10) can have the harmonic solution $x = x\exp(pt)$ etc. In particular, when the frequency of natural vibration coincides with the frequency of rotation ($p = i\Omega$) there is an unwanted situation in machine operation and this particular speed is called the critical speed. It will be computed as a root of the characteristic equation of system (3.9). Four such roots exist, in general, for this system [31]: two positive, which correspond to a motion of the type

$$x = x_0 \exp(i\omega t)\omega > 0$$

called forward whirl, and two negative, corresponding to a motion of the type

$$x = x_o \exp(-i\omega t)$$

called backward whirl. The physical significance of this technology is apparent.

3.2.2 Internal Damping

Materials and structures have several mechanisms of resistance to change in their configurations which are depending on the rate of this change. Due to friction mechanical assemblies such as compound rotors possess a great deal of this resistance. The magnitude is not proportional to the rate of change but rather to the sign of it. Therefore the system becomes non-linear. Tondl devotes a good portion of his book [7] to this non-linearity. The term internal damping is commonly adopted regarding both the elastic hysteresis of materials and the shaft fibre shear inside the hub [7, 11, 12]. When a rotating shaft undergoes a perturbation, consisting in displacement and velocity variations of a point belonging to the shaft axis with respect to dynamic equilibrium conditions, the fibres are alternatively compressed and stretched. This phenomenon occurs every time that the rotor angular speed with respect to its deflected axis line differs from the whirl speed, i.e. the angular velocity of the deflection line itself [15]. On the other hand, Timoshenko [32] and Den Hartog [33] proved the presence of a force normal to the plane of the deformed shaft, due to the fact that the neutral axis of strain does not coincide with the neutral line of stress.

Since our purpose is to develop gradually a manageable system of equations, the viscoelastic model will be used, with linear, hysteric damping. It is apparent that changes in the rotating coordinate system will result in changes of the structural configuration. Therefore, the damping force will be assumed to have the form [7, 31]

$$F_d = -\frac{\gamma k \dot{\zeta}}{\boldsymbol{\Omega \omega_n}} \tag{3.11}$$

where $\omega_n^2 = k/m$ and γ is a material constant. From here on, the first equation of (3.9 or 3.10) will be used, assuming that J and J_p are negligible. Extension to the two equations is straightforward but tedious.

Therefore

$$\left.\begin{aligned} m\ddot{\zeta} + \left(\tfrac{\gamma}{\Omega\omega_n} k + 2i\Omega m\right)\dot{\zeta} + \left(k - m\Omega^2\right)\zeta = Z(t)\exp(-i\Omega t) \\ m\ddot{z} + \tfrac{\gamma}{\Omega\omega_n} k\dot{z} + k\left(1 - \tfrac{\gamma\Omega i}{\Omega - \omega_n}\right) z = Z(t) \end{aligned}\right\} \tag{3.12}$$

3.2.3 Bearing Forces

Rotors on fluid bearings operate at some equilibrium point. Additional forces on the rotor cause the journal to move from equilibrium point. The opposite is also true. The relation of the bearing reaction to the journal motion is a highly non-linear function [34]. Such functions have been found in closed form for the most

usual fluid bearings with high speed rotor applications, the pad bearings [35]. The effect of the non-linearity will be discussed later. At present, linear behavior will be assumed, as usual [31] in the form

$$-F_b = B\delta + C\dot{\delta} \tag{3.13}$$

where B and C can be complex functions, which means that reactions are not co-linear with the deflection of the journal centre δ. Here B and C are the bearing spring and damping constants, respectively. The bearing is assumed isotropic. Otherwise, the equations should be separated into real and imaginary parts. The model and geometry of the system is shown in Fig. 3.4.

The equations for the rotor and journal motion and equilibrium are

$$\left.\begin{aligned} m\ddot{z} &= -k(z-\delta) \\ k(z-\delta) &= B\delta + C\dot{\delta} \end{aligned}\right\} \tag{3.14}$$

Eliminating δ, we obtain

$$\frac{mC}{k}\dddot{z} + m\left(1+\frac{B}{k}\right)\ddot{z} + C\dot{z} + Bz = 0 \tag{3.15}$$

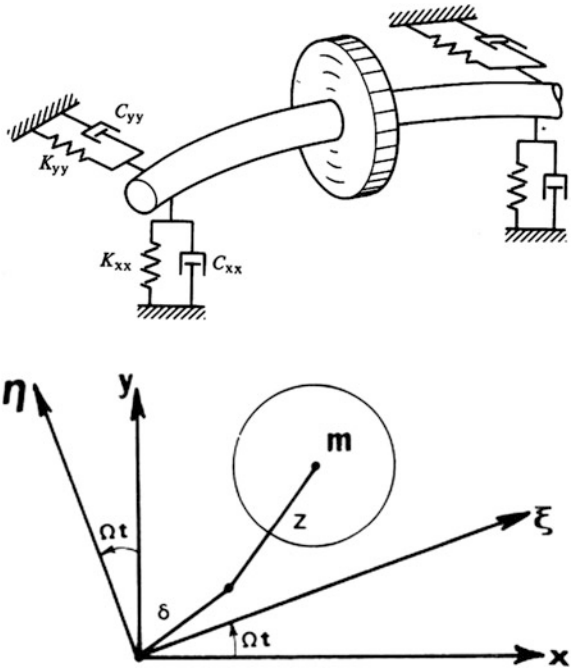

Fig. 3.4 Model and geometry of deflected rotor

3.2.4 Environmental Forces

If the disc works in a fluid or magnetic environment, forces can be exerted by the magnetic field or the fluid. We can develop a linear expansion similar to the one for the bearings. In general, this will provide us with force relations such as [31]

$$-P_x = L_{xx}x + L_{xy}y + D_{xx}\dot{x} + D_{xy}\dot{y} \tag{3.16}$$

$$-P_y = L_{yy}y + L_{yx}x + D_{yy}\dot{y} + D_{yx}\dot{x} \tag{3.17}$$

The coefficients L and D will be called midspan force gradients.

The bearings and the midspan force gradients necessitate the writing of the equations of motion explicitly in terms of x and y, in case of asymmetry. However, in most engineering systems symmetry can be assumed, which leads to $L_{xx} = L_{yy} = L,\ D_{xx} = D_{yy} = D$, where

$$-P_e = Lz + D\dot{z}. \tag{3.18}$$

3.2.5 Stability of Motion, Second-Order Equations

It has been shown that, in general, the null equation for the rotor motion of the form

$$m\ddot{z} + (c_1 + ic_2)\dot{z} + (k_1 + ik_2)z = 0 \tag{3.19}$$

Although we can deal with the solution of Eq. (3.19) directly, we can do it with a generalization of the Routh-Hurwitz criteria of complex equations. To this end, we seek after a solution $z = z_0\exp(ipt)$ to obtain the characteristic equation

$$-mp^2 + i(c_1 + ic_2)p + (k_1 + ik_2) = 0 \tag{3.20}$$

The Routh-Hurwitz criteria for stability, if the characteristic equation is of the form

$$(a_o + ib_o)p^n + (a_1 + ib_1)p^{n-1} + \ldots + (a_n + ib_n) = 0 \tag{3.21}$$

are [6], [31]

$$-\begin{vmatrix} a_o & a_1 \\ b_o & b_1 \end{vmatrix} > 0 \qquad \begin{vmatrix} a_o & a_1 & a_2 & 0 \\ b_o & b_1 & b_2 & 0 \\ 0 & a_o & a_1 & a_2 \\ 0 & b_o & b_1 & b_2 \end{vmatrix} > 0 \tag{3.22}$$

$$(-1)^n \begin{vmatrix} \ldots & \ldots & \ldots & \ldots \\ a_o & a_1 \ldots a_n & 0 & 0 \ldots \\ b_o & b_1 \ldots b_n & 0 & 0 \ldots \\ 0 & a_o \ldots a_{n-1} & a_n & 0 \ldots \\ 0 & b_o \ldots b_{n-1} & b_n & 0 \ldots \\ \ldots & \ldots & \ldots & \ldots \\ \ldots & \ldots 0 & a_o \ldots a_{n-1} & a_n \\ \ldots & \ldots 0 & b_o \ldots b_{n-1} & b_n \end{vmatrix} > 0 \tag{3.23}$$

Applied to Eq. (3.20) for

$$a_o = -m,\ b_o = 0,\ a_1 = -c_2,\ b_1 = c_1,\ a_2 = k_1,\ b_2 = k_2 :$$

the latter yields

$$-\begin{vmatrix} -m & -c_2 \\ 0 & c_1 \end{vmatrix} > 0 \tag{3.24a}$$

$$\begin{vmatrix} -m & -c_2 & k_1 & 0 \\ 0 & c_1 & k_2 & 0 \\ 0 & -m & c_2 & k_1 \\ 0 & 0 & c_1 & k_2 \end{vmatrix} > 0 \tag{3.24b}$$

Condition (3.24a) implies $mc_1 > 0$ or $c_1 > 0$: (3.24b) yields

$$-m \begin{vmatrix} c_1 & k_2 & 0 \\ -m & -c_2 & k_1 \\ 0 & c_1 & k_2 \end{vmatrix} > 0$$

or

$$c_1 c_2 k_2 + c_1^2 k_1 - m k_2^2 > 0 \tag{3.25}$$

Criteria (3.22 and 3.23) apply only for rotors with isotropy in the x and y directions, for which complex equations can be written. For other systems, for example with bearings of different vertical and horizontal stiffness, it is better to deal with equations with real coefficients. In general, these lead to characteristic equations of the form

$$a_n p^n + a_{n-1} p^{n-1} + \ldots + a_1 p + a_o = 0 \tag{3.20a}$$

In this case, Routh-Hurwitz criteria for stability are [7]

(a) that all powers of p are present and all coefficients a_i are of the same sign;
(b) that the successive determinants below are positive:

$$D_o = a_1 \quad D_1 = \begin{vmatrix} a_1 & a_o \\ a_3 & a_2 \end{vmatrix} \quad D_2 = \begin{vmatrix} a_1 & a_o & 0 \\ a_3 & a_2 & a_1 \\ a_5 & a_4 & a_3 \end{vmatrix} \tag{3.22a}$$

In engineering problems almost all factors contributing to the equations of motion are simultaneously present. However, depending on the particular application, some factors are dominant and the associated instability phenomena are labeled accordingly. The reader is warned against over-simplification of omitting factors considered less important, very commonly occurring in contemporary literature. In the following, we shall attempt to present some instability cases, with the warning that they are altogether qualitative and have a pedagogical purpose only.

Internal friction: internal friction includes the internal damping we have discussed previously, plus some other factors contributing to the same effect. The most common is the dry friction in shrink-fit joints, such as discs, gears and pulleys on the shaft. Figure 3.5 illustrates this point.

A gear G is mounted on the shaft by way of a shrink-fit. Thus, there is always a pressure p, between shaft and hub due to the gear, almost uniform. If the shaft bends, as in the figure, the upper fibres elongate and the lower ones contract. There is a friction force associated with this, if the fit slips, which produces a torque, which is a function of the deflection of the shaft. From experiments, we can incorporate this effect into the internal damping coefficient, hysteretic or viscoelastic.

In general, we shall assume that c_i represents internal damping and c_e some form of external damping, i.e. bearing damping neglecting higher derivatives in Eq. (3.15) and assuming $k \gg B$, as usually happens. Then

$$m\ddot{\zeta} + (c_1 + c_e)\dot{\zeta} + \left(k - m\Omega^2\right)\zeta + 2m\Omega i\dot{\zeta} + c_e\Omega i\zeta = 0 \tag{3.26}$$

Substituting

$$\zeta = \zeta_o \exp(ipt)$$

we obtain the characteristic equation (or characteristic polynomial)

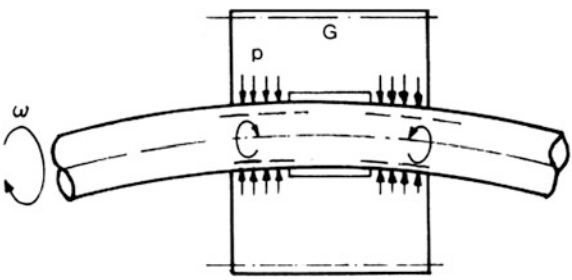

Fig. 3.5 Mechanism of damping at shrink-fit joints

$$-p^2 + i\frac{c_1 + c_e}{m}p + \left(\frac{k}{m} - \Omega^2\right) - 2\Omega p + \frac{c_e}{m}\Omega i = 0 \tag{3.27}$$

Applying the criterion (3.25) we obtain, for stability

$$\Omega < \left(1 + \frac{c_e}{c_i}\right)\omega_n \quad \omega_n = \sqrt{k/m} \tag{3.28}$$

In the absence of external damping ($c_e = 0$) we observe that for a rotating speed smaller than the critical ω_n we have stability. Furthermore, Eq. (3.28) implies that there is always a rotating speed $\Omega = (1 + c_e/c_i)\omega_n$ above which the system is unstable. Also, for any rotational speed $\Omega > \omega_n$, we can always make the system stable by providing adequate external damping.

Bearing instabilities: For a rigid rotor, $k \gg B$ and Eq. (3.15) becomes, for $B = K_d - iK_c$, $C = C_d - iC_c$

$$m\ddot{z} + (C_d - iC_c)\dot{z} + (K_d - iK_c)z = 0 \tag{3.29}$$

Stability conditions (3.25) yield

$$-C_c < 0 \quad CC_cK_c - C_c^2K - mK_c^2 > 0 \tag{3.30}$$

The first condition means that negative bearing damping always causes instability. The second condition, upon division by m, yields

$$\omega_n^2 < \frac{C}{C_c}\frac{K_c}{m} - \left(\frac{K_c}{C_c}\right)^2 \tag{3.31}$$

The right hand part of Eq. (3.31) is a function of the rotating speed ω, because so are the bearing properties. If this expression, at some value of Ω, becomes smaller than ω_n^2, this will imply instability.

Asymmetry of rotating parts: We have confined our discussion up to this point to cylindrical shafts with similar properties in both directions. If the shaft has spring constants k_η and k_ξ different along two perpendicular directions, a situation common in electric generators, we shall not have restoring forces k_η and k_ξ in the rotating coordinate system, but $k_\eta\eta$ and $k_\xi\xi$ respectively. Substituting into Eq. (3.26) and using

$$k_1 = \frac{k_\eta + k_\xi}{2} \quad k_2 = \frac{k_\eta - k_\xi}{2} \tag{3.32}$$

we obtain

$$m\ddot{\eta} + (c_e + c_i)\dot{\eta} + \left(k_1 - m\Omega^2 + k_2\right)\eta - 2m\Omega\dot{\xi} - c_e\Omega\xi = 0 \tag{3.33}$$

$$m\ddot{\xi} + (c_e + c_i)\dot{\xi} + \left(k_1 - m\Omega^2 + k_2\right)\xi - 2m\Omega\dot{\eta} - c_e\Omega\eta = 0 \tag{3.34}$$

Substituting $\eta = \eta_o \exp(ipt)$, $\xi = \xi_o \exp(ipt)$ we obtain the characteristic equation

$$\left[-p^2 + \frac{c_e c_i}{m} ip + \left(\frac{k_1}{m} - \Omega^2\right)\right]^2 - \left(2\Omega p + \frac{c_e p}{m}\right)^2 - \left(\frac{k_2}{m}\right)^2 = 0 \tag{3.35}$$

It can be shown with Routh-Hurwitz criteria [Eq. (3.22a)] that there is an additional instability region for $k_\eta < k_\xi$:

$$\sqrt{k_n/m} < \Omega < \sqrt{k_\xi/m} \tag{3.36}$$

In other words, the operation between the critical speeds defined by the two spring constants of the shaft is unstable.

Thermal imbalance: If there are stationary components around the shaft on which it might rub, there will be heat input in the rotor due to rubbing which is proportional to and in the direction of the amplitude. Therefore, there will be an imbalance in the rotating coordinate system (see Chap. 5):

$$e = \rho\zeta \tag{3.37}$$

where ρ is a complex constant depending on the geometric and thermo elastic characteristics of the system. Neglecting damping, Eq. (3.26) becomes, with the external force $m\rho\Omega^2\zeta$ due to imbalance

$$m\ddot{\zeta} + \left(k - m\Omega^2\right)\zeta + 2m\Omega i\dot{\zeta} - m\rho\Omega^2\zeta = 0 \tag{3.38}$$

Considering the characteristic equation

$$-p^2 - 2\Omega p + \left(\omega_n^2 - \Omega^2 - \rho\Omega^2\right) = 0 \tag{3.39}$$

If $\rho = u + iu$, the condition (3.25) yields

$$-(2\Omega)^2\left(\omega_n^2 - \Omega^2 - u\Omega^2\right) - m\left(\Omega^2\upsilon\right)^2 > 0 \tag{3.40}$$

or

$$-4\omega_n^2 + 4\Omega^2(1+u) - m\Omega^2\upsilon^2 > 0 \tag{3.41}$$

Finally

$$\Omega^2 > \frac{4\omega_n^2}{4(1+u) - m\upsilon^2} \tag{3.42}$$

In most practical situations, $\upsilon \approx 0$ and $u \ll 1$, so that stability occurs for a rotating speed greater than the critical speed.

3.3 The Discrete Model

The one-disc rotor representation can only be used for qualitative studies and for derivation of general results. For the analysis of specific machines, we have to take into account the complicated geometry of the rotor and accurate forms of the excitation, bearings and supports.

The transfer matrix method has been applied to stepped rotors by Landzberg [36]. This method was applied further by Vogel [37] and Lund [38]. Lumped mass systems have also been used to represent realistic rotor geometries, for example by Gasch [39], Shen [40] and Kirk [41]. Ruhl and Booker [42] used a finite element method for the modeling of a realistic rotor. Dimarogonas [32] developed a discrete model for a continuous shaft including non-linearities of the system.

The transfer matrix is powerful to model very long and complex rotors but it is strictly limited to linear systems and has certain problems of numerical instability. Lumped mass systems lead to very tedious computations, compared with the transfer matrix method, but they can be used to describe non-linear systems.

The geometry of real rotors, such as high speed turbo rotors, cannot be realized as one-mass or one-disc. Figure 3.6 depicts the configuration of such a rotor along with mass and moment of inertia distribution. The distribution of its mass and stiffness is discontinuous and very irregular. The same irregularity also characterizes the distribution of the forces acting on the rotor. In such systems successful prediction of stability behavior has been never reported. The finite element method is essentially the same as the transfer matrix method, but with a different scheme of numerical solution, and it goes through the explicit writing of the differential equations of motion, so that non-linear systems can be modeled.

Though the above methods can be applied, in principle, to analyse the stability of rotors of complicated geometries, when numerical solutions of the equations of motions are required they are usually impractical. It appears that no matter how complicated a geometry a rotor has, one can model it by way of a sufficiently large number of masses or elements, however, introduction of short shaft sections results in a "stiff" system, having very high and very low eigenvalues. This requires very

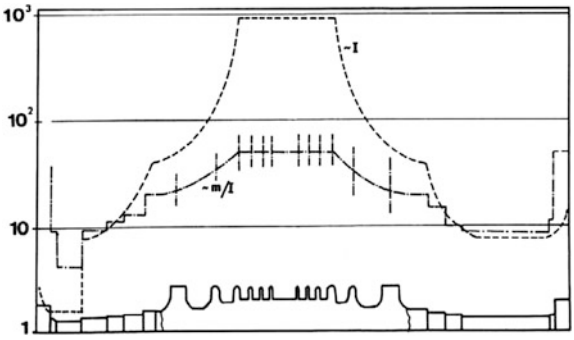

Fig. 3.6 Mass and moment of inertia distribution of a turbine rotor (from Ref. [34] by permission)

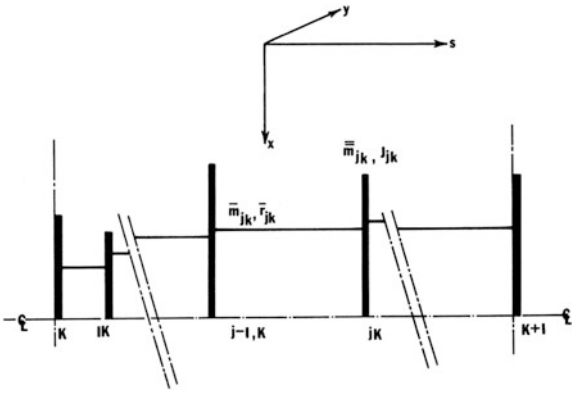

Fig. 3.7 Typical rotor element (from Ref. [34] by permission)

short integration steps which mean not only enormous computation time but also a tendency for numerical instabilities.

Since the final objective is the non-linear analysis of the system one should expect eventually to have to resort to numerical methods, namely, the numerical solution of a set of non-linear equations. Consequently, the number of equations must be reduced to an absolute minimum.

A rotor might have as many as 50 inspan conditions, such as changes in stiffness, mass applied forces, etc. The continuous rotor has an infinite number of degrees of freedom. Since the vibrations of the usual rotors observed are associated with a small number of low eigenvalues of the system, one expects that utilization of a limited number of degrees of freedom will yield adequate accuracy. In fact, for calculations of critical speeds, it has been found that with a finite element approach [42], 2–5 elements give enough accuracy for all engineering purposes, for a shaft of constant diameter. For more complicated geometries, it is obvious that a larger number of elements might be necessary.

Here, a fixed coordinate system (x, y, s) is considered with the s-axis in the direction of the geometric axis of the undeflected rotor (Fig. 3.7). It is assumed that the rotor revolves with a constant angular velocity ω. Along the rotor axis $n + 1$ nodes are considered, which identify n rotor elements. Each node is associated with 4 degrees of freedom expressed by way of four generalized coordinates: x and y are the coordinates of the node and u and v are the slopes of the rotor deflection in the planes (x, s) and (y, s) respectively. On each element there are distributed properties with a finite number (m_k) of discontinuities in the masses, flexibilities and the external forces. The subscript k denotes the element k. Furthermore, motions along the s-axis will not be considered. Finally, the rotor is assumed to be homogeneous cylindrical elastic solid of revolution.

The shape of the rotor along its length will be assumed as described by the coordinates of the $n + 1$ rotor nodes. For calculations of natural vibrations of rotors, it was found that the lower frequencies are relatively insensitive to the selection of this shape. In particular, the static deflection of the rotor between two nodes with the coordinates (deflections and slopes) at these nodes as boundary

conditions was always very successful. In view of the fact that stability analyses of practical rotors involve only very few of the lower frequencies, the static deflection curve will approximate the shape of the rotor between nodes. In the case of a uniform elastic cylinder between two nodes, the static deflection curve in the (x, s) or (y, s) plane is a third degree polynomial. This approach amounts to assuming a set of linearly independent functions $f_{ijk}(s)(i,j = 1,2;k = 1,2,\ldots,n+1)$, such that the motion of the rotor can be described as the linear combinations

$$\left.\begin{aligned} x(s,t) &= \sum_{k=1}^{n+1} [f_{11k}(s)x_k(t) + f_{12k}(s)u_k(t)] \\ u(s,t) &= \sum_{k=1}^{n+1} [f_{21k}(s)x_k(t) + f_{22k}(s)u_k(t)] \end{aligned}\right\} \tag{3.43}$$

in the (x, s) plane and similar expressions in the (y, s) plane.

This leads to four $(n + 1)$ unknown functions of the time $x_k, u_k, y_k, \upsilon_k$ describing the motion of the n + 1 nodes of the rotor. These real functions are combined into the complex functions

$$\left.\begin{aligned} z = x + iy \qquad w = u + iu \\ z_k = x_k + iy_k \quad w_k = u_k + iu_k \end{aligned}\right\} \tag{3.44}$$

Furthermore, the following vectors are defined:

$$\left.\begin{aligned} \mathbf{X} &= \{x_1 u_1 x_2 u_2 \ldots x_{n+1} u_{n+1}\} \\ \mathbf{Y} &= \{y_1 v_1 y_2 v_2 \ldots y_{n+1} v_{n+1}\} \\ \mathbf{Z} &= \{z_1 w_1 z_2 w_2 \ldots z_{n+1} w_{n+1}\} \end{aligned}\right\} \tag{3.45}$$

The shape of the rotor at time t is determined by four $(n + 1)$ generalized coordinates $x_k, u_k, y_k, \upsilon_k (k = 1,2,\ldots,n+1)$ where $(n + 1)$ is the number of nodes along the rotor. The nodes are taken on the geometric axis of symmetry of the rotor.

Between the nodes k and $k + 1$ there is a rotor element which consists of a number $m_k + 1$ of sub-elements, in the form of elastic solids of revolution, usually in the form of, but not restricted to, cylindrical sections. Between such sub-elements, discs of finite mass and moment of inertia but negligible length are admitted.

Let $\mathbf{q} = \{x \quad u\}$ or $\mathbf{q} = \{y \quad \upsilon\}$ be a vector containing the deflection and slope at the vertical or horizontal plane respectively. It will be used in the form q_{jk} and will designate the subnode jk of the element k. Each sub-element is described by a transfer matrix which relates the state vectors at the ends of the sub-elements. Let $\bar{\mathbf{D}}$ be the transfer matrix linking the state vector at subnode jk to the one at node k, and $\bar{\mathbf{R}}$ the transfer matrix linking the state vector at node $k + 1$ to one at subnode jk. Catalogues of transfer matrices for the particular beam model can be

found in Ref. [43]. If the 4 × 4 matrices $\bar{D}$ and $\bar{R}$ consist of the blocks d_{ij} and r_{ij} respectively, where i and j take the values 1 and 2, one can prove that

$$q_{jk} = f_{jk}q_{k+1} + g_{jk}q_k \tag{3.46}$$

where

$$\left.\begin{aligned} f_{jk} &= \left(d_{11}d_{12}^{-1} + r_{12}^{-1}r_{11}\right)^{-1} r_{12}^{-1} \\ g_{jk} &= \left(d_{11}d_{12}^{-1} + r_{12}^{-1}r_{11}\right)^{-1} d_{11}d_{12}^{-1}d_{11} \end{aligned}\right\} \tag{3.47}$$

Furthermore, for the sub-element jk, the end vector $\mathbf{X}_{jk} = \left\{ \mathbf{q}_j^T \vdots \mathbf{q}_j^T \right\}$ is defined. Then

$$\mathbf{X}_{jk} = \mathbf{C}_{jk}\mathbf{X}_k \tag{3.48}$$

where

$$\mathbf{C}_{jk} = \left[\begin{array}{c|c} \mathbf{g}_{jk} & \mathbf{f}_{jk} \\ \hline \mathbf{g}_{j+1,k} & \mathbf{f}_{j+1,k} \end{array}\right]$$

is a transformation matrix.

While $\mathbf{Y}_k$ has an apparently similar meaning, $\mathbf{X}_k$ is the end vector of the element k. The rotor configuration of the sub-element jk will be expressed by a function satisfying the boundary conditions $\mathbf{X}_{jk}$. The simpler function will be a third degree polynomial:

$$x = \varphi_1(s)x_{j-1} + \varphi_2(s)x_j + \varphi_3(s)u_{j-1} + \varphi_4(s)u_j \tag{3.49}$$

$$u = \varphi_1'(s)x_{j-1} + \varphi_2'(s)x_j + \varphi_3'(s)u_{j-1} + \varphi_4'(s)u_j \tag{3.50}$$

where, if l is the length of the sub-element

$$\begin{aligned} \varphi_1(s) &= \left(1 - \zeta^2 + 2\zeta^3\right) \\ \varphi_2(s) &= 3\zeta^2 - 2\zeta^3 \\ \varphi_3(s) &= l\left(\zeta - 2\zeta^2 + \zeta^3\right) \\ \varphi_4(s) &= \left(-\zeta^2 + \zeta^3\right)l \\ \zeta &= \frac{s}{l} \end{aligned}$$

Differentiating with respect to time:

$$\dot{x} = \varphi_1(s)\dot{x}_{j-1} + \varphi_2(s)\dot{x}_j + \varphi_3(s)\dot{u}_{j-1} + \varphi_4(s)\dot{u}_j \tag{3.51}$$

$$\dot{u} = \varphi_1'(s)\dot{x}_{j-1} + \varphi_2'(s)\dot{x}_j + \varphi_3'(s)\dot{u}_{j-1} + \varphi_4'(s)\dot{u}_j \tag{3.52}$$

Similar expressions hold for y, υ, $\dot{y}$, $\dot{\upsilon}$.

The kinetic energy of the sub-element jk will be

$$\mathrm{T}_{jk} = \frac{1}{2}\sum_{p=1}^{4}\sum_{q=1}^{4}\dot{x}_p\dot{x}_q\overline{\overline{\mathbf{M}}}_{pq} + \frac{1}{2}\overline{\overline{m}}_{jk}\dot{x}_j^2 + \frac{1}{2}J_{jk}\dot{x}_s^2 + \omega\sum_{q=1}^{4}\sum_{p=1}^{4}\dot{x}_p y_q\overline{\overline{\mathbf{N}}}_{pq} - \omega\sum_{q=1}^{4}\sum_{p=1}^{4}x_p\dot{y}_q\overline{\overline{\mathbf{N}}}_{pq} \tag{3.53}$$

where J_{jk} is the moment of inertia of the disk attached at the subnode jk, $\overline{\overline{m}}_{jk}$ the mass of the same disk,

$$\overline{\overline{\mathbf{M}}}_{pq} = \overline{m}_{jk}\Phi_{pq} + \bar{r}_{jk}^2\Psi_{pq}$$

$$\overline{\overline{\mathbf{N}}}_{pq} = \overline{m}_{jk}\bar{r}_{jk}^2\int_0^{l_{jk}}\varphi_p\varphi_q' ds$$

$$\Phi_{pq} = \int_0^{l_{jk}}\varphi_p\varphi_q ds$$

$$\Psi_{pq} = \int_0^{l_{jk}}\varphi_p'\varphi_q' ds$$

$\bar{m}_{jk}$ the mass of the sub-element jk, $\bar{r}_{jk}$ the radius of gyration of the sub-element, and l_{jk} the length of the sub-element.

In view of Eq. (3.48), Eq. (3.53) becomes

$$T_{jk} = \frac{1}{2}\dot{\mathbf{X}}_k^T\tilde{\mathbf{M}}_{jk}\dot{\mathbf{X}}_k + \omega\dot{\mathbf{X}}_k^T\tilde{\mathbf{N}}_{jk}\mathbf{Y}_k - \omega\mathbf{X}_k^T\mathbf{N}_{jk}\dot{\mathbf{Y}}_{jk} \tag{3.54}$$

where

$$\tilde{\mathbf{M}}_{jk} = \mathbf{C}_{jk}^T\bar{\mathbf{M}}_{jk}\mathbf{C}_{jk} + \mathbf{C}_{jk}^T diag(\,m_{jk}\quad J_{jk}\quad 0\quad 0\,)\mathbf{C}_{jk}$$
$$\tilde{\mathbf{N}}_{jk} = \mathbf{C}_{jk}^T\bar{\mathbf{N}}_{jk}\mathbf{C}_{jk} + \mathbf{C}_{jk}^T diag(\,m_{jk}\quad J_{jk}\quad 0\quad 0\,)\mathbf{C}_{jk}$$
$$\bar{\mathbf{M}}_{jk} = \left[\overline{\overline{\mathbf{M}}}_{pq}\right]_{jk}\quad \bar{\mathbf{N}}_{jk} = \left[\overline{\overline{\mathbf{N}}}_{pq}\right]_{jk}$$

The kinetic energy of the element k will be the sum

$$T_k = \sum_{j=1}^{m_k}T_{jk} = \frac{1}{2}\dot{\mathbf{X}}_k^T\mathbf{M}_k^*\mathbf{X}_k + \omega\dot{\mathbf{X}}_k^T\mathbf{N}_k^*\mathbf{Y}_k - \omega\dot{\mathbf{X}}_k^T\mathbf{N}_k^*\dot{\mathbf{Y}}_k \tag{3.55}$$

The energy of the elastic deformation of the sub-element jk is

$$(Ve)_{jk} = \frac{1}{2}\int_0^{l,k} a(s)u_s^2 ds \tag{3.56}$$

After similar steps, one obtains for the energy of elastic deformation of element k:

$$Ve_k = \frac{1}{2}\mathbf{X}_k^T \bar{\mathbf{V}}_k \mathbf{X}_k \tag{3.57}$$

where

$$\bar{\mathbf{V}}_k = \mathbf{C}_{jk}^T \mathbf{S}_{jk} \mathbf{C}_{jk} \quad \mathbf{S}_{jk} = \left[s_{pq}\right]_{jk}(4\times 4)$$
$$s_{pq} = a_{jk}\int_0^{l_{jk}} \varphi_p''(s)\varphi_q''(s)ds$$

and a_{jk} is the flexural rigidity EI of the sub-element jk.

The Lagrangian function is

$$L = \sum_{k=1}^{n}(T_k - Ve_k) \tag{3.58}$$

Application of the Lagrangian equations of motion yields

$$\left.\begin{aligned} \mathbf{M}\ddot{\mathbf{X}} - \omega\mathbf{N}\dot{\mathbf{Y}} + \mathbf{K}\mathbf{X} &= \mathbf{Q}_{X-ext} \\ \mathbf{M}\ddot{\mathbf{Y}} + \omega\mathbf{N}\dot{\mathbf{X}} + \mathbf{K}\mathbf{Y} &= \mathbf{Q}_{Y-ext} \end{aligned}\right\} \tag{3.59}$$

Using the complex displacement vector $\mathbf{Z} = \mathbf{X} + \mathrm{i}\mathbf{Y}$, the Eq. (3.59) become

$$\mathbf{M}\ddot{\mathbf{Z}} + i\omega\mathbf{N}\dot{\mathbf{Z}} + \mathbf{K}\mathbf{Z} = \mathbf{Q}_{Z-ext} \tag{3.60}$$

where $\mathbf{N} = \bar{\mathbf{N}} + \mathbf{N}^T$. The matrices $\bar{\mathbf{N}}$, $\mathbf{M}$ and $\mathbf{K}$ are similar in structure. They consist of the matrices $\mathbf{N}_k^*$, $\mathbf{M}_k^*$ and $\mathbf{V}_k$, respectively. The matrices $\mathbf{M}_k^*$ have a common diagonal with the matrix $\mathbf{M}$, and they start at the row $2k-1$ overlapping with the $\mathbf{M}_{k+1}^*$ by way of adding the common elements. Matrices $\mathbf{N}$ and $\mathbf{K}$ are constructed with the matrices $\mathbf{N}_k^*$ and $\mathbf{V}_k$ in the same way.

We turn now to the computation of the linear external forces. Non-linear terms will be developed later.

External forces acting on the element nodes can be written down immediately. Forces acting on the subnodes give contributions to generalized forces which can be calculated as follows: Given a variation $\delta\mathbf{q}_k$ to the vector $\mathbf{q}_k$, the variation at the subnode jk will be

$$\delta\mathbf{q}_{jk} = g_{jk}\delta\mathbf{q}_k \tag{3.61}$$

Associated with the variation δq_{jk} there are linear forces

$$\mathbf{Q}_{jk} = \mathbf{H}_{jk}\mathbf{q}_{jk}$$

where $\mathbf{H}_{jk}$ is a 2×2 matrix of the linear external forces at the subnode jk.

The work of those forces is

$$\delta W_{jk} = \mathbf{q}_{jk}^T \mathbf{H}_{jk} \delta \mathbf{q}_{jk} \tag{3.62}$$

The total work due to $\delta \mathbf{q}_k$ will be

$$\delta W_k = \left\{ \mathbf{q}_{k-1}^T \sum_{j=1}^{m_{k-1}} \left(\mathbf{g}^T \mathbf{H} \mathbf{f}\right)_{j.k-1} + \mathbf{q}_k^T \left[\sum_{j=1}^{m_k} \left(\mathbf{g}^T \mathbf{H} \mathbf{g}\right)_{jk} + \sum_{j=1}^{m_{k-1}} \left(\mathbf{f}^T \mathbf{H} \mathbf{f}\right)_{j.k-1} \right] + \mathbf{q}_{k+1}^T \sum_{j=1}^{m_k} \left(\mathbf{f}^T \mathbf{H} \mathbf{f}\right)_{jk} \right\} \delta \mathbf{q}_k \tag{3.63}$$

The complex force vector $\mathbf{F}$ associated with the generalized coordinate vector $\mathbf{Z}$ will then be

$$\mathbf{F} = \mathbf{S}\mathbf{Z} \tag{3.64}$$

where the matrix $\mathbf{S}$ has the following 2×2 blocks:

$$\begin{aligned}
&\text{row block } k \quad \text{column block } k+1 \\
&\qquad \mathbf{S}\text{-block} = \sum_{j=1}^{m_{k-1}} \left(\mathbf{g}^T \mathbf{H} \mathbf{F}\right)_{j.k-1} \\
&\text{row block } k \quad \text{column block } k+1 \\
&\qquad \mathbf{S}\text{-block} = \sum_{j=1}^{m_k} \left(\mathbf{g}^T \mathbf{H} \mathbf{g}\right)_{jk} + \sum_{j=1}^{m_{k-1}} \left(\mathbf{f}^T \mathbf{H} \mathbf{f}\right)_{j.k-1} \\
&\text{row block } k \quad \text{columnblock } k+1 \\
&\qquad \mathbf{S}\text{-block} = \sum_{j=1}^{m_k} \left(\mathbf{f}^T \mathbf{H} \mathbf{g}\right)_{jk}
\end{aligned}$$

Additional forces arise due to the internal friction of the shaft material. This damping appears in two forms [44–46]:

(a) Hysteretic damping, which gives rise to forces proportional to the elastic forces and lagging them by an angle $\pi/2$. They can be expressed as the vector

$$\mathbf{F}_{hyst} = -i\gamma_o \mathbf{K}\mathbf{Z} \tag{3.65}$$

The factor γ_0, the loss factor due to hysteric damping is independent of the rotating speed.

(b) Linear viscoelastic damping, which is associated with forces in the direction of and in proportion to the lateral velocities in a rotor-fixed coordinate system. In the system (x, y, s) it can be expressed as

$$\mathbf{F}_{visc} = -\gamma_1 \mathbf{K}\dot{\mathbf{Z}} + \gamma i\omega_1 \mathbf{K}\mathbf{Z} \tag{3.66}$$

where γ_1 is the viscoelastic loss factor, dependent on speed (Eq. 3.12).

Finally, the equations of motion become

$$\mathbf{M}\ddot{\mathbf{Z}} + (\gamma_1 \mathbf{K} + i\omega \mathbf{N})\dot{\mathbf{Z}} + [1 - i(\gamma_o + \gamma_1 \omega)]\mathbf{K}\mathbf{Z} = \mathbf{S}\mathbf{Z} + \mathbf{F}\left(\mathbf{Z}, \dot{\mathbf{Z}}\right) \tag{3.67}$$

where $\mathbf{F}\left(\mathbf{Z}, \dot{\mathbf{Z}}\right)$ is a vector of the non-linear forces depending, in general, on the displacements $\mathbf{Z}$ and velocities $\dot{\mathbf{Z}}$.

In the special case of a rotor with mass lumped at the nodes, the matrix $\mathbf{M}$ is diagonal, in general, it is a banded matrix, positive definite and it possesses an inverse $\mathbf{M}^{-1}$. The equations of motion take the form

$$\ddot{\mathbf{Z}} + (\gamma_1 \mathbf{L} + i\omega \mathbf{L}_2)\dot{\mathbf{Z}} + (1 - i\eta)\mathbf{L}\mathbf{Z} = \mathbf{L}_1 \mathbf{Z} + \mathbf{F}^*\left(\mathbf{Z}, \dot{\mathbf{Z}}\right) \tag{3.68}$$

where $\mathbf{L}=\mathbf{M}^{-1}\mathbf{K}$, $\mathbf{L}_1=\mathbf{M}^{-1}\mathbf{S}$ and $\mathbf{F}^*=\mathbf{M}^{-1}\bar{\mathbf{F}}$, $\mathbf{L}_2\mathbf{M}^{-1}\mathbf{N}$.

Questions about natural vibration or imbalance response can be answered by work along known lines with a linearization of Eq. (3.68) around the equilibrium point.

In general, the equilibrium state is not the static deflection of the rotor, but the solution of the system of non-linear algebraic equations

$$[(1 - i\eta)\mathbf{L} - \mathbf{L}_1]\mathbf{Z}_0 - \mathbf{F}(\mathbf{Z}_0, 0) = 0 \tag{3.69}$$

A Newton–Raphson method can be used to yield the state of equilibrium $\mathbf{Z}_0$. Since this state is usually very close to the static deflection of the rotor superposed on the equilibrium points of the bearings at the running speed, the solution $\mathbf{Z}_0$ is obtained with a small number of iterations.

The vector $\mathbf{Z}$ is now redefined with a parallel transformation $\bar{\mathbf{Z}} = \mathbf{Z} - \mathbf{Z}_0$ and the non-linear force vector $\bar{\mathbf{F}}\left(\bar{\mathbf{Z}}, \dot{\bar{\mathbf{Z}}}\right) = \mathbf{F}\left(\mathbf{Z}, \dot{\mathbf{Z}}\right) - \mathbf{F}^*(\mathbf{Z}_0, 0)$. The equations of motion become

$$\ddot{\bar{\mathbf{Z}}} + (\gamma_1 \mathbf{L} + i\omega \mathbf{L}_2)\dot{\bar{\mathbf{Z}}} + (1 - i\eta)\mathbf{L}\bar{\mathbf{Z}} = \mathbf{L}_1 \bar{\mathbf{Z}} + \bar{\mathbf{F}}\left(\bar{\mathbf{Z}}, \dot{\bar{\mathbf{Z}}}\right) \tag{3.70}$$

The equilibrium of this system is the zero vector.

If the bearings are assumed at the nodes $k1$ and $k2$, and no other non-linear forces are imposed on the system, a situation most common in rotors, the vector $\bar{\mathbf{F}}$ has only two non-zero components $\mathbf{F}_{2k1+1}$ and $\mathbf{F}_{2k2+1}$ of the form

$$\left.\begin{aligned} B_1 = F_{2k1+1} &= \bar{g}_{11}(x_{k1}, y_{k1}) + \bar{g}_{12}(x_{k1}, y_{k1})\dot{x}_{k1} + \bar{g}_{13}(x_{k1}, y_{k1})\dot{y}_{k1} \\ B_2 = F_{2k2+1} &= \bar{g}_{21}(x_{k2}, y_{k2}) + \bar{g}_{22}(x_{k2}, y_{k2})\dot{x}_{k2} + \bar{g}_{23}(x_{k2}, y_{k2})\dot{y}_{k2} \end{aligned}\right\} \tag{3.71}$$

The linearised form of these forces is obtained by a Maclaurin expansion, retaining only linear terms in $x, y, \dot{x}$ and $\dot{y}$:

$$B_j = \left[K_{jxx}K_{jyx}C_{jxx}C_{jyx}\right]\{x \quad y \quad \dot{x} \quad \dot{y}\} + i\left[K_{jyy}K_{jxy}C_{jyy}C_{jxy}\right]\{x \quad y \quad \dot{x} \quad \dot{y}\} \tag{3.72}$$

where j takes the values 1 and 2 and the coefficients K and C are the spring and damping coefficients of the bearings. These forces are incorporated in two matrices $\bar{\mathbf{V}}$ and $\bar{\mathbf{W}}$ to yield equations of motion in the form

$$\ddot{\bar{\mathbf{Z}}} + (\gamma_1\mathbf{L} + i\omega\mathbf{L}_2)\dot{\bar{\mathbf{Z}}} + (1 - i\eta)\mathbf{L}\bar{\mathbf{Z}} = \mathbf{L}_1\bar{\mathbf{Z}} + \mathbf{V}\bar{\mathbf{Z}} + \mathbf{W}\dot{\bar{\mathbf{Z}}} + \mathbf{R} \tag{3.73}$$

Where $\mathbf{V} = \mathbf{M}^{-1}\bar{\mathbf{V}}$ and $\mathbf{W} = \mathbf{M}^{-1}\bar{\mathbf{W}}$, while $\mathbf{R}$ is a vector with the higher order terms of Maclaurin expansion.

It is very unlikely that one will have the full form of Eq. (3.73) in actual systems. In fact, the most common situations are the following:

(a) Electrical machines, motors and generators. The linear terms $\mathbf{L}_1$ are very small and $\mathbf{L}_1$ is diagonal. The matrices $\mathbf{V}$ and $\mathbf{W}$ contain both coupling and cross-coupling terms which are functions of the rotating speed ω.
(b) Turbines, compressors. In cases where certain non-diagonal elements of the matrix $\mathbf{L}_1$ have a significant value, tilting pad bearings are utilized which do not have significant cross-coupling terms in the matrices $\mathbf{V}$ and $\mathbf{W}$. The matrix $\mathbf{L}_1$ is a function of the speed and load of the machine.

In these situations two types of instability are encountered:

(a) In the process of accelerating the rotor, there is a threshold speed after which the operation is unstable. Usually at this stage the load-dependent matrix $\mathbf{L}_1$ has only zero components. The problem is to find the rotor speed ω for which the system is unstable.
(b) When the rotor reaches its normal operating speed the load starts increasing and at a certain critical value the operation becomes unstable. At this stage the speed-dependent matrices $\mathbf{V}$ and $\mathbf{W}$ remain constant while the load-dependent matrix $\mathbf{L}_1$ changes with the load.

Finally, the system of Eq. (3.73) will be normalized as follows: The perturbation vector

$$\mathbf{x} = \left\{\mathbf{x}_1 \vdots \mathbf{x}_2 \vdots \ldots \vdots \mathbf{x}_{n+1}\right\}$$

is defined where

$$\mathbf{x}_j = \left\{x_j u_j y_j v_j \dot{x}_j \dot{u}_j \dot{y}_j \dot{v}_j\right\}$$

Then Eq. (3.73) becomes

$$\dot{\mathbf{x}} = \mathbf{A}\mathbf{x} + \mathbf{f}(x) \tag{3.74}$$

where the matrix **A** consists of $(n + 1)^2$ blocks a_{ij} ($i, j = 1,2,\cdots n + 1$), and the vector **f** contains higher order terms of the non-linear forces. One should assume that the non-linear functions of the vector **f** are continuous and have a sufficient number of continuous partial derivatives, in the case of non-linear forces due to dry friction with stationary components, these features does not usually exist and one has to resort to numerical methods.

According to Liapunov's first theorem, [47–50] Eq. (3.74) is asymptotically stable if all the eigenvalues are given by the equation

$$|\mathbf{A} - \lambda \mathbf{I}| = 0 \tag{3.75}$$

where **I** is the diagonal unit matrix and λ the eigenvalue. The imaginary parts of the roots of this algebraic equation are the damped natural frequencies of the system at the operating speed ω. These frequencies will coincide with the critical speeds if we set $\omega = \lambda$ in the elements of the matrix $\mathbf{A}(\omega, \sigma)$.

Let $\mathbf{A}(\omega, \sigma)$ be the matrix of Eq. (3.74). The threshold of instability is at the point where the real part of one eigenvalue of Eq. (3.75) becomes positive, crossing the zero line. Because of the continuity, we can conclude that at the threshold one eigenvalue of the system has only an imaginary part. The substitution $\lambda = i\omega_n$ in Eq. (3.75) yields the determinant

$$|\mathbf{A}(\omega, \sigma) - i\omega_n \mathbf{I}| = 0 \tag{3.76}$$

The two types of instability mentioned before, namely speed-and load-controlled, correspond to the following formulation:

(a) *Speed-controlled instability* ($\sigma = 0$)

$$F(\omega, \omega_n) = |\mathbf{A}(\omega, 0) - i\omega_n \mathbf{I}| = 0 \tag{3.77}$$

(b) *Load-controlled instability* ($\omega = constant$)

$$F(\sigma, \omega_n) = |\mathbf{A}(\omega, \sigma) - i\omega_n \mathbf{I}| = 0 \tag{3.78}$$

Each equation yields two algebraic, real and non-linear equations in the unknowns ω, ω_n, and σ, ω_n respectively. The existence of such solutions will mean instability. This question was investigated by means of a digital computer and the Newton-Raphson method. Application to turbo rotors yielded the following observations:

(a) For speed-controlled instability, an unstable speed was found associated with a whirl speed ω_n of the order of the critical speed. Many unsuccessful attempts were made for higher whirl speeds.

(b) For load-controlled instability, if the operating speed is below the unstable speed, there is a threshold load σ at whirl speeds ω_n, again of the order of the critical speed. The deviation of the whirl speed from the critical speed is due to the gyroscopic terms of ω in Eq. (3.76). Instabilities at high whirl speeds were not discovered. Details of numerical examples are given in Ref. [31].

In case of load-controlled instabilities of large steam turbines the following sequence of events was observed: At low speeds the rotor has a synchronous vibration due to residual imbalance. At increasing loads a whirl starts developing at speeds close to the first critical speed with amplitude which is a monotonic function of the load. At a load as high as 200 % of the load at which the whirl started, the whirl orbit jumps to a very high amplitude. At this point, the orbit is sometimes not only unstable, but shows an almost random character.

The low level, stable whirl occurs at a wide range of loads and it would be an unnecessary limitation to consider as unstable the operations at the appearance of the whirl, which must be the instability predicted with the first Liapunov theorem. Therefore, other methods must be employed for the study of the system.

To this end, Eq. (3.74) has been solved as an initial value problem with numerical integration. Fourth-order Runge–Kutta and as Adams–Moulton predictor–corrector methods were used.

The fact that the number of degrees of freedom is small is equivalent to observing the system operation from a window of a low number of frequencies, which makes the numerical methods sufficiently stable. The assurance of numerical stability is obtained by way of using half the integration step. A sample layout of such an integration, for a large steam turbine rotor is given in Figs 3.8, 3.9, 3.10 corresponding to limit cycle (engineering stability), stability, and instability, respectively.

The obvious place to look for limit cycles is the non-linearity of the bearings. To do this, we shall study the case of load-controlled instability. In this case the bearings are of the tilting pad type and, for simplicity; four-pad bearings are considered which are isotropic. Therefore the equations can be considered in the complex form.

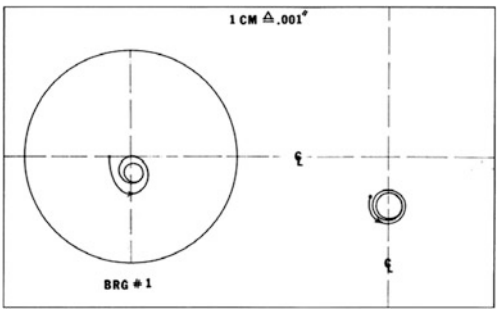

Fig. 3.8 Limit cycles of rotor orbits (from Ref. [34] by permission)

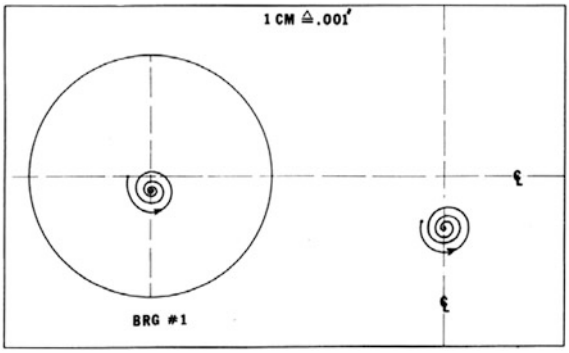

Fig. 3.9 Stable rotor orbits (from Ref. [34] by permission)

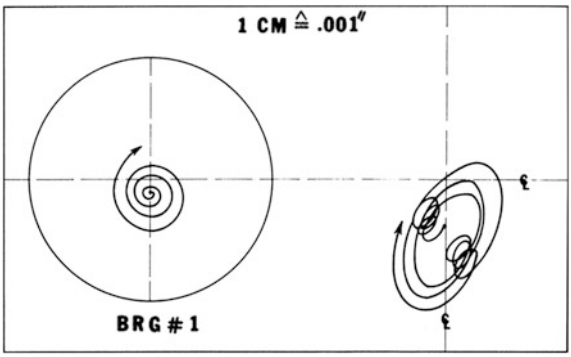

Fig. 3.10 Unstable rotor orbits (from Ref. [34] by permission)

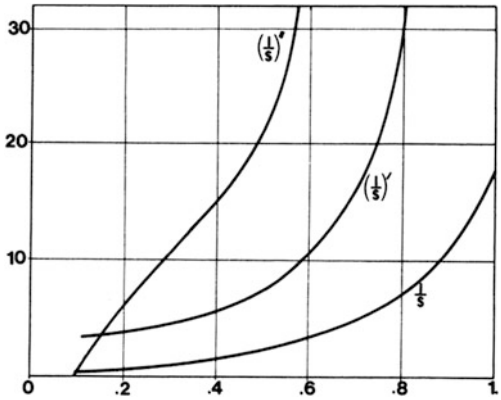

Fig. 3.11 Derivatives of the force-eccentricity function (from Ref. [32] by permission)

The bearing force R is given [32] as a function of the eccentricity ratio as

$$R = f(e) = f\left(\frac{|z|}{c}\right) \tag{3.79}$$

where c is the bearing radial clearance and e is the eccentricity ratio.

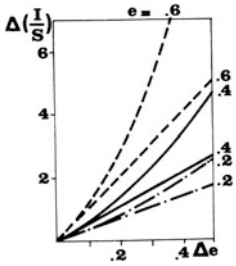

Fig. 3.12 Non linear force-functions (from Ref. [34] by permission)

An expansion of the function R around the point of equilibrium yields

$$R = ef' + \frac{e^2}{2}f'' + \ldots|_{e=eo} \tag{3.80}$$

The first derivative $f'(e)$ at $e = e_o$ is the bearing spring coefficient ε_o and the second $f''(e)$ at $e = e_o$ is the second bearing coefficient ε_1. For $\bar{z}$ denoting deviations from the equilibrium, one obtains

$$R - R_0 = \varepsilon_0 \bar{e} + \frac{\varepsilon_1}{2}\bar{e}|\bar{e}| + \ldots \tag{3.81}$$

where $\bar{e} = \bar{z}/c$.

For a tilting four-pad bearing [50], the function $f(e)$ and its derivatives have been plotted on Fig. 3.11.

For values of the Sommerfeld number equal to 0.2, 0.4 and 0.6, which cover the range of typical turbine bearings, Fig. 3.12 illustrates the bearing force versus the deviation from equilibrium $\bar{e}$, based on data from Ref. [51].

The non-linearity is apparent. For example, for a vibration amplitude $\bar{e} = 0.3$, which is within acceptable limits for turbomachinery, the deviation from linearity is 19, 39, 63 % for e = 0.2, 0.4 and 0.6, respectively.

For general bearings the situation is more complicated because the nearing forces depend on x and y and not only on z. this situation is treated in detail elsewhere [35, 52–58]

To study the feasibility of a limit cycle, solutions are sought in the form

$$\bar{\mathbf{Z}} = \boldsymbol{\rho}\exp(ipt) \tag{3.82}$$

The components of $\mathbf{R}$ will be $\varepsilon_j \boldsymbol{\rho}_j^2 \exp(ipt)$ where ε_j are the coefficients of the second-order term, if the Maclaurin expansion of the non-linear bearing forces, Eq. (3.67) becomes

$$\left[-mp^2\mathbf{I} + ip(\gamma_1\mathbf{L} + i\omega\mathbf{L}_2) + (1 - \eta i)\mathbf{L} - \mathbf{L}_1 - \mathbf{V} - ip\mathbf{W}\right]\boldsymbol{\rho} + \varepsilon\boldsymbol{\rho}_0\boldsymbol{\rho} = 0 \tag{3.83}$$

where $\boldsymbol{\rho}_o = diag\left(\rho_1\rho_2\ldots\rho_{n+1}\right)$. Equation (3.80) has of course a trivial solution but, under certain conditions, it has additional solutions because of its non-

linearity. To demonstrate this, the simplest case of one node will be considered. Equation (3.83) becomes

$$\left(-mp^2 + K + iS + ipC\right)\rho + \varepsilon\rho^2 = 0 \tag{3.84}$$

where K is the bearing spring constant, C its damping constant, S the force due to steam flow, ε the bearing second stiffness coefficient. Equation (3.84) yields

$$p = \frac{S}{C}\,\rho = \frac{m(S/C)^2 - K}{\varepsilon} \tag{3.85}$$

The limit orbit has to be positive. This yields

$$S > C\sqrt{K/m} \tag{3.86}$$

At the onset $S = C\sqrt{K/m}$, the whirl frequency is

$$p = \sqrt{K/m} = \omega_{cr} \tag{3.87}$$

where ω_{cr} is the critical speed. This, qualitatively, confirms experimental observations. Applying finite perturbation to the limit orbit solution (Eq. 3.84) it was proved that this solution is stable for all values of the parameters involved, admissible under Eq. (3.87). The jumping phenomenon observed in practice and in numerical solutions cannot be observed in this model, without taking higher order approximations to the bearing non-linearities.

3.4 Summary and Conclusions

Up to this point we have discussed special shafts of very simple geometry. Such models are useful in extracting qualitative results and general features. For many engineering systems, one has to take into account realistic geometries and boundary conditions thus, leading to the application of direct methods of analysis as the ones presented in this chapter. Of course, masses concentrated at a point, rigid bodies, elastic massless members, and linear properties do not exist in nature. But if one can conceive such systems, they can have exact solutions. The most commonly used method for engineering systems is the transfer matrix method. Attention must be paid to the fact of coupling between horizontal and vertical vibration. If there is an element in the system, such as a fluid bearing, which couples the vertical and horizontal vibration, the state vector should include the state parameters in both directions. Analysis in two planes needs to be used with great care and only if the cross-coupling terms due to the bearings and gyroscopic effects are of substantial magnitude. Thermal unbalance due to rubbing effects, and bending of shafts, depending on the geometric and thermoelastic characteristics of the system, has to be also considered, this issue is presented in detail in Chap. 8. Rotor dynamic analyses are coded in Refs. [31, 55] followed by illustrating

examples. Codes for analyses refer to vibration modes with animation, torsional critical speeds, dynamic response, nonlinear response, cracked or misaligned rotor response, nonlinear analysis, vibration analysis, and balancing.

References

1. Newkirk, B.L., Taylor, H.D.: Shaft whipping due to oil action in journal bearings. Gen. Electric Rev. **28**, 559–568 (1925)
2. Newkirk, B.L.: Shaft whipping. Gen. Electric Rev. **27**, 169–178 (1924)
3. Kimpball, A.L.: Internal friction theory of shaft whipping. Gen. Electric Rev. **27**, 244–251 (1924)
4. Kimpball, A.L.: Measurement of internal friction in a revolving deflected shaft *Gen*. Electric Rev. **28**, 554–558 (1925)
5. Stodola, A.: Steam and Gas Turbines. McGraw-Hill, New York (1927)
6. Dimentberg, F.M.: Flexural vibration of rotating shafts (Transl. from Russian). Butterwortths, London (1961)
7. Tondl, A.: Some problems of rotor dynamics (Transl. From Chech.). Chapman and Hall, London (1965)
8. Ehrich, F.: Handbook on Rotordynamics. McGraw-Hill, New York (1992)
9. Childs, D.: Turbomachinery Rotordynamics: Phenomena, Modeling and Analysis. Wiley, New York (1993)
10. Lalanne, M., Ferraris, G.: Rotordynamics Prediction in Engineering, 2nd ed. Wiley, New York (1998)
11. Yamamoto, T., Ishida, S.: Linear and Nonlinear Rotor Dynamics. John Wiley, New York (2001)
12. Loewy, R., Piarulli, V.J.: Dynamics of Rotating Shafts. Naval Publishing and Printing Office Service, Washington D.C. (1971)
13. Hagg, A.C., Sankey, G.O.: Oil film properties for unbalance vibration calculations. J. Appl. Mech. Trans. ASME **25**(4), 141–143 (1958)
14. Dimarogonas, A.D.: Newkirk effect: thermally induced dynamic instability of high speed rotors. ASME Paper Issue 73 GT-26, 1–11 (1973)
15. Vatta, F., Vigliani, A.: Internal damping in rotating shafts. Mech. Mach. Theory **43**, 1376–1384 (2008)
16. Dimentberg, M.F.: Vibration of a rotating shaft with randomly varying internal damping. J. Sound Vibr. **285**(3), 759–765 (2005)
17. Samantaray, A.K., Mukherjee, A., Bhattacharyya, R.: Some studies on rotors with polynomial type non-linear external and internal damping. Int. J. Non-Linear Mech. **41**, 1007–1015 (2006)
18. Montagnier, O., Hochard, C.: Dynamic instability of supercritical drive shafts mounted on dissipative supports—effects of viscous and hysteretic internal damping. J. Sound Vibr. **305**, 378–400 (2007)
19. Rimpel, A., Kim, D.: Rotordynamic performance of flexure pivot tilting pad gas bearings with vibration damper. J. Tribol. **131**(2), 1–12 (2009)
20. Cloud, C.H., Maslen, E.H., Barrett, L.E.: Rotor stability estimation with competing tilting pad bearing models. Mech. Syst. Signal Process. **29**, 90–106 (2012)
21. Schweizer, B.: Total instability of turbocharger rotors—physical explanation of the dynamic failure of rotors with full-floating ring bearings. J. Sound Vibr. **328**(1, 2), 156–190 (2009)
22. Moore, J.J.: Three-dimensional CFD rotordynamic analysis of gas labyrinth seals. J. Vib. Acoust. Trans. ASME 125(4), 427–433 (2003)

23. Gao, L., Dai, Y., Wang, Z., Xu, Y., Ma, Q.: Rotordynamic stability under partial admission conditions in a large power steam turbine. Proc. ASME Turbo Expo 6 (Part B), 795–802 (2009)
24. Pennacchi, P., Vania, A.: Analysis of the instability phenomena caused by steam in high-pressure turbines. Shock Vibr. **18**(4), 593–612 (2011)
25. Pugachev, A.O., Kleinhans, U., Gaszner, M.: Prediction of rotordynamic coefficients for short labyrinth gas seals using computational fluid dynamics. J. Eng. Gas Turbines Power **134**, 062501 (2012)
26. Jiang, P.N., Wang, W.Z., Liu, Y.Z., Meng, G.: Influence of steam leakage through vane, gland, and shaft seals on rotordynamics of high-pressure rotor of a 1,000 MW ultra-supercritical steam turbine. Arch. Appl. Mech. **82**(2), 177–189 (2012)
27. Duchemin, M., Berlioz, A., Ferraris, G.: Dynamic behavior and stability of a rotor under base excitation. J. Vib. Acoust Trans. ASME **128** (5), 576–585 (2006)
28. Das, A.S., Dutt, J.K., Ray, K.: Active vibration control of unbalanced flexible rotor-shaft systems parametrically excited due to base motion. Appl. Math. Model. **34**(9), 2353–2369 (2010)
29. Gaganis, B. J., Zisimopoulos, A. K., Nikolakopoulos, P. G., Papadopoulos, C. A.: Modal analysis of rotor on piecewise linear journal bearing under seismic excitation, Trans. ASME. J. Vib. Acoust. Trans. ASME **121**(2), 190–196 (1999)
30. Bückner, H.F.: Notes on Mechanics. Rennselaer Polytechnic Institute, Troy, N.Y. (1970)
31. Dimarogonas, A. D.: Vibration for Engineers Second Edition Prentice Hall Upper Saddle River, New Jersey (1996)
32. Timoshenko, S.: Thèorie des Vibrations. Beranger, Paris (1947)
33. den Hartog, P.: Mechanical Vibrations. Mc Graw-Hill, New York (1956)
34. Dimarogonas, A.D.: A general method for stability analysis of rotating shafts. Ing. Arch. **44**, 9–20 (1975)
35. Andritsos, F.E., Dimarogonas, A.D.: Nonlinear pad functions for static analysis of tilting pad bearings, ASME Trans. J. Lubrication Technol. **102/25**, 25–33 (1980)
36. Landzberg, A.H.: Stability of a turbine-generator rotor including the effects of certain types of steam and bearing exictations. ASME Trans. J. Appl. Mech. **27**, 410–420 (1960)
37. Vogel, D.H.: Das Schwingungs und Stabilitatsverhalten unwuchthchafteter, mehrfeldriger Wellen auf Gleitlagern. Konstruction **22**, 461–466 (1970)
38. Lund, J.W.: Stability and damped critical speeds of a flexible rotor in fluid-film bearings. ASME-paper 73-DET-103 (1973)
39. Gasch, R.: Selbsterregte biegeschwingungen rotierender wellen. Konstruktion **23**, 5 (1971)
40. Shen, F.A.: Transient flexible-rotor dynamics analysis; Part I-theory. Trans. ASME J. Eng. Ind. **94**, 531-542 (1972)
41. Kirk, R.G.: Nonlinear transient analysis of multi-mass flexible rotors-theory and applications. NASA CR-2300 (1973)
42. Ruhl, R.L., Booker, J.F.: A finite element model for distributed parameter turborotor systems. ASME-Paper 71-Vibr-56 (1971)
43. Pestel, E.C., Leckie, F.A.: Matrix Methods in Elastomechanics. McGraw-Hill, New York (1963)
44. Lazan, B.J.: Damping of Materials and Members in Structural Mechanics. Pergamon Press, Oxford (1968)
45. Thomas, H.J.: Instabile eigenschwingungen von turbinenlaufern, angefacht durch die spaltstromungen in stopfbuchsen und beschaufelungen. Bull. de l' AIM **71**, 1039–1064 (1958)
46. Gunter, E.J., Jr.: Dynamic stability of rotor-bearing systems. NASA Report No NAS3-6473 (1966)
47. Pontryagin, L.S.: Ordinary differential equations (Transl. from Russian). Addison-Wesley, Reading, Mass (1962)
48. Lasalle, J., Lefschetz, S.: Stability by Liapunov's Direct Method. Pergamon Press, New York, London (1961)

49. Routh, E.J.: The Advanced Part of a Treatise on the Dynamics of a System of Rigid Bodies, 6th edn. Dover, New York (1955)
50. Hourwitz, A., Courant, R.: Vorlesungen überallgemeine Funktionen-theorie und Elliptische Funktionen. Springer, Berlin (1939)
51. Mechanical Technology, Inc.: Rotor-bearing dynamic design technology, Part III: design handbook for fluid film type bearings, AFAPL-TR-65-45 (1965)
52. Dimarogonas, A.D.: A brief history of rotor dynamics. In: Rotordynamics, vol. 92. Springer, Venice (1992)
53. Dimarogonas, A. D.: Limit cycles for pad beatings under fluid excitation. STLE Transactions **31**(1), 66–70 (1987)
54. Dimarogonas, A. D.: MELAB: Computer programs for Mechanical Engineers. Englewood Cliffs N.J., Prentice-Hall (1993)
55. Dimarogonas, A.D., Gomez-Mancilla, J.: Flow excited turbine rotor instability. Int. J. Rotating Mach. **1**(1), 37–51 (1994)
56. Dimarogonas, A.D.: Vibration of cracked structures—a state of the art review. Eng. Fract. Mech. **55**(5), 831–857 (1996)
57. Ji, Z., Zu, J.W.: Method of multiple scales for vibration analysis of rotor-shaft systems with non-linear bearing pedestal model. J. Sound Vibr. **218**(2), 293–305 (1998)
58. Bonello, P., Brennan, M.J.: Modelling the dynamic behaviour of a supercritical rotor on a flexible foundation using the mechanical impedance technique, J. Sound Vibr. **239**(3), 445–466 (2001)

Chapter 4
Flow-Induced Vibration of Rotating Shafts

Abstract Chapter 4 deals with flow-induced vibration of rotors and in particular with the most important case, known as 'steam whirl', often appearing in large steam turbines. Stability criteria, Thomas Stability Criterion and Torque-Deflection Number are applied and compared. Vibration of rotors in fluid annuli occurs due to dynamic interaction of cylinders with the surrounding fluid in parallel or cross-flow. The integrated effect of pressure and dynamic fluid forces generated results to imbalance. Application of Hurwitz-Routh determinants is used for checking stability conditions. Self-excited vibration of a rotating hollow shaft partially filled with viscous liquid occurs within a certain range of rotating speed. Approximate solutions of the equations of motion for the non-dimensional time-dependent radial and circumferential velocity of a small internal liquid element yield non-dimensional liquid forces and, furthermore, stability limits for the rotor. The marginal condition under which the system becomes absolutely stable is investigated.

4.1 The Steam Whirl Problem

In the 1940s, two non-condensing turbines built by General Electric Company, designed very differently from the previous ones, and having very flexible rotors, experienced violent whirl at high loads [1]. This whirl could not be corrected by balancing and appeared at high loads only. To cure the trouble, the machines were modified with completely new rotors or pad bearings or both. It was later recognised that forces due to steam flow contributed to this instability. Alford [2] reported that modification to the steam path largely eliminated the problem. There is conflicting information of these two cases. We know, however, that an empirical stability criterion resulted from an investigation related to these two unstable turbines, the Torque Deflection Number (TDN). Later, in 1956, Thomas [3] reported similar problems with AEG turbines, and the efforts to study this

A. D. Dimarogonas et al., *Analytical Methods in Rotor Dynamics*,
Mechanisms and Machine Science 9, DOI: 10.1007/978-94-007-5905-3_4,

phenomenon both analytically and experimentally. Thomas indicated some of the sources of the excitation, and developed a stability criterion based on a combination of analytical results and experimental calibration. He concluded that the excitation originated from the steam flow through the packing clearances, and the stabilizing effect came from damping forces. He also reported that the problem was corrected mainly by decreasing the span and thus raising the critical speed, and sometimes by bearing changes. Thomas and Alford agreed that the vibration occurred at frequencies equal to the critical speed of the rotor. Alford, however, stated that variation of the whirl speed in jet engines was associated with a wide range of parameters, depending on the amplitude and the test conditions.

In the late 1960s the problem arose again, and several papers published in Germany dealt with the problem along the lines followed by Thomas [4–7]. Later, Black [8] applied simplified analyses for similar phenomena on high speed centrifugal pump rotors. He also identified instabilities due to local reversed flows at very low flow rates of the pumps. Shapiro and Colsher [9] studied the influence of bearings on steam whirl; Pollman et al. [10] and Wright [11] concentrated on the development of the excitation mechanisms due to flow in turbines and reported on measurements of the forces due to flow. The excitation coefficient for labyrinth seals and shrouded blade row seals for whirling shafts is calculated assuming standard fluid dynamic behavior by Kwanka et al. [11] and Pugachev et al. [12] Rotor bearing instability, effect of the destabilizing steam forces on the rotor at the first row, effect of the seal rotordynamic forces and the valve opening sequence on the rotor stability were studied analytically to interpret vibrations affected to 300 MW steam turbine rotors at certain loads [13].

A case history of a steam turbine that experienced a heavy steam-whirl instability though the stability margin in design conditions, calculated by the turbine manufacturer according to a consolidated methodology, was sufficiently high was studied by Bachschmid et al. [14], Pennacchi et al. [15] studied instability phenomena in steam turbines caused by certain characteristics of the steam flow as well as of the mechanical and geometrical properties of the seals. They modeled the eigenvalues and eigenvectors change due to the cross coupled coefficients from steam pressure and velocity, and the seal stiffness. The threshold level of the steam flow that causes instability conditions was analyzed and used to define the stability margin of the power unit [16].

Dimarogonas [17–19] presented a method of treating the problem in a very general way and some results of this analysis, applicable to the whirl problem of turbine rotors, are presented in this chapter.

Thomas [3] was the first to identify one of the stimuli, the forces due to leakage flow through the packing clearances. Figure 4.1 shows an eccentric stage. We observe that at the area of smaller clearances there is less leakage, and therefore more steam is available to produce shaft work. Consequently the peripheral force at this point will be greater than at the area of high clearances. The result is a net force perpendicular to the deflection and in the direction of rotation. Assuming that the efficiency of the stage is, to a first approximation, a linear function of the clearance, we can conclude that the lateral force is proportional to the deflection. The coefficient of proportionality K_s will be called the steam force gradient, $K_s = \partial U/\partial\delta$.

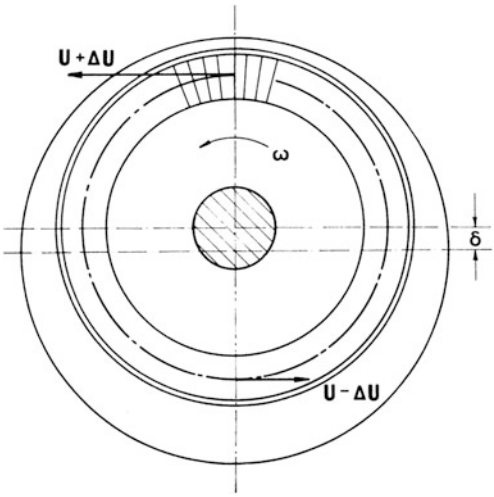

Fig. 4.1 Unequal tangential forces in an eccentric stage

The same situation exists for flow through the shaft packings. Therefore, the steam force gradient K_s consists of two terms and we have [3]

$$\frac{\partial U}{\partial \delta} = \frac{U}{2h}\left[a\left(\frac{d_n}{d_m}\right)^2 \frac{\varphi\sqrt{2gH}}{C_2 \sin a_2\sqrt{z}} + \beta\left(1 + \frac{h}{d_m}\right)\right] \tag{4.1}$$

where

U = peripheral force,
δ = shaft deflection,
h = nozzle height,
d_n = shaft diameter,
d_m = pitch diameter of stage,
H = adiabatic drop of stage,
ϕ = velocity coefficient,
C_2 = absolute exit velocity,
α_2 = exit angle,
Z = number of packing teeth,
g = acceleration due to gravity.

We recognise immediately the two terms in the bracket as representing a gradient due to leakage at the shaft and bucket packings, respectively. The two coefficients α and β are calibration constants determined experimentally. They account for secondary factors, such as circumferential flow, pressure equalising holes and other effects on efficiency. Thomas determined them experimentally. Therefore, in his work, other mechanisms for steam gradients have also been taken into account in these constants. A more accurate expression for the term due to bucket leakage can be used, similar to one for the shaft packings [4–6, 20].

Thomas [3] derived a criterion for stability based on these forces and considering the damping as a logarithmic decrement. Although Thomas's work has theoretical

flaws, it could be used for comparison of stability, even for prediction, for similar machines, since enough empirical factors have been introduced which are established by experiments in similar machines. It is unfortunate that this work, carried out in 1955, has not stimulated further interest in the subject at an earlier stage.

Alford [2] proposed another model for the axial flow around a bucket cover, assuming no effects of circumferential flow and considering variation of static pressure in a two-teeth bucket packing due to the motion of the shaft. This phenomenon appears to contribute to the problem only when the upstream tooth clearance is greater than the downstream one, and does not seem to have a considerable effect in practical situations.

Flow around eccentric cylinders without axial flow effects has been studied by Yamada et al. [21–23]. The result of this flow is that the misalignment is accompanied by a force which is not in phase with it but which has radial and circumferential components. Their magnitude appears to be small compared with the Thomas model. However, this model does not take into account axial flow, nor the fact that the steam entering the cavity might have a peripheral velocity greater than the peripheral velocity of the stage.

Adequate treatment of this subject is not available yet. In general, we shall consider the force due to an eccentricity of the stage i as a linear function of δ:

$$F_s = \delta s_r i_r + \delta s_t i_t \tag{4.2}$$

where S_r and S_t are constants of the particular stage at the rated steam flow. This is not a necessary restriction for the calculation method [19] but it is a convenient way of extracting general features of the whirl phenomenon. Information of this type is commonly available from the turbine manufacturers.

Another factor stimulating instability is the internal damping of the material and dry friction between the rotor components [24, 25]. This is expressed as a material damping factor γ which, in this work, is defined as follows: Assuming that the shaft runs in very small bearing clearances at a constant speed Ω, a vertical displacement δ results in a horizontal force perpendicular to the displacement δ and in the direction of rotation with magnitude (see Chap. 3):

$$F_t = \frac{k_r \gamma \Omega}{\Omega - \omega_n} \tag{4.3}$$

We consider γ invariant with speed, at least in the ranges of interest. Lazan gives values of γ for several rotor materials [25]. The internal damping alone has shown itself capable of inducing instability. From its definition we see that it is very similar to the steam force gradients and thus the steam and the internal damping whirl phenomena are of a similar nature. In fact, in most practical situations they coexist and both contribute to instability. A very interesting difference is that the steam force gradient is proportional to the absolute deflection of the rotor from the concentric position, no matter how the journals move, whereas the internal damping force is proportional to the deflection of the rotor itself, i.e. the deflection of the midspan from a straight line which connects the journals.

Therefore, for very stiff rotors, the internal damping is negligible and the steam force prevails. In the case of more elastic rotors, the internal damping possesses an increasing importance.

Fluid bearings react to displacements and velocities of the journals around the equilibrium with proportional forces [26]. The coefficients of proportionality are called spring and damping coefficients respectively. These forces have components along the displacements or velocities and the associated coefficients are called direct terms. The forces perpendicular to the disturbances are associated with constants called cross-coupling terms. We observe that the latter forces act in the same sense as the other stimulating forces. For that reason, in rotors with appreciable values of the other stimuli, they use pad bearings which have very small cross-coupling forces. The magnitude of these forces depends mainly on Hertzian contact effects and the inertia of the pads. Useful information for pad bearings can be found in Refs. [27–30]. In general, the coefficients for the vertical and horizontal directions are not equal. For four-pad bearings they are given in Refs. [27, 31]. In other types they do not differ too much.

Our purpose is to study general features of the system. Our method will be to reduce the system to a small number of parameters in order to make a qualitative study possible. Numerical results with specific cases should be obtained with more detailed analyses [19, 32]. Here, we shall assume the following:

1. the rotor is a uniform cylinder of diameter d and length l;
2. at the ends, the rotor is supported by two identical orthotropic bearings;
3. steam force gradients appear at the midspan only.

The simplest way to model the rotor is to divide it into two equal distributed mass finite elements (Fig. 4.2). For such a system the equations of motion will be (see Chap. 3)

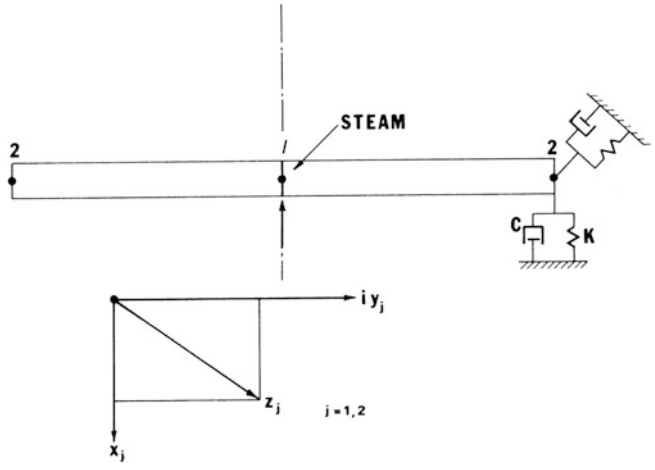

Fig. 4.2 A two-finite element rotor model

$$\left.\begin{aligned} w_1\ddot{z}_1 + K_r\left(1 - i\gamma\frac{\omega}{\Omega-\omega}\right)(z_1 - z_2) - (S_r + iS_t)z_1 = 0 \\ w_2\ddot{z}_2 + C\ddot{z}_2 + Kz_2 - \frac{1}{2}K_r\left(1 - i\frac{\omega}{\Omega-\omega}\gamma\right)(z_1 - z_2) = 0 \end{aligned}\right\} \tag{4.4}$$

where w is a function defined, neglecting rotary inertia effects, as

$$w_1 = \frac{8}{15}m \text{ and } w_2 = \frac{1}{10}m \tag{4.5}$$

m is the mass of the rotor,
z_1, z_2 complex perturbations defined in Fig. 4.2,
C damping constant of the bearing,
K the spring constant of the bearing.

Furthermore, Eq. (4.5) can be written as

$$\left.\begin{aligned} \frac{w_1}{m}\frac{\ddot{z}_1}{\omega_n^2} + \left(1 - ig\frac{\omega_n}{\Omega-\omega_n}\right)(z_1 - z_2) - (r + it)z_1 = 0 \\ \frac{w_2}{m}\frac{\ddot{z}_2}{\omega_n^2} + C\frac{z_2}{\omega_n} + kz_2 - \frac{1}{2}\left(1 - i\gamma\frac{\omega_n}{\Omega-\omega_n}\right)(z_1 - z_2) = 0 \end{aligned}\right\} \tag{4.6}$$

where

$$\omega_n^2 = \frac{kt}{m} \quad r = \frac{St}{kr} \quad t = \frac{St}{kr} \quad c = \frac{C}{\omega_n m} \quad k = \frac{k}{k_r}$$

The quantities ω_n, r, t, c, k are the governing parameters of the system. One could proceed with a study of the stability of the system (4.6) with the usual methods. This, however, will lead to an 8th degree polynomial which will force us to resort eventually to numerical methods. Therefore, the method from Ref. [19] was utilized with the model of Fig. 4.2.

The results have been plotted in a dimensionless form. Table 4.1 gives the several parameter constellations which correspond to Figs. 4.3, 4.4, 4.5, 4.6 and 4.7. We have used two values for γ, namely 10^{-3} and 10^{-4} which are, in the opinion of the authors, extreme values for rotor materials. Higher values correspond to 12 Cr material used extensively for high pressure rotors. Lower values correspond to CrMoV. We can see immediately the effect of the rotor's material on stability.

Table 4.1 Parameters for stability charts of Figs. 4.3–4.7

Figure number	Internal damping	Radial steam gradient	Tangential steam gradient
4.3	0	0	Parameter
4.4	0.0001	0	Parameter
4.5	0.001	0	Parameter
4.6	0.0001	Parameter	0
4.7	0.001	Parameter	0

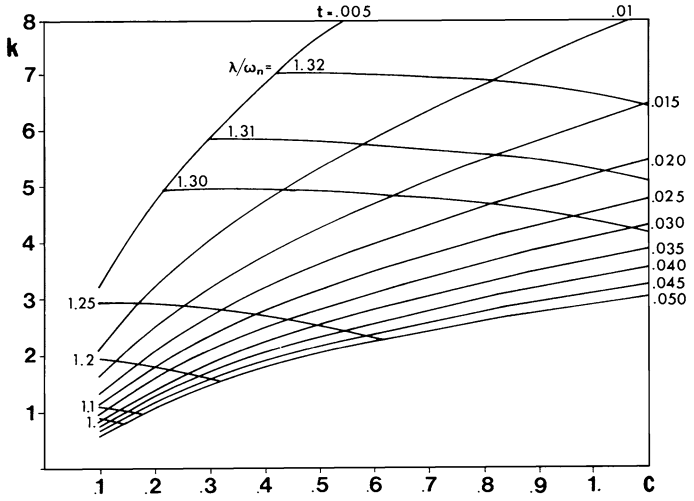

Fig. 4.3 Stability chart, $\gamma = 0.0001$, $S_t, = 0$

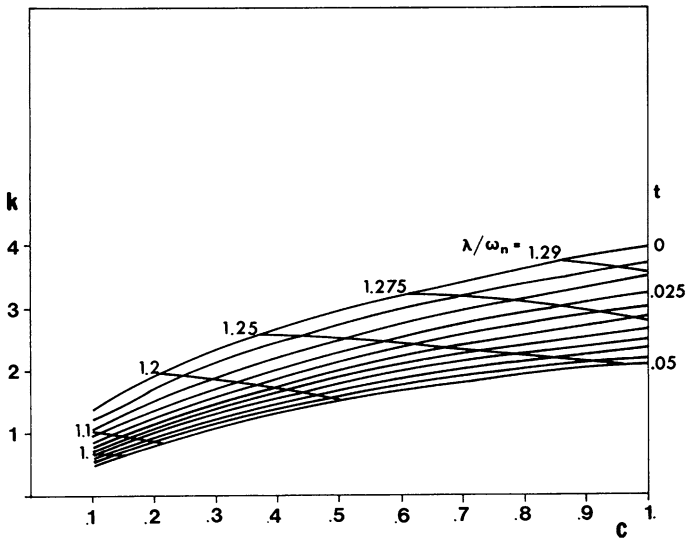

Fig. 4.4 Stability chart, $\gamma = 0.001$, $S_t, = 0$

We should point out that in stability due to internal damping is influenced by the load only to the extent that the increased temperatures influence the damping properties of the material. We note also that for normal rotors, internal damping can induce instability (in this case even at no load) only for extreme conditions in the bearings.

The stiffness and damping parameters of the bearings are used as coordinates, and the steam force parameters, either tangential or radial, are used as parameters.

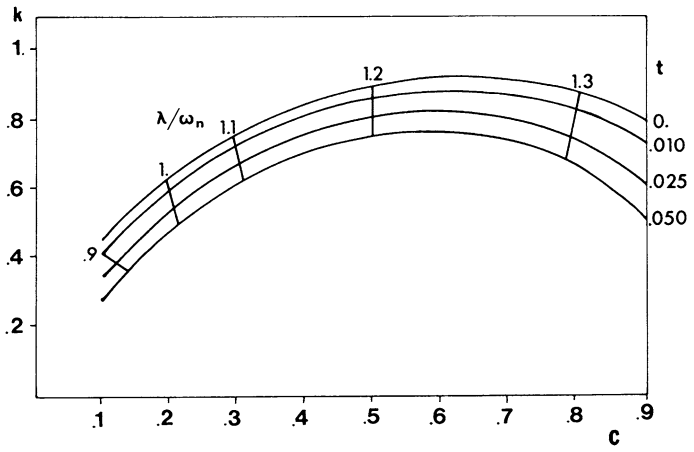

Fig. 4.5 Stability chart, $\gamma = 0.001$, S_t, $= 0$

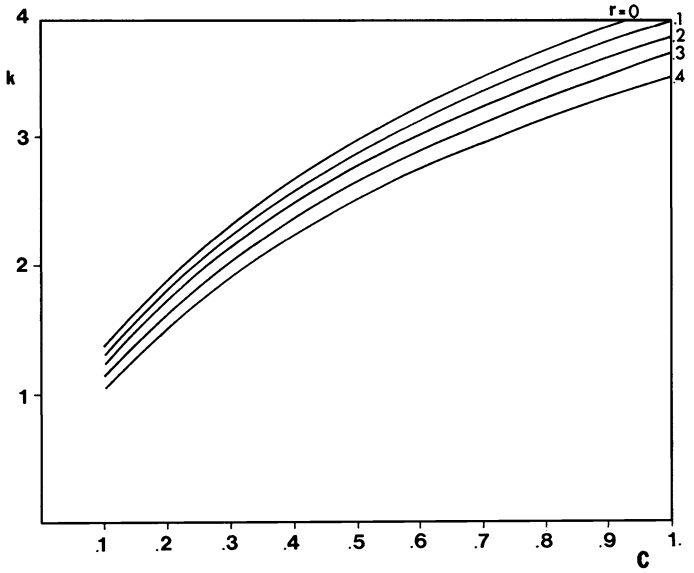

Fig. 4.6 Stability chart, $\gamma = 0.0001$, S_t, $= 0$

For a specific rotor, the bearing properties determine a point in the diagram with the appropriate parameters. This point corresponds to a value of the parameter of the plot (either r or t). If this value is higher than the value of the parameter for the rotor under consideration, the rotor is stable. Therefore, every curve $r =$ constant or $t =$ constant separates the (c, k) plane into stable and unstable regions. A measure for the deviation from stability is the ratio $g(c, k)/g_0$ where $g(c, k)$ is the value of the steam force gradient ratio, r or t which corresponds to the bearing

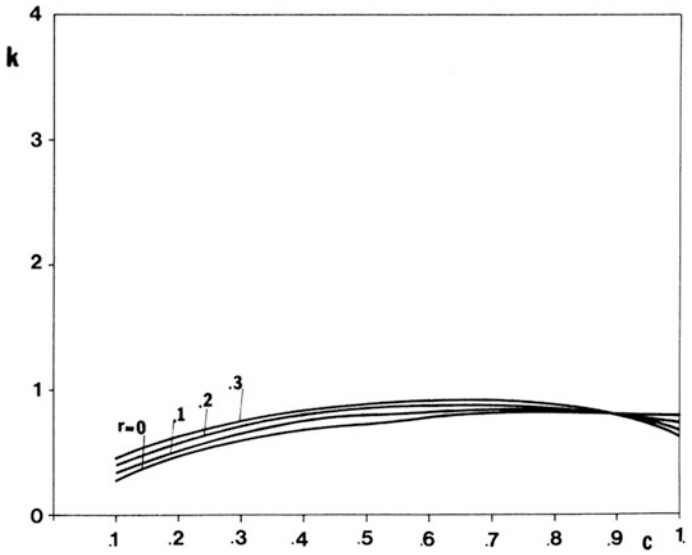

Fig. 4.7 Stability chart, $\gamma = 0.001$, $S_t, = 0$

parameters c and k, and g_o is the value of the same parameter for the rotor under consideration at rated load.

If we call this ratio the Load Stability Criterion (LSC), we observe that values of LSC above 1 indicate instability. Its deviation from I indicates how far we are from the onset of instability. This criterion is very useful for comparing similar rotors for stability behaviour.

In these graphs we did not consider radial and tangential steam force gradients acting simultaneously. In cases where this is important, additional studies have to be carried out if a sum of the values given by these graphs is not satisfactory.

By inspection, one can conclude the following:

1. The steam force gradients greatly influence the stability of the rotor. It is evident, however, that they are not the only factors influencing stability. We observe also that tangential steam gradients have far more effect than equal radial ones. However, that does not reflect the situation in turbo machinery because this might be offset by much greater radial gradients. In stabilising an unstable machine, one has to decrease these gradients. From Eq. (4.1) we see that we cannot change them very much without redesigning the machine. The only thing that we can change is the clearance, which is not involved in Eq. (4.1); therefore an increase in clearance has only secondary effects upon stability, due to the fact that Eq. (4.1) is only a first approximation. The only tool available for improvement is the bearings. Indeed, from Figs. 4.3 and 4.4 it is apparent that the bearings are the most important factor in stability.
2. Turning attention to the bearings, we observe a remarkable property. It is obvious that both stiffness and damping determine the stability of the system.

In fact, we see that stiffness has, in a way, much greater influence on stability than damping. Changing the bearing parameters in order to achieve higher damping does not necessarily result in improvement of stability, because it is always accompanied by a change in stiffness. In the area of practical interest, we observe that lines of constant steam force gradients have the form

$$C/K^2 = \text{constant}$$

From this, we conclude that the factor that one should minimise in order to optimise stability is the damping function

$$D = K^2/C$$

where K and C are the bearing spring and damping coefficients, respectively. Using graphs of the spring and damping coefficients for a four-pad bearing [27], the damping function has been constructed (Fig. 4.8). We can see that this is not a monotonous function of the Sommerfeld number, nor of its ingredients. This is a very important observation, because it cautions against deriving general results from experience or tests. Indeed, an increase of Sommerfeld number, for example, by way of reducing the oil temperature and thus increasing viscosity, might improve stability in one case and make things worse in another, with the same machine, if the increase is large enough. We can largely influence the bearing behaviour because there are many parameters which could be changed without much difficulty, such as bearing clearance, length, oil viscosity and preload. The latter is probably the most drastic tool available: we can see its influence from several graphs given in Ref. [27]. However, we should be very careful in abusing this tool because, as the pads wear with start-ups, the shape of the pad, after some time, will be the same as that of the journal and then the whirl will return, probably after years.

3. The rotor flexibility is a very important factor, in the form ω_n/ω. This is the most difficult parameter to change: therefore we are not going to discuss it any further. However, we point out the well-known fact that a stiffer rotor improves stability, if mass is not increased proportionally. We can express it better by saying that increasing the critical speed improves stability.

4.2 Stability Criteria

In Sect. 3.2.5, the stability conditions were stated for a complex second-order differential equation of motion. In Sect. 3.2.3, it was shown that an adequate description of the single-mass elastic rotor with elastic bearings requires a third-order complex equation of the form Eq. (3.15)

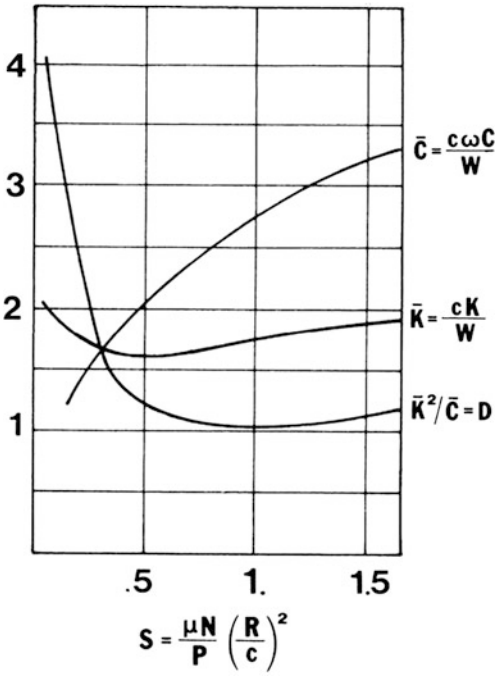

Fig. 4.8 Dynamic properties of a four-pad journal bearing (from Ref. [23])

$$\frac{mC}{k}\dddot{z} + m\left(1+\frac{B}{k}\right)\ddot{z} + C\dot{z} + Bz = 0 \tag{4.7}$$

where B and C are spring and damping constants of the bearings, respectively, and k is rotor stiffness. To account for a steam force gradient S_t, operating on the rotor deflection z, Eq. (4.7) assumes the form

$$\frac{mc}{k}\dddot{z} + m\left(1+\frac{B}{k}\right)\ddot{z} + C\left(1+l\frac{s_t}{k}\right)\dot{z} + \left[B + iS_t\left(1+\frac{B}{k}\right)\right]z = 0 \tag{4.8}$$

It has the general form

$$a_0\dddot{z} + (a_1+ib_1)\ddot{z} + (a_2+ib_2)\dot{z} + (a_3+ib_3)z = 0 \tag{4.9}$$

with

$$\alpha_0 = mC/k \quad \alpha_1 = m(1+B/k) \quad b_1 = 0$$

$$\alpha_2 = C \quad b_2 = m(1+B/k) \quad b_3 = S_1(1+B/k)$$

Substituting $z = \exp(i\lambda t)$ in Eq. (4.9) yields

$$a_0 i\lambda^3 + (a_1+ib_1)\lambda^2 + (-a_2+ia_2)\lambda + (a_3+ib_3) = 0 \tag{4.10}$$

The Routh-Hurwitz conditions require that for stability the following successive determinants should be positive (see Chap. 3):

$$-\begin{vmatrix} 0 & \alpha_1 \\ a_0 & b_1 \end{vmatrix} > 0 \, or \, a_0 a_1 > 0 \tag{4.11}$$

$$\frac{m^2 c}{k}(1 + B/k) > 0 \tag{4.12}$$

For turborotors under study for steam whirl, the bearing properties B and C are real and positive (no coupling terms-pad bearings) and condition (4.12) is always fulfilled.

$$\begin{vmatrix} 0 & \alpha_1 & b_2 & -\alpha_3 \\ \alpha_0 & b_1 & -\alpha_2 & -b_3 \\ 0 & 0 & \alpha_1 & b_2 \\ 0 & \alpha_0 & b_1 & -\alpha_2 \end{vmatrix} \tag{4.13}$$

$$a_0\left(a_1 b_1 b_2 - a_0 a_1 a_3 + a_1^2 a_2 - a_0 b_2^2 - a_0 b_2^2\right) > 0 \tag{4.14}$$

Substituting:

$$\left(1 + 2\frac{B}{k}\right)\frac{mk}{c^2}\left(1 + \frac{B}{k}\right) > \left(\frac{S_t^2}{k^2}\right) \tag{4.15}$$

Condition (4.15) is always satisfied for engineering systems, since $S_t \ll k$ and $mk/C^2 \gg 1$.

$$-\begin{vmatrix} 0 & \alpha_1 & b_2 & -\alpha_3 & 0 & 0 \\ \alpha_0 & b_1 & -\alpha_2 & -b_3 & 0 & 0 \\ 0 & 0 & \alpha_1 & b_2 & -\alpha_3 & 0 \\ 0 & \alpha_0 & b_1 & -\alpha_2 & -b_3 & 0 \\ 0 & 0 & 0 & \alpha_1 & b_2 & -\alpha_3 \\ 0 & 0 & \alpha_0 & -b_1 & -\alpha_2 & -b_3 \end{vmatrix} \tag{4.16}$$

or, expanding the determinant (4.16)

$$a_0 b_1 a_2 b_3 a_1 b_2 a_3 \left(\frac{1}{b_3} - \frac{2a_1}{a_2 b_2} + \frac{b_2}{a_2 a_3} + \frac{b_1 a_3}{a_2 b_3 b_2} + \frac{a_2 a_1}{b_1 b_3 b_2} + \frac{b_3 a_1^2}{b_1 a_2 b_2 a_3} + \frac{a_1}{b_1 a_3} + \right.$$
$$\left. \frac{a_0 b_2}{b_1 b_3 a_1} - \frac{a_0}{b_1 a_2} + \frac{a_0 b_2^2}{b_1 a_2 a_1 a_3} + \frac{a_0 a_3}{a_2 b_3 a_1} - \frac{a_0 a_3}{b_1 b_3 b_2}\right] < 0 \tag{4.17}$$

Substituting and observing that $\alpha_0 \alpha_1 \alpha_2 \alpha_3 b_2 b_3 > 0$ for the systems under consideration, we see that the stability, after proper substitutions becomes

$$1 > \frac{B}{k}\left(1+\frac{B}{k}\right)\left\{(\frac{S_t}{B})2\left[\frac{mk\left(1+\frac{B}{k}\right)^3}{c^2}+\frac{c^2B}{mk^2\left(1+\frac{B}{k}\right)^2}-1\right]+\left(\frac{S_t}{B}\right)^4\frac{c^2B^2}{mk^3\left(1+\frac{B}{k}\right)}\right\} \tag{4.18}$$

Further, the following dimensionless quantities are defined:

Bearing fraction of critical damping $4mB/C^2 = \zeta^2$
Bearing/rotor stiffness ratio $\xi = B/k$
Steam force gradient ratio $\eta = S_t/B$

The stability condition can be written as

$$1 > \xi(1+\xi)\left\{\eta^2\left[-1+\frac{\zeta^2(1+\xi)^3}{4\xi}+\frac{\xi^2}{\zeta^2(1+\xi)^2}\right]+\frac{4\xi^2}{\xi^2(1+\xi)^2}\eta^4\right\} \tag{4.19}$$

The threshold of instability will be determined by the quadratic equation in η^2

$$\frac{4\xi^2}{\xi^2(1+\xi)^2}\eta^4+\left[-1+\frac{\zeta^2(1+\xi)^3}{4\xi}+\frac{4\xi^2}{\zeta^2(1+\xi)^2}\right]\eta^2-\frac{1}{\xi(1+\xi)}=0 \tag{4.20}$$

Since; $\zeta \ll 1$ and $\xi = 0(1)$, it is apparent that Eq. (4.20), to a good approximation can be written as

$$\eta^4+\eta^2-\frac{\zeta^2(1+\xi)}{4\xi^3}=0 \tag{4.21}$$

from which

$$\eta^2 = -\frac{1}{2}+\sqrt{\frac{1}{4}+\frac{\zeta^2(1+\xi)}{4\xi^3}} \tag{4.22}$$

This function is plotted in Fig. 4.9.

It can be concluded that the parameters controlling stability are

$$\eta = S_t/B \qquad \zeta^2(1+\xi)/4\xi^3 = \varphi$$

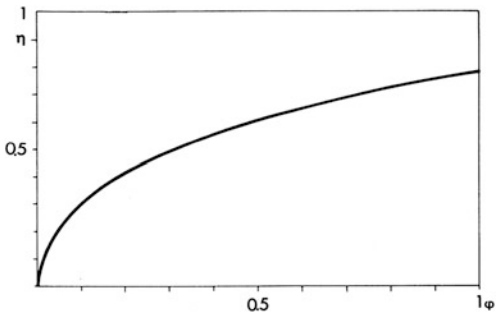

Fig. 4.9 Threshold of instability, (Eq. 4.22)

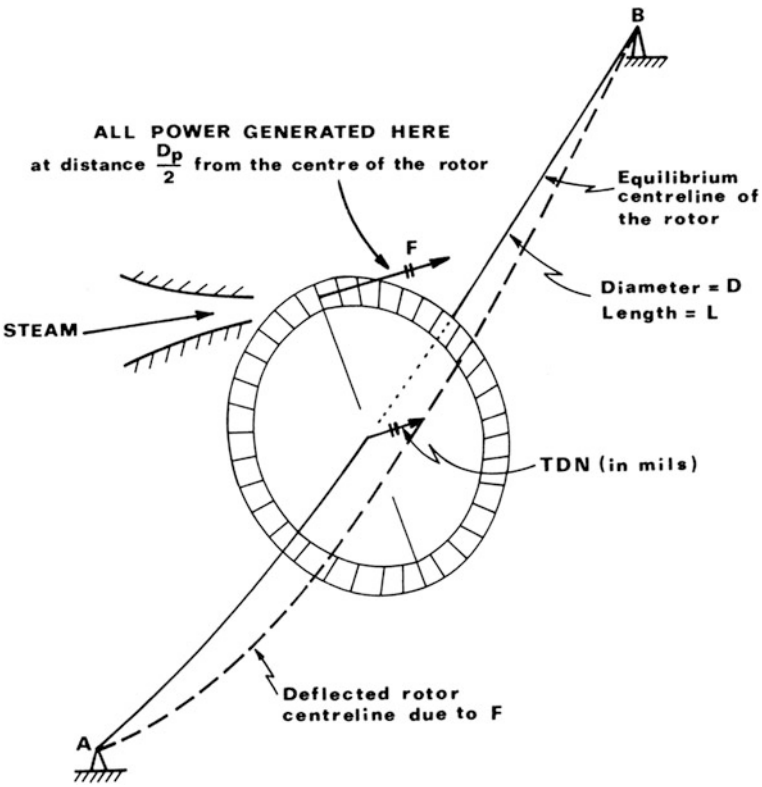

Fig. 4.10 Definition of the torque deflection number

and that there is always a value of the steam force gradient S_t, which makes the system unstable.

In view of the approximation $\zeta \ll 1$ and noting that generally $n \ll 1$, the stability condition (4.19) becomes

$$1 > \frac{\xi^3 \eta^2}{\zeta^2(1+\xi)} = \frac{B^4}{C^2} \frac{4m}{k^5\left(1+\frac{B}{k}\right)} S_t^2 \tag{4.23}$$

This is a rational stability criterion since the model used is adequately accurate and the parameters ξ and ζ can be measured or computed by well-known methods.

At this point it is interesting to discuss other stability criteria used by turbine manufacturers. As mentioned earlier, in the beginning of this Chapter, due to the instability problems of the two General Electric machines in the 1940s [2], a stability criterion called Torque Deflection Number (TDN), was established based on experience with these machines. One definition of the Torque Deflection Number (TDN) is as follows (Fig. 4.10): We assume that all of the power generation on the rotor occurs in one stage, usually in the middle of the span.

In addition, the forces F which generate the torque are concentrated on one bucket. These forces produce torque and power but also bend the shaft to the direction shown in Fig. 4.10. The maximum deflection of the rotor, considered as a simply supported beam, in mils, is called TDN.

Simple calculations using known design parameters lead to the following formula:

$$\text{TDN} = \frac{169400 y_{max} kw}{d_m W n} \tag{4.24}$$

where

$y_{\max}$ = maximum static deflection due to the rotor's own weight (min),
kW = rotor kilowatts,
d_{m} = average bucket pitch diameter (in),
W = rotor's weight (lbs),
n = speed of rotation.

TDN was considered for long to be the most successful criterion for rotor stability similarity. However, this criterion was misleading rather than guiding. The main weakness of the TDN is that it does not give a full account of the steam forces and it does not consider what happens in the bearings. For this reason its success in steam whirl prediction is limited.

The first attempt at a quantitative evaluation of steam whirl was made by Thomas [3]. He used a one-mass rotor and lumped flexibility of the rotor and bearing in a linear spring. On this rotor he imposed a steam force gradient, caused by the leakage through the bucket cover spill strips and the packings. Furthermore, he used the system's damping as a logarithmic decrement of system's vibration, which he determined experimentally. Although Thomas confused the bearing damping, which opposes the destabilizing forces, with the rotor's internal damping (a destabilizing factor), his results are valid because of the experimental determination of the damping. Thus, comparing the steam forces S for a circular orbit of unit radius with the damping forces D he gives the inequality

$$\frac{S}{D} < 1 \tag{4.25}$$

as the stability criterion.

Since the steam force S is a linear function of the load, he calculates the maximum load N_k that the rotor can carry as

$$N_k = m\omega_k^2 \theta \omega S \tag{4.26}$$

where

m = mass of the rotor,
ω_k = critical speed of the rotor (rad/s),
θ = logarithmic decrement,
ω = running speed (rad/s).

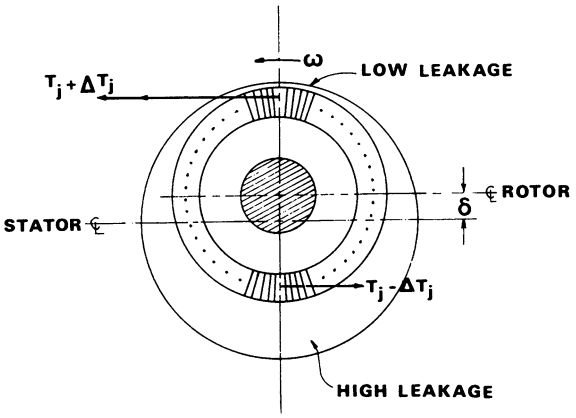

Fig. 4.11 Tangential force variation in a deflected stage

$$S = \frac{hd_m}{\pi\gamma}\gamma = \alpha\left(\frac{d_n}{d_m}\right)^2 \frac{\sqrt{2gH}}{c_2\sqrt{Z}} + \beta\left(1 + \frac{h}{d_m}\right) \tag{4.27}$$

where

h	= bucket height,
d_m	= bucket pitch diameter,
d_n	= packing diameter,
$\sqrt{2gH}$	= available stage energy,
C_2	= exit velocity from previous stage,
Z	= number of packing teeth.

Constants α and β have been determined experimentally.

Thomas [3] introduces two mechanisms of steam forces. First, an axisymmetric stage j is assumed in which N_j kilowatts of power are generated from a steam flow G_j. The steam flow results in tangential forces T_j which, because of symmetry, give the generated torque of the stage (Fig. 4.11).

The second mechanism is of a similar type. The same displacement δ results in an unequal packing clearance (Fig. 4.12). More energy is available in the upper part of the stage through the nozzle because of smaller losses through the packing. Therefore, the torque generated on the bucket will be more than in the lower part, resulting in a force perpendicular to the deflection, as in the previous model.

Here, a physical explanation of the constants α and β is in order: In the first mechanism, the disturbance of the flow due to the non-uniform flow around the buckets will show up as an eddy loss and this is taken into account by the constant β which assumes values of 0.6–1.5, the higher value for free buckets and the lower for covered buckets. In the second mechanism, in the part of the packing with the smaller clearance, because of the smaller leakage part of the available steam is not going to be gained through the nozzle but will flow towards the high clearance area. On the other hand, the non-uniformity of the leakage flow will disturb the

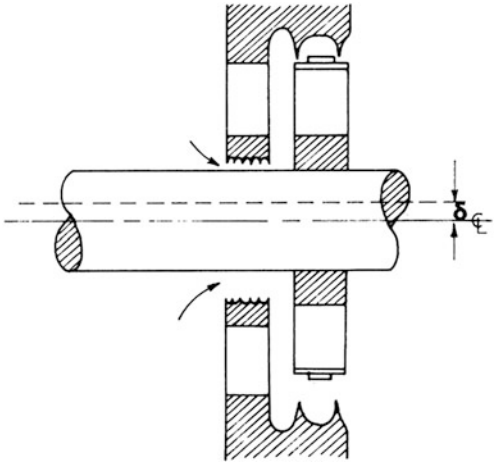

Fig. 4.12 Deflected rotor in a packing clearance

flow through the buckets. The two effects are combined in a constant α which assumes values of 1.6 for stages with and 2.0 for stages without pressure equalisation holes through the wheels.

Thomas proved also that for his model rotor the stability of the one-mass rotor expressed as the stability of the solution of a second-order linear ordinary differential equation is equivalent to the equilibrium of the steam and damping forces assuming a circular orbit.

Numerous conclusions can be derived from Thomas's work: The most important factor for stability or, in terms of Eq. (4.2), for load-carrying capacity, is the critical speed, which enters in the second power. Rotor's mass, running speed, damping, bucket height and pitch diameter enter linearly. Steam parameters enter in the parameter y as secondary effects. To express Thomas criterion in terms of TDN we rewrite Eq. (4.25) as follows:

$$Th = \frac{N}{N_k} = \frac{\pi N \gamma}{h d_m \omega_k^2 \theta \omega} \tag{4.28}$$

where N is the rotor load.

For stable operation, unstable load N_k should be greater than rotor load N; therefore the stability criterion is

$$Th < 1 \tag{4.29}$$

In terms of the TDN, Thomas Stability Criterion can be written as

$$Th = \frac{\pi}{2} \frac{TDN}{h} \frac{\gamma}{\theta} < 1 \tag{4.30}$$

Equation (4.30) shows the relation between TDN and Thomas Stability Criterion. The latter, however, contains some additional terms:

1. The bucket height h enters in the denominator. This partially explains the fact that low pressure rotors or nuclear ones with high TDN are stable because they have longer buckets.
2. The bearing damping θ enters in the denominator too. That explains the well known influence of damping on stability. Thomas gives values for θ

$$\theta = 0.05 \qquad \text{for } \omega_k \leq 0.5\omega$$

$$\theta = 0.1 \qquad \text{for } \omega_k > 0.5\omega$$

3. The factor y contains secondary effects because of the steam path, such as effect of clearances, reaction ratio, etc.

If bearing damping coefficients C are available, the log decrement can be calculated as follows:

$$\theta = \frac{\omega_k C m}{\pi}$$

Thomas Stability Criterion, although incomplete, is more rational than Torque Deflection Number.

4.3 Rotor Dynamics for Annular Flows

In the previous sections it was demonstrated that severe vibration may be imposed upon a rotating shaft due to the mechanism of power generation in fluid machinery.

In fluid machines there are well-known phenomena of dynamic interaction of cylinders with the surrounding fluid in parallel or cross-flow. A thorough review of the pertinent literature was reported by Paidoussis [33]. This type of flow is common in power reactors, heat exchangers, etc.

The effect of fluids surrounding rotating shafts can be distinguished on the basis of the relation of the clearance annulus to the rotor radius C/R. Journal bearings constitute a typical case with a C/R ratio of the order of 10^{-3} In this section we shall discuss rotor-fluid interaction in annuli of the order 10^{-1} for C/R, which corresponds to seals, passages, etc.

Whenever solids move in contact with fluids, fluid pressures are generated as a result of this motion. Fluid forces occur on these solids due to the integrated effect of pressure. Stokes analysed the case of an incompressible, frictionless fluid filling the space between two coaxial cylindrical surfaces. He found that, if the outer cylinder were stationary and the inner cylinder were accelerated, then the fluid force on the inner cylinder would be [34]

$$F_H = -\frac{b^2 + a^2}{b^2 - a^2}\pi\rho L a^2 \ddot{X} \tag{4.31}$$

This force may be associated with a 'hydrodynamic mass', m_{H}, defined by

$$F_H = -m_H \ddot{X} \tag{4.32}$$

where

$$m_H = \frac{b_2 + a_2}{b^2 - a^2} \pi \rho L a^2 \tag{4.33}$$

This expression reduces to

$$m_H = \frac{\pi R^3 \rho L}{c} \tag{4.34}$$

for a thin annulus for which $R \gg C$. For these relations:

F_{H} = hydrodynamic force,
a = inner radius of outer stationary cylinder,
b = outer radius of inner cylinder,
C = b–a,
L = length of cylinder ($L \gg b$),
P = fluid mass density,
$\ddot{X}$ = inner cylinder acceleration ($X \ll C$).

Next, the dynamic fluid forces can be estimated for a cylinder rotating at constant speed, as shown in Fig. 4.13. The fluid is incompressible and flows circumferentially in a thin annulus. Figure 4.13 shows the angles

$$\psi = \theta + \phi \tag{4.35}$$

where

ψ = angular coordinate of annular position. This angle is fixed in the laboratory system and is considered as an independent variable
$\phi = \phi(t)$ = location of minimum h (annular thickness)
$\theta = \theta(\psi,t)$ = angular coordinate of annular position which rotates with the cylinder. θ is measured from the location of minimum h.

For $C/R \ll 1$

$$h = C(1 - \varepsilon \cos\theta) \tag{4.36}$$

where $\varepsilon = \delta/C$, δ = maximum deflection of the rotating cylinder centre.

From Eqs. (4.35) and (4.36)

$$\dot{h} = -C\dot{\varepsilon}\cos\theta - c\varepsilon\dot{\phi}\sin\theta \tag{4.37}$$

The equation of continuity and Eq. (4.37) yield

$$\frac{1}{R}\frac{\partial hu}{\partial \psi} = c\dot{\varepsilon}\cos\theta + c\varepsilon\dot{\phi}\sin\theta \tag{4.38}$$

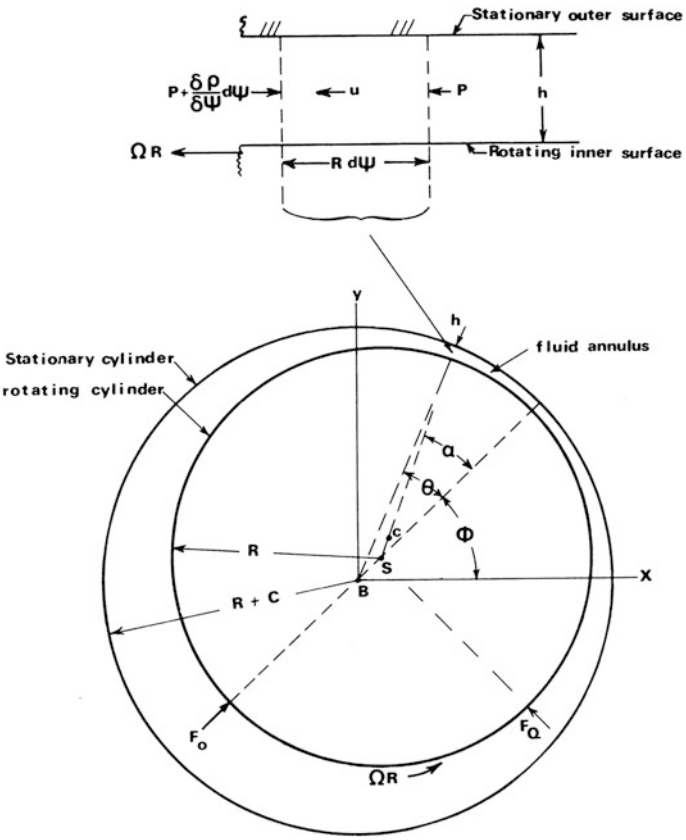

Fig. 4.13 Geometry of a rotating cylinder in a fluid annulus. (*Courtesy* ASME [35, 36])

Integrating Eq. (4.38), by using Eq. (4.35)

$$hu = q(t) + RC\dot{\varepsilon}\sin\theta - RC\,\varepsilon\dot{\phi}\cos\theta \tag{4.39}$$

where $q(t)$ is a constant of integration. If $\varepsilon = \dot{\varepsilon} = 0$; $h = C$, then, from Eq. (4.39) and the geometry of Fig. 4.13.

$$\frac{q}{C} = \frac{\Omega R}{2} \tag{4.40}$$

Substituting Eq. (4.40) into Eq. (4.39) and using Eq. (4.36) results in

$$u = \frac{\Omega R}{2(1-\varepsilon\cos\theta)} + \frac{R\dot{\varepsilon}\sin\theta}{1-\varepsilon\cos\theta} - \frac{R\varepsilon\dot{\phi}\cos\theta}{1-\varepsilon\cos\theta} \tag{4.41}$$

In the following analysis, ε will be treated as a small quantity ($\varepsilon \ll 1$). On this basis Eq. (4.41) can be approximated by

$$u = \frac{\Omega R}{2}(1 + \varepsilon \cos\theta) + R\dot{\varepsilon}\sin\theta - R\varepsilon\dot{\phi}\cos\Theta \tag{4.42}$$

Since

$$u = \frac{\Omega R}{2} + V \tag{4.43}$$

$$V = \frac{\Omega R}{2}\varepsilon\cos\theta + R\dot{\varepsilon}\sin\theta - R\varepsilon\dot{\phi}\cos\Theta \tag{4.44}$$

From Eqs. (4.35) and (4.42)

$$\begin{aligned}\dot{u} = &\frac{1}{2}\left[\dot{\varepsilon}\cos\theta + \varepsilon\dot{\phi}\sin\theta\right] - R\ddot{\varepsilon}\sin\theta - R\dot{\varepsilon}\dot{\phi}\,\mathrm{s}\cos\theta \\ &- R\dot{\varepsilon}\dot{\phi}\,\mathrm{s}\cos\theta - R\varepsilon\ddot{\phi}\,\mathrm{s}\cos\theta - R\varepsilon\dot{\phi}\,\mathrm{s}^2\sin\theta\end{aligned} \tag{4.45}$$

$$\frac{\partial u}{\partial\psi} = \frac{\Omega R}{2}(-\varepsilon\sin\theta) + R\dot{\varepsilon}\cos\theta + R\varepsilon\dot{\phi}\sin\theta \tag{4.46}$$

Substituting Eqs. (4.41), (4.44) and (4.49) into the momentum equation [35, 36] for the fluid, and rearranging results (still neglecting terms in ε [2]):

$$\begin{aligned}\frac{1}{\rho R}\frac{\partial P}{\partial\psi} = &\cos\theta\left(-\Omega R\dot{\varepsilon} + 2R\dot{\varepsilon}\dot{\phi} + R\varepsilon\ddot{\phi} - \frac{\Omega R}{2}\varepsilon F + R\varepsilon\dot{\phi}F\right) \\ &+ \sin\theta\left(-\frac{\Omega R}{2}\varepsilon\dot{\phi} - R\ddot{\varepsilon} + R\varepsilon\dot{\phi}^2 + \frac{\Omega^2}{4}R\varepsilon - \frac{\Omega}{2}R\varepsilon\dot{\phi} - R\varepsilon F\right)\end{aligned} \tag{4.47}$$

The fluid forces whose directions are shown in Fig. 4.13 are evaluated from

$$F_0 = -\int_0^{2\pi} LRP\cos\theta d\theta \tag{4.48}$$

$$F_Q = -\int_0^{2\pi} LRP\sin\theta d\theta \tag{4.49}$$

In the above relations the parameter F takes the values [35, 36] for turbulent flow ($Re > 5000$)

$$F_T = 0.0556\frac{\Omega R n}{CRe} \tag{4.50}$$

where, n is a flow profile parameter $= 1.14$ for the $-1/7$ power law, Re the Reynolds number, and for vortex (Taylor number > 60) flow

$$F_v = 1.52\frac{\Omega Rn}{c}\left(\frac{c}{R}\right)^{0.261}\mathrm{Re}^{-0.478} \tag{4.51}$$

Integrating Eq. (4.47) to obtain P and substituting into Eqs. (4.48) and (4.49) yields

$$-F_Q = m_H C\left(\varepsilon\ddot{\phi} + 2\dot{\varepsilon}\dot{\phi} - \Omega\dot{\varepsilon} - \frac{\Omega}{2}\varepsilon F + F\varepsilon\dot{\phi}\right) \tag{4.52}$$

$$-F_0 = m_H C\left(\ddot{\varepsilon} - \varepsilon\dot{\phi}^2 + \Omega\varepsilon\dot{\phi} - \frac{\Omega^2}{4}\varepsilon + F\dot{\varepsilon}\right) \tag{4.53}$$

where

$$m_H = \frac{\pi R^3 \rho L}{c} \tag{4.34}$$

For a rotor of mass M flexibly connected to a rotating shaft, a spring force is generated equal to $K\delta$ where δ is the radial deflection of the rotor from its central position. The rotor is assumed to have the shape of a long cylinder surrounded by a thin fluid annulus ($C/R \ll 1$). The fluid in the annulus is assumed to flow tangentially with negligible (net) axial flow. We are interested in the vibrations of this rotor due to imbalance. The equations of motion are

$$\left.\begin{aligned} M\left(\ddot{\delta} - \delta\dot{\phi}^2\right) &= -m_H\left(\ddot{\delta} - \delta\dot{\phi}^2 + \Omega\delta\dot{\phi} - \frac{\Omega^2}{4}\delta + F\dot{\delta}\right) - k\delta + M\Omega^2 e\cos a \\ M\left(\delta\ddot{\phi} - 2\dot{\delta}\dot{\phi}\right) &= -m_H\left(\delta\ddot{\phi} + 2\dot{\delta}\dot{\phi} - \Omega\dot{\delta} - \frac{\Omega}{4}F\delta + F\delta\dot{\phi}\right) + M\Omega^2 e\sin a \end{aligned}\right\} \tag{4.54}$$

The inertial reaction on M (left sides of Eqs. (4.54)) was taken from Page [37]. Terms multiplying m_H are the fluid reaction terms from Eqs. (4.52) and (4.53). The last term is the centrifugal force due to imbalance (see Fig. 4.14) to define e and α.

Assuming a stable whirl at steady amplitude δ, $\dot{\delta} = \ddot{\phi} = 0$ and $\phi = \Omega$, Eq. (4.54) become

$$\left.\begin{aligned} -\left(M + \tfrac{m_\mathrm{H}}{4}\right)\delta\Omega^2 + k\delta &= M\Omega^2 e\cos a \\ \tfrac{m_\mathrm{H} F\Omega\delta}{2} &= M\Omega^2 e\sin a \end{aligned}\right\} \tag{4.55}$$

Solving for δ/e, Eqs. (4.45) and (4.55) are squared and added. The result is

$$\frac{\delta}{e} = \frac{\Omega^2}{\left[(1+\beta)^2\left(\Omega_0^2 - \Omega^2\right)^2 + 4\beta^2 F^2\Omega^2\right]^{1/2}} \tag{4.56}$$

where $\beta = m_\mathrm{H}/4\,M$ (m_H from Eq. (4.34).

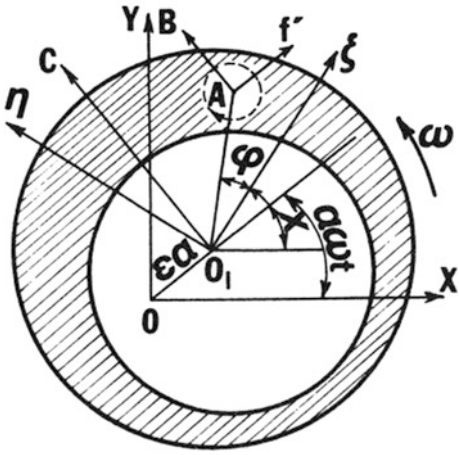

Fig. 4.14 Fluid forces in a hollow rotor partially filled with a liquid. (*Courtesy* ASME [38])

$$\Omega_0^2 = \frac{K}{M + \frac{m_H}{4}} = \frac{K/M}{1+\beta} \tag{4.57}$$

Ω_0 is the undamped ($F = 0$) critical speed. The amplification at the undamped critical speed is

$$[\delta/c]_M = \frac{\Omega}{2\beta F} \tag{4.58}$$

To analyse for stability, it is convenient to write Eqs. (4.54) referred to Cartesian coordinates in the stationary coordinate system. To this end, Eq. (4.54) give

$$(M + m_H)\left(\ddot{\delta} - \delta\dot{\phi}^2\right) = -m_H\left(\Omega\delta\dot{\phi} - \frac{\Omega^2}{4}\delta + F\dot{\delta}\right) - K\delta + M\Omega^2 e\cos a \tag{4.59}$$

$$(M + m_H)\left(\delta\ddot{\phi} - 2\dot{\delta}\dot{\phi}\right) = -m_H\left(\Omega\dot{\delta} - \frac{\Omega}{4}F\delta + F\delta\phi\right) + M\Omega^2 e\sin\ a \tag{4.60}$$

The transformation

$$\left.\begin{aligned} X &= \delta\cos\phi \\ Y &= \delta\sin\phi \end{aligned}\right\} \tag{4.61}$$

on the equations of motion, for the fixed coordinate system, yield

$$(M + m_H)\ddot{X} + F\dot{X} + \left(K - \frac{m_H\Omega^2}{4}\right)X + m_H\Omega\dot{Y} + \frac{m_H\Omega F}{2}Y = M\Omega^2 e\cos(\phi + a) \tag{4.62}$$

$$(M+m_{\mathrm{H}})\ddot{Y}+F\dot{Y}+\left(K-\frac{m_{\mathrm{H}}\Omega^2}{4}\right)Y-m_{\mathrm{H}}\Omega\dot{X}-\frac{m_{\mathrm{H}}\Omega F}{2}X=M\Omega^2 e\sin(\phi+a) \tag{4.63}$$

The homogeneous equation is analysed for stability; that is, Eqs. (4.62) and (4.63), setting the right side to zero. Replacing the coefficients of Eqs. (4.62) and (4.63) by more convenient symbols, $m = M + m_{\mathrm{H}}$, $C_1 = F$, etc., we obtain

$$m\ddot{X}+C_1\dot{X}+K_1X+C_2\dot{Y}+K_2Y=0 \tag{4.64}$$

$$m\ddot{Y}+C_1\dot{Y}+K_1Y-C_2\dot{X}+K_2X=0 \tag{4.65}$$

Assuming $X = X_0 \exp(\lambda t)$ and $Y = Y_0 \exp(\lambda t)$, and substituting into Eqs. (4.64) and (4.65) gives

$$(\mathrm{m}\lambda^2+C_1\lambda+K_1)X_0+(C_2\lambda+K_2)Y_0=0 \tag{4.66}$$

$$-(C_2\lambda+K_2)X_0+(\mathrm{m}\lambda^2+C_1\lambda+K_1)Y_0=0 \tag{4.67}$$

In order to allow non-zero solutions for X_0, Y_0 the determinant of Eqs. (4.66) and (4.67) must be zero, or

$$\left(m\lambda^2+C_1\lambda+K_1\right)^2+(C_2\lambda+K_2)^2=0$$

which may be written

$$m^2\lambda^4+2mC_1\lambda^3+\left(C_1^2+2mK_1+C_2^2\right)\lambda^2+2(C_1K_1+C_2K_2)\lambda+K_1^2+K_2^2=0 \tag{4.68}$$

Applying Hurwitz-Routh determinants to check for stability conditions, the determinants reduce to

$$2mC_1>0 \tag{4.69}$$

and

$$2mC_1\left(C_1^2+2mK_1+C_2^2\right)>2m^2(C_1K_1+C_2K_2) \tag{4.70}$$

which can be simplified to

$$C_1^2+C_2^2>m\left(\frac{c_2}{c_1}K_2-K_1\right) \tag{4.71}$$

and

$$\begin{aligned}2mC_1\left(C_1^2+2mK_1+C_2^2\right)2(C_1K_1+C_2K_2)>4m^2C_1^2\left(K_1^2+K_2^2\right)\\+4m^2(C_1K_1+C_2K_2)^2\end{aligned} \tag{4.72}$$

which simplifies to

$$\frac{c_1k_1 + c_2k_2}{k_2} > \frac{mk_2}{c_1} \tag{4.73}$$

and, finally

$$K_1^2 + K_2^2 > 0 \tag{4.74}$$

Comparing Eqs. (4.73), (4.63), (4.64) and (4.65), the coefficients are

$$m = M + m_{\mathrm{H}} \tag{4.75}$$

$$C_1 = F \tag{4.76}$$

$$K_1 = K - \frac{m_H\Omega^2}{4} \tag{4.77}$$

$$C_2 = m_{\mathrm{H}}\Omega \tag{4.78}$$

$$K_2 = \frac{m_{\mathrm{H}}F\Omega}{2} \tag{4.79}$$

Substituting these values in the following:
From Eq. (4.69)

$$2(M + m_{\mathrm{H}})m_{\mathrm{H}}F > 0 \tag{4.80}$$

From Eq. (4.71)

$$m_H^2\left(F^2 + \Omega^2\right) > (M + m_{\mathrm{H}})\left[\frac{\Omega}{F}\frac{m_{\mathrm{H}}F\Omega}{2} - \left(K - \frac{m_{\mathrm{H}}\Omega^2}{4}\right)\right] \tag{4.81}$$

which simplifies to

$$\left(F^2 + \Omega^2\right) > \frac{M + m_{\mathrm{H}}}{m_{\mathrm{H}}}\left[\frac{\Omega^2}{4} - \frac{K}{m_{\mathrm{H}}}\right] \tag{4.82}$$

From Eq. (4.75)

$$\left[\frac{m_HF\left(k - \frac{m_{\mathrm{H}}\Omega^2}{4}\right) + \frac{m_{\mathrm{H}}F\Omega^2}{2}}{\frac{m_{\mathrm{H}}F}{2}}\right] > \left[\frac{(M + m_{\mathrm{H}})m_{\mathrm{H}}F\Omega}{2m_{\mathrm{H}}F}\right] \tag{483}$$

which simplifies to

$$\Omega < 2\sqrt{\frac{k}{M}} \tag{4.84}$$

And finally, from Eq. (4.74)

$$\left(k - \frac{m_H \Omega^2}{4}\right)^2 + \left(\frac{m_H F \Omega}{2}\right)^2 > 0 \tag{4.85}$$

Equation (4.80) is inherently satisfied for a physical system where the values in the equation are all positive real quantities. Assume that condition (4.86) is met, so that

$$\frac{\Omega^2}{4} + B = \frac{k}{M} \quad B > 0 \tag{4.86}$$

Substituting Eq. (4.86) into (4.82), and letting $M/m_H = \gamma$

$$F^2 + \Omega^2 > (1+\gamma)\left(\frac{\Omega^2}{4} - \gamma\frac{\Omega^2}{4} - \gamma B\right) \tag{4.87}$$

This simplifies to

$$F^2 + \frac{\Omega^2}{4}\left(3+\gamma^2\right) + (1+\gamma)\gamma B > 0 \tag{4.88}$$

Since all terms have positive real values, inequality (4.88) is automatically satisfied if (4.84) is satisfied. And likewise for (4.74) $\sqrt{(K/M)}$ is the critical angular frequency of the rotor in a vacuum (that is, without fluid effects) and may be denoted by Ω_C.

The resulting condition for stability is relation (4.84) which states that the rotational speed Ω must be less than twice the critical speed Ω_C where Ω_C is determined in the absence of fluid effects.

4.4 Dynamics of a Hollow Rotor Partially Filled with a Liquid

In a rotating hollow shaft partially filled with viscous liquid, self-excited vibration occurs [39, 40] within a certain range of rotating speed. The investigations into this vibration reported hitherto can be divided into two schools: in one the liquid is considered to be inviscid [41, 42] and in the other the viscosity of liquid is taken into account [43–50].

Such a situation appears frequently due to condensation in the bore holes of rotating shafts, centrifugal casting of pipes, etc. In Fig. 4.14, O and O_1 represent the centre of the stationary coordinates X−Y and the centre of the rotating hollow shaft, respectively. $\xi-\eta$ are the coordinates fixed to the rotating shaft. Now O_1 is whirling around O with the small amplitude $\varepsilon\alpha$ ($\varepsilon \ll 1$) and frequency $\alpha\omega$. The equation of motion for the non-dimensional time-dependent radial velocity U of the small liquid element at point A can be written as [46]

$$R^3\frac{\mathrm{d}^4U}{\mathrm{d}R^4}+6R^2\frac{\mathrm{d}^3U}{\mathrm{d}R^3}+\left[3R-i(\alpha-1)\mathrm{Re}R^3\right]\frac{\mathrm{d}^2U}{\mathrm{d}R^2}-3\left[1-i(\alpha-1)\mathrm{Re}R^2\right]\frac{\mathrm{d}U}{\mathrm{d}R}=0 \tag{4.89}$$

and the equations of the non-dimensional time-dependent circumferential velocity V and pressure P are [8]

$$V=-iU-iR\frac{\mathrm{d}U}{\mathrm{d}R} \tag{4.90}$$

$$P=-2i(\alpha-1)R^2\frac{\mathrm{d}U}{\mathrm{d}R}-2i(\alpha+1)RU+2\alpha^2R+\frac{2}{\mathrm{Re}}\left(R^2\frac{\mathrm{d}^3U}{\mathrm{d}R^3}+4R\frac{\mathrm{d}^2U}{\mathrm{d}R^2}\right) \tag{4.91}$$

Boundary conditions are given as [46]
at $R=1$,

$$U=0 \tag{4.92}$$

$$V=0 \tag{4.93}$$

and at $R=H$,

$$R\frac{\mathrm{d}^2U}{\mathrm{d}R^2}+\frac{\mathrm{d}U}{\mathrm{d}R}=0 \tag{4.94}$$

$$U=-\gamma P \tag{4.95}$$

where
R = r/a, the dimensionless radius at A,
Re = Reynolds number ($a^2\omega/v$),
a = inner radius of the hollow shaft,
v = fluid viscosity

Equation (4.89) can be solved, for example, exactly by using the Bessel function, [45] or numerically by using the finite difference method [46]. Saito and Someya [47] solved the equation approximately by using the assumption in which the relative depth of liquid to the radius of hollow shaft is small.

The following equations are obtained by substituting $R=1-T$ into Eqs. (4.89–4.91) and regarding the coefficients of the equations so obtained as constants. This approximation is correct in the case of $T\ll 1$.

$$\alpha_1\frac{\mathrm{d}^4U}{\mathrm{d}T^4}-6\alpha_2\frac{\mathrm{d}^3U}{\mathrm{d}T^3}+[3\alpha_3-i\alpha_1(\alpha-1)Re]\frac{\mathrm{d}^2U}{\mathrm{d}T^2}+3[1+i\alpha_2(\alpha-1)Re]\frac{\mathrm{d}U}{\mathrm{d}T}=0 \tag{4.96}$$

$$V=-iU+i\alpha_3\frac{\mathrm{d}U}{\mathrm{d}T} \tag{4.97}$$

$$P = 2i\alpha_2(\alpha - 1)\frac{dU}{dT} - 2i\alpha_3(\alpha + 1)U + 2\alpha_3\alpha^2 - \frac{2}{\mathrm{Re}}\left(\alpha_2\frac{d^3U}{dT^3} - 4\alpha_3\frac{d^2U}{dT^2}\right) \quad (4.98)$$

where

$$\alpha_1 = {}^1\!/_{T_0}\int_{1-T_0}^{1} R^3 dR = 1 - \frac{3}{2}T_0 + T_0^2 - \frac{1}{4}T_0^3$$

$$\alpha_2 = {}^1\!/_{T_0}\int_{1-T_0}^{1} R^2 dR = 1 - T_0 + \frac{1}{3}T_0^2$$

$$\alpha_3 = {}^1\!/_{T_0}\int_{1-T_0}^{1} R dR = 1 - \frac{1}{2}T_0$$

$$T_0 = 1 - H$$

The characteristic equation for Eq. (4.96) can be obtained by assuming $U = C\exp(\lambda T)$:

$$\alpha_1\lambda^4 - 6\alpha_2\lambda^3 + [3\alpha_3 - i\alpha_1(\alpha - 1)Re]\lambda^2 + 3[1 + i\alpha_2(\alpha - 1)Re]\lambda = 0 \quad (4.99)$$

Regarding the solution of Eq. (4.96) as λ_j (j = 1−4)

$$U = \sum_{j=1}^{4} C_j\ exp\ (\lambda_j)T \quad (4.100)$$

Substituting Eq. (4.100) into Eqs. (4.97) and (4.98) results in

$$V = \sum_{j=1}^{4} (\alpha_3\lambda_j - 1)\ exp\ (\lambda_{jT})C_j \quad (4.101)$$

$$P = \sum_{j=1}^{4} \beta_j\ exp\ (\lambda_{jT})C_j + 2\alpha_3\alpha^2 \quad (4.102)$$

where

$$\beta_j = 2i\left[\alpha_2(\alpha - 1)\lambda_j - \alpha_3(\alpha + 1)\right] - \frac{2}{Re}\left(\alpha_2\lambda_j^3 - 4\alpha_3\lambda_j^2\right)$$

Substituting Eqs. (4.100, 4.102) into the boundary conditions (4.92–4.95)

$$\sum_{j=1}^{4} C_j = 0 \quad (4.103)$$

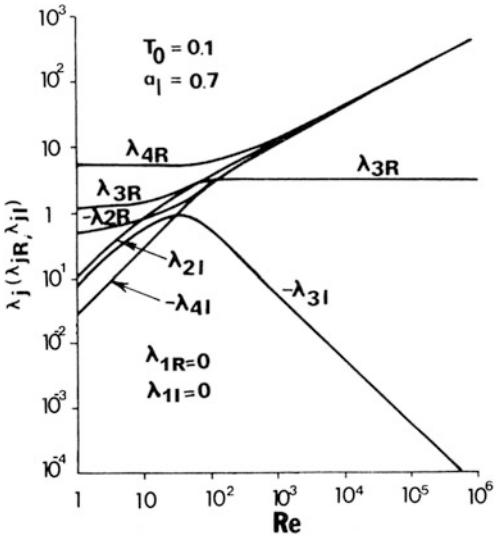

Fig. 4.15 Solution of Eq. (4.99). (*Courtesy* ASME [50])

$$\sum_{j=1}^{4} (\alpha_3 \lambda_j - 1) C_j = 0 \tag{4.104}$$

$$\sum_{j=1}^{4} (\alpha_3 \lambda_j - 1) \ \exp\ (\lambda_{jT}) C_j = 0 \tag{4.105}$$

$$\sum_{j=1}^{4} (1 + \gamma \beta_j) \ exp\ (\lambda_{jT}) C_j = -2\alpha_3 \gamma \alpha^2 \tag{4.106}$$

U, V and P can be obtained by solving Eqs. (4.103–4.106) for the unknown constants C_j ($j = 1-4$) and substituting them into Eqs. (4.100–4.102). The non-dimensional fluctuation of the free surface of liquid η^* and the non-dimensional liquid force F^* are given as [50]

$$\eta^* = -[P]_{T-T_0} / [2(1 - T_0)] \tag{4.107}$$

$$F^* = \pi [P]_{T=0} \tag{4.108}$$

Figure 4.15 shows an example of the solution $\lambda_{jR} + i\lambda_{jI} (j = 1 - 4)$ of Eq. (4.99). In the region $Re > 10^3$, as the Re number increases, $\lambda_{2R}|$, $|\lambda_{2I}|$, $|\lambda_{4R}|$ and $|\lambda_{4I}|$ increase and $|\lambda_{3I}|$ approaches zero, but $|\lambda_{3R}|$ remains constant and λ_{1R} as well as λ_{1I} are zero. Accordingly, in the case of a large Re number, $\exp(\lambda_{1T})$ and $\exp(\lambda_{3T})$ represent the term independent of T and the term that increases exponentially with $T (\lambda_{3R} > 0)$, respectively.

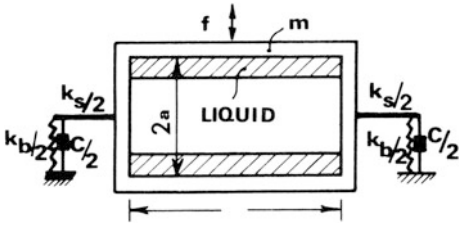

Fig. 4.16 Model of a flexible shaft on soft journal bearings. (*Courtesy* ASME [43])

And, $\exp(\lambda_{2T})$ as well as $\exp(\lambda_{4T})$ mean the terms of T that change with "high frequency". As T increases, the envelope of $\exp(\lambda_{2T})$ decreases rapidly $(\lambda_{2R} \ll 0)$, while that of $\exp(\lambda_{4T})$ increases rapidly $(\lambda_{4R} \gg 0)$.

The rapid increase of $|\lambda_{2I}|$ and $|\lambda_{4I}|$ corresponds to the fact that the thickness of the dynamic boundary layer decreases [49] rapidly as the Re number increases. As the increase of $|\lambda_{2R}|$, $|\lambda_{2I}|$, $|\lambda_{4R}|$and $|\lambda_{4I}|$ is approximately proportional to $\sqrt{Re}$ in the region $Re > 10^3$, and the term in Eqs. (4.103–4.106) that gives the maximum change is $\exp(\lambda_{jT0})$, it is considered that the non-dimensional term $T_0\sqrt{Re}$ or $T_0^2 Re$ plays an important role in this problem.

One of the applicability limits of this approximate solution depends on whether Eqs. (4.103–4.106) can be solved numerically or not. If the Re number or T_0 increases, $\exp(\lambda_{4T0})$ in Eqs. (4.105) and (4.106) becomes excessively large in comparison with the other terms and the solution could be less accurate due to the truncation error involved in the computations. Trial calculations have shown that the theory is applicable within the range $T_0^2 Re \leq 10^4$.

Figure 4.16 shows a model of a flexible shaft on soft journal bearings. The rotating hollow shaft is assumed to be rigid, and only the motion of the parallel mode is analyzed. The equations of motion are

$$m\ddot{X} + k_s(X - x) = f \tag{4.109}$$

$$\frac{k_s}{2}(X - x) = \frac{k_b}{2}x + \frac{c}{2}\dot{x} \tag{4.110}$$

where X and x are the displacements at the hollow shaft and at the journal, respectively; k_s, k_b and c are shaft stiffness, bearing stiffness, and bearing damping, respectively.

Assuming $X = \varepsilon\alpha \exp(i\alpha\omega t)$ and $x = \alpha \exp(i\alpha\omega t)$

$$\varepsilon\alpha f^* \exp(i\alpha\omega t)(\varepsilon,\ \delta \ll 1) - -m\alpha^2\omega^2\varepsilon + k_s(-\delta) = \varepsilon f^* \tag{4.111}$$

$$k_s(\varepsilon - \delta) = k_b\delta + ic\alpha\omega\delta \tag{4.112}$$

From Eq. (4.112)

$$\delta = \frac{k_s}{k_s + k_b + ic\alpha\omega}\varepsilon \tag{4.113}$$

Substituting Eq. (4.113) into Eq. (4.111) and rearranging:

$$(k_s - m\alpha^2\omega^2)(k_s + k_b + ic\alpha\omega) - k_s^2 = f^*(k_s + k_b + ic\alpha\omega) \tag{4.114}$$

Expressing Eq. (4.114) in the non-dimensional form:

$$(1 - \alpha^2\Omega^2)(1 + \mu + 2i\zeta\alpha\Omega) - 1 = \frac{m^* F^* \Omega^2}{2\pi}(1 + \mu + 2i\zeta\alpha\Omega) \tag{4.115}$$

The above equation can be solved by Newton-Raphson method and the stability of rotor systems is investigated [50–52]. Substituting $F* = F_R^* \pm iF_I^*$ and $\alpha = \alpha_{\mathrm{I}}$ into Eq. (4.115), and separating the real part from the imaginary one:

$$2\pi[\mu - (1 + \mu)\alpha_I^2\Omega^2] - (1 + \mu)\, m^*\Omega^2 F_R^* + 2m^*\zeta\alpha_I\Omega^3 F_I^* = 0 \tag{4.116}$$

$$4\pi\zeta\alpha_I\left(1 - \alpha_I^2\Omega^2\right) - 2m^*\zeta\alpha_I\Omega^2 F_R^* - (1 + \mu)\, m^*\Omega^2 F_I^* = 0 \tag{4.117}$$

Regarding g_1 and g_2 as the left sides of Eqs. (4.116) and (4.117), respectively, and expanding these functions in a Taylor series around α_{I0} and Ω_0:

$$g_1 = g_{10} + \left(\frac{\partial g_1}{\partial \alpha_I}\right)_0 (\alpha_I - \alpha_{Io}) + \left(\frac{\partial g_1}{\partial \Omega}\right)_0 (\Omega - \Omega_0) + \ldots \tag{4.118}$$

$$g_2 = g_{20} + \left(\frac{\partial g_2}{\partial \alpha_I}\right)_0 (\alpha_I - \alpha_{Io}) + \left(\frac{\partial g_2}{\partial \Omega}\right)_0 (\Omega - \Omega_0) + \ldots \tag{4.119}$$

Regarding the values of Eqs. (4.118) and (4.119) as zero:

$$\begin{pmatrix} \alpha_1 \\ \Omega \end{pmatrix} = \begin{pmatrix} \alpha_{I0} \\ \Omega \end{pmatrix} \begin{pmatrix} \partial g_1/\partial \alpha_I & \partial g_1/\partial \Omega \\ \partial g_2/\partial \alpha_I & \partial g_2/\partial \Omega \end{pmatrix}^{-1} \begin{pmatrix} g_{I0} \\ g_{20} \end{pmatrix} \tag{4.120}$$

From Eq. (4.120), values more accurate than α_{I0} and Ω_0: can be obtained. Therefore, by the above-mentioned procedure, non-dimensional frequency α_{I} and non-dimensional stability limit Ω can be calculated. The values $\partial g_j/\partial \alpha_{\mathrm{I}}$ and $\partial g_j/\partial \Omega$ ($j = 1, 2$), which are necessary in solving Eq. (4.120) are obtained by differentiating Eqs. (4.116) and (4.117). In Eq. (4.115), the following replacement is made:

$$g = \left(1 - \alpha^2\Omega^2\right)(1 + \mu + 2i\zeta\alpha\Omega) - 1 - \frac{m^*\Omega^2}{2\pi}(1 + \mu + 2i\zeta\alpha\Omega)F^* \tag{4.121}$$

Equation (4.121) is expanded in a Taylor series:

$$g = g_0 + \left(\frac{\partial g}{\partial \alpha}\right)_0 (\alpha - \alpha_0) + \ldots \tag{4.122}$$

Setting $g = 0$ into Eq. (4.122):

$$\alpha = \alpha_0 - g_0 / \left(\frac{dg}{d\alpha}\right)_0 \tag{4.123}$$

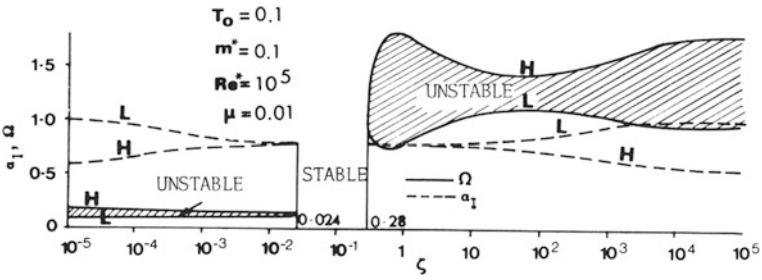

Fig. 4.17 Stability threshold for $T_0 = 0.1$, $m^* = 0.1$, $Re^* = 10^5$, $\mu = 0.01$. (*Courtesy* ASME [50])

Therefore, the non-dimensional complex eigenvalue a $(= \alpha_I - i\alpha_R)$ can be calculated by the procedure as mentioned in the foregoing paragraph.

Stability limits are given by a double root under a certain condition to be discussed later. In this paragraph the method of solving α_I, Ω and ζ, under the double root condition is presented.

The following function is defined:

$$h = g_1 + Zg_2 \tag{4.124}$$

where g_1 and g_2 stand for the left sides of Eqs. (4.116) and (4.117), respectively, and Z is an unknown constant. The differentiation of Eq. (4.124) by a_I and Ω gives

$$g_3 = \frac{\partial h}{\partial \alpha_I} = \frac{\partial g_1}{\partial \alpha_I} + Z\frac{\partial g_2}{\partial \alpha_I} \tag{4.125}$$

$$g_4 = \frac{\partial h}{\partial \Omega} = \frac{\partial g_1}{\partial \Omega} + Z\frac{\partial g_2}{\partial \Omega} \cdots \tag{4.126}$$

If a_I, Ω, ζ and Z, which satisfy $g_j = 0$ $(j = 1{-}4)$ can be calculated, a stability limit under the double root condition is obtained.

Expanding $g_j = 0$ $(j = 1{-}4)$ in a Taylor series around a_{I0}, Ω_0, ζ_0, and Z_0 and substituting $g_j = 0$ $(j = 1{-}4)$ into the equations obtained, the more accurate values for a_I, Ω, ζ and Z are calculated by the same method as mentioned in the paragraph on stability limits (Sect. 4.2). Figure 4.17 shows an example of a calculated stability limit in the case of $T_0 = 0.1$, $m^* = 0.1$, $Re^* = 10^5$, and $\mu = 0.01$. The solid curve and the dotted curve represent the stability limit and the whirling frequency, respectively. In order to distinguish the stable region from the unstable one, the complex eigenvalue has been calculated and is shown in Fig. 4.18.

The rotor system is unstable under the condition $a_R > 0$; therefore the discrimination between the stable region and the unstable one results in a form such as shown in Figs. 4.17 and 4.19.

In Fig. 4.17, if the non-dimensional rotating speed Ω is elevated at a given ζ, the system becomes unstable at the marginal curve *L*, and becomes stable again at

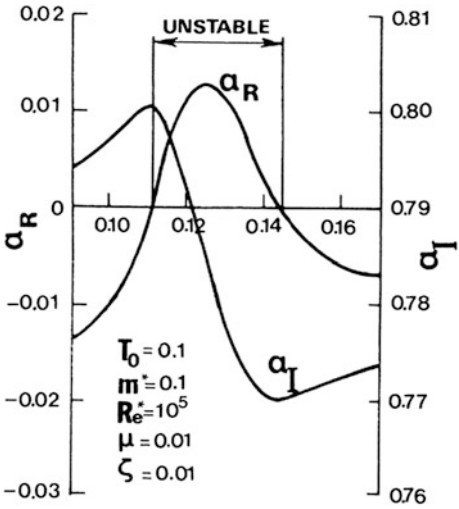

Fig. 4.18 Complex eigenvalue. (*Courtesy* ASME [50])

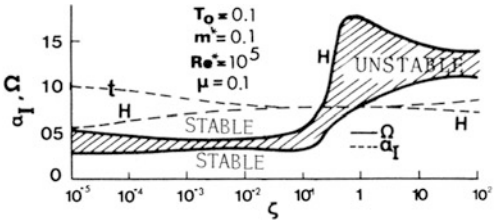

Fig. 4.19 Stability chart. (*Courtesy* ASME [50])

the marginal curve *H*. The whirling frequencies at the stability limits *L* and *H* are given by the values of frequency curves *L* and *H*, respectively. Within the unstable region, the non-dimensional whirling frequency a_I decreases with increasing Ω, as shown in Fig. 4.18, from the value of the curve *L* to that of *H*.

Next, in Fig. 4.17, the influence of non-dimensional external damping ζ on the stability limit is illustrated. If $\zeta \to 0$, it is clear from Eq. (4.117) that $F_I^* \to +0$. The two whirling frequencies (a_I), which satisfy $F_I^* \to +0$, exist as shown previously. These are named a_{I1} and a_{I2} ($a_{I1} < a_{I2}$). As $F_R^* = 0$ at $a_I = a_{I1}$ (normally 0.55–0.56), the stability limit is given by Eq. (4.116) as follows:

$$\Omega = \frac{1}{\alpha_I}\sqrt{\frac{\mu}{1+\mu}} \approx 0.181 \tag{4.127}$$

and as $F_R^* \approx 6$ at $a_I = a_{I2}$ (= 1), the stability limit is

$$\Omega \approx \sqrt{\frac{2\pi\mu}{(1+\mu)(2\pi a_I^2 + m^* F_R^*)}} \approx 0.095 \tag{4.128}$$

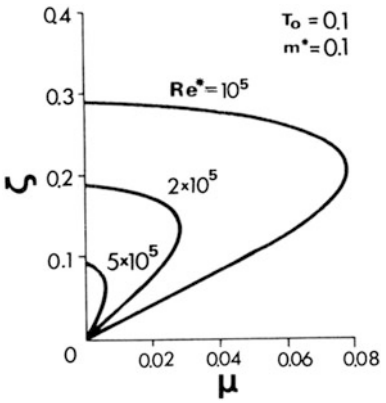

Fig. 4.20 Relation of ζ and μ for a stable system. (*Courtesy* ASME [43])

The unstable region becomes narrow gradually as the external damping increases, and vanishes in this example at $\zeta \approx 0.024$. The whirling frequencies approach each other and become equal at $\zeta = 0.024$. Under the condition $\zeta \approx 0.024$–0.28, the unstable region does not exist (absolutely stable). The condition under which the rotor system becomes absolutely stable as in this example is discussed in the following paragraph. The unstable region appears again in the region above $\zeta \approx 0.28$, and the stability limit is substantially larger than that in $\zeta < 0.024$. The cause for this change is found in the fact that the excessively large damping plays the same role as the large stiffness of the support bearing and the damped critical speed approaches that of simple support [49–56].

At $\zeta \to \infty$, the condition $F_I^* \to +0$ has to be satisfied to keep the last term of the left side of Eq. (4.116) finite. a_I which satisfies $F_I^* \to +0$ has the same value as that of $\zeta \to 0$. The following equation can be obtained from Eq. (4.117) as $F_R^* = 0$ at $a_I = a_{I1}$:

$$\Omega \approx \frac{1}{\alpha_I} = 1.81 \tag{4.129}$$

And, as $F_R^* \approx 6$ at $a_I = a_{I2}$, one obtains similarly

$$\Omega \approx \frac{1}{\alpha_I}\sqrt{\frac{2\pi}{2\pi a_I^2 + m^* F_R^*}} \approx 0.955 \tag{4.130}$$

In addition, the critical speeds under the conditions $\zeta \to 0$ and $\zeta \to \infty$ are given by Eqs. (4.128) and (4.129), respectively.

The calculated result of a stability limit under the same conditions as in Fig. 4.17, except for μ, is shown in Fig. 4.19. In this figure, though Ω and a_I under $\zeta > 10^2$ are not shown, these values are the same as in Fig. 4.17. It is found that the ζ value which makes the rotor system absolutely stable does not exist if μ is large, as in this case.

Re^*, T_0 and m^* are other factors that influence the stability limit. The larger these factors are, the smaller the stability limit of the rotor. And finally, the region in which the system is absolutely stable disappears.

As mentioned already, the instability of the rotor system does not exist in a certain range of ζ and the other factors. For example, the solutions a_I and Ω, of Eqs. (4.116) and (4.117) can be regarded as double roots at $\zeta = 0.024$ as well as at $\zeta = 0.28$. Therefore, the marginal condition under which the system becomes absolutely stable may be obtained by the method by which a double root is calculated.

The relationship between ζ and μ which make the system absolutely stable, is computed under the condition $T_0 = 0.1$ and $m^* = 0.1$, and is shown in Fig. 4.20, where Re^* is taken as a parameter. In this figure, the rotor system is absolutely stable in the region enclosed by the curved line of a given Re^* and the ζ-axis. It is found that the more μ or Re^* increases, the more the range of ζ decreases. This makes the system absolutely stable, and finally the absolutely stable region disappears.

References

1. Den Hartog, J.P.: Mechanical Vibrations, 3rd edn. McGraw- Hill, New York (1947)
2. Alford, J.S.: Protecting turbomachinery from self-excited rotor whirl. J. Eng. Power, Oct (1965)
3. Thomas, H.J.: Unstable Oscillations of Turbine Rotors due to Steam Leakage in the Clearance of Rotor and Bucket Packings, AEG Technical Publication No. 1150 (1956)
4. Gasch, R.: Stabiler Lauf von Turbinenrotoren. Konstruktion, **17**(11), 447–452 (1965)
5. Kraemer, E.: Selbsterregte Schwingungen. Brenn.- Waerme- Kraft, **20**, 7 (1968)
6. Vogel, D.H.: The vibration and stability behavior of unbalanced multi span shafts. Konstruktion **2**(2), 12 (1970)
7. Vogel, D.H.: The Stability of Turbomachine Rotors on Journal Bearings. Dissertation, Technical University of Munich (1971)
8. Black, H.F.: Lateral Stability and Vibrations of High Speed Centrifugal Pump Rotors, IUTAM Symposium on Dynamics of Rotors. Springer, Berlin (1974)
9. Shapiro, W., Colsher, R.: Rotor Whirl in Turbomachinery, Mechanisms, Analysis and Solution Approaches, ASME Winter Annual Meeting, Atlanta, Nov (1977)
10. Pollman, E., Schwerdtfeger, H., Termuehlen, H.: Flow excited vibrations in high pressure turbines (Steam Whirl). ASME J. Eng. Power **100**, 219–228 (1978)
11. Kwanka, K., Ortinger, W.: Rotordynamic coefficients of long staggered labyrinth gas seals. Int. J. Rotating Mach. **1**(3–4), 285–291 (1995)
12. Pugachev, A.O., Kleinhans, U., Gaszner, M.: Prediction of rotordynamic coefficients for short labyrinth gas seals using computational fluid dynamics J. Eng. Gas Turbines Power **134**, (062501) (2012)
13. Kubiak, S.z., J., Childs, D., Rodriguez, M., García, M.C.: Investigation into a "steam whirl" which affected HP rotors of 300 MW steam turbines Proceedings of the ASME Power Conference 291–298 (2007)
14. Bachschmid, N., Pennacchi, P., A.: Vania, Steam-whirl analysis in a high pressure cylinder of a turbo generator. Mech. Syst. Sign. Proc. **22**, 121–132 (2008)

15. Pennacchi, P., Vania, A.: Analysis of the instability phenomena caused by steam in high-pressure turbines. Shock Vibr. **18**(4), 593–612 (2011)
16. Wright, D.V.: Air Model Tests of Labyrinth Seal Forces on a Whirling Rotor. ASME J. Eng. Power **100**, 533–543 (1978)
17. Dimarogonas, A.D.: Analysis of steam whirl. General Electric Technical Information Series, DE-71-LS-48. Schenectady, NY (1971)
18. Dimarogonas, A.D.: A linear rotor stability analysis. General Electric Technical Information Series, DF-72-LS-32. Schenectady, NY (1972)
19. Dimarogonas, A.D.: A general method for stability analysis of rotating shafts. Ing. Arch. **44**, 9–20 (1975)
20. Pfleiderer, C.: Stroemungsmachinen. Springer, Berlin (1952)
21. Yamada, Y., Nakabayashi, K.: On flow between eccentric rotating cylinders. Bull. JSME, **11**(45), (1955)
22. Yamada, Y., Nakabayashi, K., Sujuki, Y.: Viscous frictional moment between rotating cylinders. Bull. JSME, **12**(53) (1956)
23. Yamada, Y., Nakabayashi, K. and Maeda, K. Pressure drop measurements of a flow through eccentric cylinders, Bull. JSM E, **12**(53), 1956
24. Kimball, A L.: Internal friction theory of shaft whipping. General Electric Review, **27**, 244–251 (1924)
25. Lazan, B.J.: Damping of Materials and Members in Structural Mechanics. Pergamon Press, Oxford (1968)
26. Pincus, O., Sternlight, B.: Theory of Hydrodynamic Lubrication. McGraw-Hill, New York (1961)
27. Mechanical technology, INC.: Design handbook for fluid film type bearings, AFAPL-TR-65-45 (1965)
28. Haag, A.C., Sankey, G.O.: Some dynamic properties of oil film journal bearings, for application to unbalance vibration calculation. ASME Trans. **78**, 302–306 (1959)
29. Haag, A.C., Sankey, G.O.: Elastic and damping properties of oil-film journal bearings. J. Appl. Mech. **23**, 101–108 (1956)
30. Booser, E.R., Missana, A., Ryan, F.D.: Performance of oil- large steam turbine journal bearings. ASME Trans. **13**(4), 262–268 Oct (1970)
31. Andritsos, F.E., Dimarogonas, A.D.: Nonlinear pad functions for static analysis of tilting pad bearings. ASME Trans. J. Lubrication Technol. **102**, 25–33 (1980)
32. Ruhl, R.L., Booker, J.F.: A finite element model for distributed parameter turborotor systems. ASME Paper 71-Vibr.-56 (1971)
33. Paidoussis, M.P.: Fluid elastic vibration of cylinder arrays in axial and cross flow: state of the art. J. Sound Vibr. **76**(3), 329 (1981)
34. Stokes, G.G.: On some cases of fluid motion, Cambridge Philosophical Soc. Proc. **8**, 105–37, May (1843)
35. Fritz, R.J.: The effect of an annular fluid on the vibrations of a long rotor. Dissertation, Rennselaer Polytech. Inst., Troy, New York (1968)
36. Fritz, R.J.: The effect of an annular fluid on the vibrations of a long rotor. J. Basic Eng. **92**, 923 (1970)
37. Page, L.: Introduction to Theoretical Physics, 2nd edn. Van Nostrand Co., Inc, Princeton (1935)
38. Saito, S., Someya, T.: Self-excited vibration of a rotating hollow shaft partially filled with a liquid, ASME Paper 79-DET-62. Design Engineering Technology Conference, St. Louis (1979)
39. Kollmann, F.G.: Experimentelle und theoretische untersuchungen uber die kritischen drehzahlen flüssigkeitsfüllter hohlkörper. Forsch. Ing. Wes **28**(4), 115–123 (1962)
40. Kollmann, F.G.: Experimentelle und theoretische untersuchungen uber die kritischen drehzahlen flüssigkeitsfüllter hohlkörper. Forsch. Ing. Wes **28**(5), 147–153 (1962)
41. Wolf, J.A., Whirl, J.R.: Dynamics of a rotor partially filled with liquid. Trans. ASME J. Appl. Mech. **35**(4), 676–682 (1968)

42. Daich, I.M.: A non-conservative problem of the vibrations of a rigid body with a cavity filled with an ideal liquid. Prikl. Mech. **7**, 44–48 (1971). (in Russian)
43. Ehrich, F.F.: The influence of trapped fluids on high speed rotor vibration. Trans. ASME, J. Eng. Ind. **89**, 806–812 (1967)
44. Daich, I.M., Bar, I.L.: Vibrations of a rotating rigid body with a cavity partly filled with a viscous liquid. Prikl. Mech. **7**(5), 64–69 (1973) (in Russian)
45. Daich, I.M., Kazdan, L.S.: Vibration of a rotating rigid body with a cavity partly filled with an arbitrary viscous liquid. Sov. Appl. Mech. **9**(8), 888–891 (1975)
46. Saito, S., Someya, T.: Investigation into the vibration of a rotating hollow shaft partially filled with liquid—part 1, numerical solution of liquid force by the finite difference method. Trans. JSME **44**(388), 4115–4122 (1978) (in Japanese)
47. Saito, S., Someya, T.: Investigation into the vibration of a rotating hollow shaft partially filled with liquid—part 2, approximate solution of liquid force by regarding coefficients as constants. Trans. JSME **44**(388), 4123–4129 (1978) (in Japanese)
48. Phillips, O.M.: Centrifugal waves, 1. Fluid Mech. **7**, 340–352 (1960)
49. Saito, S., Someya, T.: Investigation into the vibration of a rotating hollow shaft partially filled with liquid—part I, influence of the amount of damping and bearing/shaft rigidity ratio on the damping ratio. Trans. JSME **43**(376), 4474–4484 (1977) (in Japanese)
50. Saito, S.: Self-excited vibration of a rotating hollow shaft partially filled with a liquid. J. Mech. Des. Trans. ASME **102**(1), 185–192 (1980)
51. Dimarogonas, A.D.: Limit cycles for pad bearings under fluid excitation, STLE Transactions. **31**(1), 66–70 (1987)
52. Holm-Christensen, O., Traeger, K.: Note on rotor instability caused by liquid motions. J. Appl. Mech. Trans. ASME **58**(3), 804–811 (1991)
53. Dimarogonas, A.D.: MELAB: computer programs for mechanical engineers. Englewood Cliffs N.J., Prentice-Hall (1993)
54. Dimarogonas, A.D., Gomez-Mancilla, J.: Flow excited turbine rotor instability. Int. J. Rotating Mach. **1**(1), 37–51 (1994)
55. Sato, Y., Morii, S., Nagamine, T., Ishikawa, Y.: Stability of a rotating hollow rotor partially filled with liquid (effect of discharging liquid by centrifugal force). Nihon Kikai Gakkai Ronbunshu, C Hen/Trans. Japan Soc. Mech. Eng. Part C **71**(2), 359–365 (2005)
56. Krämer E.: Models for computation of turbomachine vibrations. ASME paper 85-DET-138 (1985)

Chapter 5
Heat-Flow-Induced Vibration of Rotating Shafts: The Newkirk Effect

Abstract Packing rub effect is the unstable vibration induced by friction forces and generated heat on a rotor when it rubs on a clearance annulus. Its main controlling factors are friction characteristics at the sliding contact and the dynamic response of the rotor, bearings, supports and foundation system. In Chapter 5 rotor instabilities are investigated, resulting from friction heating, a phenomenon known as the 'Newkirk effect'. The interaction between vibration characteristics and heat generation leads to a non-linear feedback system exhibiting either stable or unstable behavior.

5.1 Introduction

Around rotating shafts there exist stationary components such as packings, seals and oil deflectors, used to separate two fluids and to ensure mechanical limitations. When rotating parts come into contact with stationary elements, heat is generated which deforms the parts, and finally imbalance and vibration are produced [1–4]. On other occasions, due to normal or accidental presence of fluids in the gaps between rotating and stationary components, heat may be generated due to an abnormal flow of these fluids, or the abnormal energy dissipation within their bulk, leading to the same results as above.

The usual form of seals, subject to rotor rubbing phenomena, is of the labyrinth type used in turbines. With these seals the designer has to choose between materials which wear quickly and with a low coefficient of friction, or harder materials resisting wear but with a high coefficient of friction. The materials selected must meet additional requirements, such as corrosion and erosion resistance, high thermal conductivity, and strength at high temperatures. At the places of contact between

A. D. Dimarogonas et al., *Analytical Methods in Rotor Dynamics*, Mechanisms and Machine Science 9, DOI: 10.1007/978-94-007-5905-3_5,

stationary and rotating parts, considerable forces may appear as friction forces or shock forces in case of violent interaction [5]. The combined effect of heating imbalance, and direct forces, can be either amplifying or a stabilising. In case of amplification, a continuous increase in amplitude and phase angle usually appears and a polar presentation of these quantities exhibits an outward spiral curve [6].

The rotating parts may also be surrounded by a fluid environment, which can exert considerable influence. For example, the phenomenon of fluid-induced instability in bearings has been observed with high-speed machinery, as well as with other cases in which the rotors are working in a fluid environment such as steam and gas turbines, pumps, etc. Under certain circumstances, vibration can be induced by fluids trapped within the annuli between stationary and rotating parts [7] (see Chap. 4).

Vibration can also be initiated or amplified by structural instabilities arising from transmitted forces (buckling), or torques (torsional buckling).

The packing rub effect occurs when a rotating shaft, R (Fig. 5.1), due to its bow, O_2O_1, and due to the displacement of its centre of rotation from O to O_1 comes into contact with a stationary part, S. In the above model, a circular and synchronous orbit of the geometric centre of the rotor O_2 about O, has been assumed. At angle ωt contact occurs at point D, which moves on the rotor circumference between points C and B. A portion of the friction heat generated goes into the rotor between B and C and bows the rotor because the resulting temperature field is non-uniform. Depending on the dynamic characteristics of the rotor, vibration can decrease (if imbalance is at location U_z), or increase (if the imbalance is at location U). Generally there is also a phase shift between the position of the original bow and the location of the thermal bow produced which can be synthesized vectorially, so that the result is a spiral pattern respectively converging or diverging.

In the latter case the result is usually severe damage of the interacting parts, sometimes leading to catastrophic failure. In last decades, many such incidents

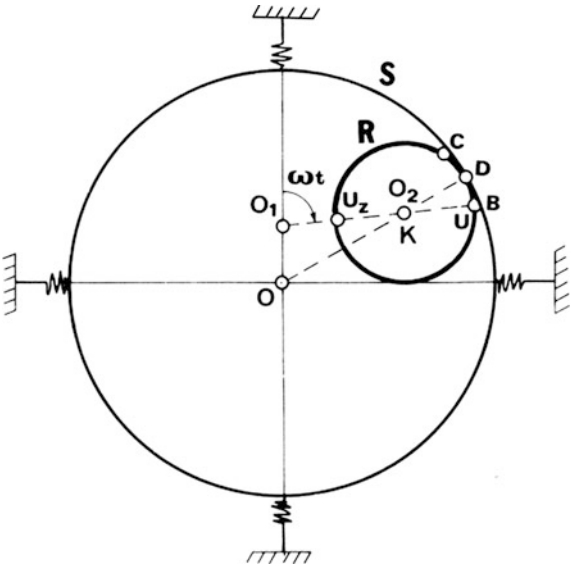

Fig. 5.1 Diagram of a bowed, eccentric rotor in contact with a flexible stator

have been reported with a variety of machines, such as steam and gas turbines, pumps, compressors and aircraft engines.

Rubbing problems were identified and reported in 1925 [8] for a vertical hydroelectric turbine-generator. Newkirk [4] noticed the thermal character of the phenomenon and gave a correlation with the critical speeds. At the same time tests were performed by Taylor [9] to verify the hypothesis of Newkirk that rubbing instability occurs below the critical speeds while above the critical speed there is a self-stabilizing effect because of the reversal of the phase angle between the exciting force (imbalance due to thermal deflection) and dynamic deflection. Taylor used a 'bent shaft' model. When light rub was applied below the critical speed, the amplitude built up slowly at first and then faster. Tests above the critical speed showed that with light rubbing the vibration level decreased. Newkirk and Taylor also noticed a backward rubbing whip in tests when the rubbing accidentally became very hard. The direction of rotation and its speed was slightly higher than the rotor's critical speed. An explanation of this can be given by considering the friction forces developing during rubbing. At higher speeds these forces have little influence, since heat propagation is so rapid that their effect is minimized.

Kroon and Williams [6, 10] noticed the spiral character of the packing rub effect. Keeping track of the amplitude and the associated phase angle they tried to correlate the experimental results mathematically to provide an analytical tool predicting the rubbing response.

The first attempt for a direct analytical attack on the problem was made by Sweets [11]. He considered a shaft bowed by heat input from a packing rub. To simplify the problem he ignored axial conduction along shaft's axis, which is the main limitation of his analysis.

A good step towards a more accurate analytical solution of the dynamic part of the problem was made by Boley [12] for thermally induced vibration in beams and plates. This analysis does not consider rotation and assumes two-dimensional temperature distribution to make the calculation of the temperature field easier; the same assumption has been made by Sweets and Kroon and Williams in their models.

The three-dimensional problem is quite elaborate and is usually resolved by the turbine manufacturers with numerical methods [13].

To make possible a prediction of the areas of instability and of the movement of the rotor, an analytical approach to the problem is necessary. In the following part of this chapter, analytical models are developed for the physical phenomenon, calibrated and verified with experimental investigation.

5.2 Analytical Model

Consider a packing of circular cross-section, Fig. 5.2. Let O be its centre if rubbing does not take place. We assume packing to be capable of translation perpendicular to its axis; a restoring force is assumed to act on the packing at the point O' of its actual centre in the direction of $O'O$. Consequently, the position with centre O is

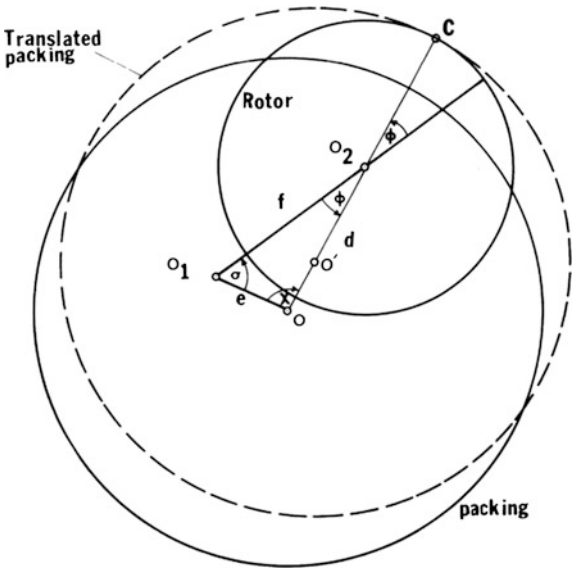

Fig. 5.2 Geometry of packing-rotor interaction

one of static equilibrium. The rotor with geometric centre at O_2 is assumed to revolve about the fixed pole O_1. The distance O_1O_2 gives the absolute value f of the dynamic bow; the line O_1O_2 is fixed to the rotor. The eccentricity e of the system is given by the distance OO_1. Let c be the clearance, i.e. the difference of the radii of packing and rotor. If $d = OO_2$ is less than c, the packing has its centre at O; if $d > c$, then rubbing occurs, and the packing will yield to the rotor and move to a position with centre O' such that O, O' and O_2 are on a straight line and such that packing and rotor touch one another. Rubbing takes place at the point C of the contact. It is important to describe the motion of C on the rotor as well as on the packing. To this end we introduce angles σ, φ, χ for triangle O_1O_2O; here σ gives the actual position of the rotor at any moment; φ measures the position of C in the rotor-fixed reference system and χ measures the position of C in the packing-fixed reference system. The angles are counted positive as indicated by the arrows in Fig. 5.2. For reasons of symmetry it suffices to consider the case $0 \leq \sigma \leq \pi$. We have $\sigma = \pi - \varphi - \chi$. In general φ is not a monotonous function of σ, and it takes several distinctions of parameter constellations c, e, f in order to describe the relationship properly.

Observing that rubbing can take place only if

$$e + f \geq c \tag{5.1}$$

and imposing the conditions

$$e < c \quad f < c \tag{5.2}$$

under which rubbing occurs in actual machine operation, we can render our task considerably easier. We have

$$f^2 = e^2 + d^2 - 2ed\cos\chi \geq e^2 + d^2 \geq c^2 \tag{5.3}$$

for $\cos\chi \leq 0$. But this contradicts (5.2) and $\cos\chi \leq 0$ cannot occur; likewise $\cos\chi \leq 0$ is impossible for a situation of rubbing. This leads to

$$0 \leq \varphi \qquad \chi \leq \pi/2 \tag{5.4}$$

But

$$f\sin\varphi = e\sin\chi \tag{5.5}$$

Conditions (5.4) and (5.5) imply that φ and χ increase and decrease simultaneously. Since $\sigma = \pi - \varphi - \chi$ we have to conclude that φ as well as χ is a monotonously decreasing function of σ. We have

$$d^2 = e^2 + f^2 - 2ef\cos\sigma \tag{5.6}$$

This makes d a monotonously increasing function of σ. We have

$$d = e + f \geq c$$

for $\sigma = \pi$ and

$$d = |e - f| < c$$

for $\sigma = 0$.

Clearly rubbing occurs if and only if $\sigma_0 \leq \sigma \leq \pi$ with $d = c$ for $\sigma = \sigma_0$. The angles φ and χ vary between zero and values $\alpha/2$ and $\Omega/2$, respectively. The latter ones are taken for $\sigma = \sigma_0$. Figure 5.3 shows the situation.

We find

$$\left.\begin{aligned}\cos\tfrac{\alpha}{2} &= \tfrac{c^2+f^2-e^2}{2cf}\\ \cos\tfrac{\Omega}{2} &= \tfrac{e^2+c^2-f^2}{2ec}\end{aligned}\right\} \tag{5.7}$$

Finally, lifting the restriction $0 \leq \sigma \leq \pi$, we can state that the intervals

$$\left.\begin{aligned}-\tfrac{\alpha}{2} \leq \varphi \leq \tfrac{\alpha}{2}\\ -\tfrac{\Omega}{2} \leq \chi \leq \tfrac{\Omega}{2}\end{aligned}\right\} \tag{5.8}$$

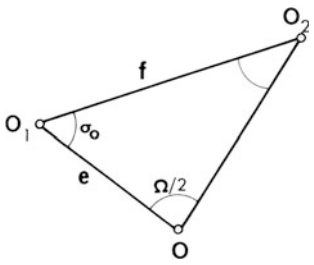

Fig. 5.3 Angles associated with ring geometry

are monotonously swept by C during one rotor revolution of the. Rubbing generates heat at an average rate

$$Q = \frac{\mu \bar{F} \alpha \Omega \omega}{2\pi J} \tag{5.9}$$

where μ is the coefficient of friction, $\bar{F}$ the normal force acting on the packing, α the outer radius of the rotor, ω its angular velocity, and J the mechanical equivalent of heat. The heat, somehow distributed over the interval $-\alpha/2 \leq \varphi \leq \alpha/2$ enters the rotor and causes a thermal deflection. Consequently the total bow f and the direction of O_1O_2 will change with respect to a rotor-fixed reference system. Even so it is reasonable to assume that the change of O_1O_2 in relation to the rotor is negligible during one revolution. This will permit us to retain Eqs. (5.7–5.9). The angle φ takes on a new meaning. We must set

$$\varphi = \theta - \Psi \tag{5.10}$$

where θ and Ψ are polar angles, measured with respect to the centre of the rotor in a rotor-fixed coordinate system. Ψ indicates the midpoint of the segment of rubbing while θ characterises the points C of contact. From here on we consider Ψ, α, Ω, f, Q as functions of time t.

We turn now to an investigation of the thermal bow. We expect rubbing to be highly localised and we assume that the length L of the rotor is large compared with the length l of the heating zone. Figure 5.4 shows the situation for a rotor extending along the z-axis of a Cartesian coordinate system with axes x, y, z and bent in the (x, z) plane due to rubbing of its outer cylindrical surface in the zone $-l/2 \leq z \leq l/2$.

Assuming that the portions of the rotor outside the rubbing zone stay straight or exhibit negligible bend only, the bow can be expressed approximately as

$$B = \frac{L\bar{\omega}}{4} \tag{5.11}$$

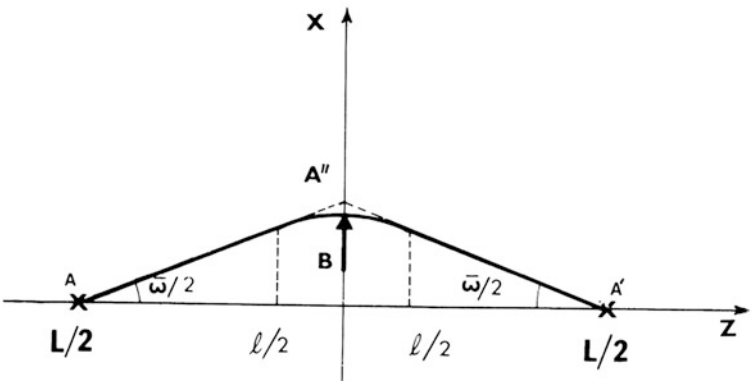

Fig. 5.4 Geometry of a locally bowed rotor

where $\bar{\omega}$ is the angle of flexural rotation of one end relative to the other. Equation (5.11) has an error due to substituting triangle A, A′, A″ for the exact shape of the bowed rotor; however, this error is believed to be quite negligible [1].

In order to apply Eq. (5.11) we must determine angle $\bar{\omega}$. Let T denote the temperature in the rotor as a function of location and time, the temperature field caused by rubbing. For a prismatic bar, extending along the z-axis and bending in the (x, z) plane under the action of T. Goodier [14] defines 'a mean thermoelastic flexural rotation of one end relative to the other' by the integral

$$\bar{\omega} = \frac{1}{I}\int_V \varepsilon T x \, \mathrm{d}x\mathrm{d}y\mathrm{d}z \tag{5.12}$$

over the volume V of the bar. I represents the moment of inertia of the bar cross-section with respect to the y-axis, and ε is the thermal expansion coefficient. Goodier's formula is based on Betti's reciprocity theorem. Its angle $\bar{\omega}$ is not exactly the angle of Eq. (5.11) but since it appears that the difference is irrelevant, we shall ignore it. If bowing is not restricted in the (x, z) plane, it is useful to let B be complex such that Re{B}, Im{B} give the bow in the x- and y-directions, respectively. Since we are concerned with rotors in the form of hollow cylinders made of isotropic material, the moment I is the same for the x- and the y-axis. This permits us to set up the complex bow in the form

$$B = \frac{L\varepsilon}{4I}\int_V T(x+iy)\, \mathrm{d}x\mathrm{d}y\mathrm{d}z \tag{5.13}$$

We turn now to the relevant features of the temperature field. It is convenient to refer it to cylindrical coordinates r, θ, z, where $x = r\cos\theta$, $y = r\sin\theta$. If the inner rotor surface has a radius b and the outer one has a radius a, then the rotor can be described by $b \le r \le a$ and $-L/2 \le z \le L/2$.

We write $T = T(r, \theta, z)$ and observe that Eq. (5.13) can be given in the form

$$B = \frac{L\varepsilon}{4I}\int_b^a \int_0^{2\pi} \int_{-L/2}^{L/2} T(r,\theta,z;t) r^2 \exp(i\theta)\, \mathrm{d}z\mathrm{d}\theta\mathrm{d}r \tag{5.14}$$

T must satisfy the partial differential equation

$$\frac{\partial^2 T}{\partial r^2} + \frac{1}{r}\frac{\partial T}{\partial r} + \frac{1}{r^2}\frac{\partial^2 T}{\partial \theta^2} + \frac{\partial^2 T}{\partial z^2} = \frac{1}{K}\frac{\partial T}{\partial t} \tag{5.15}$$

and the initial condition

$$T = 0 \quad \text{for} \quad t < 0$$

if rubbing does not begin before $t = 0$. Equation (5.15) has to be supplemented by boundary conditions. We set

$$\left.\begin{aligned} \frac{\partial T}{\partial z} &= 0 \text{ for } z = \pm\frac{L}{2} \\ -k\frac{\partial T}{\partial r} + h_b T &= 0 \text{ for } r = b \end{aligned}\right\} \tag{5.16}$$

$$k\frac{\partial T}{\partial r} + h_a T = g(\theta, z; t) \quad \text{for} \quad r = a \tag{5.17}$$

Here k, $-k$, h_a, h_b are thermodynamic constants; $g(\theta, z; t)$ gives the heat rate density per unit area, generated by rubbing at the point θ, z of the outer cylinder $r = a$.

It is remarkable that we need not specify $g(\theta, z; t)$ in every detail.

Introducing the integrals

$$\left.\begin{aligned} Z(r, \theta; t) &= \int_{-\frac{L}{2}}^{\frac{L}{2}} T(r, \theta, z; t)\mathrm{d}z \\ \bar{g}(\theta, t) &= \int_{-\frac{L}{2}}^{\frac{L}{2}} g(\theta, t)\mathrm{d}z \end{aligned}\right\} \tag{5.18}$$

We observe that Eq. (5.14) requires the knowledge of Z only; on the other hand, from Eqs. (5.15) and (5.16) it follows that

$$\frac{\partial^2 Z}{\partial r^2} + \frac{1}{r}\frac{\partial Z}{\partial r} + \frac{1}{r^2}\frac{\partial^2 Z}{\partial \theta^2} = \frac{1}{K}\frac{\partial Z}{\partial t} \tag{5.19}$$

Furthermore, Eq. (5.17) is satisfied with T replaced by Z and finally

$$\left.\begin{aligned} -k\tfrac{\partial Z}{\partial r} + h_b Z &= 0 \quad \text{for } r = b \\ k\tfrac{\partial Z}{\partial r} + h_a Z &= \bar{g}(\theta, \mathrm{z}; \mathrm{t}) \quad \text{for } r = a \end{aligned}\right\} \tag{5.20}$$

The bow can be expressed in the form

$$\left.\begin{aligned} B &= \tfrac{L\varepsilon}{4I}\int_b^a r^2 W(r, t)\mathrm{d}r \\ W(r, t) &= \int_0^{2\pi} Z(r, \theta; t)\, \exp(i\theta)\, \mathrm{d}\theta \end{aligned}\right\} \tag{5.21}$$

$W(r, t)$ represents (divided by π) a complex Fourier component of Z with respect to θ. It satisfies

$$\frac{\partial^2 W}{\partial r^2} + \frac{1}{r}\frac{\partial W}{\partial r} - \frac{W}{r^2} = \frac{1}{K}\frac{\partial W}{\partial t} \tag{5.22}$$

and the boundary conditions

$$\left.\begin{array}{l} k\frac{\partial W}{\partial r} + h_a W = w(t) \\ w(t) = \int_0^{2\pi} \bar{g}(\theta, t) \exp(i\theta) \mathrm{d}\theta \end{array}\right\} \tag{5.23a}$$

for $r = a$ and

$$-k\frac{\partial W}{\partial r} + h_b W = 0 \tag{5.23b}$$

for $r = b$.

W also satisfies Eq. (5.15), i.e. $W = 0$ for $t < 0$. The function $W(r, t)$ can be found by Laplace transform. Introducing

$$\bar{W}(r, p) = \int_0^{\infty} \exp(-pt) W(r, t) \mathrm{d}t \tag{5.24}$$

as the transform of W. In similar vein we introduce $\bar{w}$ and $\bar{B}$ as transforms of $w(t)$ and of $B(t)$ respectively.

Furthermore we set $\lambda^2 = p/K$. From Eq. (5.22) and from $W = 0$ for $t < 0$ it follows that

$$\bar{W}'' + \frac{1}{r}\bar{W}' - \frac{1}{r^2}\bar{W} - \lambda^2 \bar{W} = 0 \tag{5.25}$$

Consequently

$$\bar{W} = \gamma I_1(\lambda r) + \delta K_1(\lambda r) \tag{5.26}$$

where I_1 and K_1 are modified Bessel functions of the first order. The coefficients γ and δ must be determined from Eq. (5.23a, b) which remain valid if W, w are replaced by $\bar{W}$, $\bar{w}$ respectively. The boundary conditions yield

$$\left.\begin{array}{l} a_{11}\gamma + a_{12}\delta = \frac{a\bar{w}}{k} \\ a_{21}\gamma + a_{22}\delta = 0 \end{array}\right\} \tag{5.27}$$

where

$$\left.\begin{array}{ll} a_{11} = a\lambda I_1'(\lambda a) + u I_1(\lambda a) & a_{12} = a\lambda K_1'(\lambda a) + u K_1(\lambda a) \\ a_{21} = b\lambda I_1'(\lambda b) + v I_1(\lambda b) & a_{22} = b\lambda K_1'(\lambda b) + \upsilon K_1(\lambda b) \end{array}\right\} \tag{5.28}$$

$$u = \frac{h_a}{k} \qquad \upsilon = \frac{h_b}{k}$$

Since

$$zI_1'(z) = zI_0(z) - I_1(z) \quad zK_1'(z) = zK_0(z) - K_1(z)$$

we also have

$$
\begin{aligned}
a_{11} &= \lambda a I_0(\lambda a) + (u-1) I_1(\lambda a) \\
a_{12} &= \lambda a K_0(\lambda a) + (u-1) K_1(\lambda a) \\
a_{21} &= \lambda b I_0(\lambda b) + (u+1) I_1(\lambda b) \\
a_{22} &= \lambda b K_0(\lambda a) + (u+1) K_1(\lambda b)
\end{aligned}
$$

The solution of Eq. (5.27) is

$$
\left.
\begin{aligned}
\gamma &= \tfrac{a_{22} a \bar{w}}{k\Delta} \\
\delta &= -\tfrac{a_{21} a \bar{w}}{k\Delta}
\end{aligned}
\right\} \tag{5.29}
$$

with

$$\Delta = a_{11} a_{22} - a_{12} a_{21}$$

The computation of the determinant Δ is somewhat simplified if one uses the well-known expression for the Wronskian:

$$I_0(z) K_1(z) + I_1(z) K_0(z) = 1/z$$

We obtain

$$\Delta = \lambda^2 ab D_{00} + \lambda a(v+1) D_{01} + \lambda b(u-1) D_{10} + (u-1)(v+1) D_{11} \tag{5.30}$$

with

$$D_{mn} = I_m(\lambda a) K_n(\lambda b) - (-1)^{\mathrm{m+n}} I_n(\lambda b) K_m(\lambda a)$$

where $m, n, = 0, 1$. We are now in a position to represent $\bar{B}$ in a closed form. From Eq. (5.21) it follows that

$$\bar{B} = \frac{L\varepsilon}{4I} \int_b^a \bar{W} r^2 \mathrm{d}r \tag{5.31}$$

Since Eq. (5.25) can be rewritten in the form

$$\lambda^2 r^2 \bar{W} = r^2 \bar{W}'' + r\bar{W}' - \bar{W} = \left(r^2 \bar{W}' - r\bar{W}\right)' \tag{5.32}$$

it follows right away

$$\lambda^2 \int_b^a \bar{W} r^2 dr = \left(r^2 \bar{W}' - r\overline{W}\right)|_b^a \tag{5.33}$$

It remains to use Eqs. (5.26) and (5.29). After some elementary steps we arrive at

$$\bar{B} = \frac{L\varepsilon}{4Ik} a^4 \bar{P} \bar{W} \tag{5.34}$$

and

$$P = \frac{ab\lambda^2 D_{00} + a(\upsilon+1)\lambda D_{01} - 2b\lambda D_{10} - 2(v+1)D_{11} + b/a(1-\upsilon)}{a^2\lambda^2\left[ab\lambda^2 D_{00} + a(\upsilon+1)\lambda D_{01} + b(u-1)\lambda D_{10} + (u-1)(\upsilon+1)D_{11}\right]} \tag{5.35}$$

P represents Laplace transform of a function $P(t)$. Under the circumstances (by virtue of the convolution theorem) we may write

$$B(t) = \frac{La^4\varepsilon}{4Ik}\int_0^t P(t-s)w(s)\mathrm{d}s \tag{5.36}$$

We shall apply this general formula to the special case in which $w(t)$ represents the influence of heat flow into the rotor due to rubbing.

Our first concern is to link the function $\bar{g}(\theta,t)$ to the rate of heat $Q = Q(t)$ is given by Eq. (5.9). In view of Eq. (5.10) we set

$$g(\theta,t) = h(\varphi,t) \quad \text{for } -\frac{\alpha}{2} \le \varphi \le \frac{\alpha}{2} \tag{5.37}$$

On the function h we impose the conditions

$$h(\varphi,t) = h(-\varphi,t)$$

and

$$a\int_{-\alpha/2}^{\alpha/2} h(\varphi,t)\mathrm{d}\varphi = Q(t) \tag{5.38}$$

We postulate now that $h =$ constant with respect to φ for $|\varphi| \le \frac{a}{2}$. This leads to

$$h = \frac{Q(t)}{a\alpha} \quad \text{for } -\frac{\alpha}{2} \le \varphi \le \frac{\alpha}{2} \tag{5.39}$$

The function $w(t)$ is

$$w(t) = \frac{Q(t)}{a\alpha}\exp(i\Psi)\int_{-\alpha/2}^{\alpha/2}\exp(i\varphi)\mathrm{d}\varphi = \frac{Q(t)}{a}\frac{2\sin(\alpha/2)}{\alpha}\exp(i\Psi) \tag{5.40}$$

While the choice of h appears to be rather arbitrary, it can be hoped nevertheless that $w(t)$ is not much affected by our choice. As an example, let us consider another possibility for h, namely

$$h(\varphi,t) = \frac{6Q(t)}{a\alpha^3}\left(\frac{\alpha^2}{4} - \varphi^2\right) \quad \textit{for } -\frac{\alpha}{2} \le \varphi \le \frac{\alpha}{2} \tag{5.41}$$

This function complies with the conditions formulated above. It decreases to zero as φ goes to $\pm a/2$. The associated function $w(t)$ is

$$\left.\begin{aligned} w(t) &= \tfrac{Q(t)}{a}\tfrac{2\sin(\alpha/2)}{\alpha}\mathrm{A}(\alpha)\exp(i\Psi) \\ \mathrm{A}(\alpha) &= \tfrac{6}{\alpha^2}(2-\cot\alpha/2) \end{aligned}\right\} \tag{5.42}$$

The computations leading to Eqs. (5.41) and (5.42) are elementary and left to the reader. As we see, the function of (5.42) differs from that of (5.40) by a factor $A(\alpha)$. As is to be expected, $A(\alpha) \to 1$ as $\alpha \to 0$. For small angles α, the difference between the two $w(t)$ is certainly negligible. Let us now take the largest α admissible. This is $\alpha = \pi$, and we find $A(\alpha) = 12/\pi^2$. In this case the deviation is of the order of 20 %. In view of the fact that the coefficient of friction μ in Eq. (5.9) for $Q(t)$ is not well-known and that the thermodynamic constants may also be somewhat uncertain, our choice of Eq. (5.39) and the associated Eq. (5.40) is justified on practical grounds. From here on we deal with Eqs. (5.39) and (5.40) only.

Since $Q(t)$ is proportional to $\Omega(t)$, we can link $B(t)$ to $\Omega(t)$, and

$$B(t) = nL\int_0^t P(t-s)q(s)\mathrm{d}s \tag{5.43}$$

where

$$q(s) = \Omega(s)\exp(i\Psi(\mathrm{s}))2\frac{\sin(\alpha(s)/2)}{\alpha(s)}$$

This formula follows from Eqs. (5.36) and (5.40) along with Eq. (5.9). Note that Ψ, and α must be considered as functions of time in accordance with the statements in Sect. 5.1. The constant n is

$$\eta = \frac{\bar{F}a^4\omega\varepsilon\mu}{8\pi IkJ} \tag{5.44}$$

Since the integrand in Eq. (5.43) is dimensionless ($P\mathrm{d}s$ has no dimension), and since B has the dimension of L, n is dimensionless.

We turn now to a discussion of $P(t)$. This function has nothing to do with the rubbing process in its details. It depends on the quality of Eqs. (5.11) and (5.12) exclusively. We shall try to find a simple approximation for it, one to be compatible with the errors affecting function $w(t)$ in Eq. (5.40). To this end we consider P in some detail. For large values of $|z|$ and for $|\arg z| < \pi/2$ we use the well-known asymptotic formulae

$$\left.\begin{aligned} I_n(z) &= (1+0(1))\tfrac{\exp(z)}{\sqrt{2\pi z}} \\ K_n(z) &= (1+0(1))\sqrt{\tfrac{\pi}{2\pi z}}\exp(-z) \end{aligned}\right\} \tag{5.45}$$

This implies for the coefficients D_{mn} introduced in Eq. (5.30)

$$D_{mn} = (1 + 0(1)) \frac{\exp(\lambda(a-b))}{2\lambda\sqrt{ab}} \quad \text{as } |\lambda| \to \infty \quad |\arg \lambda| < \pi/2 \tag{5.46}$$

so that

$$D_{mn}/D_{00} \to 1 \quad \text{as} |\lambda| \to \infty \tag{5.47}$$

If we set $D_{mn}/D_{00} = 1$ then Eq. (5.35) yields the asymptotic formula

$$\bar{P} \approx \frac{a\lambda - 2}{a^2\lambda^2(a\lambda + u - 1)} \quad \text{for large } \lambda \text{ and} \quad |\arg \lambda| < \pi/2 \tag{5.48}$$

In particular

$$a^2\lambda^2\overline{P} \to 1 \quad \text{as } |\lambda| \to \infty \tag{5.49}$$

For very small values of $|\lambda|$ Eq. (5.25) indicates that the function $\bar{W}$, due to $h > 0$, will be regular analytic with respect to λ^2 in some neighbourhood of $\lambda^2 = 0$. This means that $\bar{P}$ approaches a limit value as $\lambda \to 0$. In order to find the latter value we can either use asymptotic formulae for the behaviour of Bessel functions for small arguments or we can directly determine $\bar{W}$ by setting $\lambda = 0$ in Eq. (5.25). The latter procedure is quite simple and leads to

$$\overline{W} = \overline{\gamma} r + \frac{\overline{\Delta}}{r} \tag{5.50}$$

The coefficients $\bar{\gamma}$, $\bar{\delta}$ are determined by the boundary conditions for $r = a, b$. We find

$$\bar{\gamma} = \frac{a^2(\upsilon + 1)\bar{w}}{kN} \quad \overline{\delta} = \frac{a^2b^2(\upsilon - 1)\bar{w}}{kN}$$

with

$$\begin{aligned} N &= a^2(u+1)(\upsilon+1) - b^2(u-1)(\upsilon-1) \\ &= \left(a^2 - b^2\right)(u\upsilon + 1) + \left(a^2 + b^2\right)(u + \upsilon) \end{aligned} \tag{5.51}$$

Since

$$\int_b^a \bar{W} r^2 dr = \frac{1}{4}\left(a^2 - b^2\right)\left[\overline{\gamma}\left(a^2 + b^2\right) + 2\delta\right] \tag{5.52}$$

Finally, we obtain

$$\bar{P}(0) = \rho = \frac{(a^2 - b^2)}{4a^2} \frac{(a^2 - b^2)u + a^2 + 3b^2}{(a^2 - b^2)(u\upsilon + 1) + (a^2 + b^2)(u + \upsilon)} \tag{5.53}$$

For a thick-walled rotor, and if $u \gg 1$, $\upsilon \gg 1$, we may use the approximation

$$\rho = \frac{(a^2 - b^2)}{4ua^2} \tag{5.54}$$

Let us now seek a rational function $\tilde{P}$ of λ having the same behavior as $\bar{P}$ for $\lambda \to 0$ and for $\lambda \to \infty$ and which approximates $\tilde{P}$ for positive λ within an error bound of say 1 %. Such a function $\tilde{P}$ should not present great difficulties as we try to retransform it into a function of time. Since λ is proportional to $p^{1/2}$ it would be preferable (if at all possible) to make $\tilde{P}$ a rational function of λ^2 i.e. of p itself. The latter seems promising since the behaviour of $\bar{P}$ for small and large $|\lambda|$ points to λ^2. Therefore, let us try to find a $\tilde{P}$ of the form

$$\tilde{P} = \frac{\left(a^2\lambda^2 + \rho\delta_1\delta_2\right)}{\left(a^2\lambda^2 + \delta_1\right)\left(a^2\lambda^2 + \delta_2\right)} = \frac{\rho_1}{\left(a^2\lambda^2 + \delta_1\right)} - \frac{\rho_2}{\left(a^2\lambda^2 + \delta_2\right)} \tag{5.55}$$

where

$$\rho_1 = \frac{(\rho\delta_2 - 1)\delta_1}{(\delta_2 - \delta_1)} \quad \rho_2 = \frac{(\rho\delta_1 - 1)\delta_2}{(\delta_2 - \delta_1)} \quad \rho_1 - \rho_2 = 1$$

This approximation has indeed the desired asymptotic behaviour. It depends on the two parameters $\delta 1$, $\delta 2$, which, for example, might be determined by collocation.

Collocation leads to two linear equations for $\delta 1$, $\delta 2$ and $\delta 1 + \delta 2$. Out of these quantities $\delta 1$, $\delta 2$ can be derived as roots of the quadratic

$$\delta^2 - (\delta_1 + \delta_2) + \delta_1\delta_2 = 0$$

An example of approximation by collocation is shown in Fig. 5.5. It is apparent that good agreement between $\bar{P}$ and $\tilde{P}$ has been obtained. Further improvement could be obtained by optimizing the selection of the points of collocation. For the purpose of this study the accuracy in Fig. 5.5 appears to be sufficiently good.

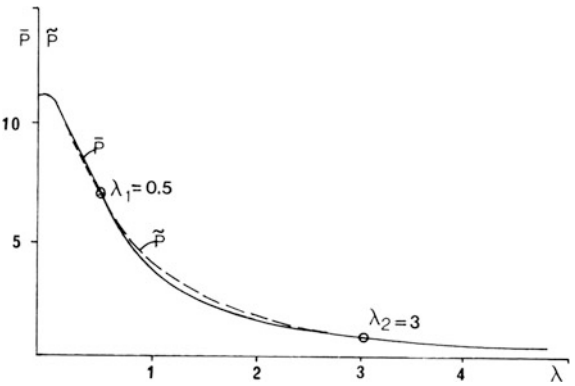

Fig. 5.5 Approximation of the Laplace transform (*Courtesy* ASME [2])

The inverse transform of $\tilde{P}$ is readily obtained. First we substitute $\lambda = \sqrt{p/k'}$ in Eq. (5.56):

$$\tilde{P} \approx \frac{k'\rho_1}{P + k'\delta_1} - \frac{k'\rho_2}{P + k'\delta_2} \quad k' = \frac{K}{a^2} \tag{5.56}$$

The fractions in Eq. (5.56) have well-known inverse transforms and

$$P(t) = k'\rho_1 \exp(-k'\delta_1 t) - k'\rho_2 \exp(-k'\delta_2 t) \tag{5.57}$$

Equation (5.43) now assumes the form of the approximation

$$B(t) = nL \int_0^t [k'\rho_1 \exp(-k'\delta_1(t-s)) - k'\rho_2 \exp(-k'\delta_2(t-s))]q(s)\mathrm{d}s \tag{5.58}$$

By differentiation we can show that Eq. (5.58) is equivalent to

$$lB = Mg \tag{5.59}$$

where

$$\begin{aligned} l &= \frac{\mathrm{d}^2}{\mathrm{d}t^2} + k'(\delta_1 + \delta_2)\frac{\mathrm{d}}{\mathrm{d}t} + k'^2\delta_1\delta_2 \\ M &= nL\left[k'^2(\rho_1\delta_2 - \rho_2\delta_1) + k'(\rho_1 - \rho_2)\frac{\mathrm{d}}{\mathrm{d}t}\right] \\ &= nL\left[k'^2\delta_1\delta_2\rho + k'\frac{\mathrm{d}}{\mathrm{d}t}\right] \end{aligned}$$

supplemented by the initial conditions

$$B(0) = 0 \quad \dot{B}(0) = nk'Lq(0) \tag{5.60}$$

It was assumed that rubbing does not occur before $t = 0$. This does not exclude the rotor possessing an initial bow B_0 at $t = 0$; the bow B_0 can represent a permanent deformation of the rotor, to give just one example. We refer B_0 to the same rotor-fixed coordinate system in which we measure B (Fig. 5.6); without loss in general the coordinate system can be chosen so that B_0 is real and positive if $B_0 \neq 0$. It is still necessary to express the bow which causes rubbing in appropriate vector form. From what was said in Section I we conclude that we must introduce

$$F = f\exp(i\Psi) \tag{5.61}$$

as the total bow. It is measured in the rotor-fixed coordinate system. In the preceding sections we established a chain of analytic expressions linking F–B. In order to obtain a model for packing rub effect we must provide a new and independent link from B to F.

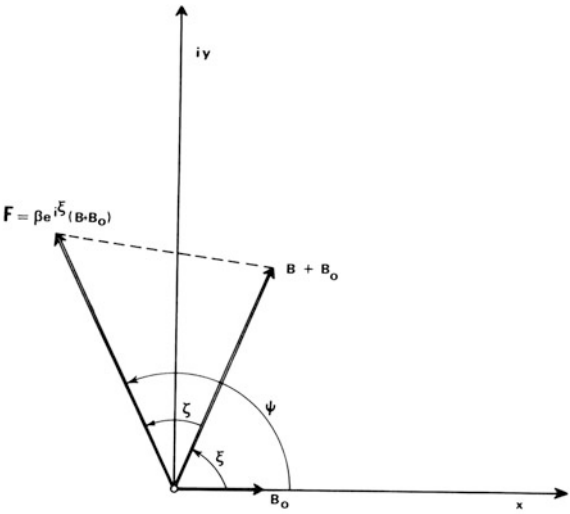

Fig. 5.6 Dynamic bow vector diagram

We expect that F depends on the sum $(B + B_0)$ only. We set up

$$F = \beta \exp(i\zeta)(B + B_0) \tag{5.62}$$

with real constants $\beta > 0$, ζ. Such a relation can be expected, and does indeed hold [9, 11–22] if one considers elastic rotor vibrations of the bending mode in the rotor-fixed coordinate system, and if the effect of bearings is also taken into account.

In connection with Eq. (5.62) we set

$$B + B_0 = r \exp(i\xi) \tag{5.63}$$

This leads to

$$f = \beta r \quad \psi = \xi + \zeta \tag{5.64}$$

Furthermore, we write

$$q = \Phi \exp(i\psi) = H(f) \exp(i(\xi + \zeta)) \tag{5.65}$$

with $\Phi = H(f)$ defined by

$$\begin{aligned} H(f) \quad &= 0 && \text{for } f < c - e \\ &= \Omega \tfrac{2 \sin d/2}{d} && \text{for } c - e < f < c \end{aligned} \tag{5.66}$$

with

$$\begin{aligned} &cos\,\tfrac{\alpha}{2} = \tfrac{c^2 + f^2 - e^2}{2cf} && cos\,\tfrac{\Omega}{2} = \tfrac{e^2 + c^2 - f^2}{2ec} \\ &0 < \tfrac{\alpha}{2} \leq \tfrac{\pi}{2} && 0 \leq \tfrac{\Omega}{2} < \tfrac{\pi}{2} \end{aligned}$$

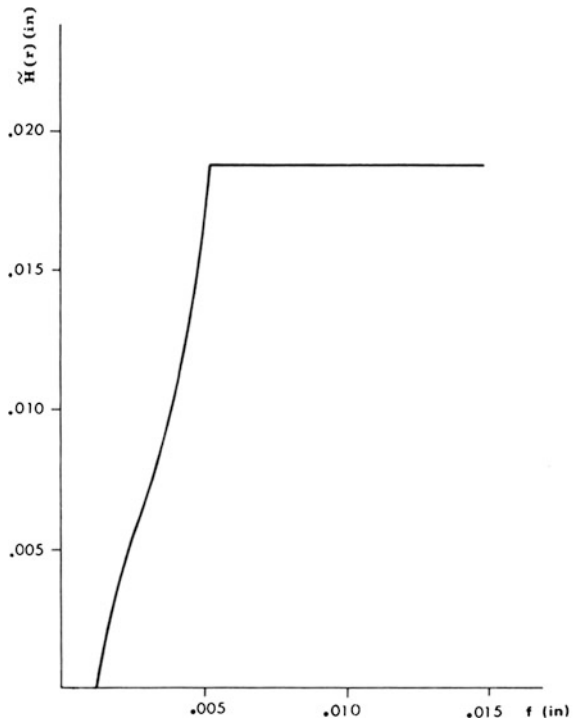

Fig. 5.7 Heat function

A typical graph of the function $\tilde{H}(f) = nL\rho H(f)$ is shown in Fig. 5.7. The function $\tilde{H}(f)$ representing heat input produced by rubbing, we can in retrospect define or change our model by specifying $H(f)$ directly.

As an example, we may substitute for the $\tilde{H}(f)$ of Fig. 5.7 the following function:

$$\left.\begin{array}{ll} H_c(f) = 0 & \text{for } f < -e + c \\ H_c(f) = 2\frac{(f+e-c)}{2c-e}\sqrt{1-\frac{e^2}{4c^2}} & \text{for } f > c \\ H_c(f) = constant & \text{for } f > c \end{array}\right\} \tag{5.67}$$

This function takes the same values as $\tilde{H}(f)$ of Fig. 5.7 at $f = e + c$ and at $f = c$. We may also use it in order to lift the former restrictions on f, e by substituting $e < 2c$ for them, while f is permitted to take any non-negative value.

In actual numerical computations $H_c(f)$ did not induce much difference in the results versus $H(f)$ [Eq. (5.67)].

In this study we assumed that the stiffness of the spring which backs the packing is negligible compared to the preload. If, however, this is not the case we may modify the heat function by multiplying by a factor

$$S_k(f - f_0)$$

where S_k is spring constant. We are now prepared to express our model by the differential equation

$$\mathfrak{E}(\mathrm{r}\,\exp(i\xi)) = M[H(\beta r)\,\exp(i(\zeta+\xi))] + k'^2\delta_1\delta_2 B_0 \tag{5.68}$$

with boundary conditions

$$\left.\begin{array}{cc} r = B_0 & \xi = 0 \\ r + ir = \eta k' L(\rho_1 - \rho_2) & H(\beta r)\,\exp(i\xi) \end{array}\right\} \quad \text{at } t = 0 \tag{5.69}$$

If we multiply Eq. (5.68) by $\exp(-i\xi)$ and split the result into real and imaginary parts, then

$$\begin{aligned} &\ddot{r} - r\dot{\xi}^2 + k'(\delta_1+\delta_2)\dot{r} + k'^2\delta_1\delta_2 r - k'^2\eta L(\rho_1\delta_2 - \rho_2\delta_1)\Phi\cos\zeta \\ &\quad - k'(\rho_1-\rho_2)\eta L\left(\dot{\Phi}\cos\zeta - \Phi\dot{\xi}\sin\zeta\right) - k'^2\delta_1\delta_2 B_0\cos\xi \\ &\quad = 0 \end{aligned} \tag{5.70}$$

$$\begin{aligned} &r\ddot{\xi} - 2\dot{r}\dot{\xi} + k'(\delta_1+\delta_2)r\dot{\xi} - k'^2\eta L(\rho_1\delta_1 - \rho_2\delta_2)\Phi\sin\xi \\ &\quad - k'(\rho_1-\rho_2)\eta L\left(\dot{\Phi}\sin\zeta + \Phi\dot{\xi}\cos\zeta\right) + k'^2\delta_1\delta_2 B_0\sin\xi \\ &\quad = 0 \end{aligned} \tag{5.71}$$

The initial conditions assume the final form

$$r = B_0 \quad \xi = 0 \quad \dot{r} = \eta k' L(\rho_1 - \rho_2)H(\beta B_0)\cos\zeta$$

$$B_0 = \eta k' L(\rho_1 - \rho_2)H(\beta B_0)\sin\zeta$$

Equations (5.70), (5.71) are in general non-linear. They become equivalent to linear equations in those time intervals at which no rubbing takes place, so that $H = 0$. In this case it is preferable to deal with the quantity B immediately to obtain

$$B(t) = A_1\exp(-k'\delta_1 t) + A_2\exp(-k'\delta_2 t) \tag{5.72}$$

as the general solution for B. In the case of non-linear equations, we are primarily interested in what happens in the long run; in particular we shall be interested in finding phenomena of stability and instability.

In order to study such features we shall ignore the initial conditions. Let us assume that we possess solutions $r = r(t)$, $\xi = \xi(t)$ tending to finite limits, $\bar{r}$, $\bar{\xi}$ as $t \to \infty$, while simultaneously their derivatives approach zero. In this case the differential equations demand

$$\left.\begin{array}{c} \bar{r} - B_0\cos\bar{\xi}_0 - \tilde{H}(\beta\bar{r})\cos\bar{\xi} = 0 \\ B_0\sin\bar{\xi} - \tilde{H}(\beta\bar{r})\sin\zeta = 0 \\ \tilde{H} = \eta L\rho H \end{array}\right\} \tag{5.73}$$

where

$$\rho = \frac{\rho_1}{\delta_1} - \frac{\rho_2}{\delta_2}$$

[see also Eq. (5.56)]. Equations (5.73) lead to

$$\bar{r} \sin \zeta = B_0 \sin\left(\zeta + \bar{\xi}\right) \tag{5.74}$$

$$\bar{r}^2 - 2\bar{r}\tilde{H} \cos \zeta + \tilde{H}^2 = B_0^2 \tag{5.75}$$

We must add the condition $0 < \beta\bar{r} < c$.

From Eq. (5.75) the value of $\bar{r}$ can be computed, provided that a solution of this equation exists. We note that this equation is identical to the cosine law for the triangle. Therefore, a triangle should exist with sides $\tilde{H}$, B_0, and angle ζ (between $\bar{r}$ and $\tilde{H}$ (Fig. 5.8). In the following, $H^*(\bar{r})$ will designate the value of $\tilde{H}$ computed from this triangle or from Eq. (5.75).

As is well known, the locus of all points A at which the fixed line $A_1\ A_2$ of length B_0 appears under the angle ζ is a circular arc, as shown in Fig. 5.8. Therefore, if

$$|\zeta| < \pi/2$$

the function $H^*(\bar{r})$ is single-valued and monotonously decreasing. In the case of

$$|\zeta| < \pi/2$$

$H^*(\bar{r})$ is double-valued.

We plot the graphs of the functions $\tilde{H}$ and H^* in Fig. 5.9. Their intersection gives the value of $\bar{r}$. The angle ξ can be computed either from Eq. (5.74) or from the first one of Eq. (5.73). If a solution $\bar{r}$ to Eq. (5.75) exists, then Fig. 5.8 yields $\bar{\xi}$ from Eq. (5.74).

The constant state $r = \bar{r}, \xi = \bar{\xi}$ can be stable or unstable. In order to check this point we introduce the complex quantity

$$\frac{1}{\bar{r}} \exp\left(i\left(\xi - \bar{\xi}\right)\right) - 1 = z \tag{5.76}$$

as a measure of deviation from the constant state, and we now linearise Eq. (5.68) with respect to z.

Writing also $z = x + iy$, we find that

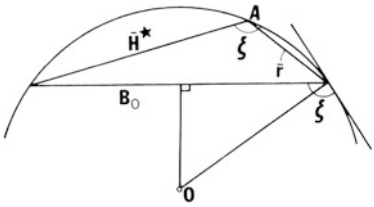

Fig. 5.8 Geometric interpretation of Eq. (5.76)

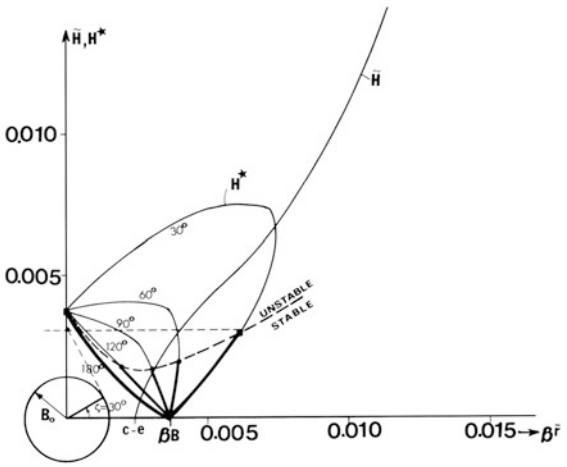

Fig. 5.9 Stability limits

$$\frac{r}{\bar{r}} - 1 \approx x \quad \xi - \bar{\xi} = y$$

and

$$\exp\left(i\left(\xi - \bar{\xi}\right)\right) - 1 \approx iy$$

Putting these relations to use we find that Eq. (5.68) yields the linearised form

$$\mathfrak{E}(x + iy) = \exp(i\zeta) M\left(\tau x + \tau' iy\right) \tag{5.77}$$

with

$$\tau = \beta H'(\beta\bar{r}) \quad \tau' = H(\beta\bar{r})/\bar{r}$$

This equation can be rewritten in the form of a vector equation

$$\mathfrak{E}\mathbf{w} = M\mathbf{A}\mathbf{w}$$

$$\mathbf{w} = \begin{pmatrix} x \\ y \end{pmatrix}$$

$$\mathbf{A} = \begin{pmatrix} \tau\cos\xi & \tau'\sin\xi \\ \tau\sin\xi & \tau'\cos\xi \end{pmatrix} \tag{5.78}$$

This has a solution of the form

$$\mathbf{w} = \mathbf{w}_0 \exp(pt)$$

where $\mathbf{w}_0$ is a constant two-vector while p is a real or complex constant; moreover $\mathbf{w}_0$ has to be an eigenvector of $\mathbf{A}$, so that $\mathbf{A}\mathbf{w}_0 = \lambda\mathbf{w}_0$ with λ, an associated eigenvalue. Consequently

$$L(p) - \lambda M(p) = 0 \tag{5.79}$$

where

$$L(p) = \exp(-pt)\mathfrak{E}(\exp(pt)) \quad M(p) = \exp(-pt)M(\exp(pt))$$

and λ satisfying

$$\lambda^2 - \lambda(\tau + \tau')\cos\xi + \tau\tau' = 0 \tag{5.80}$$

From Eqs. (5.79) and (5.80) we derive

$$L^2 - LM(\tau + \tau')\cos\xi + M^2\tau\tau' = 0 \tag{5.81}$$

The constant state $r = \bar{r},\ \xi = \bar{\xi}$ is stable if the roots p of Eq. (5.81) are in the left half plane $\mathrm{Re}(p) < 0$. We can check on this feature by investigating Eq. (5.79) for the roots λ of Eq. (5.80), or we can deal with Eq. (5.81) as it is. In this case Routh criterion of stability yields the following conditions:

$$\left.\begin{array}{c} a_1 = 4\lambda_0 + \mu_1(\tau + \tau')\ \cos\ \xi\ >\ 0 \\ a_2 = 4\lambda_0^2 + 2\mu_1^2\tau\tau' + (\tau + \tau')(\mu_0 + 2\lambda_0\mu_1)\ \cos\ \zeta \\ a_3 = 4\lambda_0 + 2\mu_0\mu_1\tau\tau' + (2\lambda_0\mu_0 + \mu_1)(\tau + \tau')\ \cos\ \zeta \\ a_0 = 1 \\ a_2 - a_0a_3/a_1\ >\ 0 \end{array}\right\} \tag{5.82}$$

and

$$\lambda_0 = \frac{\delta_1 + \delta_2}{2\sqrt{\delta_1\delta_2}} \quad \mu_0 = \eta Lp \quad \mu_1 = \frac{\eta L}{\sqrt{\delta_1\delta_2}}$$

Without going into much detail we can derive from Eq. (5.81) the result that $\cos\zeta = -1$ means stability. Indeed we can rewrite

$$L(p) + \tau M(p) = 0 \quad L(p) + \tau' M(p) = 0 \tag{5.83}$$

Since these equations represent quadratic equations with positive coefficients, their roots are in the left hand half plane. This first result permits the conjecture that stability will exist if

$$\cos\zeta < \cos\xi^*$$

where $\cos\xi^*$ is some number depending on the coefficients of L, M only. Examples given elsewhere in this chapter illustrate this point.

For the homogeneous case, $B_0 = 0$ and for suitable parameter constellations Eq. (5.68) admits solutions of the type

$$r\exp(i\xi) - 1 = \bar{r}\exp(ipt + ip'))\tag{5.84}$$

where r, p, p', are real constants. This represents an undesirable type of operation and we shall refer to it as the 'spiralling mode'. Here, we can state already (more details follow at a later stage) that this mode can be observed in actual practice. The quantities p, $\bar{r}$ have to be determined from the following condition:

$$L(ip) = R\exp(i\zeta)M(ip) \quad R = H(\beta\bar{r})/\bar{r} \tag{5.85}$$

where L and M are the polynomials introduced in Eq. (5.79). Since R must be positive, the imaginary part of $L(ip)M(-ip)\exp(-\mathrm{i}\zeta)$ has to vanish. This leads to a cubic equation for p, namely

$$p\left[(\lambda_1\mu_0 - \lambda_0\mu_1) + \mu_1 p^2\right]\cos\xi + \left[-\mu_0\lambda_0 - \mu_1\lambda_1 + \mu_0 p^2\right]\sin\xi = 0 \tag{5.86}$$

This equation always has one real root, which, once found, one has to ascertain that quantity R is positive and that $\bar{r}$ can be found in accordance with it.

While the constant states and the 'spiralling' modes can be found easily from rather simple equations for two unknowns, more information about the model has to be obtained the hard way, i.e. by solving the differential equation (5.68) with the associated initial conditions, which was obtained by a Runge–Kutta method. Since all numerical methods involve errors, while in the case of initial value problems the errors sometimes build up with time, two particular solutions were chosen in order to check the quality of the method and of the program. In the long run the solutions would either approach a constant state or become indistinguishable from a spiralling mode. Therefore the final data, furnished by numerical solutions of differential equation (5.68), could be checked by an independent and rather accurate computation of the final data. These checks confirmed that the program for the differential equation comes up to engineering requirements.

To obtain the asymptotic values of the constant mode the solution of two transcendental equations is necessary, namely Eqs. (5.74) and (5.75). For the spiralling mode, utilising Eq. (5.85), the following explicit expressions for p and $\bar{r}$, were found:

$$\bar{r} = \eta L\rho\pi\left(\cos\zeta + \sqrt{\left(\cos^2\zeta + 4\frac{\delta_1\delta_2}{(\delta_1+\delta_2)^2}\sin^2\zeta\right)}\right) \tag{5.87}$$

$$p = \frac{2\pi\eta L k'\rho\delta_1\delta_2\sin\zeta}{\bar{r}(\delta_1+\delta_2)} \tag{5.88}$$

The asymptotes calculated for the numerical example show very good agreement with the numerical solution of the non-linear differential equation. A fourth-order Runge–Kutta method was used.

Figure 5.10 shows an example of both the asymptotic and the non-linear solution.

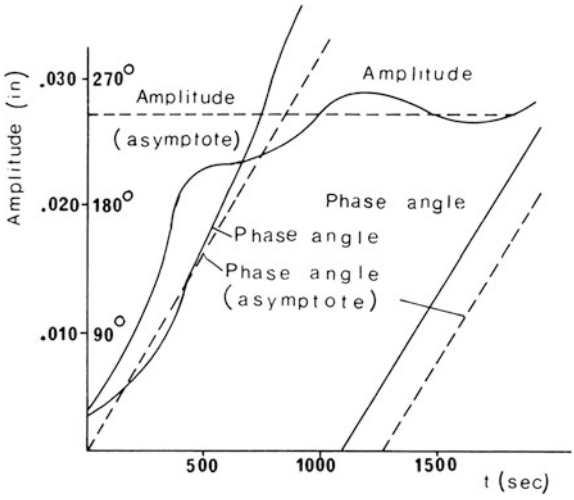

Fig. 5.10 Asymptotic behaviour (*Courtesy* ASME [2])

5.3 Modes of the Newkirk Effect

Certain general observations can be made by observing the behaviour of the solutions for different parameter constellations [3, 23–30]:

1. The system response can have three modes:
   a. The spiralling mode. The amplitude and phase angle increase continuously up to some point where the amplitude varies harmonically around a maximum value while the phase angle increases continuously.
   b. The oscillatory mode. The amplitude oscillates around a value close to the initial bow of the system.
   c. The constant mode. The amplitude reduces to a constant value where it remains, with the phase angle exhibiting the same behaviour.
2. This response can be initiated only by an initially unbalanced or bowed rotor.
3. The mode of the Newkirk effect depends primarily on the dynamic response of the system, namely on the phase angle between static and resulting dynamic bow at the operating speed. It also depends on the friction characteristics, but this effect is secondary.

As a test case, a typical turbine rotor was used, with properties described in the Appendix.

The first critical speed of the test rotor was 1,450 rpm and the second 2,400 rpm.

Figure 5.11 shows a typical unstable mode. There are two calculated responses: wear = 0 means that the wear or the material is very small compared to the

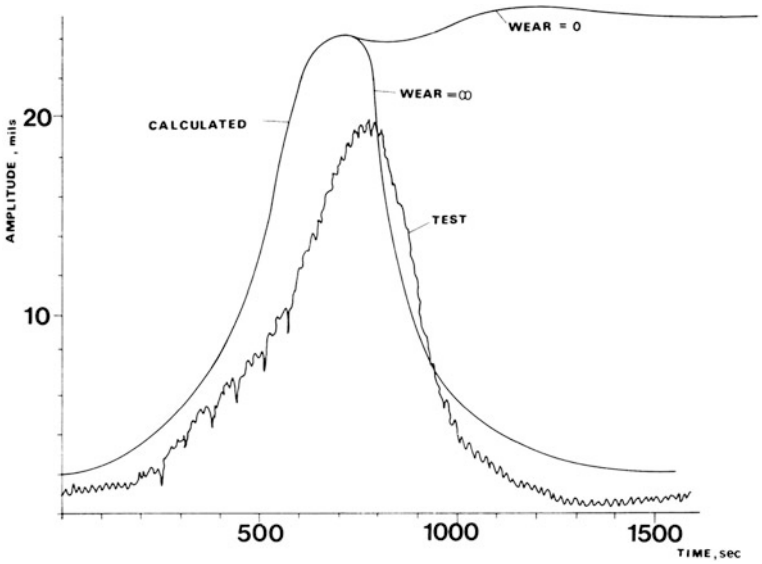

Fig. 5.11 Rubbing response at 1,200 rpm (from Ref. [3], by permission)

clearance and the bow. Therefore, the heat generation continues for a long time and maintains maximum bow of the rotor. The test results are from Ref. [3]. Wear $= \infty$ means that the material wears so fast that the clearance is never less than the maximum vibration amplitude. Therefore, after the rotor bow reaches a maximum, heat generation stops, the rotor cools rapidly and the bow resumes the initial value. This performance actually occurred with the tests because the packing ring consists of very thin teeth of soft brass which wear very quickly.

Figure 5.12 shows a typical oscillatory mode. Again, because of the wear of the teeth the oscillatory motion predicted by the analysis did not appear in the test, and for all practical purposes such performance can be accepted as stable.

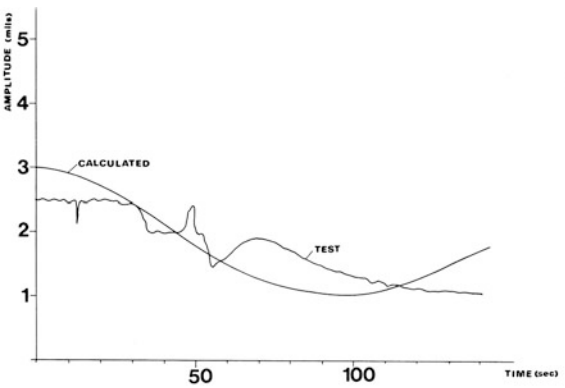

Fig. 5.12 Rubbing response at 1,800 rpm (from Ref. [3], by permission)

In all modes, after a time long enough to wear the teeth, the rotor will return to its initial bow, provided the rubs were mild enough to avoid permanent bow. However, this result does not have practical importance because we are only interested in the stability of the system at the start of the rub. If the system is unstable, the resulting bow is so high that operation of the machine must be stopped to avoid major damage.

In Fig. 5.13, a typical stable mode is plotted. Figures 5.14, 5.15, 5.16 show the same cases as in Figs. 5.11, 5.12, 5.13, respectively, in polar form.

Figures 5.11, 5.12, 5.13, 5.14, 5.15, 5.16, 5.17 use the following parameters:

B_0 static initial bow of the rotor at the rubbing position;
b dynamic vibration amplitude on a rotor-fixed coordinate system;
ξ phase angle between initial static bow and dynamic bow at time t;
C radial clearance of the packing annulus;
ζ phase angle between static and dynamic bow at time t.

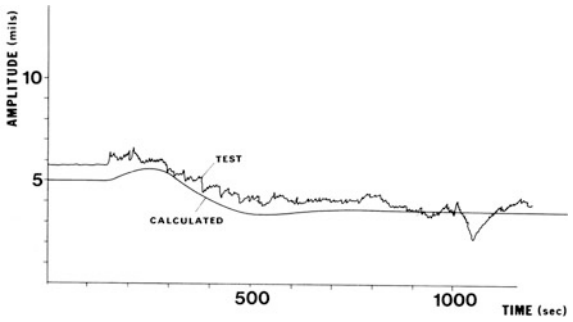

Fig. 5.13 Rubbing response at 3,000 rpm (from Ref. [3], by permission)

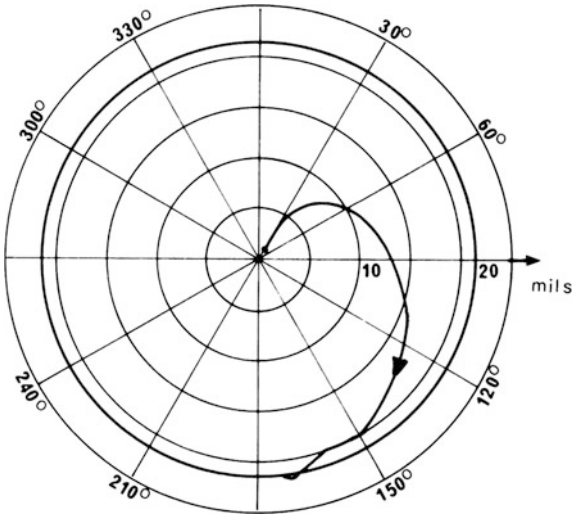

Fig. 5.14 Rubbing response at 1,200 rpm (from Ref. [3], by permission)

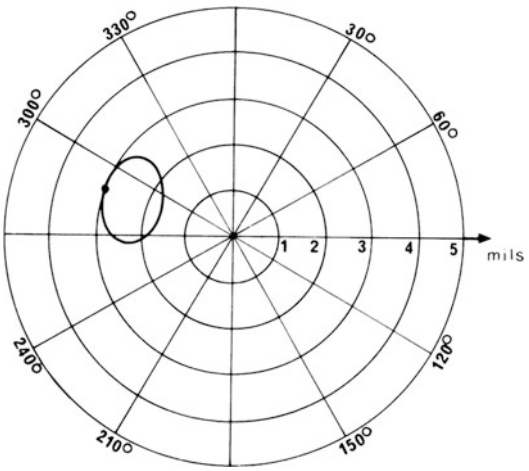

Fig. 5.15 Rubbing response at 1,800 rpm (from Ref. [3], by permission)

In general, it was found that the main factor controlling the rubbing stability of a system is the phase angle ζ. Generally, at $\zeta = 0$ the mode is always spiralling and at $\zeta = \pi$ the mode is always converging. Around the middle, at $\zeta = \pi/2$ or $\zeta = 3\pi/2$, an oscillatory response is obtained. Based on these results, the chart in Fig. 5.17 was constructed. In areas where more than one mode overlaps each other, the behaviour depends on other parameters of the system and the phase angle alone cannot determine the mode characteristics of the system. This observation agrees with the test results and with an early observation of Taylor [9], who noticed that at running speeds above critical, light rubbing did not have any effect. When the rubbing force was increased, then the vibration amplitude decreased.

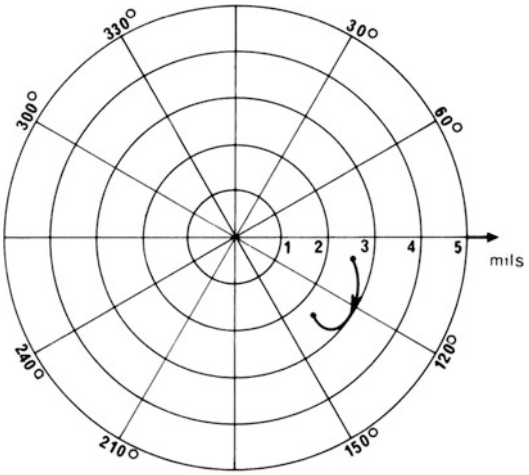

Fig. 5.16 Rubbing response at 3,000 rpm (from Ref. [3], by permission)

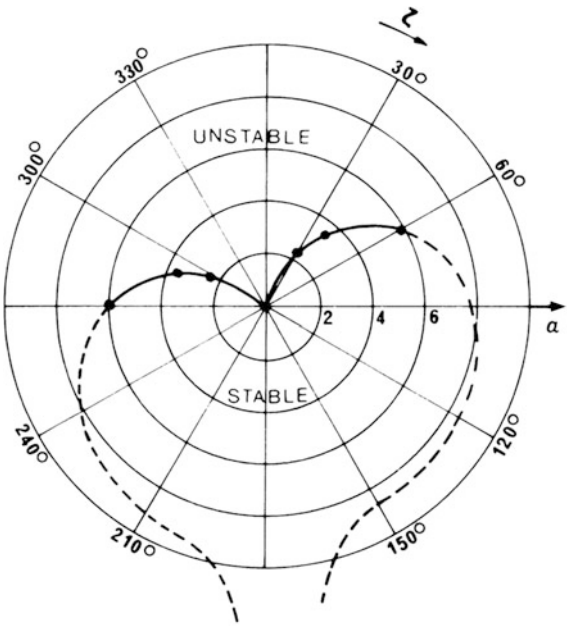

Fig. 5.17 Packing rub effect stability chart (from Ref. [3], by permission)

Appendix: Numerical Example

Unless otherwise indicated the following numerical values have been used, corresponding to the test conditions [3]:

Rotor geometry:	
Outer radius	$a = 0.19$ m
Inner radius	$b = 0.038$ m
Length	$L = 3.0$ m
Thermodynamic properties:	
Thermal conductivity	$k = 60$ W/m °C^{-1}
Thermal diffusivity	$\alpha = 12.6 \times 10^{6}$m^2/s
Heat transfer coefficients	$h_a = 116$ m^{-1}
	$h_b/k = 29{\cdot}2$ m^{-1}
Coefficient of thermal expansion	$\varepsilon = 10.8 \times 10^{-6}$ °C^{-1}
Friction properties:	
Friction force	$F = 89.2$ N
Friction coefficient	$\mu = 0.5$
Heat distribution coefficient	$\alpha = 0.75$
Interaction properties:	
Initial bow	$B_0 = 22.8$ μm
Clearance	$c = 254$ μm
Eccentricity	$\varepsilon = c$

The heat parameter η is

$$\eta = \frac{Fa^4 \omega \varepsilon \mu}{8\pi IkJ}.$$

Where ω is rotating speed, I is the moment of inertia, and J is the mechanical equivalent of heat.

This example corresponds to a medium-size steam turbine or to a large gas turbine. The results of the calculations presented are not directly applicable to different designs. However, the general features of the model are valid also for a wide range of designs. One could plot stability charts for the constellation of the parameters involved, which could be used directly by the designer. This is a major undertaking and certainly beyond the aim of this book.

References

1. Dimarogonas, A.D.: Packing rub effect in rotating machinery. Dissertation, Rennselaer Polytechnic Institute, Troy (1970)
2. Dimarogonas, A.D.: Newkirk effect: Thermally induced dynamic instability of high speed rotors. In: ASME paper 73-GT-26, Gas turbine conference, Washington (1973)
3. Dimarogonas, A.D.: A study of the Newkirk effect in turbomachinery. Wear **28**, 369–382 (1974)
4. Newkirk, B.L.: Shaft rubbing. Mech. Eng. **4**(8), 830 (1926)
5. Black, H.F.: Interaction on a whirling rotor with a vibrating stator across a clearance annulus. J. Mech. Eng. Sci. Trans. IFToMM **10**(1), 1–12 (1968)
6. Kroon, R.P., Williams, W.A.: Spiral vibration of rotating machinery. In: Proceedings of 5th International Congress Applied Mechanics, p. 712. Wiley, New York, (1939)
7. Ehrich, F. The influence of trapped fluids on high speed rotor vibration. In: ASME paper 67-Vibration-29
8. Thoma, D.: Selbsterregte schwingungen von turbinenrotoren. Vereines Deutscher Ingenieure **2**(5), 985 (1925)
9. Taylor, H.D.: Rubbing Shafts Above and Below Resonant Speed, General Electric Technical Information Series, 16709 (1924)
10. Kroon, R.P.: Erratic vibration, a case for the specialist. Power **6**(6), 212 (1940)
11. Sweets, W.J.: Analysis of Rotor Rubbing, General Electric Technical Information Series. DF-66-LS-70 (1966)
12. Boley, B., Barner, A.: Dynamic response of beams and plates to rapid heating. J. Appl. Mech. **24**, 413–416 (1957)
13. Mokrushin, S.A., Gusak, Y.M.: Computation of temperature field and stress in the cooled rotor of a gas turbine on starting. Energomashinostroyeniye **7**(11), (1964) (in Russian)
14. Goodier, J.N.: Formulas for overall thermoelastic deformation. In: Proceedings of 5th International Congress Applied Mechanics. Wiley, New York (1958)
15. Rabinowicz, E.: High temperature friction in controlled atmospheres up to 2,000 °F, US Air Force, Technical Report, 59−603 (1960)
16. Kruschov, M.M., Semenov, A.P., et al.: Investigation of anti friction bronzes and brasses subjected with and without lubrication, friction and wear in machinery. ASME Trans. **17**, 31(1967)
17. Bisson, E.: Etude du frottement et de l'usure a des températures èlevées (jusqu'a 815 °C) ou tres basses (−250 °C). Rev. Inst. Franc. Pétrole **4**, 485 (1961)

18. Jaeger, J.C.: Moving sources of heat and the temperature at sliding contacts. Proc. Roy. Soc. N.S.W. **56**, 203–224 (1942)
19. Holm, R.: Calculation of the temperature at sliding contacts. J. Appl. Phys. **1**(9), 361 (1948)
20. Ling, F.F., Pu, S.L.: Probable interface temperature of solids in sliding contact. Wear **7**, 23 (1964)
21. Archard, J.F.: The temperature of rubbing surfaces. Wear **2**, 438 (1958/1959)
22. Bishop, R.E.D.: The vibration or rotating shafts. J. Mech. Eng. Sci. **1**(1), 50 (1959)
23. Kellenberger, W.: Spiral vibrations due to the seal rings in turbogenerators. Thermally induced interaction between rotor and stator. In: ASME paper 79-DET-61, design engineering technical conference, St. Louis (1979)
24. Kwanka, K., Ortinger, W.: Rotordynamic coefficients of long staggered labyrinth gas seals. Int. J. Rotating Mach. **1**(3–4), 285–291 (1995)
25. Dimarogonas, A.D., Sandor, G.N.: Packing-rub effect in rotating machinery. I. State of the art review. Wear **14**, 153–170 (1969)
26. Dimarogonas, A.D.: Vibration of cracked structures: A state of the art review. Eng. Fracture Mech. **55**(5), 831–857 (1996)
27. Dimarogonas, A.D.: Vibration for Engineers, 2nd edn. Prentice-Hall, Upper Saddle River (1996)
28. Zhao, H., Stango, R.J.: Effect of flow-induced radial load on brush seal/rotor contact mechanics. J. Tribol. **126**(1), 208–215 (2004)
29. Kubiak, S.J., Childs, D., Rodriguez, M., García, M.C. Investigation into a “steam whirl” which affected HP rotors of 300 MW steam turbines. In: Proceedings of the ASME Power Conference, pp. 291–298 (2007)
30. Pugachev, A.O., Kleinhans, U., Gaszner, M.: Prediction of rotordynamic coefficients for short labyrinth gas seals using computational fluid dynamics. J. Eng. Gas Turbines Power **134** (2012) (062501)

Chapter 6
Dynamics of Cracked Shafts

Abstract The problem of cracked rotor dynamics is discussed in Chap. 6. Analytical formulation for crack local flexibility in relation to crack depth yields a supervisory instrument which can give an early crack warning. Fracture mechanics methods provide stress intensity factors for the investigation of rotor's dynamic performance for varying crack depth. Open cracks lead to linear systems, while closing cracks lead to non-linear ones. Analytical solutions are obtained, which can be used to monitor crack propagation or to identify cracks in service.

6.1 Introduction

The behavior of a rotating shaft with a transverse surface crack first attracted attention in the late 1960s in connection with the possibility of crack identification on a large steam turbine where there was a suspicion that one of the rotors had such a crack. Dimarogonas [1] observed the local flexibility of the shaft due to the crack and developed an analytical formulation for the crack local flexibility in relation to the crack depth; he also showed the influence of the crack upon the dynamic response of the rotor. Due to the turbine rotor failures at Southern California Edison's Mohave station in 1970 and 1971, industry's attention was focused on problems of turbine-generator shaft failures, caused by transmission system operation and system faults leading to fatigue cracks. Metallurgical examination revealed that the failure was due to fatigue-propagated cracks in the rotors. A sister machine had similar loading history and it was suspect for having the potential for a forthcoming failure of the same type [2].

A. D. Dimarogonas et al., *Analytical Methods in Rotor Dynamics*,
Mechanisms and Machine Science 9, DOI: 10.1007/978-94-007-5905-3_6,

As a result of Dimarogonas and his colleagues' efforts, the problem was the subject of a thorough investigation and led to the development of a supervisory instrument which can give an early crack warning. The manufacturer released this instrument for general use in the early 1970s [3]. After 1975 there were a number of publications dealing with this problem [1, 2, 4, 5].

Gash [6] and Henry and Okah-Avae [7] considered the non-linear mechanism of a closing crack with different flexibilities for open and closed cracks. Applying this principle on a De Laval rotor they derived the equations of motion on both the rotating and the stationary coordinate systems, which were solved by an analogue computer. The crack flexibility was determined experimentally.

Mayes and Davies [8] performed a detailed analytical and experimental investigation for turbine shafts with cracks. They derived a rough analytical estimate of crack compliance based on Paris energy principle and measured it on a test rig. Although they considered the nonlinear equations for a simple rotor, they obtained analytical solutions by considering an open crack which led to a shaft with dissimilar moments of inertia in two normal directions, a problem with a known analytical solution.

Grabowski [9] argues that in shafts of practical interest the shaft deflection, due to its own weight, is greater than the vibration amplitude by several orders of magnitude. Therefore, he suggests that non-linearity does not affect shaft response, since the crack opens and closes regularly with rotation. Therefore, the equations of motion can be considered linear with variable coefficients. Further, he uses modal analysis, like Mayes and Davies [8], and numerical integration of the resulting system of equations for a multi-degree of freedom shaft. Similar results are also presented by Ziebarth et al. [10].

The influence of a peripheral crack upon the torsional dynamic behaviour of a rod was introduced in 1980 by Dimarogonas and Massouros [11]. The assumption of a torsional linear spring model for the peripheral crack led to the conclusion that, because of added flexibility, the introduction of a crack leads to lower torsional natural frequencies. Experimental results confirmed the analysis closely. The results showed that the change in dynamic response due to the crack was high enough to allow for the detection of the crack and estimation of its location or magnitude for moderate and deep cracks. Since early 1980s substantial body of academic research on the monitoring and early warning of cracked rotors was performed [12–18].

Concerning dynamic response of rotors and other structures with cracks, there were three basic methods to deal with the problem: equivalent reduced section, local flexibility from fracture mechanics, cracked continuous beam. Among those methods the lumped crack flexibility gained wider acceptance. The effect of a notch on a structure is usually simulated by a local bending moment or reduced section, with magnitudes, estimated experimentally or analytically or with fine-mesh finite element techniques. Also, an important observation was the identification of vibration coupling due to cracks as well as parametric vibration and bilinear and non-linear effects characterizing vibration of cracked rotating shafts [1–4].

Although there is extensive literature on the vibration of cracked shafts attention is restricted to theoretical methods to assess the effect of cracks on overall

dynamics. Such estimates were made numerically or by introducing the concept of crack local flexibility. It must be stated here that there is extensive confusion in the literature in distinguishing between a notch and a crack. Many authors treat cracks as notches, experimentally, analytically or numerically. Saw cuts are used to model cracks. It must be understood that no matter how thin a saw cut is, never behaves as a crack. In fact, in the authors' experience, a thin cut results in a local flexibility substantially less than the local flexibility associated with a fatigue crack [1–6].

Christides and Barr [19, 20] extended Hu-Washizu [21, 22] theory for the uncracked bar to develop the theory for the torsional vibration of the cracked rod based on the general variational principle and independent assumptions concerning displacement, momentum, strain and stress fields of the cracked rod. The equations of motion for a uniform rod in torsional vibration were derived, where the rod had one or more circumferential open edge cracks along its length. This restriction on crack geometry avoided coupling of torsional and flexural motion, which follows a non-symmetric crack configuration. The cracks were regarded as constantly open to avoid non-linearity associated with the compressive stresses over a closing crack face. Further, for the stress field about the crack an exponential decay stress and strain distribution determined experimentally was used.

A continuous cracked beam vibration theory was developed by Chondros et al. [23, 24], with adequate assumptions for the stress field determined by fracture mechanics, for the prediction of the dynamic response of a cracked shaft considering it in a more fundamental way as a one-dimensional elastic continuum, presented in Chaps. 9 and 10 [25].

6.2 Local Flexibility of a Cracked Shaft

A transverse crack of depth a is considered on a shaft of radius R (Fig. 6.1). The shaft has local flexibility due to a crack in many directions, depending on the direction of the applied forces. A complete flexibility matrix will be presented in the next chapter but here only bending deformation will be considered. Axial forces giving coupling with transverse motions of the cracked shaft will not be considered. Shear stresses are also not considered, on the assumption of a rather long shaft. Therefore, the shaft is bent by a pure bending moment $\boldsymbol{M}$ and the additional angular deflection of the one shaft end relative to the other will be computed.

Paris computed the displacement u of a cracked structure due to the action of a force P as [26]

$$u = \frac{\partial}{\partial P} \int_0^a J(a) da \tag{6.1}$$

where a is the crack depth and $J(a)$ is the strain energy density function, which for a rectangular beam with a crack of constant depth a is (for unit width) and for plane strain

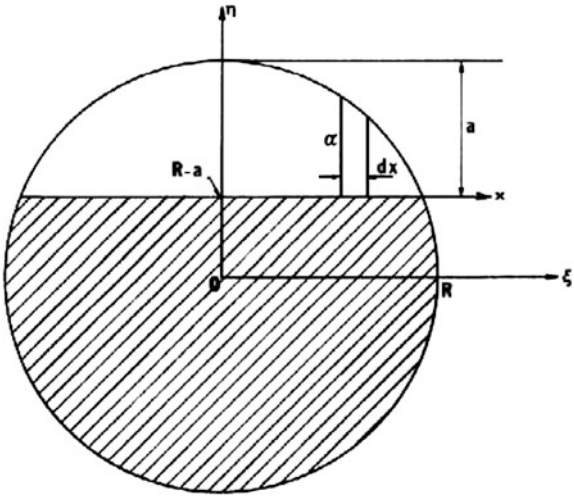

Fig. 6.1 Geometry of a cracked section of a shaft

$$J = \frac{1 - v^2}{\mathrm{E}} K_l^2 \tag{6.2}$$

For a crack with varying depth, the strain energy density function will have the form

$$J = \int_{-b}^{b} \frac{(1 - v^2) K_l^2(\xi)}{E} d\xi \tag{6.3}$$

where E is Young's modulus, v is Poisson's ratio and $2b$ the crack width.

The flexibility influence coefficient will be [1]:

$$c = \frac{\partial u}{\partial P} = \frac{\partial^2}{\partial P^2} \int_0^a \int_{-b}^{b} \frac{(1 - v^2) K_l^2(\xi)}{E} da d\xi \tag{6.4}$$

The solution for the stress intensity factor K_i is not available. The solution for the strip with width dξ and depth $\alpha = a + \sqrt{R^2 - \xi^2} - R$ will be used. This solution is [26]

$$K_l = \frac{4\mathrm{M}}{\pi R^4} \sqrt{R^2 - \xi^2} \sqrt{\pi \alpha} F_2(\alpha / h) \tag{6.5}$$

where

$$F_2(\alpha/h) = \sqrt{\frac{2\mathrm{h}}{\pi\alpha} \tan \frac{\pi\alpha}{2\mathrm{h}}} \frac{0.923 + 0.199\left(1 - \sin \frac{\pi\alpha}{2\mathrm{h}}\right)^4}{\cos \frac{\pi\alpha}{2\mathrm{h}}}$$

and h is the local height:

$$h = 2\sqrt{R^2 - \xi^2}$$

Therefore, for $P = M$, Eq. (6.4) becomes

$$c_\xi = \frac{1-\nu^2}{E}\int_0^a \int_{-b}^{b} \frac{32}{\pi^2 R^8}\left(R^2 - \xi^2\right)\pi\alpha F_2^2(\alpha/h)d\alpha d\xi \tag{6.6}$$

In dimensionless form

$$\frac{\pi^2 R^3 Ec}{1-\nu^2} = \int_0^a \int_{-b}^{b} 32\left[1 - (\xi/R)^2\right]\pi(\alpha/R)F_2^2(\alpha/h)d\left(\frac{\alpha}{R}\right)d\left(\frac{\xi}{R}\right) \tag{6.7}$$

The expression on the right is a function of a/R only and has been computed by way of numerical integration; it is plotted in Fig. 6.2. Certain experimental data are shown in this figure for comparison.

For the moment about the η-axis, the cracked shaft has another flexibility coefficient:

$$c_\eta = \frac{1-\nu^2}{E}\int_0^a \int_{-b}^{b} \frac{32\xi^2\pi\alpha F_1^2(\alpha/h)}{\pi^2 R^8} d\alpha d\xi \tag{6.8}$$

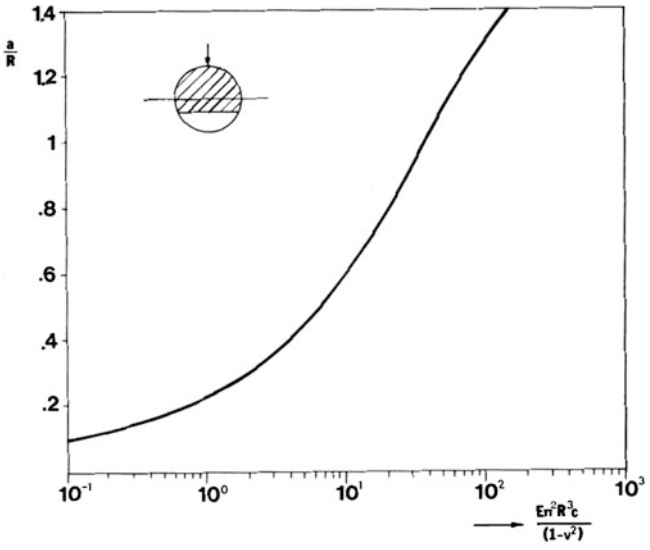

Fig. 6.2 Dimensionless flexibility or the cracked section, load direction normal to crack edge

where [26]

$$F_1(\alpha/h) = \sqrt{\frac{2h}{\pi\alpha}\tan\frac{\pi\alpha}{2h}}\frac{0.752 + 2.02(\alpha/h) + 0.37\left(1 - \sin\frac{\pi\alpha}{2h}\right)^3}{\cos(\pi\alpha/2h)}$$

In dimensionless form

$$\frac{\pi^2 R^3 Ec}{1-\nu^2} = \int_0^a \int_{-b}^b 32(\xi/R)^2 \pi(\alpha/R) F_1^2(\alpha/h) d\left(\frac{\alpha}{R}\right) d\left(\frac{\xi}{R}\right) \tag{6.9}$$

The integral on the right is a function of *a/R* and is plotted in Fig. 6.3. The integration is carried out over only half the crack width because only positive tension stresses cause extension and opening of the crack.

6.3 The Open Crack

Analysis of a system with an open crack introducing only a dissimilar moment of inertia has more than just a pedagogic purpose. Many features of rotors with dissimilar moments of inertia are found in the behavior of cracked rotors and on many occasions open cracks can be assumed for small vibration amplitudes and static deflections that are not substantial.

Consider a de Laval rotor with a disc of mass m supported by a massless elastic shaft of stiffness k without the crack, damping c and eccentricities of the mass ε_1 and ε_2 along the rotor-fixed coordinates ξ and η (see Chap. 3). The edge of the crack is along the fixed coordinate ξ. Therefore, the shaft spring constant will be

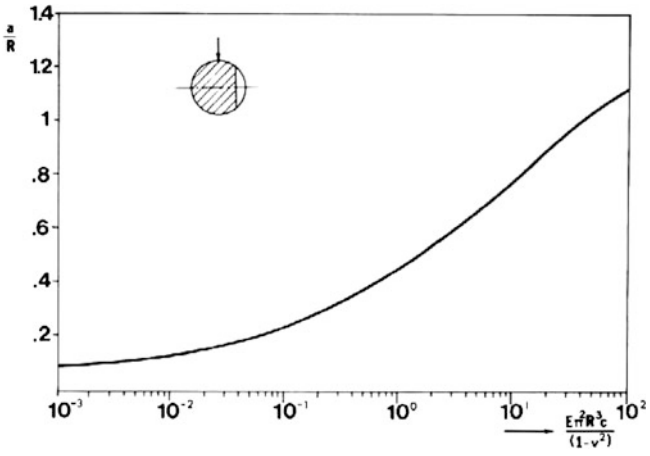

Fig. 6.3 Dimensionless flexibility of the cracked section, load parallel to cracked edge

different along the two axes ξ and η. If k_ξ and k_η are the respective spring constants, c_ξ and c_η the respective crack flexibilities, and l the shaft length, then

$$\left.\begin{aligned} k_\xi &= k/\left(1 + c_\eta k l^2/8\right) \\ k_\eta &= k/\left(1 + c_\xi k l^2/8\right) \end{aligned}\right\} \tag{6.10}$$

The equations of motion in the rotor-fixed coordinate system are

$$\left.\begin{aligned} m\left[\ddot{\xi} - 2\omega\dot{\eta} - \omega^2(\xi + \varepsilon_1)\right] + c\left(\dot{\xi} - \omega\eta\right) + k_\xi \xi &= mg\cos\omega t \\ m\left[\ddot{\eta} - 2\omega\dot{\xi} - \omega^2(\eta + \varepsilon_2)\right] + c(\dot{\eta} - \omega\xi) + k_\eta \eta &= mg\sin\omega t \end{aligned}\right\} \tag{6.11}$$

Introducing

$$\omega_n^2 = \frac{k}{m} \qquad \frac{c}{m} = 2\omega_n\zeta \qquad \frac{k_\xi}{m} = \omega_1^2 \qquad \frac{k_\eta}{m} = \omega_2^2$$

The equations of motion become

$$\left.\begin{aligned} &\ddot{\xi} + 2\omega_n\xi\left(\dot{\xi} - \omega\eta\right) - 2\omega\dot{\eta} + \left(\omega_1^2 - \omega^2\right)\xi = \varepsilon_1\omega^2 + g\cos\omega t \\ &\ddot{\eta} + 2\omega_n\xi(\dot{\eta} + 2\omega\xi) + 2\omega\dot{\xi} + \left(\omega_2^2 - \omega^2\right)\eta = \varepsilon_2\omega^2 - g\sin\omega t \end{aligned}\right\} \tag{6.12}$$

Stability of this linear system will depend on the behavior of the homogeneous system. A solution is sought in the form

$$\xi = A\exp(\lambda t) \quad \eta = B\exp(\lambda t) \tag{6.13}$$

The characteristic equation is then

$$\begin{aligned} &\lambda^4 + 4\omega_n\zeta\lambda^3 + \left(\omega_1^2 + \omega_2^2 + 2\omega^2 + 4\omega_n^2\zeta^2\right)\lambda^2 + 2\omega_n\zeta\left(\omega_1^2 + \omega_2^2 + 2\omega^2\right)\lambda \\ &\quad + \left(\omega_1^2 - \omega^2\right)\left(\omega_2^2 - \omega^2\right) + 4\omega_n^2\zeta^2\omega^2 = 0 \end{aligned} \tag{6.14}$$

Routh criterion for stability [27] demands that a characteristic equation of the form

$$a_n\lambda^n + a_{n-1}\lambda^{n-1} + \cdots + a_1\lambda^1 + a_0 = 0 \tag{6.15}$$

must have all roots with negative real parts so that

1. All coefficients a o are non-zero and of the same sign;
2. All the following successive determinants are positive:

$$D_0 = a_1 \quad D_1 = \begin{vmatrix} a_1 & a_0 \\ a_3 & a_2 \end{vmatrix} \quad D_2 = \begin{vmatrix} a_1 & a_0 & 0 \\ a_3 & a_2 & a_1 \\ a_5 & a_4 & a_3 \end{vmatrix} \quad \cdots$$

The conditions $D_0 > 0, D_1 > 0, D_2 > 0$ are always satisfied. The condition $a_0 > 0$ implies that for stability, ω should lie outside the roots of the equation in ω:

$$\left(\omega_1^2 - \omega^2\right)\left(\omega_2^2 - \omega^2\right) + 4\omega_n^2\zeta^2\omega^2 = 0 \tag{6.16}$$

which means that ω should be either

$$\omega^2 < \frac{\omega_1^2 + \omega_2^2}{2} - 2\omega_n^2\zeta^2 - \sqrt{\left(\frac{\omega_1^2 - \omega_2^2}{2}\right)^2 - 4\omega_n^2\zeta^2\left(\frac{\omega_1^2 + \omega_2^2}{2}\right) + 4\omega_n^4\zeta^4}$$

or

$$\omega^2 > \frac{\omega_1^2 + \omega_2^2}{2} - 2\omega_n^2\zeta^2 + \sqrt{\left(\frac{\omega_1^2 - \omega_2^2}{2}\right)^2 - 4\omega_n^2\zeta^2\left(\frac{\omega_1^2 + \omega_2^2}{2}\right) + 4\omega_n^4\zeta^4} \tag{6.17}$$

A first observation is that when the radical is negative there is always stability. Neglecting ζ^4, the condition for global stability is

$$\zeta^2 > \frac{\left(\omega_1^2 - \omega_2^2\right)^2}{4\omega_n^2\left(\omega_1^2 + \omega_2^2\right)} \tag{6.18}$$

If the system is undamped, Eq. (6.17) suggest that the range $\omega_1 > \omega > \omega_2$ is unstable. Damping shifts the range of instability to lower frequencies. For shallow cracks the local flexibility is small and condition (6.18) is usually satisfied. The propagation of the crack causes ω_1 and ω_2 to be progressively different from one another until inequality (6.18) is violated. At this point the instability range starts developing. As the difference between ω_1 and ω_2 increases, the influence of damping tends to be minimized and the situation gradually approaches undamped instability range $\omega_1 > \omega > \omega_2$.

Turning our attention to the forced response (Eq. 6.12), upon multiplication of the second by i and addition, becomes, for $\rho = \xi + i\eta$

$$\ddot{\rho} + 2(\omega_n\zeta + i\omega)\dot{\rho} + \left(\frac{\omega_1^2 + \omega_2^2}{2} - \omega^2 + 2i\omega\omega_n\zeta\right)\rho + \frac{\omega_1^2 - \omega_2^2}{2}\bar{\rho} = \omega^2(\varepsilon_1 + i\varepsilon_2) + g\,\exp(-i\omega t) \tag{6.19}$$

where a bar denotes the complex conjugate number. Since the problem is linear, the influence of imbalance and of the disc weight can be assessed separately.

To this end, the imbalance response is the steady state solution neglecting the term $g\,\exp(-i\omega t)$. The length of the response vector, from Eq. (6.19) is

$$|\rho_\varepsilon| = R_\varepsilon = \omega^2\frac{\sqrt{\left[\varepsilon_1\left(\omega_2^2 - \omega^2\right) + 2\zeta\omega_n\omega\varepsilon_2\right]^2 + \left[\varepsilon_2\left(\omega_1^2 - \omega^2\right) - 2\zeta\omega_n\omega\varepsilon_1\right]^2}}{\left(\left(\omega_1^2 - \omega^2\right)\left(\omega_2^2 - \omega^2\right) + 4\zeta^2\omega_n^2\omega^2\right)} \tag{6.20}$$

As one would expect, this function has maxima near the frequencies ω_1 and ω_2 and the respective amplitudes are, for small damping

$$\left.\begin{aligned}(R_\varepsilon)_{\omega=\omega_1} &= \frac{\varepsilon_1}{4\zeta^2}\frac{\left|\omega_2^2-\omega_1^2\right|}{\omega_n^2}\\ (R_\varepsilon)_{\omega=\omega_2} &= \frac{\varepsilon_2}{4\zeta^2}\frac{\left|\omega_2^2-\omega_1^2\right|}{\omega_n^2}\end{aligned}\right\} \tag{6.21}$$

These amplitudes become infinite for zero damping. Therefore, it is expected that critical speeds are present during speeding up or coasting down near the natural frequencies ω_1 and ω_2 which are both below the uncracked shaft frequency ω_n.

The influence of the disc weight can be found by neglecting the eccentricities ε_1 and ε_2 in Eq. (6.19). A solution of the resulting equation exists in the form

$$\rho_g = U\exp(i\omega t) + V\exp(-i\omega t) \tag{6.22}$$

where

$$\begin{aligned}
\mathrm{Re}\{U\} &= \tfrac{1}{2}\tfrac{g}{\Delta}\left(\omega_2^2-\omega_1^2\right)\left[\omega_1^2\omega_2^2 - 2\omega^2\left(\omega_1^2+\omega_2^2\right)\right]\\
\mathrm{Im}\{U\} &= \frac{g}{\Delta}\zeta\omega_n\omega\left(\omega_1^2-\omega_2^2\right)\left(\omega_1^2+\omega_2^2\right)\\
\mathrm{Re}\{V\} &= \frac{g}{\Delta}\left\{\left[\frac{1}{2}\left(\omega_1^2+\omega_2^2\right)-4\omega^2\right]\times\left[\omega_1^2\omega_2^2 - 2\omega^2\left(\omega_1^2+\omega_2^2\right)+\gamma\zeta^2\omega_\mathrm{n}^2\omega^2\left(\omega_1^2+\omega_2^2\right)\right]\right\}\\
\mathrm{Im}\{V\} &= \frac{g}{\Delta}2\zeta\omega_n\omega\left\{\left[\frac{1}{2}\left(\omega_1^2+\omega_2^2\right)-4\omega^2\right]\left(\omega_1^2+\omega_2^2\right)-2\left[\omega_1^2\omega_2-2\omega^2\left(\omega_1^2+\omega_2^2\right)\right]\right\}\\
\Delta &= \left[\omega_1^2\omega_2^2-2\omega^2\left(\omega_1^2+\omega_2^2\right)\right]^2+4\zeta^2\omega_n^2\omega^2\left(\omega_1^2+\omega_2^2\right)^2
\end{aligned}$$

The magnitudes of U and V are finite for all ω for non-zero ζ, because Δ is positive. For zero damping, Δ becomes zero and the amplitude becomes infinite, for a particular speed of rotation:

$$\omega_c = \frac{\omega_1\omega_2}{\sqrt{2\left(\omega_1^2+\omega_2^2\right)}} = \frac{1}{2}\omega_n\sqrt{1-\left(\frac{k_\xi-k_\eta}{k_\xi+k_\eta}\right)} \tag{6.23}$$

For small crack depth, $\omega_1 \approx \omega \approx \omega_2$, and this particular speed equals half the uncracked rotor natural frequency. This observation is used for crack detection on rotating shafts because only mechanisms of dissimilar moment of inertia can introduce such a frequency. For non-zero damping the amplitude at $\omega = \omega_\mathrm{c}$ is near maximum and this speed is called the secondary critical speed due to the weight of the disc.

If we now consider a forced response due to both imbalance and disc weight and perform the transformation

$$z = \rho\exp(i\omega t)$$

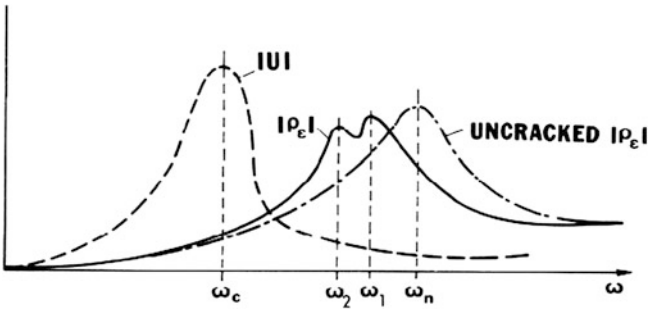

Fig. 6.4 Vibration amplitude of the cracked shaft

into the stationary coordinate system, we see that the rotor response is

$$z = U\exp(2i\omega t) + V + \rho_\varepsilon \exp(i\omega t) \tag{6.24}$$

The first term represents whirl at double the running frequency. The second term is the static deflection of the shaft. The third term is the imbalance response at running frequency. The response as a function of the running speed is shown in Fig. 6.4.

6.4 The Closing Crack

The rotation of a cracked shaft loaded laterally by its own weight or a static load, for a crack closing at positions where compressive stresses occur at the location of the crack, introduces time varying coefficients into the equations of motion. In this case, if the time $t = 0$ corresponds to a position at which the crack starts opening, Eq. (6.19) becomes

$$\begin{aligned}\ddot{\rho} + 2(\omega_n\zeta + i\omega)\dot{\rho} + \left(\frac{\omega_1^2+\omega_2^2}{2} - \omega^2 + 2i\omega\omega_n\zeta\right)\rho + \frac{\omega_1^2-\omega_2^2}{2}\bar{\rho} &= \omega^2(\varepsilon_1 + i\varepsilon_2) + g\exp(-i\omega t) \quad 0<\omega t<\pi \\ \ddot{\rho} + 2(\omega_n\zeta + i\omega)\dot{\rho} + (\omega_n^2 - \omega^2 + 2i\omega\omega_n\zeta)\rho &= \omega^2(\varepsilon_1 + i\varepsilon_2) + g\exp(-i\omega t)\end{aligned} \tag{6.25}$$

Although, in principle, these equations can be solved with the analytical methods described in Chap. 2, the usual procedure is the numerical solution of these equations. In this manner, one can take into account the non-linear behavior for sufficiently high vibration amplitudes.

For shafts with more complicated geometry, it is preferable to work in the stationary coordinate system. A shaft element in the vicinity of the crack has the following flexibility matrix in the rotating coordinate system:

$$\begin{bmatrix} c_1 & 0 \\ 0 & c_2 \end{bmatrix}$$

Multiplying by the transformation matrix, the same matrix in the stationary coordinate system is

$$\begin{bmatrix} c_2 + (c_1 - c_2)\cos^2 \omega t & \frac{1}{2}(c_1 - c_2)\sin 2\omega t \\ \frac{1}{2}(c_1 - c_2)\sin 2\omega t & c_2 + (c_1 - c_2)\sin^2 \omega t \end{bmatrix}$$

for $2\pi n < \omega t < 2\pi n + \pi$. In the second half of the period, the flexibility matrix is

$$\begin{bmatrix} c & 0 \\ 0 & c \end{bmatrix}$$

for $2\pi n + \pi < \omega t < 2\pi(n + 1)$.

Several investigators have used such equations to obtain the responses of cracked shafts [4–18, 28–33].

Whereas a slotted shaft has only two speeds at which the synchronous response becomes unbounded, the cracked shaft carries the possibility of either a range of speeds, where a bounded synchronous response does not exist, or a range of speeds where there are two possible synchronous responses. Which of these alternatives is realized depends upon the phase of the out-of-balance with respect to the crack. With the out-of-balance in phase with the crack, a band of speeds occurs where the equations have no solution; with the out-of-balance in antiphase with the crack, a band of speeds exists where there are two solutions to the equations. One of these solutions is unstable and the slightest disturbance would cause the system to jump from the unstable to the stable solution. This phenomenon (switching from one solution to another) is characteristic of non-linear systems. The time history of local flexibilities associated with a breathing crack and, furthermore, material damping in a rotating shaft has been the subject of several investigations [33–38].

A first analytical approach to the problem of a breathing crack can be made by considering the motion on the rotating coordinate system. The equation of motion for the de Laval rotor, neglecting damping and for a mass of eccentricity , will be

$$m\ddot{\xi} + 2m\omega i\dot{\xi} + \left(k - m\omega^2\right)\xi = mg\exp(-i\omega t) + m\varepsilon\omega^2 \tag{6.26}$$

where the shaft stiffness k takes the value $k(1 - \delta)$ for negative (which is equivalent to $\pi/\omega < t < 2\pi/\omega$. If k_T is the cracked shaft local stiffness to bending, the corresponding linear stiffness of the shaft in the lateral direction will be

$$\frac{1}{k(1-\delta)} = \frac{1}{k} + \frac{L^2}{16k_T} = \frac{1}{k}\left(1 + \frac{kL^2}{16k_T}\right) \tag{6.27}$$

Here, $k_T = 1/c_\xi$ where c_ξ, is given by Eq. (6.6).

The null equation has the form

$$\ddot{\xi} + 2\omega i\dot{\xi} + \left(\omega_1^2 - \omega_2^2\right)\xi = 0 \tag{6.28}$$

with $\omega = \omega_1 = \sqrt{k/m}$ for $\xi > 0$ and $\omega = \omega_2 = \omega_1\sqrt{1-\delta}$ for $\xi < 0$. It admits solutions of the form

$$\left.\begin{aligned}\xi_1 &= (A_1 \cos \omega_1 t + B_1 \sin \omega_1 t) \exp(-i\omega t)\\ \xi_2 &= (A_2 \cos \omega_2 t + B_2 \sin \omega_2 t) \exp(-i\omega t)\end{aligned}\right\} \tag{6.29}$$

during the first and second half of one rotation respectively.

If the system is forced to rotate with angular velocity Ω instability may occur (see Chap. 2). This can be demonstrated by observing some compatibility conditions:

1. At the end of the half cycle ($t = n/w$) displacements and velocity are the same;
2. At the end of the complete cycle ($t = 2n/w$) displacement and velocity are λ times greater than the values at the beginning of the cycle ($t = 0$).

These conditions lead to four homogeneous linear equations in A_1, A_2, B_1, B_2. The condition that these equations have a solution other than the trivial gives (see Eqs. 2.9–2.11)

$$\lambda^2 - 2q\lambda + 1 = 0 \tag{6.30}$$

from which

$$\lambda = q \pm \sqrt{q^2 - 1} \tag{6.31}$$

where

$$q = \cos\frac{\pi\omega_1}{\omega}\cos\frac{\pi\omega_2}{\omega} - \frac{\omega_1^2 + \omega_2^2}{2\omega_1\omega_2}\sin\frac{\pi\omega_1}{\omega}\sin\frac{\pi\omega_2}{\omega} \tag{6.32}$$

It is apparent that $\lambda > 1$ will lead to growing vibrations and instability. The threshold of instability is at $\lambda = 1$ in which case $q = 1$. The speeds at which instability occurs are given as solutions of the equation

$$q = 1 \tag{6.33}$$

or, in terms of the dimensionless parameters, $\zeta_1 = \omega_1/\omega$, and $\zeta_2 = \omega_2/\omega$, where ω is the natural frequency of the uncracked shaft.

$$q = \cos\pi\zeta_1 \cos\zeta_2 - \frac{\zeta_1^2 + \zeta_2^2}{2\zeta_1\zeta_2}\sin\pi\zeta_1 \sin\zeta_2 = 1 \tag{6.34}$$

Solutions of this equation are plotted in Fig. 6.5 as functions of the parameters δ and ω_1/ω. Out of these, δ is a function of the crack depth, as described above. The instability region for the shaft with open crack is indicated by dotted lines. It is obvious that there is a substantial difference between the two models.

When we turn our attention to the forced response, we find that a particular solution of the non-homogeneous equation is

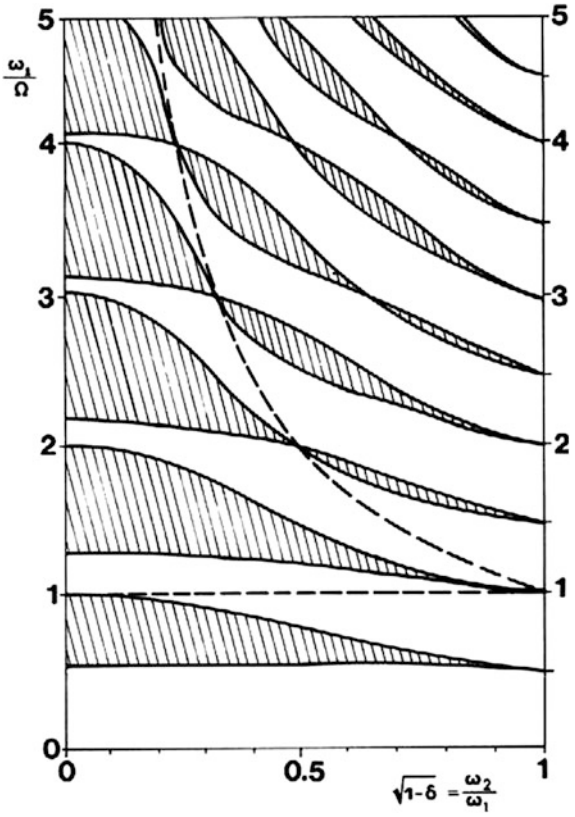

Fig. 6.5 Stability chart for a cracked shaft. Shaded areas indicate instability

$$\xi_p = \frac{m\varepsilon\omega^2}{k - m\omega^2} + \frac{mg}{k}\exp(-i\omega t) \tag{6.35}$$

The general solution is

$$\xi = \left(A_j \cos\omega_j t + B_j \sin\omega_j t\right)\exp(-i\omega t) + \frac{m\varepsilon\omega^2}{k - m\omega^2} + \frac{mg}{k}\exp(-i\omega t) \tag{6.36}$$

where the subscript j takes the values 1 and 2 in the intervals $0 < t < \pi/\omega$ and $\pi/\omega < t < 2\pi/\omega$, respectively. Application of the continuity conditions with $\lambda = 1$ for steady state will yield

$$\mathbf{La} = \mathbf{f} \tag{6.37}$$

where

$$\mathbf{a} = \{A_1\, A_2\, B_1\, B_2\}$$
$$\mathbf{f} = \{f_1 f_2 f_3 f_4\}$$

$$f_1 = \varepsilon\left[\frac{1}{(\omega_2/\omega)^2-1} - \frac{1}{(\omega_1/\omega)^2-1}\right] + g\left(\frac{1}{\omega_1^2} - \frac{1}{\omega_2^2}\right)$$

$$f_2 = -g\left(\frac{1}{\omega_1^2} - \frac{1}{\omega_2^2}\right)$$

$$f_3 = \varepsilon\left[\frac{1}{(\omega_2/\omega)^2-1} - \frac{1}{(\omega_1/\omega)^2-1}\right] - g\left(\frac{1}{\omega_1^2} - \frac{1}{\omega_2^2}\right)$$

$$f_4 = g\left(\frac{1}{\omega_1^2} - \frac{1}{\omega_2^2}\right)$$

$$\mathbf{L} = \begin{bmatrix} \cos\pi(\omega_1/\omega - 1) & \sin\pi(\omega_1/\omega - 1) & -\cos\pi(\omega_2/\omega - 1) & -\sin\pi(\omega_2/\omega - 1) \\ -\sin\pi(\omega_1/\omega - 1) & \cos\pi(\omega_1/\omega - 1) & \sin\pi(\omega_2/\omega - 1) & -\cos\pi(\omega_2/\omega - 1) \\ 1 & 1 & -1 & -1 \\ -1 & 1 & 1 & -1 \end{bmatrix}$$

Therefore, the coefficients of Eq. (6.37) are

$$\mathbf{a} = \mathbf{L}^{-1}\,\mathbf{f} \tag{6.38}$$

Then, Eq. (6.37) yields the rotor response in the rotating coordinate system and the transformation $z = \xi \exp(i\Omega t)$ will give the response in the stationary coordinate system.

The above analysis is based on the assumption that the static deflection is much greater than the vibration amplitude and that there is a sharp transition of the shaft stiffness from uncracked to cracked, at the time that the crack is vertical. This is not exactly correct at times when the crack is near the vertical position. For such cases the local stiffness is measured experimentally as a function of the angle of the crack to the vertical. The analytical procedure in this case is based on the expansion of this function in a Fourier series. To this end, proper selection of the zero time permits the shaft stiffness to be set up in the form

$$k = \sum_{i=0}^{n} A_n \cos i\omega t \tag{6.39}$$

Usually, this series converges very rapidly and no more than a few first terms are significant.

The shaft equation in the stationary coordinate system for the vertical motion will be

$$m\ddot{z} + kz = m\varepsilon\omega^2 \exp(i\omega t) + mg \tag{6.40}$$

A solution is sought in the form

$$z = \sum_{j=0}^{l} a_j \cos j\omega t \tag{6.41}$$

Substituting into Eq. (6.40) and collecting similar terms cos $k\Omega t$, after expressing the products

$$\cos a \cos b = [\cos(a+b) + \cos(a-b)]/2$$

a series of equations is obtained. The kth of the $p = l + n + 1$ equations is

$$-m\omega^2 a_k k^2 + \sum_{j=0}^{l+n} a_j \left(A_{k+j} + A_{k-j}\right) = \left\{ \begin{array}{cc} mg & for \quad k=0 \\ m\varepsilon\omega^2 & for \quad k=1 \\ 0 & \text{otherwise} \end{array} \right\} \tag{6.42}$$

The second term in the parentheses exists only if $k \geq j$.

The coefficients a_j are computed from the solution of the system of linear algebraic equations

$$\mathbf{Da} = \mathbf{f} \tag{6.43}$$

where the i, j element of the $p \times p$ matrix $\mathbf{D}$ is

$$d_{ij} = \left\{ \begin{array}{ll} A_{i+j} + A_{i-j} & for\, i > j \\ A_{2i} + A_0 - m\varepsilon\omega^2 i^2 & for\, i = j \\ A_{i+j} & for\, i < j \end{array} \right\}$$

Of course $A_i = 0$ when $i > n$. The forcing vector has only two non-zero terms:

$$\begin{aligned} f_0 &= mg \\ f_1 &= m\varepsilon\omega^2 \end{aligned}$$

$\mathbf{D}$ is a banded matrix and the width of the band depends on the number n of harmonics of the stiffness function. In general, the response has $2n$ harmonics and $l = 2n$. Then, the size of the matrix 0 is $p = 3n + 1$.

Therefore

$$\mathbf{z} = \mathbf{cD}^{-1}\mathbf{f} \tag{6.44}$$

where

$$\mathrm{c} = [1 \cos \omega t, \cos 2\omega t, \ldots, \cos(3n+1)\omega t]$$

Critical speeds will be roots of the equation

$$|\mathbf{D}| = 0 \tag{6.45}$$

Due to the term i^2 in the diagonal of matrix $\mathbf{D}$, the system has several subharmonics. Their magnitude depends strongly on b. For uncracked shafts, Eq. (6.45) degenerates to the well-known relation

$$\omega^2 = k/m$$

for $A_0 = k$, $A_1 = A_2 = \cdots = 0$.

References

1. Dimarogonas, A.D.: Vibration for Engineers, 2nd edn. Prentice Hall, New Jersey (1996)
2. Wauer, J.: On the dynamics of cracked rotors: A literature survey. Appl. Mech. Rev. **43**(1), 13–17 (1990)
3. General Electric Co.: A methodology for predicting torsional fatigue life of turbine generator shafts using crack initiation plus propagation. EL-4333, Research project 1531-1, Final report (1985)
4. Dimarogonas, A.D.: Vibration of cracked structures: A state of the art review. Eng. Fract. Mech. **55**(5), 831–857 (1996)
5. Papadopoulos, C.A.: The strain energy release approach for modelling cracks in rotors: A state of the art review. Mech Syst Signal Process **22**(4), 763–789 (2008). Special issue on crack effects in Rotordynamics
6. Gash, R.: Dynamic behavior of a simple rotor with a cross-sectional crack. In: IME Conference on Vibrations in Rotating Machinery, Paper C178/76. IME Conference Publication (1976)
7. Henry, T.A., Okah-Avae, B.E.: Vibrations in cracked shafts. ibid, Paper C162/76 (1976)
8. Mayes, I.W., Davies, W.G.R.: The vibrational behavior of a rotating shaft system containing a transverse crack. ibid, Paper C168/76 (1976)
9. Grabowski, B.: The vibrational behavior of a turbine rotor containing a transverse crack. In: Proceedings of the ASME Design Engineering Technology Conference, ASME paper 79-DET-67. St. Louis (1979)
10. Ziebarth, H., et al.: Auswirkung von Querissen auf das Schwingungsverhalten von Rotoren. VDl-Berichte **320**, 37–43 (1978)
11. Dimarogonas, A.D., Massouros, G.: Torsional vibration of a shaft with a circumferential crack. Eng. Fract. Mech. **15**(3–4), 439–444 (1981)
12. Dimarogonas, A.D., Papadopoulos, C.A.: Vibration of cracked shafts in bending. J. Sound Vib. **91,** 583–593 (1983)
13. Papadopoulos C.A., Dimarogonas, A.D.: Coupled longitudinal and bending vibrations of a rotating shaft with an open crack. J. Sound Vib. **117,** 81–93 (1987)
14. Wauer, J.: Modelling and formulation of equation of motion for cracked rotating shafts. Int. J. Solids Struct. **26**(4), 901–914 (1990)
15. Papadopoulos, C.A., Dimarogonas, A.D.: Coupled vibration of cracked shafts. J. Vib. Acoust. **114**, 461–467 (1992)
16. Edwards, S., Lees, A.W., Friswell, M.I.: Fault Diagnosis of Rotating Machinery. Shock Vib Digest **1**, 4–13 (1998)
17. Bicego, V., Lucon, E., Rinaldi, C., Crudeli, R.: Failure analysis of a generator rotor with a deep crack detected during operation: Fractographic and fracture mechanics approach. Nucl. Eng. Des. **188**, 173–183 (1999)
18. Gounaris, G.D., Papadopoulos, C.A.: Crack identification in rotating shafts by coupled response measurements. Eng. Fract. Mech. **69**, 339–352 (2002)
19. Christides, S., Barr, A.D.S.: Torsional vibration of cracked beams of non-circular cross-section. Int. J. Mech. Sci. **28**(7), 473–490 (1986)
20. Barr, A.D.S.: An extension of the Hu-Washizu variational principle in linear elasticity for dynamic problems. Trans. ASME J. Appl. Mech. **33**(2), 465 (1966)
21. Washizu, K.: On the Variational Principles of Elasticity and Plasticity. Technical report 25–18, contract no. N5–07833. Massachusetts Institute of Technology, Cambridge, Mass (1955)
22. Hu, H.C.: On some variational principles in the theory of elasticity and plasticity. Sci. Sinica **4**, 33–55 (1995)
23. Chondros, T.G., Dimarogonas, A.D., YAO, J.: A consistent cracked bar vibration theory. J. Sound Vib. **200**, 303–313 (1997)

24. Chondros, T.G., Dimarogonas, A.D., Yao, J.: A continuous cracked beam vibration theory. J. Sound Vib. **215**, 17–34 (1998)
25. Chondros, T.G.: Variational formulation of a rod under torsional vibration for crack identification. Fatigue Fract. Eng. Mater. Struct. **44**(1), 95–104 (2005)
26. Tada, H., Paris, P.: The Stress Analysis of Cracks Handbook. Del Research Corp., Hellertown, Pennsylvania (1973)
27. Gibson, J.E.: Nonlinear Automatic Control. McGraw-Hill, New York (1963)
28. Papadopoulos, C.A., Dimarogonas, A.D.: Coupling of bending and torsional vibrations of a cracked timoshenko shaft. Ing. Arch. (Replaced by Arch. Appl. Mech.) **57**(4), 257–266 (1987)
29. Papadopoulos, C.A., Dimarogonas, A.D.: Coupled longitudinal and bending vibrations of a cracked shaft. J. Vib. Acoust. Stress Reliab. Des. **110**(1), 1–8 (1988)
30. Papadopoulos, C.A., Dimarogonas, A.D.: Stability of cracked rotors in the coupled vibration mode. J. Vib. Acoust. Stress Reliab. Des. **110**(3), 356–359 (1988)
31. Papadopoulos, C.A.: Torsional vibrations of rotors with transverse surface cracks. Comput. Struct. **51**(6), 713–718 (1994)
32. Gounaris, G.D., Papadopoulos, C.A., Dimarogonas, A.D.: Crack identification in beams by coupled response measurements. Comput. Struct. **58**(2), 299–305 (1996)
33. Tondl, A.: The Effect of Internal Damping on the Stability of Rotor Motion and the Rise of Self Excited Vibrations, Some Problems of Rotor Dynamics, pp. 1–6. Publishing House of Czechoslovak Academy of Sciences, Prague (1965)
34. Zorzi, E.S., Nelson, H.D.: Finite element simulation of rotor- bearing systems with internal damping. J. Eng. Power Trans. ASME **99**, 71–76 (1977)
35. Muszynska, A.: Rotor Dynamics. CRC Press, Taylor (2005)
36. Georgantzinos, S.K., Anifantis, N.K.: An insight into the breathing mechanism of a crack in a rotating shaft. J. Sound Vib. **318**, 279–295 (2008)
37. Chouksey, M., Dutt, J.K., Modak, S.V.: Modal analysis of rotor-shaft system under the influence of rotor-shaft material damping and fluid film forces. Mech. Mach. Theory **48**, 81–93 (2012)
38. Rubio, L., Fernández-Sáez J.: A new efficient procedure to solve the nonlinear dynamics of a cracked rotor, Nonlin. Dynam **70**(3), 1731–1745 (2013)

Chapter 7
Identification of Cracks in Rotors and Other Structures by Vibration Analysis

Abstract The question of crack detection from dynamic measurements is further extended and discussed in Chap. 7. A general stiffness matrix for cracked structural members is introduced, to model the respective dynamic system. This stiffness matrix can be further utilized for static, dynamic or stability analysis of a structure with cracked members of rectangular or circular cross-section. Off-diagonal terms indicate vibration coupling. The change in dynamic response is analytically evaluated for simple systems and by means of approximate methods for more complicated ones. The outlined procedure can be used for engineering analysis in two ways: (a) as a design tool, to assist in structural optimization with the objective of achieving certain specific dynamic characteristics; and (b) as a maintenance and inspection tool, to identify structural flaws, such as cracks, by linking the variations in service of the structure's natural frequencies to structural changes due to the cracks.

7.1 Flexibility Matrix of Cracked Structural Members

In the previous chapter it was shown that the presence of a crack on a rotating shaft may change to a measurable, even substantial, extent its dynamic characteristics.

A crack on a structural member introduces a local flexibility, which is a function of the crack depth. This flexibility changes the dynamic behavior of the system and its stability characteristics. In this chapter, the problem of identification of the crack from the resulting change in the dynamic behavior of the system containing the crack will be examined. It must be emphasized that non-propagating cracks will be examined.

A. D. Dimarogonas et al., *Analytical Methods in Rotor Dynamics*, Mechanisms and Machine Science 9, DOI: 10.1007/978-94-007-5905-3_7,

The local flexibility of a cracked beam was studied by Irwin [1], who related this flexibility (compliance) to the stress intensity factor.

The effect of the local flexibility of a cracked column upon its buckling load was studied by Liebowitz et al. [2, 3] and Ocamura [4]. These authors identified the compliance of a cracked column to a bending moment. Rice and Levy [5] recognized coupling between bending and extensional compliance of a cracked column in compression.

The effect of cracks upon the dynamic behavior of cracked beams was studied by Dimarogonas [6] and by Chondros and Dimarogonas [7, 8]. The effect of peripheral cracks upon the torsional vibration of a rod of circular cross-section was studied by Dimarogonas and Massouros [9].

The investigation of cracked rotors behavior in torsional vibration and the development of crack detection methods for rotating shafts were initiated at about 1970. In a literature survey on the dynamics of cracked rotors by Wauer [10] it is stated that obviously the first work was done by the General Electric Company. The problem was further examined by Dimarogonas [11] and Pafelias [12], at the Turbine Department of the General Electric Company in Schenectady. Metallurgical examination revealed that failure was due to fatigue-propagated cracks in the rotors.

Circumferential cracks often appear in a variety of machinery such as gas and steam turbines and aircraft engines, especially in welded rotors. Identification of cracks and their depth in service is of paramount importance for system planners who must modify operating practices before large amounts of shaft fatigue life have gone astray. The problem of crack modeling is one of the most significant issues in this area. The theory of strain energy release meets the rotordynamics in the early 1970s, when the detection of fatigue crack became a necessity in power plants.

Since the early 1980s, there has been a substantial amount of academic research on the monitoring and early warning of cracked rotors. A state of the art review by Dimarogonas [11] on the vibration of cracked structures provided a detailed description of the papers that followed the initial investigations reported by Wauer [10, 13] and Gasch [14] including analytical, numerical and experimental investigations.

The fundamental frequency vibration problem has been investigated experimentally and analytically by Dimarogonas [6, 11] to assess the possibility of crack detection without interrupting the operation of the machine. For a stepped rotor, the transfer matrix technique was used to compute the change in critical speed of a shaft due to a crack. The results confirmed that for small crack depths the change in critical speed is proportional to $(\alpha/D)^2$, where α is the crack depth and D is the shaft diameter, but it was concluded that the measurement of the change at critical speed is not an efficient way to monitor rotor cracks.

Cracks in rotors are initiated on a microscopic level and are not detectable until the shaft has suffered extensive damage. Continued exposure to system disturbances could result in crack growth and subsequent shaft fatigue failure. A case of a generator rotor, in which a transverse fatigue crack could grow to a very large

extent for several years until its extension reached 60 % of the rotor section area, without being detected, is presented by Bicego et al. [15].

A continuous cracked rod torsional vibration theory proposed by Christides and Barr [16, 17] was adopted by Chondros [18, 19] and independent assumptions about displacement, momentum, strain and stress fields of the cracked rod were considered for the derivation of the equations of motion for a uniform rod in torsional vibration, where the rod has one circumferential open edge crack along its length. Since fracture mechanics methods appear in the literature for the evaluation of stress intensity factors for different cracks configurations, the method can be extended to multiple cracks, stepped rods, etc., without adding complexity to the problem, as the same differential equation will be used with different forms of the stress disturbance function [20]. This theory will be presented in Chaps. 9 and 10.

7.1.1 Prismatic Cracked Beam Element

To study the effect of a crack on the dynamic response of an elastic structure, one has to establish local stiffness or flexibility matrix of the cracked member under general loading. To this end, a prismatic bar with a crack of depth a along the y-axis with a uniform depth along the z-axis is considered.

The beam has height h and width b. The beam is loaded with an axial force P_1, shear forces P_2, P_3 and bending moments P_4 and P_5 (Fig. 7.1).

The basic modes of crack surface displacements, also shown in Fig. 7.1 correspond to: I—the crack surfaces move directly apart (symmetric to the x–y and

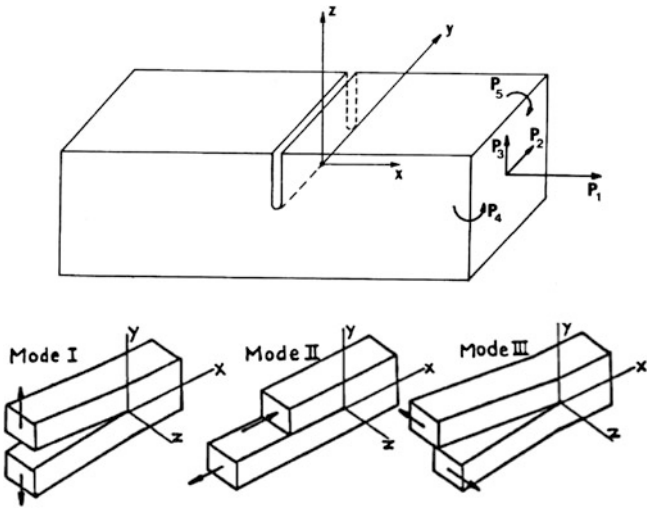

Fig. 7.1 Loaded beam element with transverse crack, and the basic modes of crack surface displacements [21]

y–z planes), II—the edge sliding mode, and III—tearing [21]. Under general loading, the additional displacement u_{i} along the direction of force P_i due to the presence of the crack will be computed using Castigliano's theorem and by generalization of the Paris equation [21].

To this end, if U_T is the strain energy due to a crack, Castigliano's theorem demands that the additional displacement is

$$u_i = \partial U_T / \partial P_i$$

along the force P_i. The strain energy will have the form [1]

$$U_T = \int_0^a \frac{\partial U_{\mathrm{T}}}{\partial a} da = \int_0^a J da \tag{7.1}$$

where $J = (\partial U_T / \partial a)$, the strain energy density function. Therefore

$$u_{\mathrm{i}} = \frac{\partial}{\partial P_{\mathrm{i}}} \left[\int_0^a J(a) da \right] \text{ (Paris equation)} \tag{7.2}$$

the flexibility influence coefficient c_{ij} will be

$$c_{\mathrm{ij}} = \frac{\partial u_{\mathrm{i}}}{\partial P_{\mathrm{j}}} = \frac{\partial^2}{\partial P_{\mathrm{i}} \partial P_{\mathrm{j}}} \int_0^a J(a) da \tag{7.3}$$

The strain energy density function J is the general form

$$\mathrm{J} = \frac{1}{E'} \left[\left(\sum_{i=1}^{5} K_{\mathrm{II}} \right)^2 + \left(\sum_{i=1}^{5} K_{\mathrm{III}} \right)^2 + a \left(\sum_{i=1}^{5} K_{\mathrm{IIII}} \right) \right] \tag{7.4}$$

where $E' = E$ for plane stress, $E' = E/(1 - \nu^2)$ for plane strain, $\alpha = 1 + \nu$; E and ν are Young's modulus and Poisson's ratio, respectively. Then, integrating along the cut (y-axis):

$$c_{\mathrm{ij}} = \frac{1}{E' b} \int_0^a \left[\frac{\partial^2}{\partial P_{\mathrm{i}} \partial P_{\mathrm{j}}} \sum_m \int_0^b (e_{\mathrm{m}} \sum_n K_{\mathrm{mn}})^2 dy \right] da \tag{7.5}$$

where $e_m = \alpha$ for $m = \mathrm{III}$ and $e_m = 1$ for $m = \mathrm{I}, \mathrm{II}$. Furthermore, K_{mn} is the stress intensity factor of mode m ($m = \mathrm{I}, \mathrm{II}, \mathrm{III}$) due to the load P_n ($n = 1, 2, 5$) since the strain energy is additive. Adequate information is available for all K_{mn} except K_{14} which will be assumed variable along the y-axis and the plane solution will be used with the beam bending stress due to P_4 at location y. Then

$$K_{11} = \frac{P_1}{bh}\sqrt{\pi a}F_1(a/h) \tag{7.6}$$

$$K_{15} = \frac{6P_5}{bh^2}\sqrt{\pi a}F_2(a/h) \tag{7.7}$$

$$K_{14} = \frac{12P_4}{b^3h}y\sqrt{\pi a}F_1(a/h) \tag{7.8}$$

$$K_{12} = K_{13} = 0$$

$$K_{\mathrm{II}\,1} = K_{\mathrm{II}\,2} = K_{\mathrm{II}\,4} = K_{\mathrm{II}\,5} = 0$$

$$K_{\mathrm{II}\,3} = \frac{2P_3}{bh\pi a}F_{\mathrm{II}}(a/h) \tag{7.9}$$

$$K_{\mathrm{III}\,1} = K_{\mathrm{III}\,3} = K_{\mathrm{III}\,4} = K_{\mathrm{III}\,5} = 0$$

$$K_{\mathrm{III}\,2} = \frac{2P_2}{bh\pi a}F_{\mathrm{III}}(a/h) \tag{7.10}$$

where [21]

$$\begin{aligned}
F_1(a/h) &= \sqrt{\tfrac{2h}{\pi a}\tan\tfrac{\pi a}{2h}}\,\frac{0.752+2.02(a/h)+0.37\left(1-\sin\frac{\pi a}{2h}\right)^3}{\cos\frac{\pi a}{2h}}\\
F_2(a/h) &= \sqrt{\tfrac{2h}{\pi a}\tan\tfrac{\pi a}{2h}}\,\frac{0.923+0.199\left(1-\sin\frac{\pi a}{2h}\right)^4}{\cos\frac{\pi a}{2h}}\\
F_{\mathrm{II}}(a/h) &= \frac{1.122-0.561(a/h)+0.085(a/h)^2+0.180(a/h)^3}{\sqrt{1-a/h}}\\
F_{\mathrm{III}}(a/h) &= \sqrt{\tfrac{\pi a}{h}/\sin\tfrac{\pi a}{h}}
\end{aligned}$$

Using Eqs. (7.6–7.10) in Eq. (7.5), we obtain

$$c_{11} = \frac{\Phi_{11}}{E'b^3h^2}\;\; c_{14} = \frac{12\Phi_{11}}{E'b^3h^2}\;\; c_{15} = \frac{6\Phi_{12}}{E'b^3h^3} \tag{7.11}$$

$$c_{44} = \frac{48\Phi_{11}}{E'b^4h^2}\;\; c_{45} = \frac{72\Phi_{12}}{E'b^3h^3}\;\; c_{11} = \frac{\Phi_{11}}{E'b^3h^2} \tag{7.12}$$

$$c_{22} = \int_0^a \frac{4aF_{\mathrm{III}}^2(a/h)}{E'b^2h^2\pi(a/h)}d(a/h) \tag{7.13}$$

$$c_{33} = \int_0^a \frac{4F_{\mathrm{II}}^2(a/h)}{E'b^2h^2\pi(a/h)}d(a/h) \tag{7.14}$$

$$\Phi_{\mathrm{ij}} = \int_0^a \frac{\pi a}{h}F_{\mathrm{i}}(a/h)F_{\mathrm{j}}(a/h)da.$$

The local flexibility matrix for the crack will have the form

$$\mathbf{C} = \begin{bmatrix} c_{11} & 0 & 0 & c_{14} & c_{15} \\ 0 & c_{22} & 0 & 0 & 0 \\ 0 & 0 & c_{33} & 0 & 0 \\ c_{41} & 0 & 0 & c_{44} & c_{45} \\ c_{51} & 0 & 0 & c_{54} & c_{55} \end{bmatrix}. \tag{7.15}$$

Due to reciprocity, matrix $\mathbf{C}$ is symmetric.

Some of the terms of matrix $\mathbf{C}$ can be found also in the literature. Okamura [4] and Liebowitz et al. [2, 3] have computed c_{55}; Rice and Levy [5] have computed the terms c_{11}, c_{15}, c_{55}; and Dimarogonas and Massouros have computed the term c_{22} [9]. Dimarogonas and Papadopoulos [22–24] and Dimarogonas [25, 26] generalized the Irwin method of the computation of local compliances, extending it for six degrees of freedom.

7.1.2 Circular Cracked Rod

Direct application of fracture mechanics methods for the computation of local flexibility of a shaft with an edge crack could not be done, because solutions for the stress intensity factor, for a cylindrical shaft with an edge crack, were not available. Dimarogonas [11, 12] used the approximation to consider the section as consisting of elementary strips of varying height which were perpendicular to the crack tip and parallel to the axis of symmetry of the cylindrical shaft (Fig. 7.2). Each was considered as a rectangular cross-section beam with an edge crack, assuming that there was no traction between the strips, for which the cracked region local flexibility, for plane strain, is computed using the fracture mechanics relations between the strain energy release rate and stress intensity factor and Castigliano theorem, Eqs. 7.1–7.4 [1–3, 11]. The effect of a crack upon the dynamic behavior of a beam with a circular cross section under general loading and a surface crack of depth α along the y axis is considered by Papadopoulos and Chondros [27–32]. The beam is loaded with axial force P_1, shear forces P_2, P_3, and bending moments P_4, P_5, P_6 (Fig. 7.2).

The values of the stress intensity factors for a strip of unit thickness with a crack propagating on its own plane are known from the literature [1-11, 21]. Since the energy density is a scalar, it is permissible to integrate along the tip of the crack assuming that the crack depth is variable and that the stress intensity factor is given for the elementary strip. Then, for the circular cross-section of radius R shown in Fig. 7.2, the stress intensity factors K for a strip of unit thickness with a transverse crack under different loading conditions, as shown in Fig. 7.2 are [11]:

$$K_{I1} = \sigma_1 \sqrt{\pi\alpha} F_1\left(\alpha/h\right),\ \sigma_1 = P_1/\left(\pi R^2\right)$$

$$K_{I4} = \sigma_4 \sqrt{\pi\alpha} F_1\left(\alpha/h\right),\ \sigma_4 = 4P_4 x/\left(\pi R^4\right)$$

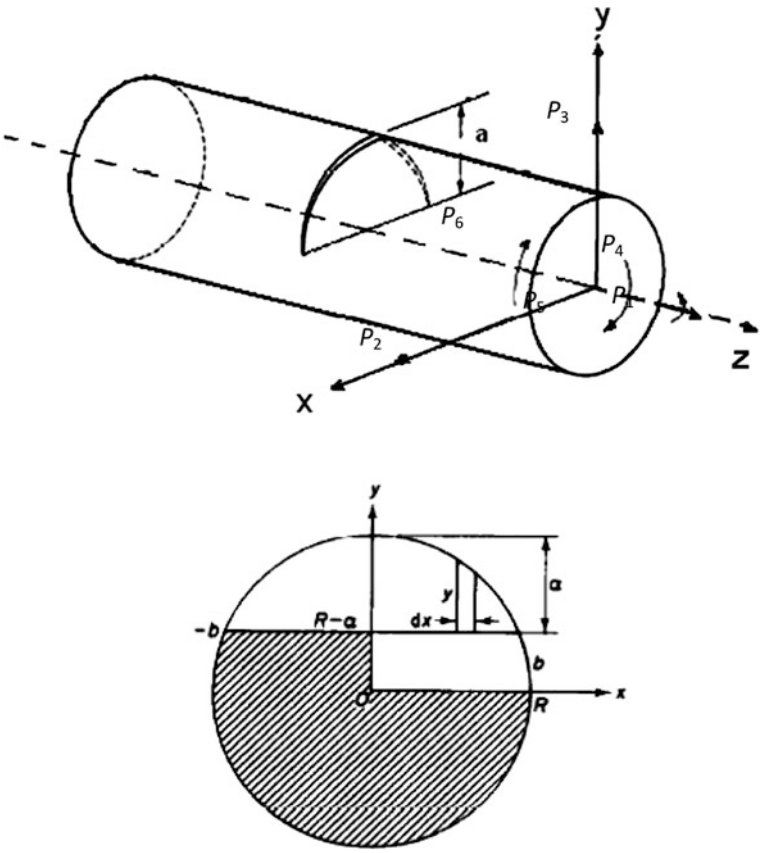

Fig. 7.2 A cracked rod element in general loading and cracked section geometry

$$K_{I5} = \sigma_5\sqrt{\pi\alpha}F_2\left(\alpha/h\right),\ \sigma_5 = 4P_5\sqrt{R^2 - x^2}\Big/\left(\pi R^4\right)$$

$$K_{I2} = K_{I3} = K_{I6} = 0,$$

$$K_{II3} = \sigma_3\sqrt{\pi\alpha}F_{II}\left(\alpha/h\right),\ \sigma_3 = P_3k/\left(\pi R^2\right) \tag{7.15}$$

$$K_{II6} = \sigma_{6II}\sqrt{\pi\alpha}F_{II}\left(\alpha/h\right), \sigma_{6II} = 2P_6x/\left(\pi R^4\right)$$

$$K_{II1} = K_{II2} = K_{II4} = K_{II5} = 0$$

$$K_{III2} = \sigma_2\sqrt{\pi\alpha}F_{III}\left(\alpha/h\right),\ \sigma_2 = kP_2/\left(\pi R^2\right).$$

$$K_{III6} = \sigma_{6III}\sqrt{\pi\alpha}F_{III}\left(\alpha/h\right) \quad \sigma_{6III} = 2P_6\sqrt{R^2 - x^2}\Big/\left(\pi R^4\right)$$

$$K_{III1} = K_{III3} = K_{III4} = K_{III5} = 0$$

where K_{ij} are crack stress intensity factors (SIF) corresponding to the three modes of fracture i = I, II, III, which result for every individual loading mode j = 1, 2,…6, h and a are local strip height and crack depth, respectively, at x, and $k = 6(1 + v)/(7 + 6v)$ a shape coefficient for the circular cross section. The functions $F_1(a/h)$, $F_2(a/h)$, $F_{\mathrm{II}}(a/h)$, $F_{\mathrm{III}}(a/h)$ are the same as in the case of the prismatic beam (Sect. 7.1.1).

Combination Eqs. (7.3), (7.4), and (7.15) yields the dimensionless terms of the compliance matrix as:

$$\bar{c}_{11} = \pi ERc_{11}/\left(1-v^2\right) = 4\int_0^{\bar{a}}\int_0^{\bar{b}} \bar{x}F_{\mathrm{I}}^2(\bar{h})d\bar{x}d\bar{y}$$

$$\bar{c}_{15} = \pi ER^2c_{15}/\left(1-v^2\right) = 16\int_0^{\bar{a}}\int_0^{\bar{b}} \bar{y}\sqrt{(1-\bar{x}^2)}F_1(\bar{h})F_2(\bar{h})d\bar{x}d\bar{y}$$

$$\bar{c}_{55} = \pi ER^3c_{55}/\left(1-v^2\right) = 64\int_0^{\bar{a}}\int_0^{\bar{b}} \bar{y}(1-\bar{x}^2)F_2^2(\bar{h})d\bar{x}d\bar{y}$$

$$\bar{c}_{44} = \pi ER^3c_{44}/\left(1-v^2\right) = 32\int_0^{\bar{a}}\int_0^{\bar{b}} \bar{x}^2\bar{y}(1-\bar{x}^2)F_1^2(\bar{h})d\bar{x}d\bar{y}$$

$$\bar{c}_{14} = \pi ER^2c_{14}/\left(1-v^2\right) = 8\int_0^{\bar{a}}\int_0^{\bar{b}} \bar{x}\bar{y}F_1^2(\bar{h})d\bar{x}d\bar{y} \tag{7.16}$$

$$\bar{c}_{45} = \pi ER^3c_{45}/\left(1-v^2\right) = 64\int_0^{\bar{a}}\int_0^{\bar{b}} \bar{x}\bar{y}\sqrt{(1-\bar{x}^2)}F_1(\bar{h})F_2(\bar{h})d\bar{x}d\bar{y}$$

$$\bar{c}_{33} = \pi ERc_{33}/\left(1-v^2\right) = 4\int_0^{\bar{a}}\int_0^{\bar{b}} \bar{y}F_{II}^2(\bar{h})d\bar{x}d\bar{y}$$

$$\bar{c}_{22} = \pi ERc_{22}/\left(1-v^2\right) = 4\int_0^{\bar{a}}\int_0^{\bar{b}} \bar{y}F_{III}^2(\bar{h})d\bar{x}d\bar{y}$$

$$\bar{c}_{62} = \pi ER^2c_{62}/\left(1-v^2\right) = 8\int_0^{\bar{a}}\int_0^{\bar{b}} \bar{y}\sqrt{(1-\bar{x}^2)}F_{III}^2(\bar{h})d\bar{x}d\bar{y}$$

$$\bar{c}_{63} = \pi E R^2 c_{63} / \left(1 - \nu^2\right) = 8 \int_0^{\bar{a}} \int_0^{\bar{b}} \bar{x}\bar{y} F_{II}^2(\bar{h}) d\bar{x} d\bar{y}$$

$$\bar{c}_{66} = \pi E R^3 c_{66} / \left(1 - \nu^2\right) = 16 \int_0^{\bar{a}} \int_0^{\bar{b}} [A_1 + mA_2] d\bar{x} d\bar{y}$$

where

$$A_1 = \bar{x}^2 \bar{y} F_1^2(\bar{h}),\ A_2 = \left(1 - \bar{x}^2\right) \bar{y} F_{III}^2(\bar{h}),\ \text{and}\ \bar{x} = x/R,\ \bar{y} = y/R,\ \bar{h} = y/h,\ \bar{b} = b/R$$

Finally, the compliance matrix has the form

$$\mathbf{C} = \begin{bmatrix} \bar{c}_{11} & 0 & 0 & \bar{c}_{14} & \bar{c}_{15} & 0 \\ 0 & \bar{c}_{22} & 0 & 0 & 0 & \bar{c}_{26} \\ 0 & 0 & \bar{c}_{33} & 0 & 0 & \bar{c}_{36} \\ \bar{c}_{41} & 0 & 0 & \bar{c}_{44} & \bar{c}_{45} & 0 \\ \bar{c}_{51} & 0 & 0 & \bar{c}_{54} & \bar{c}_{55} & 0 \\ 0 & \bar{c}_{62} & \bar{c}_{63} & 0 & 0 & \bar{c}_{66} \end{bmatrix}$$

where $\bar{c}_{ij}$ is the compliance or deflection in the i direction due to the load in the j direction. Dimensionless compliances for varying crack depths are shown in Fig. 7.3. By inversion of the compliance matrix the local stiffness matrix $\mathbf{K} = \mathbf{C}^{-1}$ can be obtained. Off-diagonal terms of the flexibility matrix indicate vibration coupling.

This matrix relates the displacement vector $\{\boldsymbol{\delta}\}^+ = [\delta_1, \delta_2 \ldots \delta_6]$ to the corresponding generalized force vector $\{\boldsymbol{P}\}^+ = [P_1, P_2 \ldots P_6]$. Assuming a "small" element about the crack, its motion defined by a displacement vector $\{\boldsymbol{\delta}\} = \{\{\boldsymbol{\delta}\}^- \{\boldsymbol{\delta}\}^+\}$ and a force vector $\{\boldsymbol{P}\} = \{\{\boldsymbol{P}\}^- \{\boldsymbol{P}\}^+\}$, where $-$ and $+$ mean before and after the crack. Here, force equilibrium is maintained, while the additional displacement due to the crack is related to the force vector as

$$\{\boldsymbol{P}\}^+ = \{\boldsymbol{P}\}^-, \quad \{\boldsymbol{\delta}\}^+ - \{\boldsymbol{\delta}\}^- = [\mathbf{C}]\{\boldsymbol{P}\}^+ \tag{7.17}$$

or

$$\left\{\{\boldsymbol{P}\}^- \{\boldsymbol{P}\}^+\right\} = \begin{bmatrix} -[\mathbf{C}]^{-1} & [\mathbf{C}]^{-1} \\ -[\mathbf{C}]^{-1} & [\mathbf{C}]^1 \end{bmatrix} \left\{\{\boldsymbol{\delta}\}^- \{\boldsymbol{\delta}\}^+\right\} \tag{7.18}$$

or

$$\{\boldsymbol{P}\} = [\mathbf{K}]\{\boldsymbol{\delta}\} \tag{7.19}$$

and the stiffness matrix [**K**] of the element is computed [33].

The flexibility matrix **C** can be further utilized for static, dynamic or stability analysis of a structure with cracked members of rectangular or circular cross-section. In the previous chapter, the pertinent elements of the flexibility matrix

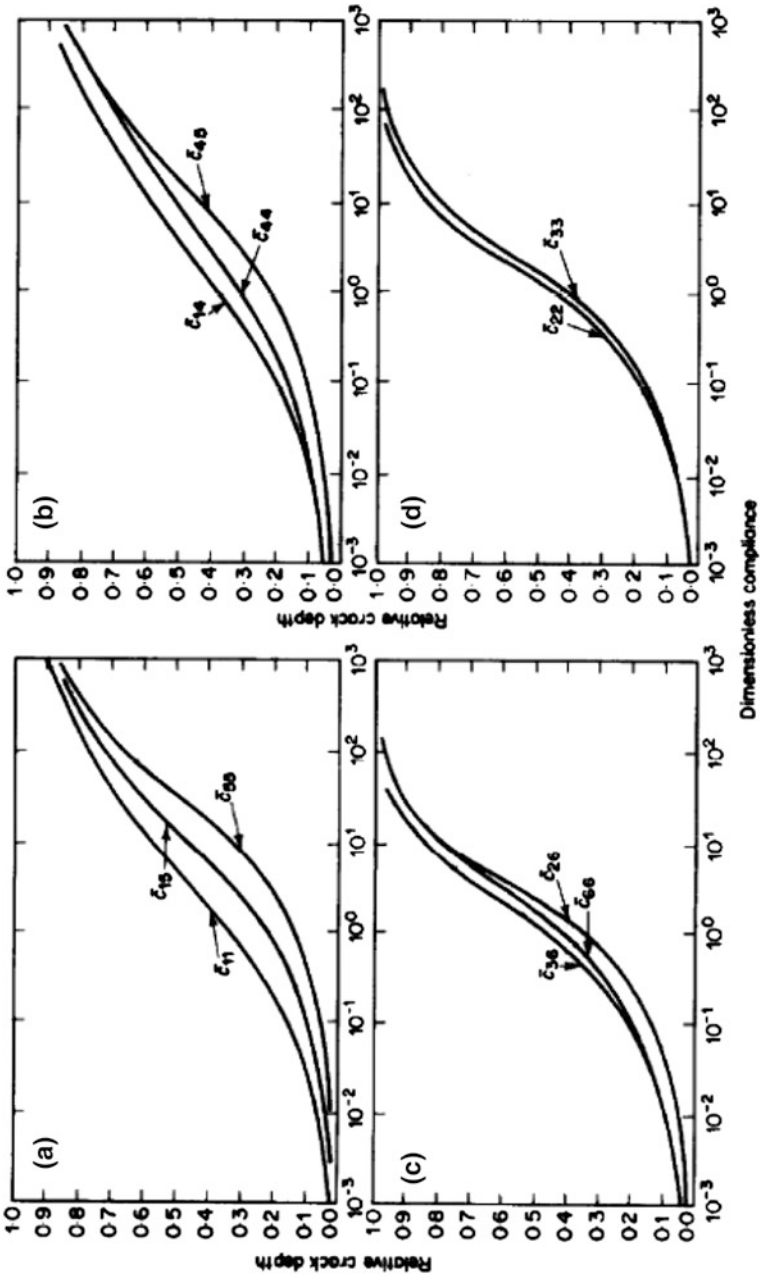

Fig. 7.3 Dimensionless compliances for varying crack depths

have been computed for circular cross-section and for a straight crack. Other cases can be treated along the same lines, if appropriate expressions for the stress intensity factor are available.

7.2 Direct Methods

Introduction of one or more cracks on an elastic structure will apparently change its dynamic response, which, in turn can be related to the change in elastic properties and these to the existence, location, and magnitude of the crack(s).

In small structures, such as uniform shafts, this can be achieved by direct analysis. In this section, some simple methods will be presented which directly relate the crack location and magnitude to the dynamic properties of the system. For systems with simple geometry, this can be obtained with relatively small computation effort.

7.2.1 Rotors with a Circumferential Crack

With a rotor with a circumferential crack, the analysis is simple because the flexibility matrix has only one element relating the torque applied to the relative rotation of the two faces of the crack.

Circumferential cracks often appear in a variety of machinery, e.g. shafts of thermal machines such as gas and steam turbines, and aircraft engines, especially in welded rotors. Identification of cracks in service is desirable, and estimation of the crack depth at the same time can be very useful, since the machine can have a programmed maintenance instead of a catastrophic failure.

The somewhat similar problem of torsional wave scattering about a penny-shaped crack was studied by Sih and Loeber [34, 35]. They studied scattering of a given torsional wave due to the penny-shaped crack by way of the field equation solved by a finite Hankel transform. Although the same procedure could be used for the problem at hand, an energy method was preferred, based on the wealth of data existing for the strain energy density function.

The strain energy in the shaft due to torque T is

$$U = \frac{T^2 c}{2} \tag{7.20}$$

where c is the local flexibility (compliance) of the shaft due to the crack, $\Delta\varphi/\Delta t$.

The strain energy release rate with respect to the crack surface $A = at$ is defined as

$$J = \frac{\partial U}{\partial A} = \frac{1}{2} T^2 \frac{\partial c}{\partial a} \frac{1}{2(\pi R - a)} \tag{7.21}$$

Irwin and Kies [36] suggested that by measuring the flexibility of a test specimen, or a component model, with various crack depths a, the value of the gradient $\partial c/\partial a$ as a function of a could be determined, leading to the determination of the strain release function.

By using virtual work arguments Irwin [37] demonstrated that energy release rate J could be related to the stress intensity factor K as

$$J = \frac{K_{\mathrm{III}}^2}{2G} \tag{7.22}$$

where G is shear modulus, and mode III stress intensity factor K_{III} is defined by the relation

$$\begin{bmatrix} \tau_{xz} \\ \tau_{yz} \end{bmatrix} = \frac{K_{\mathrm{III}}}{\sqrt{2\pi r}} \begin{bmatrix} \sin\frac{\theta}{2} \\ \cos\frac{\theta}{2} \end{bmatrix} + \text{terms of order } \mathrm{r}^0 \tag{7.23}$$

giving the shear stresses in the vicinity of the crack at distance r from its tip. Equation (7.22) is a particular case of Eq. (7.4).

Equations (7.21) and (7.22) yield

$$\frac{dc}{da} = \frac{K_{\mathrm{III}}^2}{T^2 G} 2(\pi R - a) \tag{7.24}$$

Integrating:

$$c = \int_0^a \frac{K_{\mathrm{III}}^2}{T^2 G} 2(\pi R - a) da \tag{7.25}$$

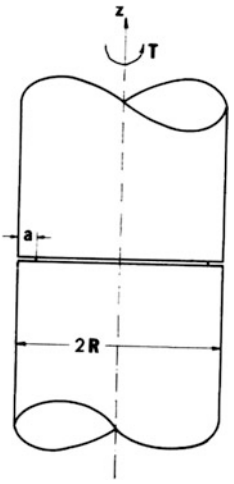

Fig. 7.4 Geometry of a rotor with a circumferential crack

An expression is needed for the stress intensity factor K_{III} for the problem at hand. For a shaft with a circumferential crack, Bueckner [38] has outlined a method for the determination of K_{III} as a function of the crack depth.

Benthem and Koiter [39] have approximated stress intensity factor K for a cylinder in torsion T with a circumferential crack by the following expression:

$$K = \frac{3}{8}\left[1 + \frac{1}{2}\lambda^2 + \frac{5}{16}\lambda^3 + \frac{35}{128}\lambda^4 + 0.208\lambda^5\right] \tag{7.26}$$

where $\lambda = (R - a)/R$, R being shaft radius (Fig. 7.4).

The dimensionless stress intensity factor K is defined by the relation

$$\tau_{z\varphi} = K\frac{2T}{\pi(R-a)^3}\left[\frac{a(R-a)}{R}\right]^{1/2}\frac{1}{\sqrt{2r}} \tag{7.27}$$

Therefore, comparison with Eq. (7.23) yields

$$K_{III} = \frac{2T}{(R-a)^3}\left[\frac{a(R-a)}{\pi R}\right]^{1/2} K \tag{7.28}$$

Dimensionless flexibility becomes (Eq. 7.25)

$$\frac{\pi R^3 \mu}{4} c = \frac{1}{R}\int_0^a \frac{a}{R}\frac{2(\pi R - a)}{R}\frac{R^5}{(R-a)^5}K^2(a)da = I(a/R) \tag{7.29}$$

where $\mu = G$ is the shear modulus of the material.

The integral $I(a/R)$ has a value

$$\begin{aligned} I(a/R) &= 0.035(1 - a/R)^{-4} + 0.001(1 - a/R) + 0.029(1 - a/R)^2 \\ &+ 0.0086(1 - a/R)^3 + 0.0044(1 - a/R)^4 + 0.0025(1 - a/R)^6 \\ &+ 0.0017(1 - a/R)^7 + 0.008(1 - a/R)^8 - 0.092 \end{aligned}$$

Values of this integral are plotted in Fig. 7.5.

Measurement of local flexibility on a plexiglas shaft was carried out indirectly on the same apparatus used for developing the fatigue crack [9]. A light shaft carries an inertia J_0 at the end, while the crack is near the support (Fig. 7.6).

In the model of Fig. 7.6, the natural frequency for torsional motion without crack is

$$\omega_0 = \sqrt{\frac{k}{J_o}} = \sqrt{\frac{\pi d^4 \mu}{32 L J_o}} \quad k = \frac{\pi d^4 \mu}{32 L} \tag{7.30}$$

while, in the presence of a crack of stiffness k_c

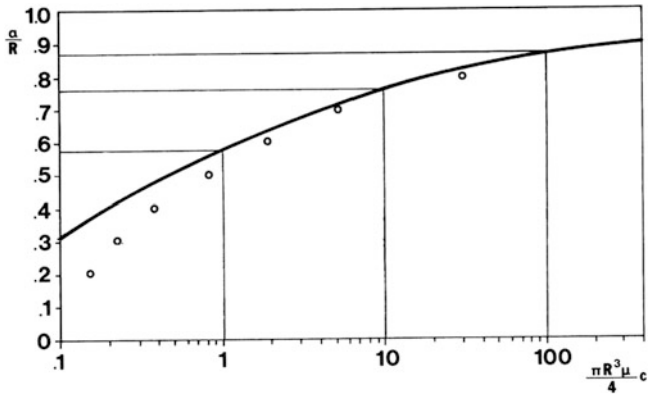

Fig. 7.5 Cracked rotor local flexibility. *Line*, analytical, Eq. (7.25); *circle*, experimental (from Ref. [9], by permission)

Fig. 7.6 Test model

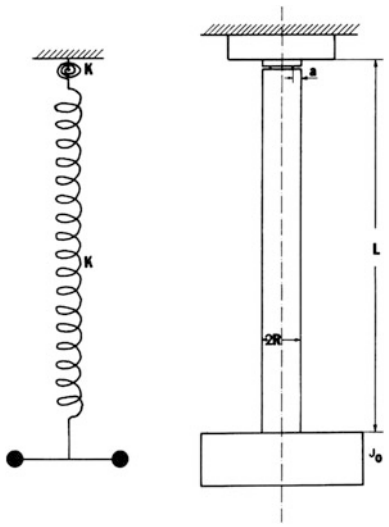

$$\frac{\omega}{\omega_o} = \frac{1}{\sqrt{1 + k/k_c}}. \tag{7.31}$$

Therefore,

$$\frac{\pi R^3 \mu}{4} c = \frac{L}{2R}\left[\frac{1}{(\omega/\omega_c)^2} - 1\right] \tag{7.32}$$

which leaves the expression $\left[1\Big/(\omega/\omega_0)^2 - 1\right](L/2R)$ the role of an experimental value of the integral $I(a/R)$ in Eq. (7.29). For comparison, experimental results are

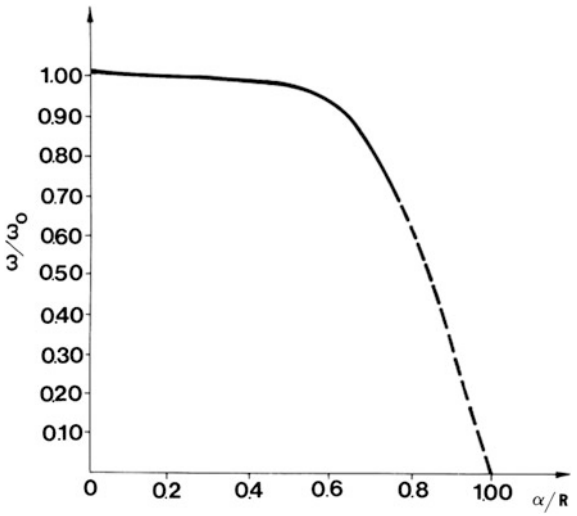

Fig. 7.7 Natural frequency versus crack depth (from Ref. [9], by permission)

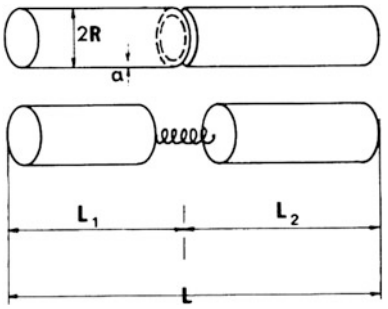

Fig. 7.8 Model of a continuous cracked shaft

plotted in Fig. 7.5 against analytical function. In the experiment, a Plexiglas shaft was used with diameter $d = 0.020$ m, length $L = 0.75$ m, $\mu = 1.1 \times 10^9 \mathrm{N/m^2}$. The measured function of the frequency change ω/ω_0 versus relative crack depth is shown in Fig. 7.7. Here, ω is torsional natural frequency with the crack and ω_0 the same frequency without the crack. From these results and Eq. (7.32), cracked shaft local flexibility parameter was computed and entered in Fig. 7.5 as a function of crack depth. At small crack depths a/R there is a considerable discrepancy between analytical and experimental results, which was expected, due to the difficulty in accurate measurement of small frequency differences of the order of 1 %, appearing for cracks with a/R in the range 0–0.4.

A continuous shaft with free ends (Fig. 7.8) and length L, at distance L_1 from the left there has a circumferential crack of depth α. Usual procedures [6] lead to the frequency equation

$$\sin\frac{\omega L_1}{\gamma}\cos\frac{\omega L_2}{\gamma} + \sin\frac{\omega L_2}{\gamma}\left(\cos\frac{\omega L_1}{\gamma} - \frac{\pi R^3 \mu c}{4}\frac{R}{L}\sin\frac{\omega L_1}{\gamma}\right) = 0 \qquad (7.33)$$

where
R is shaft diameter;
L is shaft length;
ω is shaft torsional natural frequency;
γ is torsional wave velocity $= \sqrt{\mu/\rho}$;
ρ is density of the shaft material.

Let a frequency parameter $\xi = \omega L/\gamma$, the location of the crack on the shaft $\lambda = L_1/L$, and the crack flexibility parameter $\zeta = \left(\pi R^3 \mu c/4\right)(R/L)$. Equation (7.33) becomes

$$\sin(\lambda\xi)\cos(1-\lambda)\xi + \sin(1-\lambda)\xi(\cos\lambda\xi - \zeta\sin\lambda\xi) = 0. \tag{7.34}$$

The first three solutions $\omega_1 L/\gamma,\ \omega_2 L/\gamma,\ \omega_3 L/\gamma$ of Eq. (7.34) were computed as functions of the flexibility parameter ζ with, as the other parameter, the location $\lambda = L_1/L$ of the crack on the shaft. The results are plotted in Fig. 7.9. It is obvious that in the absence of a crack ($\zeta = 0$), the first three frequency parameters are π, 2π *and* 3π. This result is known for a free cylindrical shaft in torsional vibration [6].

From Fig. 7.9 it can be seen that the crack can have a substantial influence upon the natural vibration of the shaft. In the upper part of Fig. 7.9 the crack depth a/R over the crack flexibility parameter $\zeta = \left(\pi R^3 \mu c/4\right)(R/L)$ was plotted for a shaft of different R/L ratios to allow for a direct evaluation of the frequency drop as a function of the crack depth a/R and the inverse of it. It can be seen that relatively small cracks can have a substantial influence on the torsional natural frequencies with measurable magnitude.

This gives a very useful method to identify magnitude and location of the crack. Since the change of the first three frequencies shown does not follow the same pattern it is possible to estimate location and magnitude. For rotating machinery, this is very useful because it allows for the identification of the crack without disassembling the machine, even without stopping it. Proper instrumentation can provide continuous monitoring of the machine operation and an early warning for the existence of a crack.

7.2.2 Beam with a Lateral Crack

A lateral crack on a beam of rectangular cross-section introduces local flexibility, influencing the dynamic response of the beam. This property can be used for direct identification of the crack.

The local flexibility matrix for the cracked beam was computed in Sect. 7.1. However, Chondros and Dimarogonas [7] have found that, in this case, only the diagonal term c_{55} is significant. Let K_τ be the inverse of this term, a rotational spring constant for the crack. In Ref. [7] this stiffness was determined experimentally.

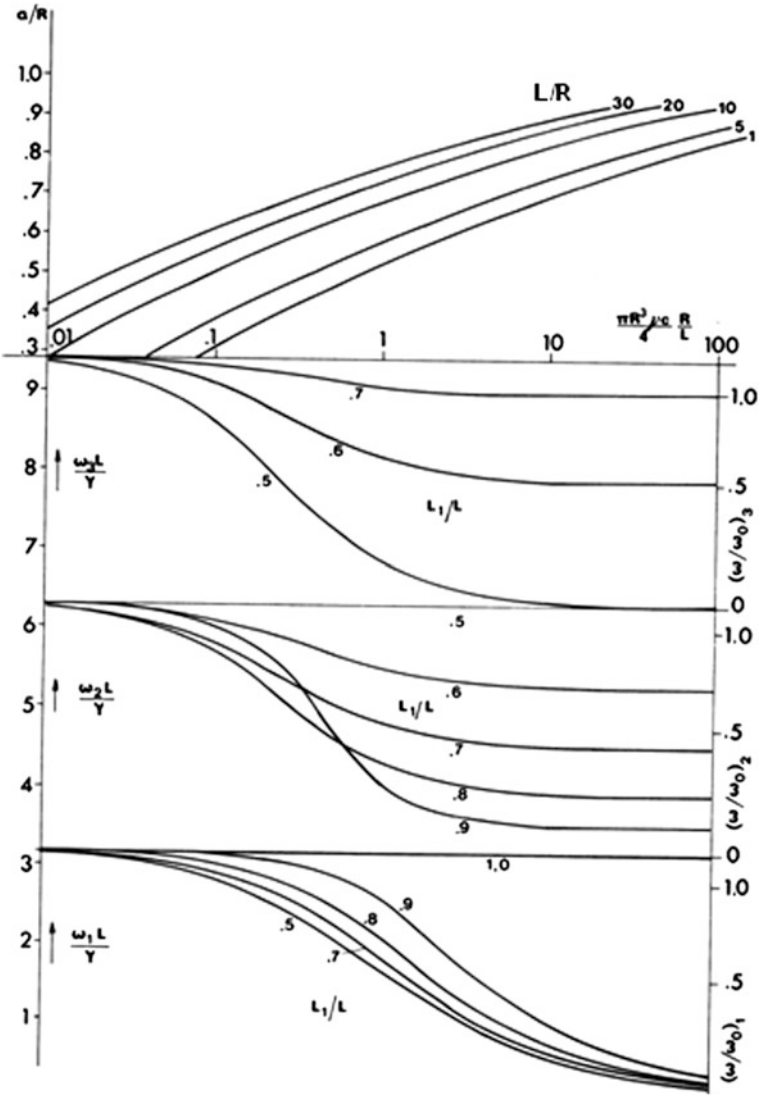

Fig. 7.9 Natural frequencies of a continuous cracked shaft (from Ref. [9], by permission)

To this end, a 300 mm cantilever beam of cross-section 20 × 20 mm^2 with a mass of 0.6 kg at the free end, welded at a base clamped to a vibrating table, was used to give the relation between the change in natural frequency of the vibrating beam and the depth of a crack at the welded edge. The crack was initiated with a saw cut and propagated to the desired depth by fatigue loading. The depth of the crack was measured directly and verified with an ultrasonic detector for uniformity and actual depth. The vibration pick-up signal was transferred to a vibration analyzer and a recorder to give plots of frequency versus vibration amplitude.

For various values of the ratio a/h, where a is the crack depth and h the initial height of the cross-section profile, the corresponding values of the ratio ω_n/ω_{n0} were measured, where ω_n is natural frequency of the beam with the existing crack and ω_{n0} is the natural frequency in the absence of the crack ($a/h = 0$).

Figure 7.10 gives this relation as found experimentally by the procedure described above. To relate the crack depth to a local flexibility parameter, the system was modeled, as shown in Fig. 7.11, by a massless elastic beam with a mass m at the free end and a torsional spring of constant K_τ at the clamped end. The load was applied at the free end of the cantilever where the deflection was also measured. This deflection consists of the beam deflection δ_1 which was measured initially without the crack and which remained unchanged with the increase of crack depth, and the deflection δ_2 due to the rigid body motion caused by the local flexibility at the clamped end. If ω_n is the natural frequency of this system and ω_{n0} the natural frequency without the crack ($K_\tau = 0$), steps of elementary nature lead to the relationship

$$\frac{\omega_n}{\omega_{no}} = \frac{1}{1 + \mu_o^2} \tag{7.35}$$

where $\mu_0^2 = 3EI/LK_\tau$, E is Young's modulus, I moment of inertia of the section, and L is the length of the beam.

Equation (7.35) and Fig. 7.11 yield the information shown in Fig. 7.12, which is a plot of the crack depth a/h against the torsional spring constant parameter LK_τ/EI. This figure can be used directly to assess the depth of crack for a system as the one shown in Fig. 7.11.

These experimental results provide a basis for an extension of the method so that it can be applied with other member geometries and other boundary conditions, since the flexibility of the crack area is a highly local phenomenon and has negligible influence on the stress field beyond a certain distance.

For a beam of constant cross-section clamped at both ends the frequency equation for transverse vibrations is [6]

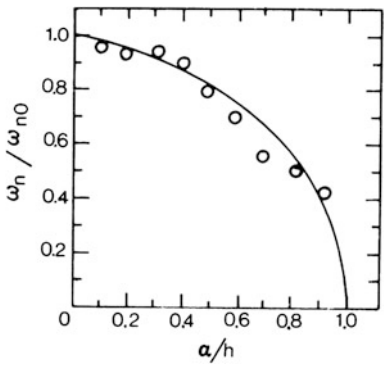

Fig. 7.10 Diagram relating crack depth a to the change in natural frequency of vibration ω_{n0} (from Ref. [7], by permission)

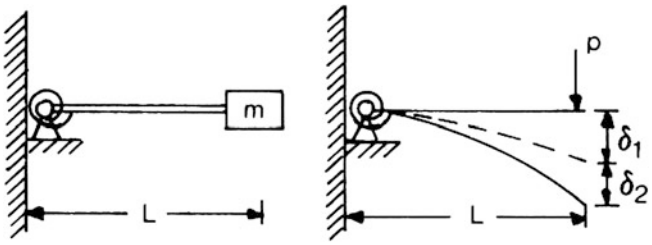

Fig. 7.11 Modelling of a cantilever beam with a mass at the free end and a crack at the welded root (from Ref. [7], by permission)

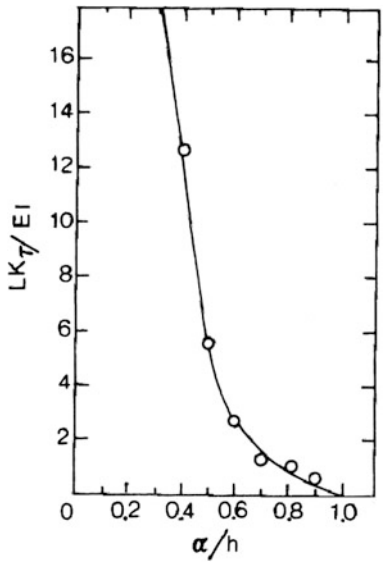

Fig. 7.12 Diagram relating crack depth α to the torsional spring constant K_τ (from Ref. [7], by permission)

$$\frac{\partial^4 w}{\partial z^4} - \lambda^4 w = 0 \tag{7.36}$$

where $\lambda = \rho F \omega^2 / EI$, F is cross-sectional area, ρe material density and w vertical displacement. The solution of Eq. (7.36) is [6]

$$w(z) = c_1 \cosh \lambda z + c_2 \sinh \lambda z + c_3 \cos \lambda z + c_2 \sin \lambda z$$

When the beam has a crack at one of the welded edges (see Fig. 7.13), the crack is treated as a torsional spring of constant K_τ, disregarding the transverse flexibility in the vertical direction. The corresponding boundary conditions are

$$w(0) = 0 \quad w(L) = 0 \quad EIw''(0) = K_\tau w'(0) \quad w'(L) = 0. \tag{7.37}$$

By applying these the frequency equation assumes the form

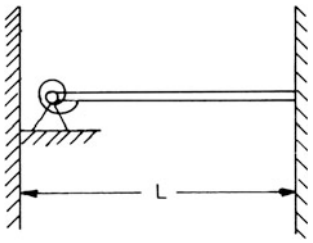

Fig. 7.13 Clamped–clamped beam with a crack at one welded edge

$$\begin{vmatrix} 1 & 0 & 1 & 0 \\ 1 & -A & -1 & A \\ \cosh \lambda L & \sinh \lambda L & \cosh \lambda L & \sin \lambda L \\ \sinh \lambda L & \cosh \lambda L & -\sinh \lambda L & \cos \lambda L \end{vmatrix} = 0 \tag{7.38}$$

where $A = K_\tau/EI$. The roots of Eq. (7.38) for different values of A were found by numerical computations and are plotted in Fig. 7.14.

For a cantilever beam (see Fig. 7.11) one proceeds in a similar manner. The boundary conditions are

$$w(0) = 0 \quad \partial^2 w(L)/\partial z^2 = 0 \quad EIw''(0) = K_\tau w'(0) \quad \partial^3 w(L)/\partial z^3 = 0. \tag{7.39}$$

The frequency equation is

$$\begin{vmatrix} 1 & 0 & 1 & 0 \\ 1 & -A & -1 & -A \\ \cosh \lambda L & \sinh \lambda L & -\cos \lambda L & -\sin \lambda L \\ \sinh \lambda L & \cosh \lambda L & \sin \lambda L & -\cos \lambda L \end{vmatrix} = 0 \tag{7.40}$$

Figure 7.15 shows the solutions of Eq. (7.40), which were obtained by numerical machine computation.

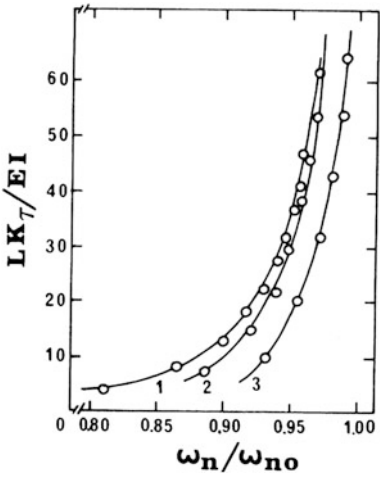

Fig. 7.14 Diagram relating the change in natural frequency (for the first three harmonics) and local flexibilities for a clamped–clamped beam (from Ref. [7], by permission)

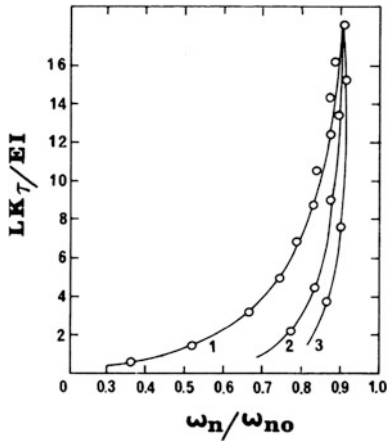

Fig. 7.15 Diagram relating the change in natural frequency (for the first three harmonics) and local flexibilities for a cantilever beam (from Ref. [7], by permission)

The graph in Fig. 7.12 the local flexibility due to the existence of a transverse crack and to the depth of the crack. This relation was obtained both experimentally and analytically using c_{55} (Eq. 7.12). The two relations are in close agreement. The local flexibility thus found was utilized to establish the relationships of the crack depth to the change of natural frequency for two cases: of a cantilever beam with a transverse crack at the welded root of the beam, and of a beam welded (clamped) at both ends with a transverse crack at one welded end. For these cases, and of course also for the case of a massless beam carrying a mass at the end and having a cracked weld at the other end which was used to establish the local flexibility of the crack, Figs. 7.10, 7.14 and 7.15 provide graphically quantitative relations between the change in natural frequency and the depth of the crack. However, these are based on the assumption of a transverse surface crack, extending uniformly along the width of the weld.

In many cases, other situations might occur, such as a crack inside the section, a non-uniform crack along the width, a crack at both ends of the clamped beam, etc. Furthermore, one might encounter other geometries and boundary conditions, such as frames, beams of non-uniform cross-section, etc. In such cases one can easily use the results of Fig. 7.12 local flexibility, to establish the analytical relations between the frequency ratio and the crack depth for the particular geometry and boundary conditions.

The experimental results of this work also have another limitation. They are based on the assumptions of a weld having a Young's modulus equal to that for the beam material, and of a rectangular cross-section of the weld and the beam. For other cross-sections, further work is needed.

For the cases investigated, nomograms were constructed directly relating crack depth to the frequency ratio (Figs. 7.16 and 7.17), from Eqs. (7.38) and (7.40), respectively, and Figs. 7.12 and 7.13. These nomograms can be used for field work. In the field, the natural frequencies can be easily measured with portable instruments and by a variety of methods. An inspection schedule can be

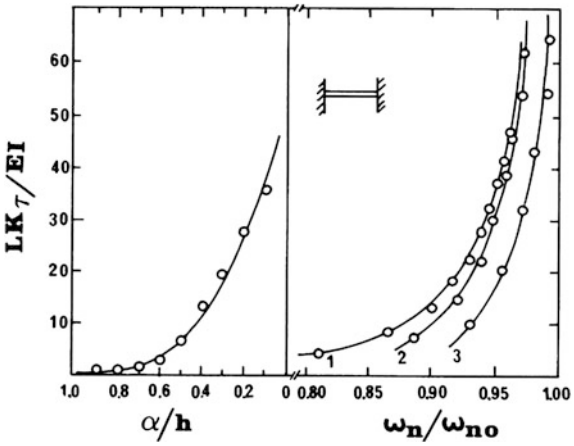

Fig. 7.16 Nomogram relating crack depth to the change in natural frequency of the first three harmonics for a clamped–clamped beam (from Ref. [7], by permission)

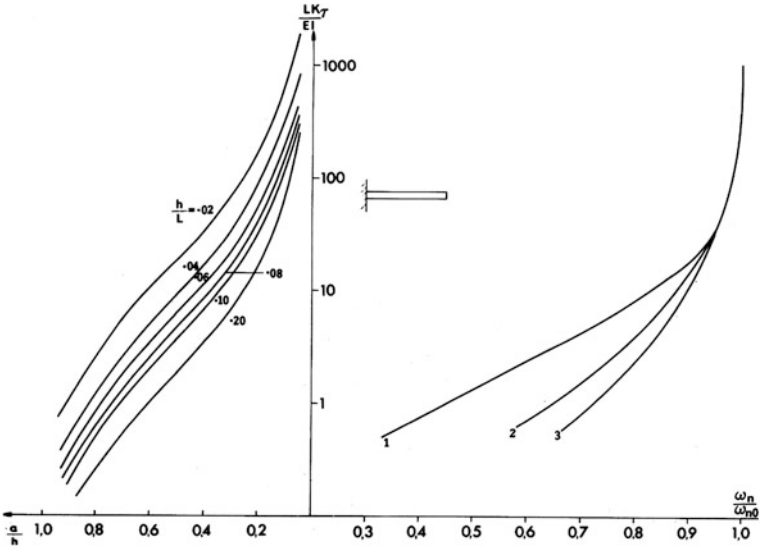

Fig. 7.17 Nomogram relating crack depth to the change in natural frequency of the first three harmonics for a cantilever beam (from Ref. [7], by permission)

established for periodic checks of the natural frequencies of the structure. With the aid of the nomograms of Figs. 7.16 and 7.17, or similar ones for other particular cases, one can follow the history of the crack development and proceed to repairs, when necessary. It is believed that this method can be developed into a useful tool for preventive maintenance and non-destructive testing of structures.

For complex structures, one does not need to establish relations such as in Figs. 7.16 and 7.17 for the whole structure, and also different ones for the crack at each of the welds, as might seem necessary. Among the large number of natural frequencies of a structure there are a certain number of frequencies associated with modes having high relative amplitudes at the location of any particular member. This simplifies the problem since one can work with simpler local structures, making proper simplifying assumptions for the boundary conditions. General guidelines for such a procedure cannot be given here, since it depends on experience for the particular type of structure.

The method is not very sensitive as compared with other methods such as ultrasonic, radiation ones, etc. Since, with modern portable digital vibration analyzers, one can obtain resolutions far better than 1 %, detection of a frequency change better than 5 % is certainly possible in practice. Once can ensure better results by following a programme of periodic inspection to indicate the trend in lowering of the natural frequency with the propagation of the crack. Therefore, as can be seen from Fig. 7.12, the crack depth detectable with confidence is of the order of 10 %. It is known that, by the other methods, one can detect much smaller cracks and thus obtain a much earlier warning of defects.

However, the method proposed has definite advantages because it is easier to apply to large structures than any other method in the field such as, for example, underwater platforms, bridges, etc. In such cases inspections with a portable instrument can be carried out, to measure the response of the structure to environmental excitation. If this excitation is considered to be white noise, the response of the structure will be, to a certain scale, the transfer function of the structure. This can also be done with telemetry, without even approaching the structure. The possibility for automation of the inspection procedure is obvious. In most cases detection with the sensitivity mentioned above is early enough from a practical stand point.

Another problem with the application of the method is that it is limited to open cracks only. The authors believe that this is not a severe limitation, given the fact that the method is intended for field application to cracks developed in service, which almost invariably affect bending and tension modes and also are the most likely ones to propagate.

The quantitative results given in this section are of course strictly applicable to a particular case of a very simple geometry, but can be likewise applied to individual members of large structures, especially if the member flexibility is substantially larger than the flexibility of the supporting members.

In the general case of a complex structure no quantitative results can be tabulated because of the large number of parameters involved. The structural analyst, however, can use this analysis as a guide to obtain quantitative results for a specific structure, treating cracks as local flexibilities at the welding points.

One should be cautious in cases where material properties may change in service, especially if changes of the elasticity modulus occur.

7.2.3 Clamped Circular Plate with a Peripheral Surface Crack

The problem of a circular plate clamped at the contour with a surface crack at the periphery was discussed by Chondros and Dimarogonas [8]. An apparatus consisting of a circular plate having a peripheral crack at the weld and subjected to vibrations with the aid of a vibrating table was used to give quantitative evidence of the influence of the peripheral crack on the dynamic behavior of the plate, to be compared with the analytical results.

For various values of the ratio a/h, where a is crack depth and h is the plate thickness, the corresponding values of the ratio ω_n/ω_{n0} were measured, where ω_n is the natural frequency for the plate with a peripheral crack and ω_{n0} is the natural frequency in the absence of a crack. The crack extends over the periphery at constant depth. Figure 7.18 gives this relation found experimentally with the above procedure for plates welded peripherally at the support and plates integral with the support. A good correlation exists for the two cases.

Assuming that the plate consists of radial parts of unit width at the periphery, each treated as a cantilever beam clamped at one end by the peripheral weld, the torsional spring constant K_τ due to the local flexibility at the crack was measured by a simple test. A cantilever beam of thickness h welded at the support with a crack at the weld of depth a was loaded in order to have a moment M at the welded support. The local rotation φ was measured and the rotational spring constant $K_\tau = M/\varphi$ was computed. This yields K_τ for a unit length peripheral crack of the plate as a function of the crack depth.

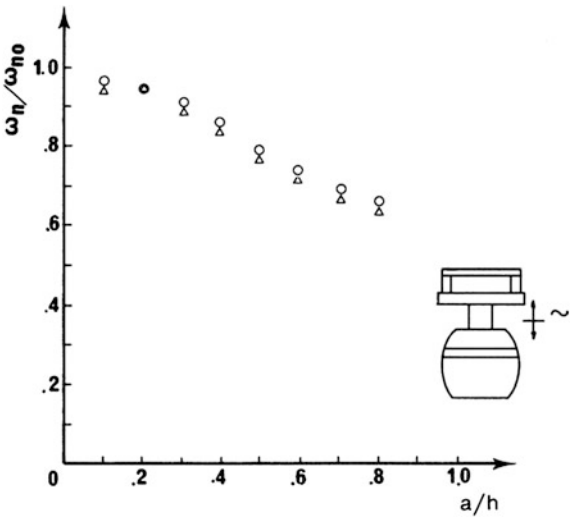

Fig. 7.18 Change of natural frequency of vibration for various values of crack depth (*Courtesy* ASME [8]) *triangle* experimental; *circle*, analytical

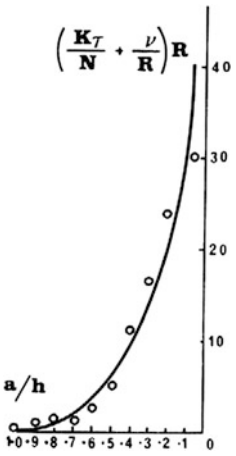

Fig. 7.19 Relation of the torsional spring constant of the crack K_τ versus the ratio a/h where a is the crack depth and h the plate thickness (*Courtesy* ASME [8]) *circle*, experimental; [8]—, Eq. (7.12)

Figure 7.19 shows the relation of a/h versus $(K_\tau/N + v/R)R$, where a is the crack depth, h the plate thickness, $N = Eh^3/12(1 - v^2)$, E is Young's modulus, v is Poisson's ratio for the plate material $(v = 0.3)$ and R is the plate radius.

In order to check the accuracy of the method and the assumptions made so far, the deflections of the plate's centre point caused by a force P acting at the centre were analytically calculated using the torsional spring constant K_τ found experimentally from cantilever beam tests and analytically using Eq. (7.16).

Next, an experimental procedure was used, in order to give the relation between the peripheral crack depth and the deflection of the plate's centre point. A circular plate welded at the contour with a peripheral crack was subjected to a constant force, P, acting at its centre. With increasing crack depth, the deflection at the centre point was measured. Figure 7.20 gives the deflections found both analytically and experimentally versus a/h, the ratio of crack depth to plate thickness. Figure 7.20 shows that the assumption made for the determination of the torsional spring constant K_τ of the crack was adequate. This was expected since the flexibility of the crack area is highly local and has a negligible influence on the stress beyond a certain distance.

With the results obtained above, one can proceed to apply the method directly to the determination of cracks in peripherally welded plates from the change in natural frequency of vibration. For this reason the solution of the frequency equation is necessary.

For a circular plate of constant thickness the equation for transverse vibrations is [40]

$$\Delta\,\Delta F - \lambda^4 F = 0 \tag{7.41}$$

where $\lambda^4 = \omega^2 \rho h/N$, ω is the frequency of transverse vibration and ρ the material density. Here, the solution is

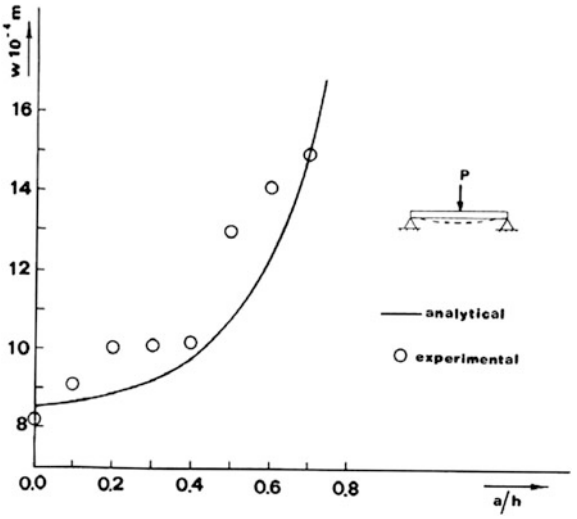

Fig. 7.20 Deflections w of the plate's centre point for various crack depths and a constant force acting at the centre. (*Courtesy* ASME [8])

$$F(r) = C_1 J_0(\lambda r) + C_2 J_0(\mathrm{i}\lambda r) \tag{7.42}$$

where J_0 is Bessel function of the first kind.

For a plate clamped at the periphery with a peripheral crack at the weld, the crack is treated as a torsional spring of constant K_τ. Here, the boundary conditions yield the following system of linear equations [41]:

$$\left\{ \begin{array}{l} C_1 J_0(\lambda R) + C_2 J_0(\lambda R) = 0 \\ C_1 - \lambda J_0(\lambda R) - \left(\mathrm{A} - \frac{1}{R}\right) J_1(\lambda R) + C_2 \lambda Io(\lambda R) + \left(\mathrm{A} - \frac{1}{R}\right) I_1(\lambda R) = 0 \end{array} \right\} \tag{7.43}$$

where I_0 is Bessel function of the second kind and,

$$A = \frac{K_\tau}{N} + \frac{v}{R}.$$

The solution of Eq. (7.43) is shown in Fig. 7.21. It is evident that the first few natural frequencies depend heavily on the crack depth, especially the fundamental one.

Figure 7.19 relates the local flexibility due to the presence of a peripheral transverse crack to the depth of the crack. This relation was found by the aid of a simple experimental procedure to confirm analytical results. The assumptions made for the determination of local flexibilities due to the presence of the crack are based on the hypothesis of a peripheral transverse surface crack extending uniformly along the peripheral weld.

On many occasions, different situations may exist, such as a crack inside the section, a crack of non-uniform depth along the weld, etc. Another limitation of the experimental results of this work is the assumptions made for a weld having the same as that of the plate material, which is not always correct.

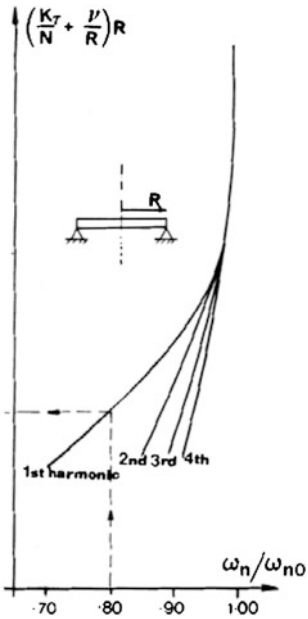

Fig. 7.21 Solution of the frequency equation for a plate with a peripheral crack at the weld (*Courtesy* ASME [8])

Figure 7.22 shows a nomogram constructed with the aid of Figs. 7.19 and 7.21 directly relating the depth of the crack to the frequency ratio. This nomogram is of importance for field work. In the field, the natural frequencies can be easily measured with portable instruments and by a variety of methods.

An inspection schedule can be established for periodic checks of the natural frequencies of the structure. With the aid of the nomogram in Fig. 7.22, or with similar ones for other particular cases, one can follow the history of the crack development and proceed to repairs when necessary. It is believed that this method can be developed into a useful tool for preventive maintenance and non-destructive testing of structures.

7.3 The Eigenvalue Sensitivity Problem

7.3.1 Introduction

Direct methods, such as the ones presented in the previous section, can be applied only to systems with simple geometry. With more complicated systems one has to use a more systematic methodology.

In general, a structure will be assumed to be modeled as a linear system described by way of stiffness and a mass matrix. The general statement of the problem is that the change in the eigenvalues and eigenvectors of a linear system is to be computed if the change in the stiffness or flexibility matrix of the system is

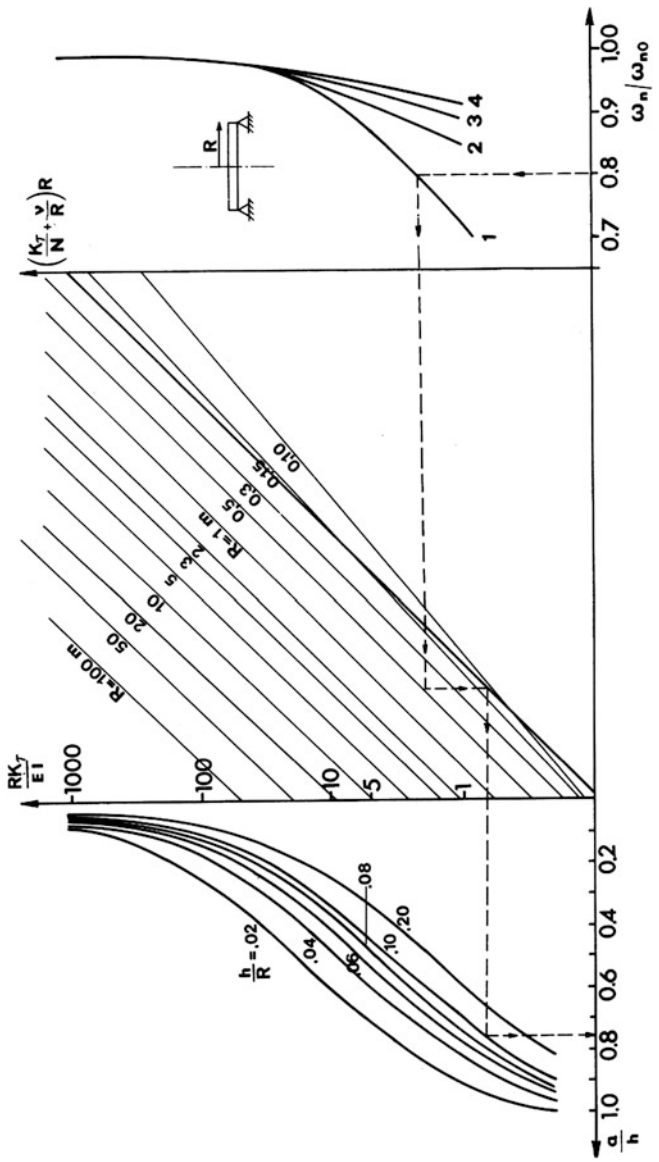

Fig. 7.22 Nomogram relating peripheral crack depth to the change of natural frequency of vibration for a circular plate welded at the periphery (*Courtesy* ASME [8])

known. In addition, it is assumed that for the unmodified structure the eigenvalue problem has been solved in advance and the procedure desired should not be to solve the eigenvalue problem for the modified structure, on two counts: first, to reduce computation effort; secondly, to reduce computation error.

Simple problems can be solved analytically and yield direct relations of change in natural frequencies of vibration to location and magnitude of cracks on structural members. With more complex engineering problems it is impractical to have direct solutions and one needs a more systematic investigation.

Weissenburger [42] developed the solution for the modified problem of the eigenvalues of the modified matrix **B*** if the diagonal eigenvalue matrix r of the matrix **B** is known, and then the matrix **B** can be expressed in the form $\mathbf{B} = \mathbf{V}^{\mathrm{T}}\boldsymbol{\Gamma}\mathbf{V}$, where **V** is an upper tridiagonal matrix. The eigenvalues of the modified matrix **B*** can then be computed by way of a procedure which is of comparable complexity to the solution of the eigenvalue problem for the matrix **B*** directly.

Zarghmee [43] computed the derivative of an eigenvalue with respect to the compliance of a member of the structure, if the mass and stiffness matrices of the structure can be written in the form

$$\mathbf{K} = \sum_{i=0}^{n} a_{\mathrm{i}}\mathbf{K}_{\mathrm{i}} \quad \mathbf{M} = \sum_{i=0}^{n} a_{\mathrm{i}}\mathbf{M}_{\mathrm{i}}$$

where α_{i} are constants and $\mathbf{K}_{\mathrm{i}}$ and $\mathbf{M}_{\mathrm{i}}$ are stiffness matrix and mass matrix, respectively, for the element *i* of the structure.

Fox and Kapoor [44] computed the variation of the eigenvalue *i* for the variation of the vector $\boldsymbol{\delta}$ containing all the parameters of the system which change, in the form

$$\frac{\partial \mathbf{L}_{\mathrm{i}}}{\partial \boldsymbol{\delta}_{\mathrm{j}}} = \mathbf{x}_i^T \left[\partial \mathbf{K}/\partial \boldsymbol{\delta}_{\mathrm{j}} - \lambda \partial \mathbf{M}/\partial \boldsymbol{\delta}_{\mathrm{j}}\right]\mathbf{x}_i$$

where $\mathbf{x}_{\mathrm{i}}$ is the eigenvector *i* of the unmodified structure and λ_{i} the corresponding eigenvalue.

Morgan [45] and Paraskevopoulos et al. [46] computed the change in the eigenvalue λ_{i} of a matrix **A** as

$$\mathrm{d}\lambda_{\mathrm{i}} = [\mathrm{tr}\,\mathbf{R}(\lambda_{\mathrm{i}})]^{-1}[\mathbf{R}(\lambda_{\mathrm{i}})]^{*}\mathrm{dA} \tag{7.44}$$

where $\mathbf{R}(\lambda)$ is the adjoint matrix for the eigenvalue λ_{i}, d**A** is the change in the matrix **A** and * means inner product of vectors.

Determination of the eigenvalue differential by Eq. (7.44) requires the computation of the adjoint matrix, which is of considerable complexity, especially for large systems.

7.3.2 Rayleigh's Quotient

Owing to the stationary character of Rayleigh's quotient [6] a simpler method was developed for the computation of the change of eigenvalues of the modified system, provided that the solution of the unmodified problem is known.

The equation of motion for a vibrating conservative system is

$$\mathbf{M}\ddot{x} + \mathbf{K}x = 0 \tag{7.45}$$

where **M** and **K** are mass and stiffness matrices, respectively. If $\mathbf{x}_\mathrm{i}$ are the eigenvectors and λ_i the corresponding eigenvalues, Rayleigh's quotient, with ω_i the corresponding natural frequencies, is

$$\lambda_i = \frac{x_i^T \mathbf{K} x_i}{x_i^T \mathbf{M} x_i} = \omega_i^2. \tag{7.46}$$

If the modification of the stiffness matrix is $\Delta\mathbf{K}$ and the corresponding changes in the eigenvalues are $\Delta\lambda_\mathrm{j}$, then

$$(\lambda_i + \Delta\lambda_i) \approx \frac{\mathbf{x}_i^T(\mathbf{K} + \Delta\mathbf{K})\mathbf{x}_i}{\mathbf{x}_i^T \mathbf{M} \mathbf{x}_i}$$

where, change in eigenvectors has been omitted, since small variations of the eigenvectors have a much smaller effect upon the eigenvalues. Using Eq. (7.46) we obtain

$$\Delta\lambda_i \approx \frac{\mathbf{x}_i^T \Delta\mathbf{K} \mathbf{x}_i}{\mathbf{x}_i^T \mathbf{M} \mathbf{x}_i}. \tag{7.47}$$

It should be noted that, again owing to the stationary behavior of the Rayleigh's quotient, small but finite changes in eigenvalues can be computed with acceptable error. Further, the eigenvector change can be computed. To this end, the eigenvalue problem which follows Eq. (7.45) is stated as

$$\mathbf{K}\mathbf{x}_i = \lambda_i \mathbf{M} \mathbf{x}_i \tag{7.48}$$

where $\lambda_\mathrm{i} = \omega_\mathrm{i}^2$ and $\mathbf{x}_\mathrm{i}$ the corresponding eigenvector. Differentiation yields

$$\mathrm{d}\mathbf{K}\mathbf{x}_i + \mathbf{K}\mathrm{d}\mathbf{x}_i = \mathrm{d}\lambda_i \mathbf{M}\mathbf{x}_i + \lambda_i \mathbf{M}\mathrm{d}\mathbf{x}_i \tag{7.49}$$

Multiplication from the left by $\mathbf{x}_\mathrm{j}^\mathrm{T}$ yields

$$\mathbf{x}_j^\mathrm{T}\mathrm{d}\mathbf{K}\mathbf{x}_i + \mathbf{x}_j^\mathrm{T}\mathbf{K}\mathrm{d}\mathbf{x}_i = \mathrm{d}\lambda_i \mathbf{x}_j^\mathrm{T}\mathbf{M}\mathbf{x}_i + \lambda_i \mathbf{x}_j^\mathrm{T}\mathbf{M}\mathrm{d}\mathbf{x}_i. \tag{7.50}$$

Since the matrices **K** and **M** are real and symmetric, Eq. (7.44) implies that

$$\mathbf{x}_i^\mathrm{T}\mathbf{K} = \lambda_\iota \mathbf{x}_\iota^\mathrm{T}\mathbf{M} \tag{7.51}$$

Equation (7.50) for $j = i$ yields

$$\mathbf{x}_i^\mathrm{T}\mathrm{d}\mathbf{K} = \mathrm{d}\lambda_\iota \mathbf{x}_\iota^\mathrm{T}\mathrm{M} \tag{7.52}$$

$$\mathrm{d}\lambda_\iota = \frac{\mathbf{x}_i^\mathrm{T}\mathrm{d}\mathbf{K}\mathbf{x}_i}{\mathbf{x}_\iota^\mathrm{T}\mathbf{M}\mathbf{x}_i} \tag{7.53}$$

which is identical to Eq. (7.47). Furthermore, Eq. (7.50), because of the orthogonality of the eigenvectors, [47] i.e.

$$\mathbf{x}_i^{\mathrm{T}}\mathbf{M}\mathbf{x}_i = 0$$

yields

$$\mathbf{x}_j^{\mathrm{T}}\lambda_i\mathbf{M}\mathrm{d}\mathbf{x}_i - \mathbf{x}_j^{\mathrm{T}}\mathbf{K}\mathrm{d}\mathbf{x}_i = \mathbf{x}_j^{\mathrm{T}}\mathrm{d}\mathbf{K}\mathbf{x}_i \tag{7.54}$$

and because of Eq. (7.51)

$$\mathbf{x}_j^{\mathrm{T}}\left(\lambda_i - \lambda_j\right)\mathbf{M}\mathrm{d}\mathbf{x}_i = \mathbf{x}_j^{\mathrm{T}}\mathrm{d}\mathbf{K}\mathbf{x}_i. \tag{7.55}$$

Let the eigenvector differential be

$$\mathrm{d}\mathbf{x}_i = \sum_{j=1}^{n} a_{\mathrm{ij}}\mathbf{x}_{\mathrm{j}} \tag{7.56}$$

where α_{ij} are appropriate differential weighing factors . Multiplying from the left by $\mathbf{x}_{\mathrm{j}}^{\mathrm{T}}\mathbf{M}$, due to the orthogonality,

$$\mathbf{x}_j^{\mathrm{T}}\mathbf{M}\mathrm{d}\mathbf{x}_i = \alpha_{ij}\mathbf{x}_j^{\mathrm{T}}\mathbf{M}\mathbf{x}_j \tag{7.57}$$

and with Eq. (7.55) we obtain

$$\alpha_{ij} = \frac{\mathbf{x}_j^{\mathrm{T}}\mathrm{d}\mathbf{K}\mathbf{x}_i}{\mathbf{x}_j^{\mathrm{T}}\mathbf{M}\mathbf{x}_j} \qquad i \neq j \tag{7.58}$$

$$\alpha_{\mathrm{ii}} = 0$$

Equations (7.53), (7.56) and (7.58) can be used to compute the eigenvalue and eigenvector change due to the modification of the stiffness matrix **K** of the structure.

To test of the accuracy of this approximation, the simple system of Fig. 7.23a was considered. The error in computation of the changes of the natural frequencies ω_1 and ω_2 with Eq. (7.43) in comparison with the changes computed exactly by analysis is shown in Fig. 7.23b. For a rather substantial change in stiffness by 10 %, the error in $\Delta\omega_1$ is 5 % and in $\Delta\omega_2$ is 0.5 % [48].

With more complicated systems, the global matrices **K** and d**K** consist of blocks describing the structural elements [49–52]. The matrix d**K** of the structural modifications due to cracks can be directly linked to the crack characteristics, as shown by the following example.

7.3.3 Torsional Vibration of a Cracked Rotor

For an infinite cylinder with a peripheral crack of depth *a,* Dimarogonas and Massouros [9] computed the torsion al local flexibility of the shaft due to the crack in the form

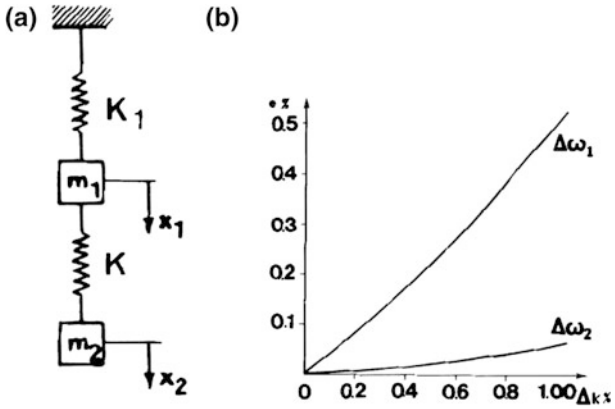

Fig. 7.23 Frequency shift calculation error for a 2-degree-of-freedom system

$$c = \frac{\Delta\varphi}{T} = f(\xi)$$

where $\xi = 1 - a/R$, R the radius of the cylinder.

$$\frac{\pi R^3 \mu}{4} c = 0.035\xi^{-4} + 0.01\xi + 0.029\xi^2 + 0.0086\xi^3 + 0.0044\xi^4 + 0.0025\xi^6 + 0.0017\xi^7 + 0.008\xi^8 - 0.092. \tag{7.59}$$

For a general rotor in torsional vibration, considered as the lumped system of Fig. 7.22, the equations of motion are [6]

$$\mathbf{J}\ddot{\Theta} + \mathbf{K}\Theta = 0 \tag{7.60}$$

where the inertia matrix

$$\mathbf{J} = \mathrm{diag}(J_1, J_2, \ldots, J_n)$$

and the stiffness matrix has the line i in the form

1	2	$3 \ldots i-1$	i	$i+1$	$\ldots n$
0	0	$0 \ldots -k_i$	$\ldots k_i + k_{i+1}$	k_{i+1}	$\ldots 0$

The natural frequencies ω_i are roots of the equation

$$|-\mathbf{J}\lambda + \mathbf{K}| = 0 \quad \lambda = \omega^2 \tag{7.61}$$

The modified problem consists of the rotor of Fig. 7.24 having a peripheral crack of depth a at section i which, without crack, has torsional stiffness k_i. The stiffness k_i^*, reduced by the presence of a crack, will be

$$\frac{1}{k_i^*} = c + \frac{1}{k_i} \quad k_i^* = \frac{1}{1 + ck_i} k_i \tag{7.62}$$

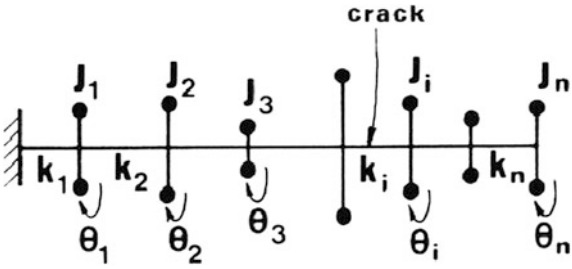

Fig. 7.24 Model of a lumped rotor

The change $\Delta\mathbf{K}$ of the stiffness matrix $\mathbf{K}$ will be an $n \times n$ matrix with all elements zero, except

$$(\Delta\mathbf{K})_{ii} = \frac{ck_\mathrm{i}}{1 + ck_\mathrm{i}} k_\mathrm{i} = (\Delta\mathbf{K})_{(i-1)(i-1)}$$

$$(\Delta\mathbf{K})_{i-1,i} = -\frac{ck_\mathrm{i}}{1 + ck_\mathrm{i}} k_\mathrm{i} = (\Delta\mathbf{K})_{i,(i-1)}.$$

For comparison, the change in natural frequencies has been computed for a shaft with 10 nodes and uniform diameter with the inertia lumped at the nodes, with a crack at midspan. The changes have been computed alternatively by the following methods:

1. 'exactly', by repeating the solution of the eigenvalue problem for the original and the cracked rotor;
2. by the classical Morgan method [22];
3. by Eq. (7.47).

For comparison, considering the processing time for the computation of the change in the first four natural frequencies with method (1) as 100, the time required for method (2) is 78.25 and 7.57 for (3).

The changes in the first three natural frequencies as a function of the change in local stiffness $1/(1 + ck_i)$ at node 4, computed with the above methods, have been plotted in Fig. 7.25.

7.3.4 Cracked Structural Members

For a structural member with rectangular cross-section (Fig. 7.1) having a transverse crack (see Sect. 7.1), a local flexibility matrix $\mathbf{C}$ describes the elastic behavior of the latter.

Due to reciprocity, matrix $\mathbf{C}$ is symmetric. The stiffness matrix is the inverse:

$$\mathbf{K} = \mathbf{C}^{-1}. \tag{7.63}$$

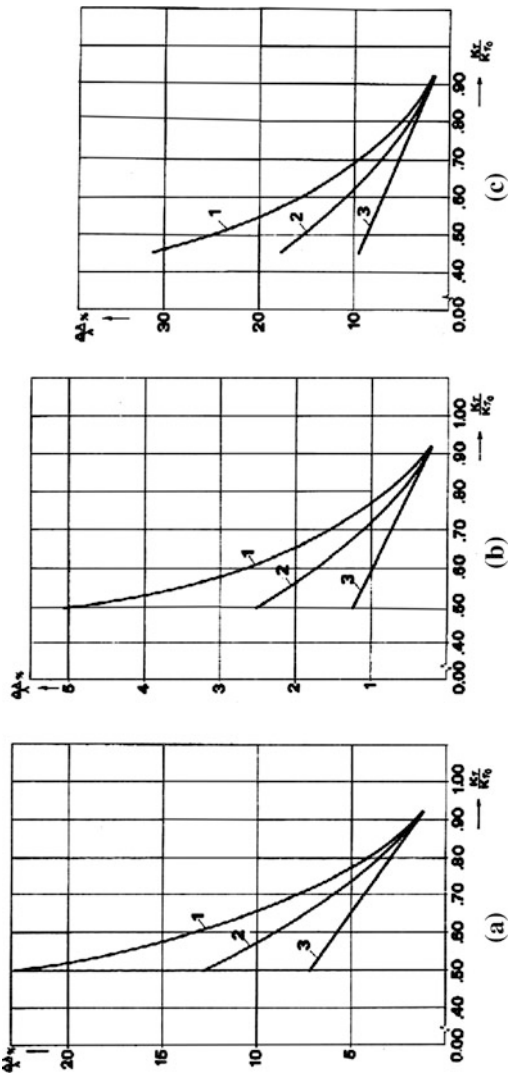

Fig. 7.25 Frequency shift of a cracked rotor in torsional vibration. **a** Harmonic 1. **b** Harmonic 2. **c** Harmonic 3. 1, 2 and 3: morgan, exact and Eq. (7.47), respectively

The change in the system eigenvalues due to the appearance of the crack can be linked directly to the local flexibility or stiffness matrix. To this end, we note that the numerator in Rayleigh's quotient is the additional strain energy due to the introduction of the crack. It can be written in the form

$$V = \frac{1}{2}\mathbf{x}_i^T \mathrm{d}\mathbf{K}\mathbf{x}_i \tag{7.64}$$

where d$\mathbf{K}$ refers to the local stiffness $\mathbf{C}^{-1}$ due to the crack. Therefore, Eq. (7.47) can be written as

$$\mathrm{d}\lambda_i = \frac{(\mathbf{x}_i)_c^T \mathbf{C}^{-1} (\mathbf{x}_i) c}{\mathbf{x}_i^T \mathbf{M} \mathbf{x}_i} \tag{7.65}$$

where crack flexibility matrix **C** for the most general loading indicated in Fig. 7.1 is given by Eq. (7.15). This links a change of natural frequencies directly to the geometry and location of the crack. The subscript c in the eigenvector denotes the components of the eigenvector describing the state of deformation in the vicinity of the crack. In Eq. (7.65) the elements of matrix **C** are functions of the geometry, location of crack and material properties. The treatment of continuous systems is very similar. Rayleigh's quotient can be written in the form

$$\mathrm{d}\lambda_i = \frac{(\mathbf{x}_i)_c^T \mathbf{C}^{-1} (\mathbf{x}_i) c}{\int \mathbf{x}_i^2 \mathrm{d}m} \tag{7.66}$$

where $\mathbf{x}_\mathrm{i}$ is the appropriate eigenvector and integration is carried over the length of the structural members.

Equations (7.47) and (7.66) provide a complete solution of the modified eigenvalue problem, especially if modification consists of a variation of the stiffness matrix. A change in the mass matrix can be treated similarly. This solution requires that the solution of the original problem of the unmodified structure be known, as usually happens. Moreover, for the computation of the change of the lowest eigenvalue, mass and stiffness change matrices are required, along with an estimate of the corresponding eigenvector which can be obtained with sufficient accuracy from the static deflection of the structure. Owing to the constancy of Rayleigh's quotient, good results can be obtained even for finite structural modifications, as can be seen from Fig. 7.25.

The method requires much less computation effort than Morgan's method. In addition, it yields higher accuracy for finite modifications and the eigenvector changes can also be computed.

The outlined procedure can be used for engineering analysis in two ways:

1. as a design tool, to assist in structural optimization with the objective of achieving certain specific dynamic characteristics;
2. as a maintenance and inspection tool, to identify structural flaws, such as cracks, by linking the variations in service of the structure's natural frequencies to structural changes due to the cracks.

7.4 Summary and Conclusions

The fact that a crack or a local defect affects the dynamic response of a structural member is known long ago. Numerous attempts to quantify local defects are reported to the literature. Dimarogonas [6] introduced the local flexibility model

for a crack for vibration analysis of cracked beams. In general there exist three basic crack models configurations: the local flexibility model, the local bending moment or the equivalent reduced cross section model, with magnitudes that were estimated by experimentation or by use of fracture mechanics methods. It must be stated here that flaws in structures may have a serious influence on their dynamic characteristics [6–11, 53, 54].

Defects in a structure may cause also changes in mass distribution and damping properties. This approach suffers from various limitations mainly from the fact that the modification of the stress field induced by the crack is decaying with the distance from the crack or flaw and a direct method relating flaw position and size with stiffness change is not easy to be developed. Such parameters affecting this approach are discussed in the papers of Dimarogonas and Chondros [20, 53, 54]. There is confusion in the literature concerning cracks. In some experimental works cuts or slots are used to simulate cracks. It would be more precise if the term crack model (local flexibility or distributed disturbance) was used. An experimental setup for initiating and propagating a fatigue crack is presented Chap. 9 [20].

During the vibration period of a cracked structural member the static deflection due to some loading component on the cracked beam (residual loads, body weight of a structure, etc.) combined with the vibration effect may cause the crack to open at all times, or open and close regularly, or completely close depending on various loads at a given time. If the static deflection due to some loading component on the beam (dead loads, own weight, etc.) are larger than the vibration amplitudes, then the crack remains open all the times, or opens and closes regularly and the problem is linear. If the static deflection is small, then the crack will open and close in time depending on the vibration amplitude. In this case the system is nonlinear. The effect of a breathing crack on the flexural and longitudinal vibration of cracked structures is discussed in the papers by Chondros and Dimarogonas [55, 56]. Besides, the change of damping of structures in case of crack initiation and growth is important for the estimation of resonance and near resonance vibrations of high-loaded structures and structural elements such as rotors of steam and gas turbines [10–14, 57–62].

References

1. Irwin, G.R.: Fracture mechanics. In: Goodier, J.N., Hoff, N.J. (eds.) Structural Mechanics, p. 557. Pergamon Press, Oxford (1960)
2. Liebowitz, H., Vanderveldt, H., Harris, D.W.: Carrying capacity of notched column. Int. J. Solids Struct. **3**, 489–500 (1967)
3. Liebowitz, H., Claus, W.D.: Failure of notched columns. Eng. Fract. Mech. **1**, 379–83 (1968)
4. Okamura, H., et al.: A cracked column under compression. Eng. Fract. Mech. **l**, 547 (1969)
5. Rice, J.R., Levy, N.: The part-through surface crack in an elastic plate. J. Appl. Mech. **39**, 185–194 (1972)

6. Dimarogonas, A.D.: Vibration for Engineers, 2nd edn. Prentice-Hall, Upper Saddle River (1996)
7. Chondros, T.G., Dimarogonas, A.D.: Identification of cracks in welded joints of complex structures. J. Sound Vibr. **69**(4), 531–538 (1980)
8. Chondros, T.G., Dimarogonas, A.D.: Identification of cracks in circular plates welded at the contour. ASME paper 79-DET-I06, Design engineering and technology conference, St. Louis (1979)
9. Dimarogonas, A.D., Massouros, G.: Torsional vibration of a shaft with a circumferential crack. Eng. Fract. Mech. **15**(3–4), 439–444 (1981)
10. Wauer, J.: On the dynamics of cracked rotors: A literature survey. Appl. Mech. Rev. **43**(1), 13–17 (1990)
11. Dimarogonas, A.D.: Vibration of cracked structures: A state of the art review. Eng. Fract. Mech. **55**(5), 831–857 (1996)
12. Pafelias, T.: Dynamic behaviour of a cracked rotor. General Electric Co., technical information series, no. DF-74-LS-79 (1974)
13. Wauer, J.: Modelling and formulation of equation of motion for cracked rotating shafts. Int. J. Sol. Str. **26**(4), 901–914 (1990)
14. Gasch, R.: A survey of the dynamic behavior of a simple rotating shaft with a transverse crack. J. Sound Vibr. **160**, 313–332 (1993)
15. Bicego, V., Lucon, E., Rinaldi, C., Crudeli, R.: Failure analysis of a generator rotor with a deep crack detected during operation: Fractographic and fracture mechanics approach. Nucl. Eng. Des. **188**, 173–183 (1999)
16. Barr, A.D.S.: An extension of the Hu-Washizu variational principle in linear elasticity for dynamic problems. Trans. ASME J. Appl. Mech. **33**(2), 465 (1966)
17. Christides, S., Barr, A.D.S.: Torsional vibration of cracked beams of non-circular cross-section. Int. J. Mech. Sci. **28**(7), 473–490 (1986)
18. Chondros, T.G.: Variational formulation of a rod under torsional vibration for crack identification. Fatigue Fract. Eng. Mater. Struct. **44**, 95–104 (2005)
19. Chondros, T.G., Labeas, G.: Torsional vibration of a cracked rod by variational formulation and numerical analysis. J. Sound Vib. **301**(3–5), 994–1006 (2007)
20. Chondros, T.G.: The continuous crack flexibility method for crack identification. Fatigue Fract. Eng. Mater. Struct. **24**, 643–650 (2001)
21. Tada, H.: The stress analysis of cracks handbook. Del Research Corp, Hellertown (1973)
22. Dimarogonas, A.D., Papadopoulos, C.A.: Vibration of cracked shafts in bending. J. Sound Vibr. **91**, 583–593 (1983)
23. Dimarogonas, A.D., Papadopoulos, C.A.: Crack detection in turbine rotors. Proceedings of the 2nd international symposium on transport phenomena, dynamics and design of rotating machinery, vol. 2, pp. 286–298. Honolulu (1988)
24. Dimarogonas, A.D., Papadopoulos, C.A.: Identification of cracks in rotors. 3rd EPRI lncip. Fail conference, Philadelphia (1990)
25. Dimarogonas, A.D.: Modeling damaged structural members for vibration analysis. J. Sound Vibr. **112**(3), 541–543 (1987)
26. Dimarogonas, A.D.: Bilinear analysis of closing cracks in rotating shafts. ISROMAC-4, Honolulu (1992)
27. Chondros, T.G.: Fatigue fracture of the Bjork-Shiley heart valve strut and failure diagnosis from acoustic signatures. Theor. and Appl. Fract. Mech. J. **54**, 71–81 (2010)
28. Papadopoulos, C.A.: The strain energy release approach for modelling cracks in rotors: A state of the art review, published in the special issue of Mechanical Systems and Signal Processing for Crack Effects in Rotordynamics, **22**(4), 763–789, (2008)
29. Papadopoulos, C.A., Dimarogonas, A.D.: Coupled longitudinal and bending vibrations of a rotating shaft with an open crack. J. Sound Vibr. **117**(1), 81–93, (1987)

30. Papadopoulos, C.A., Dimarogonas, A.D.: Coupled longitudinal and bending vibrations of a cracked shaft. J. Vib. Acoust. Stress Reliab. Des. **110**(1), 1–8, (1988)
31. Papadopoulos, C.A., Dimarogonas, A.D.: Stability of cracked rotors in the coupled vibration mode. J. Vib. Acoust. Stress Reliab. Des. **110**(3), 356–359, (1988)
32. Papadopoulos, C.A.: Torsional vibrations of rotors with transverse surface cracks. Comput. Struct. **51**(6), 713–718, (1994)
33. Papaeconomou, N., Dimarogonas, A.D.: Vibration of cracked beams. Comput. Mech. **5**, 88–94 (1989)
34. Sih, G.C., Loeber, J.E.: Torsional vibration of an elastic solid containing a penny-shaped crack. J. Acoust. Soc. Am. **44**(5), 1237–1245 (1968)
35. Loeber, J.E., Sih, G.C.: Torsional wave scattering about a penny-shaped crack on a biomaterial interface. In: Sih, G.C. (ed.) Dynamic Crack Propagation, pp. 513–528. Noordhoff, Leyden (1973)
36. Irwin, G.R., Kies, J.A.: Fracturing and fracture dynamics. Weld J. Res. Suppl. **34**, 570 (1955)
37. Irwin, G.R.: Analysis of stresses and strain near the end of a crack traversing a plate. J. Appl. Mech. **24**, 361 (1957)
38. Bueckner, H.F.: Field singularities and related integral representations. In: Sih, G.C. (ed.) Methods of Analysis and Solutions of Crack Problems, p. 239. Noordhoff, Leyden (1973)
39. Benthem, J.P., Koiter, W.T.: Asymptotic approximations to crack problems. In: Sih, G.C. (ed.) Methods of Analysis and Solutions of Crack Problems. Noordhoff, Leyden (1973)
40. Timoshenko, S., Goodier, J.N.: Theory of Elasticity. McGraw-Hill, Inc., New York (1953)
41. Szabo, I.: Höhere Technische Mechanik. Springer, Berlin (1964)
42. Weissenburger, J.T.: Effect of local modifications on the vibration characteristics of linear systems. J. Appl. Mech. **35**, 327–332 (1968)
43. Zarghmee, M.S.: Optimum frequency of structures. AJAA J. **6**(4), 749–750 (1968)
44. Fox, R.L., Kapoor, M.P.: Rates of change of eigenvalues and eigenvectors. AJAA J. **6**(12), 2426–2429 (1968)
45. Morgan, B.S.: Sensitivity analysis and synthesis of multivariable systems. IEEE Trans. Autom. Control **AC-11**(3), 36–52 (1966)
46. Paraskevopoulos, P.N., Tsonis, C.A., Tzafestas, S.G.: Eigenvalue sensitivity of linear time-invariant control systems with repeated eigenvalues. IEEE Trans. Autom. Control **AC-19**(5), 610–612 (1974)
47. Fadeev, D.K., Fadeeva, V.N.: Computational Methods of Linear Algebra. Freeman and Co., San Francisco (1963)
48. Chondros, T.G.: Influence of cracks on the dynamic behaviour of machines. Dissertation (in Greek), University of Patras, Greece (1982)
49. Kardestuncer, H.: Elementary Matrix Analysis of Structures. McGraw-Hill, New York (1974)
50. Gounaris, G., Dimarogonas, A.D.: A finite element of a cracked prismatic beam for structural analysis. Comput. Struct. **28**(3), 309-313 (1988)
51. Papadopoulos, C.A.: The strain energy release approach for modeling cracks in rotors: A state of the art review. Mech. Syst. Sig. Process. **22**(4), 763–789 (2008)
52. Naik, S.S., Maiti, S.K.: Triply coupled bending–torsion vibration of Timoshenko and Euler–Bernoulli shaft beams with arbitrarily oriented open crack. J. Sound Vib. **324**, 1067–1085 (2009)
53. Krawczuk, M., Ostachowicz, W.: Damage indicators for diagnostic of fatigue cracks in structures by vibration measurements—a survey. Mech. Teor Stosow **34**(2), 307–326 (1996)
54. Chondros, T.G., Dimarogonas, A.D.: Dynamic sensitivity of structures to cracks. J. Vibr., Acoust., Stress Reliab. Des. **111**, 251–256 (1989)
55. Chondros, T.G., Dimarogonas, A.D.: Vibration of a beam with a breathing crack. J. Sound Vib. **239**, 57–67 (2001)

56. Chondros, T.G., Dimarogonas, A.D., Yao, J.: Longitudinal vibration of a bar with a breathing crack. Eng. Fract. Mech. J. **61**, 503–518 (1998)
57. Bovsunovsky, A.P.: Experimental and analytical study of the damping capacity of multilayer steels. Strength Mater. **27**(9), 516–524 (1995)
58. Bovsunovsky, A.P.: The mechanisms of energy dissipation in the non-propagating fatigue cracks in metallic materials. Eng. Fract. Mech. **71**(16–17), 2271–2281 (2004)
59. Ezanno, A., Doudard, C., Calloch, S., Millot, T., Heuze, J-L.: Fast characterization of high-cycle fatigue properties of a cast copper–aluminum alloy by self-heating measurements under cyclic loadings. Proc. Eng. **2**, 967–976 (2010)
60. Ismail, A.E., Ariffin, A.K., Abdullah, S., Ghazali, M.J., Daud, R.: Mode III stress intensity factors of surface crack in round bars. Adv. Mater. Res. **214**, 92–96 (2011)
61. Xue, S., Cao, J., Chen,Y.: Nonlinear dynamic analysis of a cracked rotor-bearing system with fractional order damage, Trans. ASME, DETC 2011-47415, 1–6 (2011)
62. Yan, G., De Stefano, A., Matta, E., Feng, R.: A novel approach to detecting breathing-fatigue cracks based on dynamic characteristics. J. Sound Vib. **332**(2), 407–422 (2013)

Chapter 8
Thermal Effects Due to Vibration of Shafts

Abstract Chapter 8 deals with the inverse problem of the one encountered in Chap. 5, e.g. the heat generated by torsional vibration of rotating shafts. The corresponding mechanisms are associated with internal damping and plastic deformation. Practically all the energy of 476 plastic deformation is transformed into heat. For elastic deformation part of the strain energy is transformed into heat, depending on material loss factor. This phenomenon has been identified as the cause of large-scale failures of power equipment, with electrical disturbances being the cause of rotor torsional vibration. Maximum temperatures given in the form of design nomograms can assist in estimating the overheating of shaft of rotating machinery, where such phenomena are present. A typical turbo-generator shaft is analyzed for vibrations occurring during electrical transients.

8.1 Heat Propagation Due to Torsional Vibration of Shafts

Torsional vibrations of shafts result in heat generation due to material damping. In some cases, temperatures can reach high values affecting the reliability of machine members. Such a case was reported for the generator exciter shaft failures at the Southern California Edison. Mohave Station [1, 2], due to torsional vibration resulting from subsynchronous resonance or the electromechanical system. The heat generated produced high temperatures which destroyed the exciter insulation and accelerated shaft failure.

This chapter gives a quantitative account of the temperatures generated in the shaft and over its surface because of torsional vibration. The heat is generated due to material damping and, for plastic deformation, due to plastic flow.

A. D. Dimarogonas et al., *Analytical Methods in Rotor Dynamics*,
Mechanisms and Machine Science 9, DOI: 10.1007/978-94-007-5905-3_8,

Dynamic effects due to surface friction heating have been reported for rotating shafts [3–5, 7–12], Extensive studies were also reported on the effect of material damping on the vibration response of shafts [12–17].

Barenblatt et al. [18]. studied heat propagation caused by a crack in a vibrating elastic solid due to material damping. Panteliou and Dimarogonas [19–21] reported on the temperatures produced during torsional vibration of rotating shafts.

A uniform shaft is supposed to undergo forced torsional vibration. In general, vibration of this sort can have a linear mode between nodes for lumped mass systems, and a harmonic mode for continuous shafts.

Therefore, the torsional vibration amplitude will be [3]

$$\varphi_1 = \alpha z \cos \omega t \tag{8.1}$$

$$\varphi_c = C_l \cos \frac{\pi z}{L} \cos \omega t \tag{8.2}$$

where z is coordinate along shaft axis, and subscripts l and c mean lumped mass and continuous system, respectively. L is mode length and α and C_l, are vibration amplitude parameters.

The energy of elastic deformation for unit volume under shear stress τ will be

$$w = \frac{\tau^2}{2G} \tag{8.3}$$

but

$$\tau = \frac{1}{2} GD\Theta$$

where $\Theta = d\varphi/dz$, D is shaft diameter ($D = 2r$) at the point considered and G shear modulus. Therefore,

$$w = \frac{1}{2} G \left(\frac{d\varphi}{dz} \right)^2 r^2. \tag{8.4}$$

Heat generation per vibration cycle due to material damping is $\pi\gamma$w/2 [3, 12] where γ is loss factor of the material. Therefore, heat generation rate will be

$$\frac{q}{k} = \frac{\pi\gamma}{2} w = \frac{\pi\gamma}{2} \frac{nGr^2 (d\varphi/dz)^2}{2k} \tag{8.5}$$

where k is thermal conductivity and $n = \omega_n/2\pi$, vibration frequency. For plastic deformation, there will be additional heat generation. Practically all of deformation energy will be transformed into heat, so that the material loss factor should be taken as effectively equal to $2/\pi$, and an appropriate term should be added to Eq. (8.5). Heat conduction equation for the shaft becomes, for the steady state [22],

$$\frac{\partial^2 T}{\partial r^2} + \frac{1}{r} \frac{\partial T}{\partial r} + \frac{\partial^2 T}{\partial z^2} = -\frac{q}{k} = -\frac{\pi\gamma n G r^2 (d\varphi/dz)^2}{4k} \tag{8.6}$$

where $T = T(r, z)$ is temperature.

Equations (8.1) and (8.2) yield

$$\frac{d\varphi_1}{dz} = \alpha \tag{8.7}$$

$$\frac{d\varphi_c}{dz} = -\frac{\pi}{L} C_1 \sin \frac{\pi z}{L} \tag{8.8}$$

The term cos ωt was dropped at this point because heat generation was computed on the basis of averaging over one period. It should be noted that with a continuous system, L is not necessarily the total shaft length but the half cosine period of the vibration mode over the shaft. The reason is that at the points $z = 0$ and $z = L$ of this function, the twist ($d\Theta/dz$) is zero and the corresponding energy of elastic deformation and generated heat vanishes as well Fig. 8.1a. Due to symmetry, there is no heat flow along the shaft at these points; therefore the part of

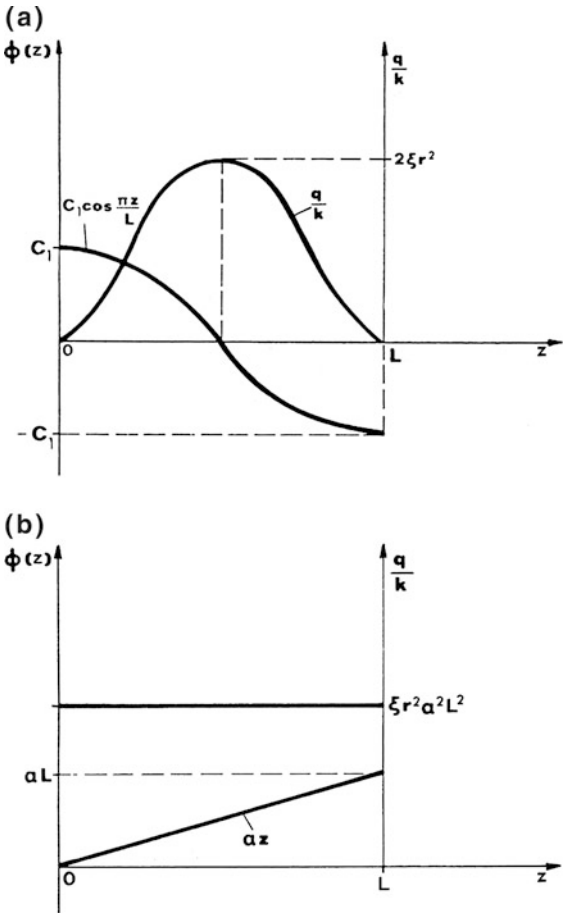

Fig. 8.1 Vibration modes and heat functions for **(a)** Continuous systems and **(b)** Lumped mass systems

the shaft of length L can be treated independently. Modes of more complicated forms, mainly due to variable diameters, can be expressed as cosine series.

Equations (8.7) and (8.8) yield

$$\frac{q_1}{k} = \frac{\pi\gamma n G r^2 \alpha^2}{4k} = \xi_1 r^2 f_1(z) \tag{8.9}$$

$$\frac{q_c}{k} = \frac{\omega\pi^2\gamma G r^2 C_1^2}{16kL^2}\left(1 - \cos 2\frac{\pi z}{L}\right) \tag{8.10}$$

$$\frac{q_c}{k} = \xi_c r^2 f_c(z) \tag{8.11}$$

where

$$\xi_c = \frac{\omega G\gamma}{4KL^2} \qquad f_c(z) = \frac{\pi^2 C_1^2}{4}\left(1 - \cos\frac{2\pi z}{L}\right) \tag{8.12}$$

$$\xi_1 = \frac{\omega G\gamma}{4KL^2} = \xi_c \qquad f_1(z) = \alpha^2 L^2. \tag{8.13}$$

Now, we turn to the heat conduction Eq. (8.6):

$$\mathcal{J}(T) = \frac{\partial^2 T}{\partial r^2} + \frac{1}{r}\frac{\partial T}{\partial r} + \frac{\partial^2 T}{\partial z^2} = -\xi r^2 f(z) \tag{8.14}$$

where ξ *and* $f(z)$ are given by Eqs. (8.12) and (8.13). In general, for $\lambda = \pi/L$

$$f(z) = \beta_1 + \beta_2 \cos 2\lambda z \tag{8.15}$$

where for a lumped system

$$\beta_1 = \alpha^2 L^2 \qquad \beta_2 = 0 \tag{8.16}$$

and for a continuous system

$$\beta_1 = \frac{\pi^2 C_1^2}{4} \qquad \beta_2 = -\frac{\pi^2 C_1^2}{4}. \tag{8.17}$$

Due to the linearity of the problem

$$T = T_1 + T_2 \tag{8.18}$$

where

$$\mathcal{J}(T_1) = -\xi r^2 \beta_1 \tag{8.19}$$

$$\mathcal{J}(T_2) = -\xi r^2 \beta_2 \cos 2\lambda z. \tag{8.20}$$

Equation (8.19) suggests that $T_1 = T_1(r)$ and $\partial T1/\partial z = 0$, Therefore,

$$T_1^{''} + \frac{1}{r} T_1^{'} = -\xi r^2 \beta_1 \tag{8.21}$$

with the boundary condition of Newtonian cooling at $r = R$

$$k \frac{dT_1}{dr} + h_a T_1 = 0 \tag{8.22}$$

where h_a is heat transfer coefficient. The resulting solution is

$$T_1(r) = \frac{\xi \beta_1 R^4}{4} \left\{ \frac{1}{Bi} + \frac{1}{4} \left[1 - (r/R)^4 \right] \right\} \tag{8.23}$$

where Bi is the Biot number, $Bi = h_a R/k$. Equation (8.20) suggests that

$$T_2(r, z) = \Theta(r) \cos 2\lambda z. \tag{8.24}$$

Therefore,

$$\frac{d^2\Theta}{dr^2} + \frac{1}{r} \frac{d\Theta}{dr} - (2\lambda)^2 \Theta = -\xi r^2 \beta_2. \tag{8.25}$$

The general solution of the homogeneous differential equation is

$$\Theta(r) = C_1 I_0(2\lambda r) + C_2 K_0(2\lambda r). \tag{8.26}$$

The boundary condition suggests that Θ be bounded for $r \to 0$, and therefore $C_2 = 0$; and at $r = R$ there is Newtonian cooling with heat transfer coefficient h_a and Biot number Bi [Eq. (8.22)]. A particular solution of Eq. (8.25) will be sought in the form.

$$\Theta_\mu(r) = a_0 + a_1 r + a_2 r^2. \tag{8.27}$$

Therefore, solving for the coefficients a_0, a_1, a_2:

$$\Theta_\mu(r) = \frac{\xi \beta_2}{4\lambda^4} + \frac{\xi \beta_2}{4\lambda^2} r^2.$$

For the non-homogeneous differential equation, the general solution will be

$$\Theta(r) = C_1 I_0(2\lambda r) + \frac{\xi \beta_2}{4\lambda^4} + \frac{\xi \beta_2}{4\lambda^2} r^2. \tag{8.28}$$

The boundary condition

$$K \frac{d\Theta}{dr} + h_a \Theta = 0$$

yields

$$C_1 = -\frac{\xi\beta_2}{2\lambda^2}\frac{\frac{Bi}{2}\left(\frac{1}{\lambda^2}+R\right)+R^2}{2\lambda RI_1(2\lambda R)+BiI_0(2\lambda R)}$$

and, therefore, from Eq. (8.28) yields

$$\Theta(r) = -\frac{\xi\beta_2}{4\lambda^2}\left\{\frac{Bi\left(1+\lambda^2R^2\right)+2\lambda^2R^2}{2\lambda RI_1(2\lambda R)+BiI_0(2\lambda R)}I_0(2\lambda r) - \left[1+(r\lambda)^2\right]\right\}. \tag{8.29}$$

Then, Eqs. (8.18), (8.23), (8.24) and (8.29) yield the solution

$$\begin{aligned} T = &-\frac{\xi\beta_2}{4\lambda^2}\left\{\frac{Bi\left(1+\lambda^2R^2\right)+2\lambda^2R^2}{2_1(2\lambda R)+BiI_0(2\lambda R)}I_0(2\lambda r) - \left[1+(r\lambda)^2\right]\right\}\times\cos 2\lambda z \\ &+\frac{\xi\beta_1R^4}{4}\left\{\frac{1}{Bi}+\frac{1}{4}\left[1-(r/R)^4\right]\right\}. \end{aligned} \tag{8.30}$$

For lumped mass systems, one can write

$$T = \frac{\xi\beta_1R^4}{4}\left\{\frac{1}{Bi}+\frac{1}{4}\left[1-(r/R)^4\right]\right\}. \tag{8.31}$$

In dimensionless form,

$$\frac{4T}{\xi\beta_1R^4} = \frac{1}{Bi}+\frac{1}{4}\left[1-(r/R)^4\right]. \tag{8.32}$$

The maximum temperature occurs at the centre of the cylinder *(r = 0)*, and the minimum one at the surface *(r = R)*. Therefore

$$\frac{4T_{\max}}{\xi\alpha^2L^2R^4} = \frac{1}{Bi}+\frac{1}{4}$$

$$\frac{4T_{\min}}{\xi\alpha^2L^2R^4} = \frac{1}{Bi}.$$

In Fig. 8.2 the maximum and minimum (surface) temperatures are shown as functions of Biot number. The temperature at the shaft centre *(r = 0* and z = 0) is given by

$$\frac{8\lambda^4T_{\max}}{\xi\pi^2C_1^2} = \frac{Bi\left(1+\lambda^2R^2\right)+2\lambda^2R^2}{2\lambda RI_1(2\lambda R)+BiI_0(2\lambda R)} - 1 + \lambda^4R^4\left(\frac{1}{Bi}+\frac{1}{4}\right). \tag{8.33}$$

The maximum surface temperature occurs for $r = \mathrm{R}$ and $z = 0$:

$$\frac{8\lambda^4T_{\text{surf}}}{\xi\pi^2C_1^2} = \frac{Bi\left(1+\lambda^2R^2\right)+2\lambda^2R^2}{2\lambda RI_1(2\lambda R)+BiI_0(2\lambda R)}I_0(2\lambda R) - \left[1+(R\lambda)^2\right] + (\lambda R)^4\left(\frac{1}{Bi}\right) \tag{8.34}$$

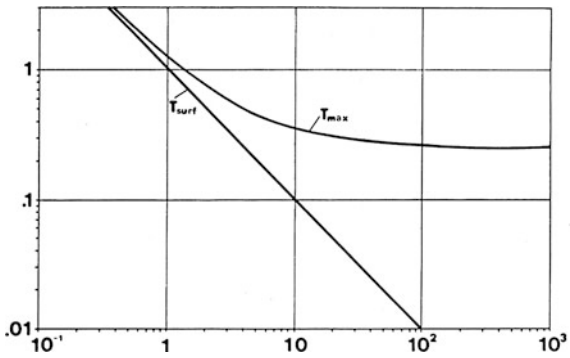

Fig. 8.2 Maximum and surface temperatures for a lumped mass shaft (from Ref. [19] by permission). Ordinate: $4T/\xi\alpha^2L^2R^4$. Abscissa: *Bi*

These temperatures are plotted in Figs. 8.3 and 8.4 as functions of Biot number and radius to length parameter $\lambda R = \pi R/L$.

From Fig. 8.2, it can be seen that, for lumped mass systems, substantial temperatures can be developed for low Biot number. With exciters for electric generators, where electrical insulation between shaft and collector exists, this

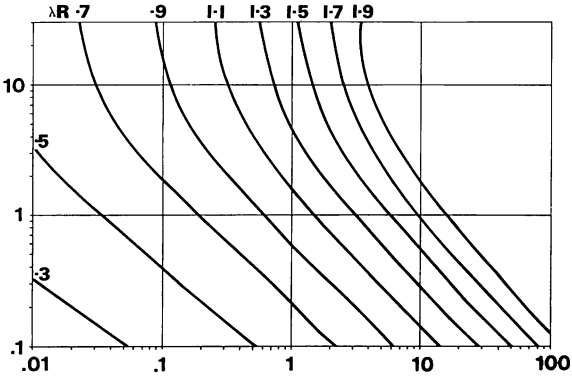

Fig. 8.3 Maximum temperatures for a uniform mass shaft (from Ref. [19], by permission). Ordinate: *Bi*. Abscissa: $8\lambda^4 T_{\max}/\xi\pi^2 C_1^2$

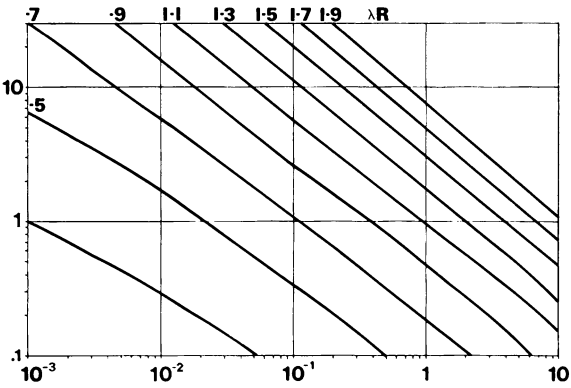

Fig. 8.4 Maximum surface temperatures for a uniform mass shaft (from Ref. 19 by permission). Ordinate: *Bi*. Abscissa: $8\lambda^4 T_{\text{surf}}/\xi\pi^2 C_1^2$

insulation has low thermal conductivity and acts as a thermal insulator as well. In this case, temperatures reach high levels and destroy the insulation. For very high values of Biot number, i.e. high rate of heat convection over the surface, surface temperatures fall with increasing Biot number but the maximum temperatures at the shaft centre decrease with an increasing Biot number, but only down to a certain level, and remain constant despite further increase of the Biot number.

Similar results are presented with continuous systems in Figs. 8.3 and 8.4. Temperatures increase rapidly with increasing diameter to length ratio. Again, substantial temperatures can be developed in the shaft centre even at very high rates of surface cooling (Biot number) and even higher temperatures at the surface in case of surface insulation (low Biot number) as previously mentioned for the electric exciter.

Equation (8.30) was used to calculate temperature field in a continuous shaft with the following characteristics:

(a)	Geometry: diameter	$2R = 0.20$ m;
	Length	$L = 2$ m;
(b)	Material properties: shear modulus, steel SAE 1045;	$G = 1.05 \times 10^{11}$ N/m^2;
	Material damping factor	$\gamma = 0.01$ Snowdon [12];
	Thermal conductivity (steel)	$k_s = 60$ W/m °C;
	Thermal conductivity (air)	$k_a = 0.095$ W/m °C;
	Viscosity (air)	$\upsilon = 0.1785 \times 10^{-4}$ m^2/s;
(c)	Vibration mode (Eq. 8.2):	
	Amplitude	$C_1 = 0.0093$ rad;
	Angular velocity	$\omega = 377$ rad/s;
	Vibration frequency	$n = 914$ Hz.

In this example, Biot number was computed for rotation of the cylinder in free air. For this case, Dorfman [23] gives the Nusselt number, for negligible effect of the free convection, based on the plain wall model, $Nu = 300$ for Reynolds number

$$\mathrm{Re} = \frac{\omega_0 R^2}{\upsilon} = \frac{377 \times 0.1^2}{0.1785 \times 10^{-4}} = 211.000$$

Biot number

$$Bi = Nu \frac{k_a}{k_s} = 0.47$$

The maximum shear stress corresponding to the above geometry and vibration characteristics can easily be computed to be $\tau_{\max} = 4.85 \times 10^6$ N/m^2. The corresponding temperatures are shown in Fig. 8.5 for different radii. It is shown that considerable temperatures will develop.

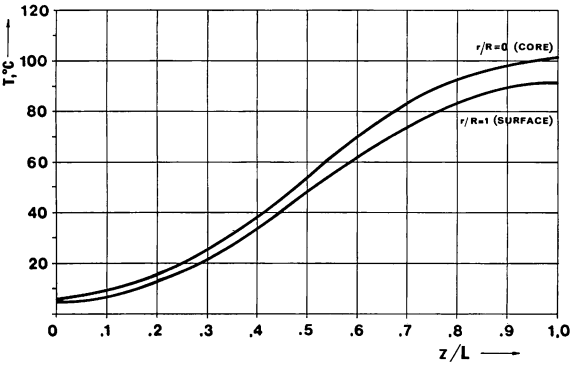

Fig. 8.5 Temperature distribution in a uniform mass shaft (from Ref. [19] by permission)

8.2 Heat Propagation in Rotating Shafts Due to Bending

A uniform shaft is supposed to rotate at constant speed and carry static loads. Because of rotation the shaft material undergoes alternating bending stresses. Due to the damping mechanism, a certain amount of heat is generated within the shaft material. Exactly the same analysis applies to any form of bending vibration of shafts or beams of circular cross-section [24].

The energy of elastic deformation for unit volume under bending stress a will be, for a static load mg at the midspan of the rotor

$$w = \frac{\sigma^2}{2E} \tag{8.35}$$

but

$$\sigma = \mathrm{M}r/I$$

where bending moment $M = mgz/2$, moment of inertia $I = R^4/4$, and R is shaft radius. Furthermore, E is elastic modulus, g acceleration of gravity, m mass of the static load, z coordinate along the shaft axis and L is shaft length. The situation is shown in Fig. 8.6. Therefore

$$w = \frac{2m^2g^2z^2r^2}{\pi^2ER^8}. \tag{8.36}$$

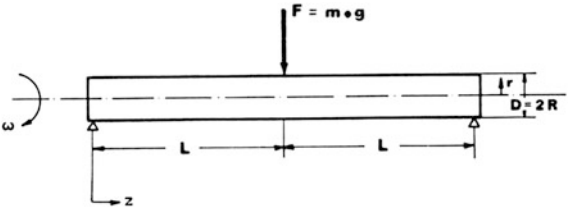

Fig. 8.6 Shaft geometry

Heat generation per time unit due to material damping is $\pi\gamma w/2$ [3, 12], where γ is loss factor of the material and rotation frequency $n = \omega_n/2\pi$. Therefore, heat generation rate will be

$$q = \frac{\pi n\gamma}{2} w = \frac{\gamma n m^2 g^2 z^2 r^2}{\pi E R^8}. \tag{8.37}$$

The heat conduction equation for the shaft becomes for the steady state [23]

$$\frac{\partial T}{\partial r} + \frac{1}{r}\frac{\partial T}{\partial r} + \frac{\partial^2 T}{\partial z^2} = -\frac{q}{k} \tag{8.38}$$

where k is thermal conductivity, and with boundary conditions

(1) Newtonian cooling at $r = R$

$$k\frac{\partial T}{\partial r} + hT = 0 \tag{8.39}$$

where h is heat transfer coefficient at the surface.

(2) due to symmetry at $z = 0$

$$\frac{\partial T}{\partial z} = 0 \tag{8.40}$$

Equations (8.36) and (8.37) yield

$$\frac{\partial^2 T}{\partial r^2} + \frac{1}{r}\frac{\partial T}{\partial r} + \frac{\partial^2 T}{\partial z^2} = -Az^2 r^2 \tag{8.41}$$

where $A = -(\gamma n m^2 g^2/\pi k E R^8)$. One can solve Eq. (8.41) using the finite cosine Fourier transform of $T(r, z)$ as follows: Let

$$F(r, \eta) = \int_0^L T(r, z)\cos\frac{\pi\eta z}{L} dz. \tag{8.42}$$

Equation (8.41) multiplied by $\cos(\pi nz/L)dz$ and integrated between 0 and L yields

$$\int_0^L \frac{\partial^2 T}{\partial r^2}\cos\frac{\pi\eta z}{L} dz = \frac{\partial^2}{\partial r^2}\int_0^L T\cos\frac{\pi\eta z}{L} dz = \frac{\partial^2 F}{\partial r^2}$$

$$\int_0^L \frac{1}{r}\frac{\partial T}{\partial z}\cos\frac{\pi\eta z}{L} dz = \frac{1}{r}\frac{\partial}{\partial z}\int_0^L T\cos\frac{\pi\eta z}{L} dz = \frac{1}{r}\frac{\partial F}{\partial z}$$

$$\int_0^L \frac{\partial^2 T}{\partial z^2}\cos\frac{\pi\eta z}{L} dz = -\left(\frac{\pi\eta}{L}\right)^2 F$$

Therefore

$$\frac{\partial^2 F}{\partial r^2} + \frac{1}{r}\frac{\partial F}{\partial r} - a^2 F = -Ar^2 \int_0^L z^2 \cos azdz$$

where $a = {}^{\pi n}/_{L}$. Since

$$\int_0^L z^2 \cos azdz = \frac{2L^3 \cos \pi\eta}{(\pi\eta)^2} = \frac{2L^3(-1)^\eta}{(\pi\eta)^2}$$

we get

$$\frac{\partial^2 F}{\partial r^2} + \frac{1}{r}\frac{\partial F}{\partial r} - a^2 F = \beta_\eta r^2 \tag{8.43}$$

where

$$\beta_\eta = \frac{2AL^3(-1)^n}{(\pi\eta)^2} \quad \eta = 1, 2, 3, \ldots$$

At this point, it should be noted that the simple model of linear bending due to a static load at the midspan was assumed. In general, the integration should be carried out for any form of the bending diagram of the shaft. This will yield a different value for β_n. In the present case, integration was carried out over half the shaft length since, due to symmetry of the bending diagram and therefore symmetry of the heat function, there is no axial flow at the midspan.

The general solution of the homogeneous differential equation is

$$F(r) = C_1 I_0(ar) + C_2 K_0(ar). \tag{8.44}$$

The boundary condition suggests that F be bounded for $r \to 0$; and therefore $C_2 = 0$; and that at $r = R$ there is Newtonian cooling:

$$k\frac{dF}{dr} + hF = 0. \tag{8.45}$$

A particular solution of Eq. (8.43) will be sought in the form

$$F_\mu(r) = d_0 + d_1 r + d_2 r^2. \tag{8.46}$$

Substituting in Eq. (8.43) and equating to zero the coefficients of powers of r, the particular solution is found as

$$F_\mu(r) = -\frac{4\beta_\eta}{a^4} - \frac{\beta_\eta}{a^2} r^2 = -\frac{\beta_\eta}{a^4}\left[4 + (ar)^2\right]. \tag{8.47}$$

The general solution for the non-homogeneous differential equation will be

$$F(r,\eta) = C_1 I_0(ar) - \frac{\beta_\eta}{a^4} 4 + (ar)^2. \tag{8.48}$$

With $Bi = hR/k$, Eqs. (8.45) and (8.48) yield,

$$C_1 = \frac{\beta_\eta}{a^4}\left\{\frac{Bi\left[4 + (aR)^2\right] + 2(aR)^2}{aRI_1(aR) + B_i I_0(aR)}\right\}.$$

Therefore,

$$F(r,\eta) = \frac{\beta_\eta}{a^4}\left[\left\{\frac{Bi\left[4 + (aR)^2\right] + 2(aR)^2}{aRI_1(aR) + I_0(aR)}\right\} I_0(aR) - 4 - (aR)^2\right]. \tag{8.49}$$

One can obtain zero-order of $F(r,n)$ as follows: Multiplying Eq. (8.41) by $\cos(\pi nz/L)dz$ and integrating between 0 and L for $n = 0$ and $F_0 = F(r,0)$:

$$\frac{d^2F_0}{dr^2} + \frac{1}{r}\frac{dF_0}{dr} = \frac{AL^3r^2}{3}. \tag{8.50}$$

But

$$\frac{1}{r}\frac{d}{dr}\left(r\frac{dF_0}{dr}\right) = \frac{d^2F_0}{dr^2} + \frac{1}{r}\frac{dF_0}{dr} = \frac{AL^3r^2}{3}.$$

Integrating twice:

$$F_0 = \frac{AL^3r^4}{48} + C_1 \ln r + C_2. \tag{8.51}$$

For F_0 bounded, C_1 must be zero.
Due to Newtonian cooling

$$R\frac{dF_0}{dr} + BiF_0 = 0 \quad r = R. \tag{8.52}$$

Equation (8.52) yields

$$C_2 = -\frac{AL^3R^4}{12}\left(\frac{1}{Bi} + \frac{1}{4}\right). \tag{8.53}$$

Therefore,

$$F_0 = \frac{R^4AL^3}{48}\left[\left(\frac{r}{R}\right)^4 - \left(\frac{4}{Bi} + 1\right)\right]. \tag{8.54}$$

Because $T(r, z)$ satisfies Dirichlet's conditions in the interval $(0, L)$ and considering Eq. (8.42), then $T(r, z)$ is given at each point of the interval $(0, L)$ by the series [23] (inverse discrete Fourier transform)

$$T(r,z) = \frac{1}{L}F(r,0) + \frac{2}{L}\sum_{\eta=1}^{\infty} F(r,\eta)\cos\frac{\pi\eta z}{L}. \tag{8.55}$$

Equations (8.49), (8.54) and (8.55) yield the following solution:

$$\begin{aligned} T(r,z) = {} & \frac{R^4AL^2}{48}\left[\left(\frac{r}{R}\right)^4 - \left(\frac{4}{Bi}+1\right)\right] + \sum_{\eta=1}^{\infty}\frac{4A(-1)^{\eta}}{a^6} \\ & \times \left[\left\{\frac{Bi\left[4+(aR)^2\right]+2(aR)^2}{aRI_1(aR)+BiI_0(aR)}\right\}I_0(ar) - 4 - (ar)^2\right]\cos az \end{aligned} \tag{8.56}$$

The temperature in dimensionless form is

$$\begin{aligned} \frac{T}{AL^6} = {} & \frac{(R/L)^4}{48}\left[\left(\frac{r}{R}\right)^4 - \left(\frac{4}{Bi}+1\right)\right] + \sum_{\eta=1}^{\infty}\frac{4A(-1)^{\eta}}{(\pi\eta)^6} \\ & \times \left[\left\{\frac{Bi\left[4+(aR)^2\right]+2(aR)^2}{aRI_1(aR)+BiI_0(aR)}\right\}I_0(ar) - 4 - (ar)^2\right]\cos\frac{\pi\eta z}{L} \end{aligned} \tag{8.57}$$

The maximum core temperature occurs at $r = 0$, $z = L$:

$$\frac{T_c}{AL^6} = \frac{-(R/L)^4}{48}\left(\frac{4}{Bi}+1\right) + \sum_{\eta=1}^{\infty}\frac{4}{(\pi\eta)^6}\left\{\frac{Bi\left[4+(aR)^2\right]+2(aR)^2}{aRI_1(aR)+BiI_0(aR)} - 4\right\}. \tag{8.58}$$

The maximum surface temperature occurs at $r = R$, z = L:

$$\begin{aligned} \frac{T_s}{AL^6} = {} & -\frac{(R/L)^4}{12Bi} + \sum_{\eta=1}^{\infty}\frac{4}{(\pi\eta)^6} \\ & \times \left[\left\{\frac{Bi\left[4+(aR)^2\right]+2(aR)^2}{aRI_1(aR)+BiI_0(aR)}\right\}I_0(aR) - 4 - (aR)^2\right]. \end{aligned} \tag{8.59}$$

These temperatures are plotted in Figs. 8.7 and 8.8 as functions of Biot number and radius to length parameter, *R/L*. From Figs. 8.7 and 8.8, it can be seen that substantial temperatures can develop at low Biot numbers and high *R/L* ratios. At low Biot numbers, maximum core and surface temperatures are very close. Surface temperatures drop drastically at higher Biot numbers, while maximum core temperatures are substantially higher [25].

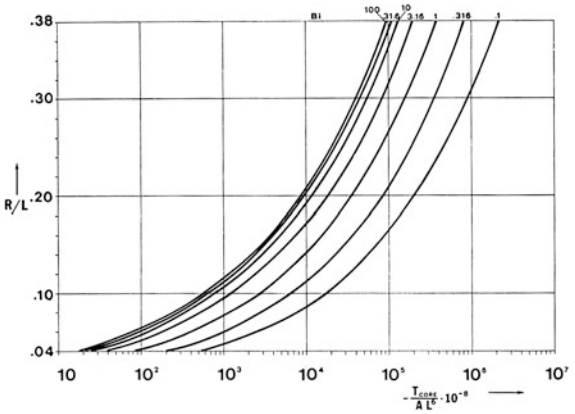

Fig. 8.7 Maximum core temperatures (*Courtesy* ASME [27])

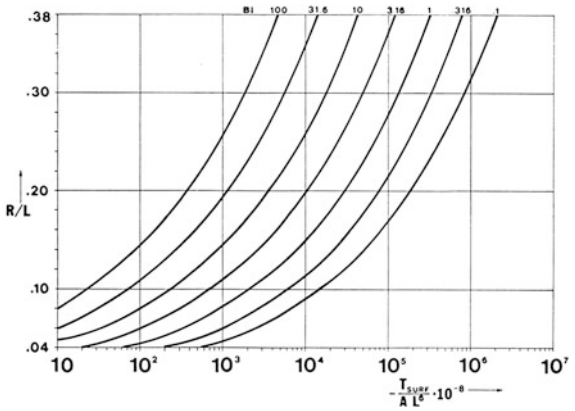

Fig. 8.8 Maximum surface temperatures (*Courtesy* ASME [27])

Equation (8.57) was used to calculate temperature field in a uniform shaft with the following characteristics:

(a)	Geometry: diameter	$2R = 1.00$ m;
	length	$2L = 20$ m;
(b)	Material properties: elastic modulus, steel SAE 1045;	$E = 2.10 \times 10^{11}$ N/ m^2;
	Material damping factor	$\gamma = 0.01$ Snowdon [12];
	Thermal conductivity (steel)	$k_s = 22$ W/m °C;
	Thermal conductivity (air)	$k_a = 0.03$ W/m °C;
	Viscosity (air)	$\upsilon = 0 \cdot 1785 \times 10^{-4}$ m^2/s;
(c)	Deflection mode: angular velocity	
	Static load at midspan	$\omega = 377$ rad/s;
		$F = 58.86 \times 10^4$ N.

In this example, Biot number was computed for rotation of the cylinder in free air. For this case, Mikheyev [26] relationship (Eq. 2.46)

$$Nu_f = 0.018\,\mathrm{Re}^{0.80}$$

yields Nusselt number (for negligible effect of the free convection, based on the plane wall model) $Nu = 4300$ for Reynolds number:

$$\mathrm{Re} = \frac{\omega R^2}{\upsilon} = \frac{377 \times 0.5^2}{0.1785 \times 10^{64}} = 5.28 \times 10^6.$$

Biot number

$$Bi = Nu\frac{k_a}{k_s} = 4300 \times \frac{0.03}{22} = 5.7.$$

The maximum bending stress corresponding to the above geometry and loading characteristics can be easily computed to be $\sigma_{\max} = 30\ \mathrm{MN/m^2}$. The corresponding temperatures are shown in Fig. 8.9 for the core ($r = 0$) and for the surface ($r = R$) [26].

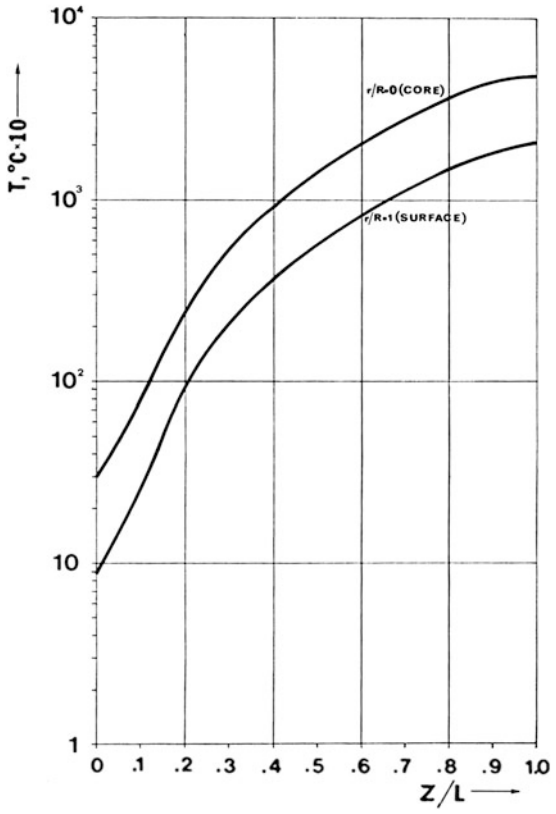

Fig. 8.9 Temperature distribution in a uniform shaft (*Courtesy* ASME [27])

8.3 Summary and Conclusions

Transient heat propagation in a rotating shaft undergoing torsional vibration of variable amplitude, or due to static load, internal damping or bending vibration was discussed. It was shown that low heat transfer coefficients over the shaft surface can lead to extremely high surface temperatures. High diameter to length ratios lead also to high surface temperatures. Surface temperatures drop rapidly with increasing heat transfer coefficients over the surface [19–21, 24, 25, 27].

Transients following switching in the network and/or the tripping of generating unit auxiliaries can excite oscillatory torques on the turbine-generator-rotor-shaft system. The oscillations can be damped or amplified with time. Damped oscillations affect the power quality and, if the oscillations grow with time, they may even lead to generating unit outages (and damages) resulting in possible system instabilities. During such transients, substantial temperatures may develop in the shafts which may affect the operation of the machine [21, 28–30].

Plastic deformation is very important because practically all the energy of plastic deformation is transformed into heat. For elastic deformation some of the strain energy is transformed into heat depending on the loss factor of the material. For machinery steels the amount of strain energy which is transformed into heat is usually below 1 %. This stresses the importance of the plastic deformation on the shaft [21].

The results of this transient analysis coincide in the limit with previously published results on steady state heat generation due to constant amplitude vibration. Maximum temperalbures are given in the form of design nomograms which can assist in estimating the overheating of shaft of rotating machinery where such phenomena are present. In particular, a typical turbo-generator shaft was analysed for vibrations occuring during electrical transients. Substantial temperatures have been computed for this ease [21, 28].

References

1. Chiriozzi, E., Spenna, A.: Effects of electrical faults on reliability of turbogenerator units in large steam power plants. Electr. Power. Syst. Res. **1**, 153–66 (1977/78)
2. Walker, D.N., et al.: Results of subsynchronous resonance tests at Mohave. IEEE Trans. on Power Apparatus and Syst. **PAS 94**(5), 1878–1888 (1975)
3. Dimarogonas, A.D.: Vibration for Engineers, 2nd edn. Prentice Hall Upper Saddle River, NJ (1996)
4. Dimarogonas, A.D.: Newkirk effect: thermally induced dynamic instability of high speed rotors. In: ASME Paper 73-GT-26. Gas Turbine Conf, Washington, D.C. (1973)
5. Dimarogonas, A.D.: A study of the Newkirk effect in turbomachinery. Wear **28**, 369–382 (1974)
6. Kellenberger, W.: Spiral vibrations due to the seal rings in turbogenerators—thermally induced interaction between rotor and stator. In: ASME Paper 79-DET-61, Design Eng. Tech. Conf., St. Louis 1979

7. Dimarogonas, A.D.: A brief history of rotor dynamics. In: Rotordynamics, vol. 92, Springer, Venice, (1992)
8. Dimarogonas, A.D.: Vibration of cracked structures—a state of the art review. Eng. Fract. Mech. **55**(5), 831–857 (1996)
9. Adams, M.L.: Rotating Machinery Vibration. Marcel Dekker Inc., New York (2001)
10. Edwards, S., Lees, A.W., Friswell, M.I.: The influence of torsion on rotor/stator contact in rotating machinery. J. Sound Vib. **225**(4), 767–778 (1999)
11. Bachschmid, N., Pennacchi, P., Vania, A.: Thermally induced vibrations due to rub in real rotors. J. Sound Vib. **299**, 683–719 (2007)
12. Lazan, B.J.: Damping of Materials and Members in Structural Mechanics. Pergamon Press, Oxford (1968)
13. Snowdon, J.C.: Vibration and Shock in Damped Mechanical Systems. Wiley, New York (1968)
14. Zorzi, E.S., Nelson, H.D.: Finite element simulation of rotor-bearing systems with internal damping. J. Eng. Power Trans. ASME **99 Ser**(1), 71–76 (1977)
15. Lalanne, M., Ferraris, G.: Rotordynamics Prediction in Engineering, 2nd edn. Wiley, Somerset, NJ (1998)
16. Montagnier, O., Hochard, C.H.: Dynamic instability of supercritical driveshafts mounted on dissipative supports-effects of viscous and hysteretic internal damping. J. Sound Vib. **305**(3), 378–400 (2007)
17. Chouksey, M., Dutt, J.K., Modak, S.V.: Modal analysis of rotor-shaft system under the influence of rotor-shaft material damping and fluid film forces. Mech. Mach. Theory **48**(1), 81–93 (2012)
18. Barenblatt, G.I., Entov, V.M., Salganik, R.L.: On the influence of vibrational heating on the fracture propagation in polymeric materials. Proceedings IUTAM Symposium on the Thermoinelasticity, East Kilbride, Scotland, Springer-Verlag, Wien, Boley, B.A., (ed.), 33–46 (1970)
19. Panteliou, S., Dimarogonas, A.D.: Heat propagation due to transient torsional vibration. J. Sound. Vib **73**(2), 239–245 (1980)
20. Panteliou, S., Dimarogonas, A.D.: Heat propagation due to transient torsional vibration. Int. Com. in Heat and Mass Transfer **10**(2), 111–122 (1983)
21. Panteliou, S., Aspragathos, N., Dimarogonas, A.D.: Thermal effects on rotating shafts due to electrical transients causing plastic deformation. Ingenieur. Archiv **53**, 173–179 (1983)
22. Carslau, H.S., Jaeger, J.C.: Conduction of Heat in Solids, 2nd edn. Oxford University Press, Oxford, New York (1959)
23. Dorfman, L.A.: Hydrodynamic Resistance and the Heat Loss of Rotating Solids. Oliver & Boyd, London (1963). (translated from Russian)
24. Pantellou, S., Dimarogonas, A.D: Heat propagation in rotating shafts due to bending. ASME winter annual meeting paper No 81-WA/DE-1, 1981
25. Pantellou, S: Heat propagation on vibrating shafts with internal damping and plastic deformation. Dissertation, University of Patras, Greece, 1983
26. Mikheyev, M.: Fundamentals of Heat Transfer. Mir Publishers, Moscow (1964)
27. Panteliou, S., Dimarogonas, A.D.: Heat propagation in rotating shafts due to damping. J. Mech. Design **104**, 675–678 (1982)
28. Dimarogonas, A.D.: Vibration of cracked structures——a state of the art review. Eng Fract Mech **55**(5), 831–857 (1996)
29. Kumar, R., Merkle, M., Leibfried,T.: A new approach for investigation of the turbine generator oscillatory behavior affecting power system quality and reliability. ASME power conference;Baltimore, MD.American society of mechanical engineers, PWR 35, pp 401–408, Power Division (Publication), 2004
30. Ziaei-Rad, S., Kouchaki, E., Imregun, M.: Thermoelastic modeling of rotor response with shaft rub. J. Appl. Mech. Trans ASME **77**(6), 2011, art. no. 061010

Chapter 9
Variational Formulation of Consistent: Continuous Cracked Structural Members

Abstract In Chap. 9, modeling and formulation of the governing dynamic equations for cracked Euler-Bernoulli beams in flexural vibration are studied. The results of three independent evaluations of the lowest natural frequency of lateral vibrations of beams with single-edge cracks and various end conditions are investigated: continuous cracked beam vibration theory, lumped crack flexibility model vibration analysis, a finite element method, and experimental results. For the case of torsional vibration of a shaft with a peripheral crack, the Hu-Washizu-Barr variational formulation is adopted for obtaining the differential equation of motion, with plausible assumptions about displacements, momentum, strain and stress fields, along with the associated boundary conditions. For the experimental procedure crack propagation and formation of stationary cracks is achieved by a vibration technique. Continuous cracked beam theory agrees better with experimental results than lumped crack theory.

9.1 Variational Formulation of Cracked Beams and Rods

Cracks on elastic structural elements introduce considerable local flexibility due to strain energy concentration around the crack tip [1, 2]. Great efforts have been expended to develop models capable of simulating the vibrational characteristics of cracked beams, however, the said models usually assume ideal geometry and material properties [3–20]. Variational approaches seem promising in such cases, as the one used by Chondros et al. [21–29] to develop a continuous vibration model for the lateral vibration of cracked Euler-Bernoulli beams with open single-edge or double-edge cracks, and torsional vibration of cracked rods. The Hu-Washizu-Barr

A. D. Dimarogonas et al., *Analytical Methods in Rotor Dynamics*,
Mechanisms and Machine Science 9, DOI: 10.1007/978-94-007-5905-3_9,

[30, 31] variational formulation was used to develop the differential equation and boundary conditions for flexural and torsional vibration of structural members with flaws considered as one-dimensional continua. Cracks are modelled as continuous flexibilities, and displacement field, found with fracture mechanics methods is investigated. This consistent continuous cracked beam vibration theory is useful in predicting changes in flexural vibration of prismatic members with single- or double open-edge surface cracks. The variational formulation along with fracture mechanics methods, provide analytical solutions, for the development of the differential equation and the boundary conditions of the cracked beam. Analytical methods are always convenient, since they deliver accurate results, are more efficient and provide deep physical insight into the problem.

In this chapter the problem of cracked beams with a single- or double-edge surface crack and various end-conditions is investigated. The cracked beam model satisfies the Euler-Bernoulli theory [27–29] i.e., the planar cross-sections of the undeformed beam remain plane after deformation, perpendicular to any axis along the length of the beam and retain original size and shape after deformation, the vibration of the cracked beam as a one–dimensional structural member is described by a linear hyperbolic partial differential equation of second order, with respect to time. Beam has open edge crack(s) along its length, and modification of the stress field in the vicinity of the crack is evaluated by fracture mechanics methods. A comparative study based on the Hu-Washizu-Barr variational formulation, a lumped crack flexibility approach and a finite element alternative is applied for the derivation of the cracked beam frequencies drop for vibration analysis and crack identification. The analytical and numerical results were correlated with experimental results, obtained from prismatic aluminium beams with open fatigue cracks.

For the case of torsional vibration of a shaft with a peripheral crack, again the Hu-Washizu-Barr variational formulation will be adopted for obtaining the differential equation of motion, with plausible assumptions about displacements, momentum, strain and stress fields, which produces the approximate equation of motion together with its associated boundary conditions. Relationships between strain and displacement, stress and strain, and momentum and displacement are also generated [27–30].

9.2 Lateral Vibration of a Continuous Cracked Beam

9.2.1 The Variational Theorem for a Simply Supported Beam

Hu-Washizu-Barr [30–32] variational principle in linear elasticity allows for independent variation of displacement, strain, and stress for the construction of approximate equations of equilibrium in elastostatic problems. Application of

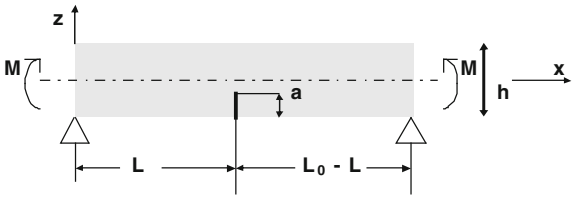

Fig. 9.1 Geometry of a simply supported beam with an edge crack

Hu-Washizu variational principle requires plausible assumptions about momentum, strain and stress fields. Christides and Barr [31] extended Hu-Washizu [30] principle further, by incorporating the perturbation in the stress and strain distributions of the beam, due to the presence of a crack through local functions which assume their maximum value at the cracked section, and decay exponentially from crack location. The equations of motion of a cracked beam-like structure are derived through Hu-Washizu-Bar [30–32] variational principle. The reduction to one spatial dimension was achieved by using integration over the cross-section after certain stress, strain, displacement and momentum fields were chosen. In particular, the modification of the stress field induced by the crack was introduced through a local experimental function, assuming an exponential decay with distance from the crack, and included a parameter that must be evaluated by experiments. Some experiments on beams with cuts simulating cracks were briefly described. The change in the first natural frequency versus crack depth matched closely with theoretical predictions. To confirm theoretical results, Shen and Pierre [33, 34] used a two-dimensional finite element approach to determine the parameter controling the stress concentration profile near the crack tip in the theoretical formulation without using experimental results. They found an agreement between theoretical and finite element results.

For an Euler-Bernoulli beam with an open single transverse surface crack as shown in Fig. 9.1, where displacement components are denoted by u_i, strain components by γ_{ij}, and stress components by σ_{ij}, with $i, j = 1, 2, 3$ referring to Cartesian axes x, y, z. Normal engineering notation will be used here with $u_1 = u$, $u_2 = \upsilon$, $u_3 = w$. Let p_i be the momentum such that $T_\mathrm{m} = 1/2\rho\delta_{\mathrm{ij}}p_\mathrm{i}p_j$ will be the kinetic energy density (δ_{ij} is Kronecker's delta). For arbitrary independent variations δu_i, $\delta\gamma_{\mathrm{ij}}$, $\delta\sigma_{\mathrm{ij}}$, and δp_i, the extended Hu-Washizu variational principle was introduced by Christides and Barr [30–32] and Chondros et al. [21–23] in the form:

$$\begin{aligned}
&\int_V \Big\{ \left[\sigma_{ij,j} + F_i - \rho\dot{p}_i\right]\delta u_i + \left[\sigma_{ij} - W_{,\gamma_{ij}}\right]\delta\gamma_{ij} \\
&+ \left[\gamma_{ij} - \left(1 - \frac{1}{2}\delta_{ij}\right)\left(u_{i,j} + u_{j,i}\right)\right]\delta\sigma_{ij} + \left[\rho\dot{u}_i - T_{m,p_i}\right]\delta_{p_i}\Big\}dV \qquad (9.1)\\
&+ \int_{S_g} [\bar{g}_i - g_i]\delta u_i dS + \int_{S_u} [u_i - \bar{u}_i]\delta g_i dS = 0
\end{aligned}$$

where, $W(\gamma_{ij})$ is strain energy density function, ρ is material density, F_i, g_i and u_i are, respectively, body forces, surface traction and surface displacement. Moreover, V is the total volume of the solid, and S_g and S_u are its external surfaces. The overbar denotes the prescribed values of the surface traction and the surface displacement. The prescribed surface tractions g_i are applied over the surface S_g and the prescribed displacements u_i are over S_u. Together S_g and S_u constitute the total surface of the solid. The differentiation with respect to time $(\partial/\partial t)$ is indicated by a dot. Commas in the subscripts indicate differentiation with respect to Cartesian axes.

To derive the governing equation and applicable boundary conditions for the transverse vibration of a cracked beam through the variational theorem, Eq. (9.1), the x axis is taken along the center line of the bar and the yz plane is the plane of the cross-section. The change in stress, strain and displacement distributions due to the crack will be expressed by a crack disturbance function for the axial displacement $f(x,z)$ introduced here.

For a uniform beam in the absence of body forces, the introduction of the displacement disturbance function $f(x,z)$ will modify Eq. (9.3) of Ref. [30] to yield:

$$\begin{aligned}
&u = -z\{[1 + f(x,z)]w(x,t)\}', \upsilon = 0, w = [1 + f(x,z)]w(x,t) p_x = 0,\ p_y = 0, p_z = P(x,t)\\
&\gamma_{xx} = -zS(x,t),\ \gamma_{yy} = \gamma_{zz} = -v\gamma_{xx},\ \gamma_{xy} = \gamma_{yz} = \gamma_{xz} = 0\\
&\sigma_{xx} = -zT(x,t),\ \sigma_{xz} = \sigma_{xz}(x,z,t),\ \sigma_{xy} = \sigma_{zz} = \sigma_{xy} = \sigma_{yz} = 0 F_x = F_y = F_z = 0
\end{aligned} \tag{9.2}$$

Following the method introduced in Ref. [30] the term σ_{xz} is applied for the lateral loading of the beam, and furthermore, it will be noted $f(x,z) = f$. Equation (9.2) can now be substituted in the general variational theorem, Eq. (9.1) and independent variations of the unknowns w, P, S and T are considered. The variations will be considered one by one as follows:

For an arbitrary and independent variation δT, the strain-displacement term of Eq. (9.1) becomes:

$$\int_V \left[\gamma_{xx} - \frac{}{\partial x}\right] \delta\sigma_{xx} dV = \int_x \left\{ \int_A \left(-zS + z[(1+f)w]''\right) - z\delta T dA \right\} dx \tag{9.3}$$

Defining the various integrals over the cross section A as:

$$I = \int_A z^2 dA, I_2 = \int_A z dA, I_4 = \int_A z^2 f'' dA, I_5 = \int_A z^2 f' dA, I_6 = \int_A z^2 (1+f) f dA,$$

the right-hand of Eq. (9.3) becomes:

$$\int_x \{(I - 2I_2)S - (I_4 w + 2I_5 w' + I_6 w'')\}\, \delta T dx \tag{9.4}$$

The stress-strain term in Eq. (9.1) is

$$\int_v \left\{ \left[\sigma_{xx} - \frac{\partial W}{\partial \gamma_{xx}} \right] \delta\gamma_{xx} - \frac{\partial W}{\partial \gamma_{yy}} \delta\gamma_{yy} - \frac{\partial W}{\partial \gamma_{zz}} \delta\gamma_{zz} \right\} \delta S dV \tag{9.5}$$

where, $W = 1/2\ \lambda e^2 + G(\gamma_{xx}^2 + \gamma_{yy}^2 + \gamma_{zz}^2) + 1/2\ G(\gamma_{xy}^2 + \gamma_{yz}^2 + \gamma_{xz}^2)$ is strain energy density, E and v are Young modulus and Poisson's ratio respectively, $e = \gamma_{xx} + \gamma_{yy} + \gamma_{zz}$ is dilatation, $G = E/[2(1+v)]$ is shear modulus, and $\lambda = vE/[(1+v)(1-2v)]$ is Lame's constant. Substituting the various quantities from Eq. (9.2), the stress-strain term (9.5) simplifies to:

$$\int_x \{(T - ES)(I - 2I_2)\} \delta S dx \tag{9.6}$$

The velocity momentum term is written using assumptions (9.2) as:

$$\int_x (\rho I_7 \dot{w} - \rho PA) \delta P dx \tag{9.7}$$

where $I_7 = \int_A [1 + f(x,z)]\, dA$.

The first term of Eq. (9.1) is the dynamic equilibrium term, leading to the equation of motion. Using the assumptions of Eq. (9.2), this term becomes:

$$\begin{aligned} &\int_V \left[\left(\frac{\partial \sigma_{xx}}{\partial x} + \frac{\partial \sigma_{xz}}{\partial z} \right) \delta u + \left(\frac{\partial \sigma_{xz}}{\partial x} - \rho \dot{P}_z \right) (1+f) \delta w \right] dV \\ &= \int_A \int_x \left\{ \left[(-zT)' + \frac{\partial \sigma_{xz}}{\partial z} \right] \left[-z\delta \left\{ (1+f)w \right\}' \right] \right. \\ &\quad \left. + \left(\frac{\partial \sigma_{xz}}{\partial x} - \rho \dot{P} \right) (1+f) \delta w \right\} dx dA \end{aligned} \tag{9.8}$$

Since,

$$\delta[(1+f)w]' \equiv \frac{\partial}{\partial x}[(1+f)\delta w] \tag{9.9}$$

the first term of Eq. (9.8) can be integrated by parts as

$$\begin{aligned} &\int_A \int_x \left\{ \left(z^2 T' - z \frac{\partial \sigma_{xz}}{\partial z} \right) \left(\frac{\partial}{\partial x} \right) [(1+f)\delta w] \right\} dx dA \\ &= \int_A \left[z^2 T' - \left(z \frac{\partial \sigma_{xz}}{\partial z} \right) \right] (1+f) \delta w\, dA \Big|_x \\ &\quad - \int_A \int_x \left[z^2 T' - \frac{\partial}{\partial x} \left(z \frac{\partial \sigma_{xz}}{\partial z} \right) \right] (1+f) \delta w dx dA \end{aligned} \tag{9.10}$$

The last term of Eq. (9.10) integrated by parts over z results in

$$\begin{aligned}&\int_x \frac{\partial}{\partial x}\left\{\int_y\int_z z\frac{\partial \sigma_{xz}}{\partial z}dzdy\right\}(1+f)\delta w dx\\&=\int_y\int_x \frac{\partial}{\partial \sigma z}(z\sigma_{xz})(1+f)\delta w dx dy|_z\\&-\int_A\int_x \frac{\partial \sigma_{xz}}{\partial z}(1+f)\delta w dx dA\end{aligned} \tag{9.11}$$

The boundary terms of Eq. (9.10) incorporated with the other boundary conditions, of the variational Eq. (9.1) yield

$$\begin{aligned}&\int_A\left\{z^2T'-z\frac{\partial \sigma_{xz}}{\partial z}\right\}(1+f)\delta w\, dA|_x\\&+\int_y\int_x \frac{\partial}{\partial x}(z\sigma_{xz})(1+f)\delta w dx\, dy|_z\end{aligned} \tag{9.12}$$

The first and second term of the right-hand of Eq. (9.10) incorporated in Eq. (9.8) reduces the latter to the form

$$\int_x\int_A\left[\left(-z^2T\right)''-\rho\dot{P}\right](1+f)\delta w dA dx \tag{9.13}$$

Performing the double differentiation indicated and integrating over the cross-section in (9.13), the dynamic equilibrium term of Eq. (9.1) can be rewritten as

$$\int_x\left\{I_2''T+2I_2'T'+(I_2-I)T''-\rho A\dot{P}\right\}|1+f|\delta w dx \tag{9.14}$$

It will be assumed that the lateral surfaces *S*g of the beams are free of external traction, i.e., that all prescribed traction on lateral surfaces are zero. The surface force is obtained from the stress components as $g_i = \sigma_{ij}n_j$ where n_j is the direction cosine of the external normal to the surfaces with the co-ordinate directions. While the beam is a uniform beam, the normal to its lateral surfaces will be at right angles to its axis so that n_x is zero. Thus, using Eq. (9.2), the surface forces g_i become:

$$\begin{aligned}g_x&=\sigma_{xx}n_x+\sigma_{xy}n_y+\sigma_{xz}n_z=\sigma_{xz}n_z,\\g_y&=\sigma_{yx}n_x+\sigma_{yy}n_y+\sigma_{yz}n_z=0,\\g_z&=\sigma_{zx}n_x+\sigma_{zy}n_y+\sigma_{zz}n_z=0\end{aligned} \tag{9.15}$$

On the other hand, over the ends of the beam $x = 0$ and $x = Lo$, there are $n_x = -1$ and $n_x = 1$, respectively (assuming plane ends normal to the beam axis).

From Eq. (9.15) g_x is reduced to $\pm\,\sigma_{xx}$ and g_z to $\pm\,\sigma_{xz}$. The forces prescribed at the ends, integrated over the section, correspond to an applied force or moment.

The surface integral in the general variational Eq. (9.1) thus takes the form, over the lateral surface of the beam at the limits of z, z_1 and z_2, and $z_2 > z_1$:

$$\int_x \int_y \left\{ [0 - \sigma_{xz}]_{z=z_2} \delta u + [0 + \sigma_{xz}]_{z=z_1} \delta u \right\} dy dx$$

which can be written as:

$$\left[\int_x \int_y -\sigma_{xz} \delta u dy dx \right] \Bigg|_{z_1}^{z_2}$$

Using the relation $\delta u = -z(1+f)\delta w'$ and integrating by parts over x, the latter surface integral becomes:

$$\left[\int_y z\sigma_{xz}(1+f)\delta w \delta y \right) \Bigg|_x - \int_y \int_x \frac{\delta}{\delta x}(z\sigma_{xz})(1+f)\delta w dx dy \Bigg] \Bigg|_{z_1}^{z_2} \tag{9.16}$$

The second term of this integral cancels the final term of Eq. (9.12). The second term of (9.12) can be integrated by parts over z, and results in a term cancelling first term of (9.16). The remaining terms of Eq. (9.12) applied to the boundaries of x are:

$$\int_y \left\{ z^2 T' + \sigma_{xz} \right\} (1+f)\delta w \, dA|_x \tag{9.17}$$

Similarly, for the prescribed forces, the surface integral of Eq. (9.1) over the ends of the beam, at $x = 0$ and $x = L_0$, assume the form:

$$\begin{aligned} &\left[\int_A \int \{(\bar{X} - \sigma_{xx})\delta u + (\bar{Z} - \sigma_{xz})(1+f)\delta w\} dA \right]_{x=L_0} \\ &+ \left[\int_A \{(\bar{X} + \sigma_{xx})\delta u + (\bar{Z} + \sigma_{xz})\delta w\} dA \right]_{x=0} \end{aligned} \tag{9.18}$$

The variation δw in term (9.17) is arbitrary and independent, expecting at boundary

$$\left\{ \sigma_{xz} = -z^2 T' \right\}\big|_x \tag{9.19}$$

From Eqs. (9.19 and 9.18) and using Eq. (9.2) for the quantities δu, δw and σxx, integration over the section can be performed. The resulting boundary terms take the form,

$$\left[\left\{-\int_A z\bar{X}dA + (I_2 - I)T\right\}\delta w' + \left\{\int_A \bar{Z}dA + (I - I_2)T' - I_2'T\right\}\delta w\right]_{x=L_0} - \left[\left\{-\int_A z\bar{X}dA - (I_2 - I)T\right\}\delta w' + \int_A \bar{Z}dA + (I - I_2)T' - I_2'T\right\}\delta w\Bigg]_{x=0} \tag{9.20}$$

On the other hand, for the prescribed displacements, the surface integral of the variational Eq. (9.1) over the ends $x = 0$, and $x = Lo$ is:

$$\left[\int_A \{(u - \bar{u})\delta\sigma_{xx} + (1 + f)(w - \bar{w})\delta\sigma_{xx}\}dA\right]_{x=L_0} - \left[\int_A \{(u - \bar{u})\delta\sigma_{xx} + (1 + f)(w - \bar{w})\delta\sigma_{xx}\}dA\right]_{x=0} \tag{9.21}$$

After substituting for u, w and σ_{xx} from Eq. (9.2) and integrating over the section, (9.21) becomes:

$$\left[\left\{(I - I_2)(1 + f)w' + \int_A \bar{u}zdA\right\}\delta T + \{(w - \bar{w})A\}\delta\sigma_{xz}\right]_{x=L_0} - \left[\left\{(I - I_2)(1 + f)w' + \int_A \bar{u}zdA\right\}\delta T + \{(w - \bar{w})A\delta\sigma_{xz}\}\right]_{x=0} \tag{9.22}$$

The entire variational statement for the vibration of cracked Euler–Bernoulli beams can now be assembled by using Eq. (9.1) and the variational terms (9.4), (9.6), (9.7) and (9.14) along with the boundary terms given in (9.20) and (9.22). The variations δw, δP, δS, δT and $\delta\sigma_{xz}$ are regarded as independent so that Eq. (9.1) implies, for arbitrary values of these variations, that each term multiplied by them in the volume integral must independently be zero, which will give the following relations directly:
the strain-displacement term (9.4) for δT yields

$$S = Q_1(x)w'' + Q_2(x)w' + Q_3(x)w \tag{9.23}$$

where: $Q_1(x) = I_6/(I - 2I_2), Q_2(x) = 2I_5/(I - 2I_2), Q_3(x) = I_4/(I - 2I_2)$, from stress-strain term (9.6):

$$T = E S, \tag{9.24}$$

from velocity momentum term (9.7):

$$P = \frac{I_7}{A}\dot{w}, \tag{9.25}$$

and from dynamic equilibrium term (9.14):

$$I_2'' T + 2I_2' T' + (I_2 - I)T'' - \rho A \dot{P} = 0 \tag{9.26}$$

or

$$[(I - I_2)T]'' + \rho A \dot{P} = 0 \tag{9.27}$$

The above Eq. (9.27) is the equation of motion. Substitution for T and P can be made in terms of displacement w by using Eqs. (9.23–9.27). The resulting equation of motion is

$$E[(I - I_2)(Q_1 w'' + Q_2 w' + Q_3 w)]'' + \rho I_7 \ddot{w} = 0 \tag{9.28}$$

where the various integrals over the cross section A have been defined as:

$$I = \int_A z^2 dA, I_2 = \int_A z dA, I_4 = \int_A z^2 f'' dA, I_5 = \int_A z^2 f' dA$$
$$I_6 = \int_A z^2 (1 + f) f dA, I_7 = \int_A [1 + f(x,z) dA,$$
$$Q_1(x) = I_6/(I - 2I_2), Q_2(x) = 2I_5/(I - 2I_2), Q_3(x) = I_4/(I - 2I_2)$$

Equation (9.28) is the differential equation expressing the consistent beam behaviour for generally distributed displacement field. The boundary conditions appropriate to equation of motion (9.28) are obtained by equating surface integral (9.20) of Eq. (9.1), to zero with prescribed external forces, and equivalent surface integral (9.22) to zero with prescribed displacements.

From Eq. (9.28) it can be seen that the displacement disturbance factor $f(x,z)$ affects the displacement $w(x,t)$ through the function $I_7(x)$ directly. The displacement disturbance factor $f(x,z)$ will be evaluated by fracture mechanics methods available in the literature, in the next paragraph.

If there are no cracks in the beam, the functions f, I_2, I_4, I_5, Q_2, Q_3 are zero, Q_1 is unity and function I_7 is replaced by area A. The equation of motion (9.28) will then reduce to [3]

$$EI\ \partial^4 w(x,t)/\partial x^4 + A\rho\ \partial^2 w(x,t)/\partial t^2 = 0. \tag{9.29}$$

9.2.2 The Crack Disturbance Function

For the redistribution of stress in a structural member due to the presence of a crack or notch, linear-elastic stress analysis methods have been used. The high

elevation of stresses in the vicinity of the crack tip, which usually is accompanied by some plasticity and other non-linear effects, is confined within a linear elastic field surrounding the crack tip [36–43] The influence of crack surfaces on stress distribution in the vicinity of the crack tip prevails against remote stress-free surfaces. Other loading forces and boundary conditions have a lesser effect on the intensity of this local stress field.

Griffith's concept, relating fracture stress to crack size, for brittle materials lay the foundations of fracture mechanics as [36–40]:

$$\sqrt{GE} = \sigma\sqrt{\pi\alpha} \tag{9.30}$$

where E is Young's modulus, G is strain energy release rate, σ is applied stress, and a is crack's half-length. The energy release rate is the amount of energy, per unit length along the crack edge, supplied by the elastic energy in the body and by the loading system in creating the new fracture surface area.

Stress fields near crack tips are divided in three basic types, the opening mode *I*, the sliding mode *II*, and the tearing mode *III*, each associated with a local mode of deformation (Fig. 7.1). By the superposition of these three modes, the most general case of local crack-tip deformation and stress fields is sufficiently described.

Irwin's relationship for energy release rate in terms of stress intensity factors [1, 2]:

$$G = G_I + G_{II} + G_{III} = \frac{1}{E'}\left(K_I^2 + K_{II}^2 + \frac{K_{III}^2}{1-v}\right) \tag{9.31}$$

provides the means to describe the redistribution of load paths for transmitting force past a crack through the parameters K_{I}, K_{II}, K_{III}, the crack tip stress field intensity factors for the corresponding three modes of fracture. Two different models for the stress intensity factor for plane stress and plane strain exist, and their values are determined by the other boundaries of the structural element and the loads imposed. A complete stress analysis of a given configuration and loading yields their evaluation [35–40].

In order to establish the local flexibility matrix of the cracked part for the prismatic beam shown in Fig. 9.1, the additional displacement u_i along the direction of the force $P_{i,}$ due to the presence of a transverse surface crack of uniform depth a under general loading will be considered. Under general loading, applying Castigliano's theorem Paris equation [36–40] relates the additional displacement and strain energy release rate as:

$$u_i = \frac{\partial}{\partial P_i}\int_0^a J(\alpha)dy \tag{9.32}$$

where: *J(a)* is strain energy release rate and P_i the corresponding load. *J(a)* depends on crack depth and applied generalized forces responsible for the different mode of fracture (opening, shearing or tearing). For general loading of the cracked cross section, strain energy release rate for plane strain is defined as:

$$J(\alpha) = \frac{1-v^2}{E}\left[\left(\sum_{i=1}^{6} K_{Ii}\right)^2 + \left(\sum_{i=1}^{6} K_{IIi}\right)^2 + (1+v)\left(\sum_{i=1}^{6} K_{IIIi}\right)^2\right] \tag{9.33}$$

where: E is Young modulus, v Poisson's ratio, and K Stress Intensity Factors (SIF) for fracture modes *I, II, III* respectively. The stress intensity functions depend on the cracked section geometry and the loads applied.

From Paris equation the local flexibility matrix $[c_{ij}]$ per unit width has components

$$c_{ij} = \frac{\partial u_i}{\partial P_j} = \frac{\partial^2 u_i}{\partial P_i \partial P_j}\int_0^a J(\alpha)dy \tag{9.34}$$

A simply supported cracked beam of length L_0 as shown in Fig. 9.1 is loaded with a bending moment M. The cross sectional width and height are b and h respectively. The crack is located at the lower edge of the beam at $x = L$. The lateral displacement w_0 and the axial displacement u_0 at the free end of the uncracked beam are [35, 42]:

$$w_0 = M/2EI\left(L_0^2 + v\left(h^2/4\right)\right), u_0 = -hML_0/2EI \tag{9.35}$$

Under general loading, the additional displacements w^*, u^* and θ^* due to the presence of the initial moment M and the crack, will be computed by Castigliano's theorem. If U_T is strain energy due to the crack, Castigliano's theorem demands that additional rotation θ^* is:

$$\theta^* = \partial U_T/\partial M \tag{9.36}$$

due to the initial moment M and the crack. The strain energy U_T and the strain energy density J_s have respectively the form[29–32]:

$$U_T = \int_0^a \frac{\partial U_T}{\partial a}da = b\int_0^a J_s da \tag{9.37}$$

where b is beam thickness, and strain energy density J_s has the general form

$$J_s = \frac{K_I^2}{E'} = \frac{1-v^2}{E}\sigma_0^2 \pi a F_I^2(\alpha) \tag{9.38}$$

for plane strain, K_I is stress intensity factor, E and v are Young modulus and Poisson's ratio respectively, and $E' = E/(1-v^2)$.

The stress intensity factor for a single-edge cracked beam specimen under pure bending M (Fig. 9.1), is [29, 30]:

$$K_I = \sigma_0 \sqrt{\pi\alpha} \cdot F_I(\alpha) \tag{9.39}$$

where, $\sigma_0 = 6M/bh^2$, $\alpha = a/h$, and $F_1(\alpha) = 1.12 - 1.40\alpha + 7.33\alpha^2 - 13.1\alpha^3 + 14.0\alpha^4$. $F_1(\alpha)$ has an accuracy of ± 0.2 % for $a/h \leq 0.6$, b is thickness, and h is height of the cross-section of the beam. Then, Eq. (9.37) yields

$$b \int_0^a J_s(a)da = bh^2 \frac{(1-\nu^2)}{E} \left(\frac{6M}{bh^2}\right) \pi \Phi_1(a) e^{i\theta} \tag{9.40}$$

where $\Phi_I(a) = 0.6272a^2 - 1.04533a^3 + 4.5948a^4 - 9.9736a^5 + 20.2948a^6 - 33.0351a^7 + 47.1063a^8 - 40.7556a^9 + 19.6a^{10}$ and hence, the additional rotation θ^* will be:

$$\theta^* = \partial U_T / \partial M = 72\pi(1-\nu^2) M \Phi_I(\alpha)/Ebh^2 \tag{9.41}$$

or

$$\theta^* = 6\pi(1-\nu^2) Mh \Phi_I(\alpha)/EI \tag{9.42}$$

On the other hand, assuming that u_0 and u^* are the total elongation of the lower surface of the beam due to the bending moment and the existence of the crack respectively, the following geometric relations hold

$$\theta^*/\theta_0 = u^* |x - L - L_0/2|/L_0 h \tag{9.43}$$

where $\theta_0 = L_0 M/EI$ and consequently

$$\theta^* = 2u^*/|x - L - L_0/2|/L_0 h \tag{9.44}$$

From Eq. (9.2) it is

$$u^* = -zf' w_0 \tag{9.45}$$

Consequently, the crack disturbance derivative will be:

$$f' = -3\pi\left(1-\nu^2\right) h^2 \Phi_I(\alpha)(x - L - L_0/2)/zL_0\left(L_0^2 + \nu h^2/4\right) \tag{9.46}$$

Integrating Eq. (9.46) yields the crack disturbance function:

$$f = -3\pi\left(1-\nu^2\right) h^2 \Phi_I(\alpha)(x - L - L_0/2)^2/zL_0\left(L_0^2 + \nu h^2/4\right) \tag{9.47}$$

where $a = a/h$.

Combining the above Eqs. (9.46) and (9.47) with the systems of Eqs. (9.8–9.10), the frequency shifting ratio can be calculated for cracked Euler-Bernoulli beam with different boundary conditions and varying crack depth a.

9.2.3 Natural Frequencies of Cracked Beams

Let a beam as in Fig. 9.1, with an open-edge crack at a distance L from the left end. The differential Eq. (9.28) for the natural modes can be written as [23]:

$$c_0^2\left[(I_7 w)^{iv}\right] + I_7 \ddot{w} = 0 \tag{9.48}$$

where $c_0^2 = EI/(\rho A)$ material constant, and I the appropriate area moment.

By separation of variables, the general solution of Eq. (9.28) can be set as

$$w(x,t) = W(x)T(t) \tag{9.49}$$

Substituting it into the above partial differential Eq. (9.48), the following equation yields

$$c_0^2\left\{\partial^4\left[\frac{I_7(x)W(x,t)}{\partial x^4}\right]\right\}T = [I_7(x)W(x)]\frac{\partial^2 T}{\partial t^2} = 0 \tag{9.50}$$

From Eq. (9.50) two ordinary differential equations are derived,

$$[I_7(x)W(x)]^{iv} + \left(\frac{\omega_n^*}{c_0}\right)^2 [I_7(x)W(x)] = 0 \tag{9.51}$$

and

$$\ddot{T} + \omega_n^{*2} T = 0 \tag{9.52}$$

where $\omega_{\mathrm{n}}*$ are natural frequencies of cracked beam.

Equation (9.51) is the differential equation for the natural modes of vibration considering the beam as a continuous system while, Eq. (9.53) corresponds to the breathing crack problem [26]. The general solution of Eq. (9.51) for a continuous cracked beam with an open crack is [23]:

$$\begin{aligned} W(x) = {} & G_n\left(\cos\beta_{\mathrm{n}}^* x + \cosh\beta_{\mathrm{n}}^* x\right) + H_n\left(\cos\beta_{\mathrm{n}}^* x - \cosh\beta_{\mathrm{n}}^* x\right) \\ & + A_n\left(\sin\beta_{\mathrm{n}}^* x + \sinh\beta_{\mathrm{n}}^* x\right) + D_n\left(\sin\beta_{\mathrm{n}}^* x - \sinh\beta_{\mathrm{n}}^* x\right) \end{aligned} \tag{9.53}$$

where $\omega_n* = c_o\beta_n^{*2}$ are natural frequencies of the cracked beam, $c_0^2 = EI/(\rho A)$ is material constant, and I the appropriate second area moment. G_{n}, H_{n}, A_{n}, and D_{n} are unknown constants. For the cracked beam with a crack the natural modes of vibration become:

$$w(x) = I_7(x)W(x) \tag{9.54}$$

where I_7(x) is related to the crack disturbance function $f(x,z)$, evaluated earlier with fracture mechanics methods.

The boundary conditions appropriate to the equation of motion (9.28), for beams with different end-conditions, are summarized as:

1. simply supported beam, zero deflection and shear forces at both ends of the beam, i.e.

$$w|_{x=0} = 0, \partial^2 w/\partial x^2|_{x=0} = 0, w|_{x=Lo} = 0, \partial^2 w/\partial x^2|_{x=Lo} = 0 \tag{9.55}$$

2. cantilever beam, zero deflection and slope at the clamped end and zero moments and shear forces at the free end of the beam:

$$w|_{x=0} = 0, \partial w/\partial x|_{x=0} = 0, \partial^2 w/\partial x^2|_{x=Lo} = 0, \partial^3 w/\partial x^3|_{x=Lo} = 0 \tag{9.56}$$

3. free-free beam, zero moments and shear forces at both ends of the beam:

$$\partial^2 w/\partial x^2|_{x=0} = 0, \partial^3 w/\partial x^3|_{x=0} = 0, \partial^2 w/\partial x^2|_{x=Lo} = 0, \partial^3 w/\partial x^3|_{x=Lo} = 0 \tag{9.57}$$

Similarly, for clamped–clamped beam, zero deflection and slope at both ends of the beam.

The set of Eqs. (9.55–9.57) possess a solution if the determinant of the coefficients of the unknowns G_n, H_n, A_n and D_n is zero.

The set of Eqs. (9.55–9.57) can be solved directly for the exact solution β^*_n through a numerical method and results are shown in Figs. 9.2, 9.3 and 9.4.

For the simply supported cracked beam, the boundary conditions at $x = 0$ and $x = L_0$ yield the characteristic equation

$$I_7'(L_0)/I_7(L_0)\left[\cos(\beta_n^* L_0) - \sin(\beta_n^* L_0)\mathrm{cth}(\beta_n^* L_0)\right] + \beta_n^* \sin(\beta_n^* L_0) = 0 \tag{9.58}$$

This implicit natural frequency Eq. (9.58) is solved directly for an exact solution β_n^* through a numerical method or solved analytically and results are shown in Fig. 9.2. Results from a simply supported beam with a breathing crack, found with a perturbation method, are also shown in Fig. 9.2 for comparison [26].

Results for a cracked cantilever beam, with boundary conditions described by the set of Eq. (9.56) and application of the variational theorem, are shown in Fig. 9.3, along with results from a lumped crack flexibility approach presented below (Eq. 9.66).

Similarly, the results of the above analysis, for a cracked free-free beam, with open cracks, and boundary conditions described by the set of Eq. (9.57) are shown in Figs. 9.4, 9.5 and 9.6 for the first three natural frequencies, along with results from a lumped crack flexibility approach presented below (Eq. 9.67). Continuous beam theory results agree well with experimental data for crack depths up to 60 %.

Results shown in Figs. 9.4, 9.5 and 9.6 refer to aluminium 2024-T351 beam, length 0.235 m, cross-section width 0.007 m, cross-section height 0.023 m, $E = 7.2E10\ N/m^2$, material density 2,800 kg/m^3 and Poisson's ratio 0.35.

9.2.4 The Beam with Lumped Crack Flexibility

The above procedure distributes the flexibility added due to the crack over the length of the beam. For comparison, the natural frequencies of a cracked beam,

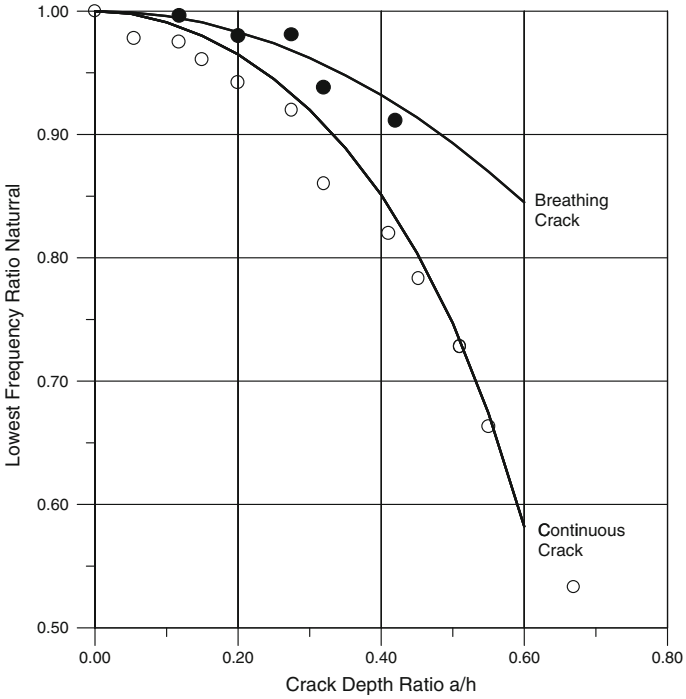

Fig. 9.2 Lowest transverse natural frequency ratio ω_1^*/ω_1 for a simply supported aluminum beam with a surface crack at 40 % of span, versus the crack depth ratio $\alpha = a/h$. Analytical results: Continuous crack model, Eqs. (9.55, 9.58). Breathing crack from Ref. [26]. Experimental results *small circles*

considering the crack as a local flexibility, as previously reported in the literature was found [23–27]. The local flexibility can be found from Eq. (9.36) as

$$c = 6\pi\left(1 - \nu^2\right)h\Phi_I(\alpha)/EI \tag{9.59}$$

Assuming that the effect of the crack is apparent in its neighbourhood, the beam can be treated as two uniform beams, connected by a torsional spring of local flexibility c at crack location. Considering the modes of harmonic vibration on the two segments of the beam, left and right of the crack respectively, an alternative configuration for the mode shapes will be employed as follows:

With harmonic flexural vibration of Euler–Bernoulli beams, the dimensionless equation of motion for a uniform beam of rectangular cross-section (Fig. 9.1) is given as [3]:

$$EI\frac{d^4W(X)}{dX^4} - \Omega^2 W(X) = 0 \tag{9.60}$$

where the non-dimensional variables are defined as $X = x/L_0$, $\Omega^2 = \omega_i^2 \mathrm{A} L_0^4 \rho/EI$, x the crack position from the beam left end, L_0 the length of the beam, ρ = mass of

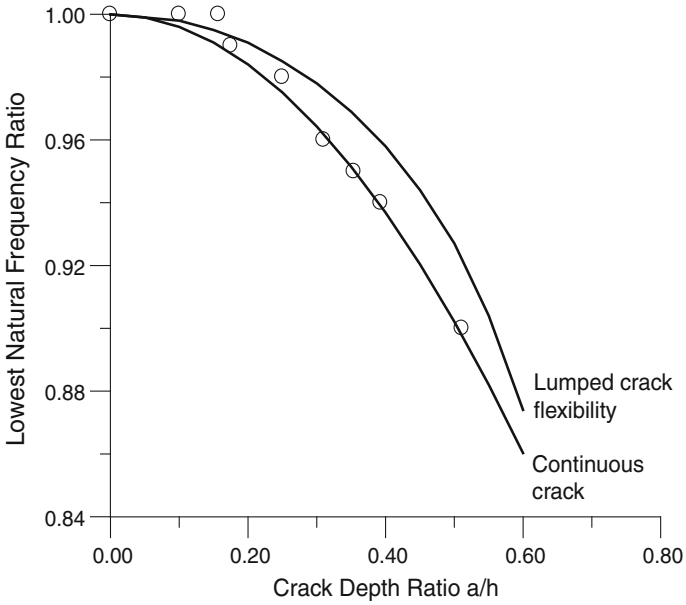

Fig. 9.3 Lowest transverse natural frequency ratio $\omega 1^*/\omega 1$ for a cantilever aluminum beam with a surface crack at 40 % of span, versus the crack depth ratio $\alpha = a/h$. Analytical results: Continuous crack model, Eq. (9.56). Lumped crack model, Eq. (9.66). Experimental results *small circles*

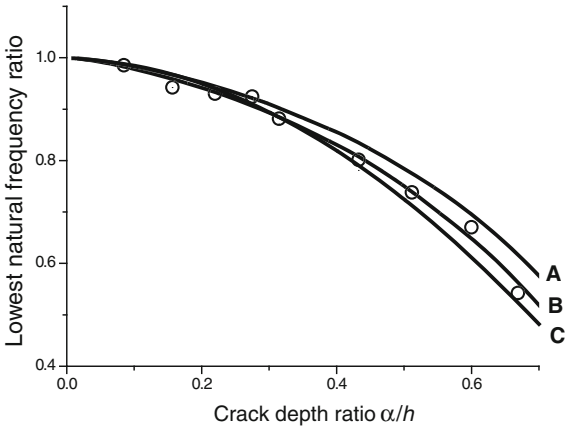

Fig. 9.4 Lowest transverse natural frequency ratio ω_1^*/ω_1 for a free-free aluminum beam with a surface crack at 40 % of span, versus the crack depth ratio Analytical results: *A* lumped crack model, Eq. (9.67), *B* continuous crack model, Eqs. (9.51, 9.56), *C* FEA model, Eq. (9.8). Experimental results *small circles*

the beam per unit length (kg/m), ω_i natural frequency of the *i*th mode (rad/sec), E = modulus of elasticity (N/m^2) and I the area moment of inertia for the beam cross-section (m^4).

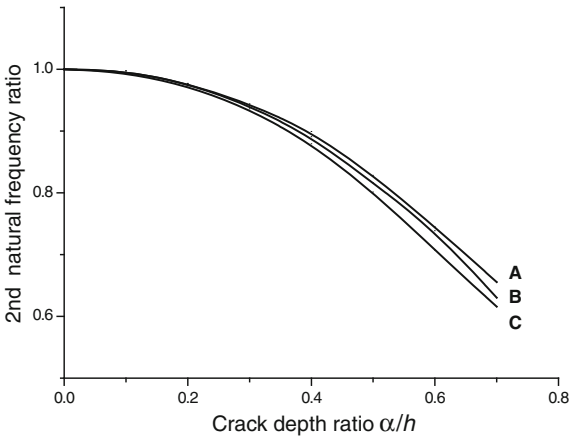

Fig. 9.5 Second transverse natural frequency ratio $\omega 2^*/\omega 2$ for a free-free aluminum beam with a surface crack at 40 % of span, versus the crack depth ratio $\alpha = a/h$. Analytical results: *A* lumped crack model, Eq. (9.67), *B* continuous crack model, Eqs. (9.51 and 9.56), *C* FEA model, Eq. (9.68)

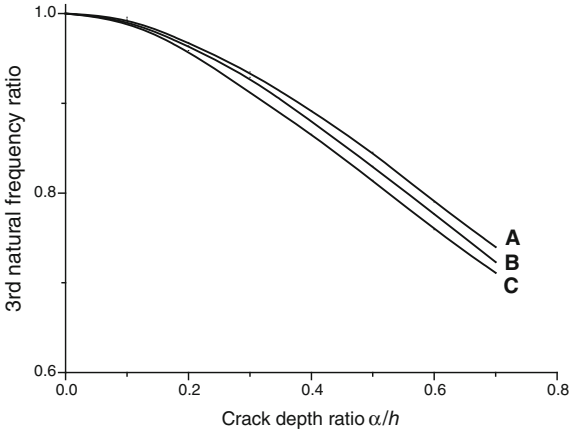

Fig. 9.6 Third natural frequency ratio $\omega 3^*/\omega 3$ for a free-free aluminum beam with a surface crack at 40 % of span, versus the crack depth ratio $\alpha = a/h$. Analytical results: *A* lumped crack model, Eq. (9.67), *B* continuous crack model, Eqs. (9.51), (9.56), *C* FEA model, Eq. (9.68)

Solution of Eq. (9.60) is given by

$$W(X) = A\cos\lambda X + B\sin\lambda X + C\cosh\lambda X + D\sinh\lambda X \tag{9.61}$$

If the bending mode of vibration dominates as in the present study, the crack is modeled as a torsional spring with a lumped flexibility c. Based on this model, the beam is divided into two segments: the left part before the crack and the right after the crack. The cracked beam is modeled by applying Eq. (9.61) to each segment of the crack independently. Then, the mode shapes for both segments of the beam as illustrated in Fig. 9.1 are:

$$W_1(X) = A_1\cos\lambda X + B_1\sin\lambda X + C_1\cosh\lambda X + D_1\sinh\lambda X \tag{9.62}$$

$$W_2(X) = A_2\cos\lambda X + B_2\sin\lambda X + C_2\cosh\lambda X + D_2\sinh\lambda X \tag{9.63}$$

In order to use Eqs. (9.62 and 9.63) for the purposes of crack identification the following assumptions are made: (1) The crack is open. As a result of this assumption the crack is replaced by a torsional spring. (2) The open-edge crack is uniform in propagation over the surface of one side of the specimen. (3) shear deformation and rotary inertia effects are ignored.

The eight unknown coefficients in the set of Eqs. (9.62 and 9.63) can be found by substituting this solution into the boundary conditions. Assuming constant properties along the beam, in addition to the boundary conditions as described in Eqs. (9.55–9.57), the continuity conditions at the crack position require equal displacements, moments and shear forces at both ends of the crack. Defining a non-dimensional crack position parameter measured from the left end $\xi = L/L_0$, where L_0 is the total beam length (m), and L is the distance from the left end of the beam to the crack location, an additional boundary condition simulating the torsional spring crack model follows:

$$\partial W_2(X)/\partial X|_{x=\xi} - \partial W_1(X)/\partial X|_{x=\xi} = (EIc/L)\partial^2 W_1(X)/\partial X^2|_{x=\xi} \tag{9.64}$$

where EIc/L is the dimensionless cracked section flexibility.

The boundary conditions result in a set of homogeneous linear algebraic equations for the unknown coefficients in Eqs. (9.62 and 9.63).

For a nontrivial solution the determinant for the unknown coefficients must be zero, thus providing the natural frequency equation for the beam with lumped crack flexibility as shown in Figs. (9.2, 9.3, 9.4), based on the assumption that the crack flexibility does not depend on the frequency of vibration.

Assuming that the effect of the crack is apparent in its neighbourhood only, the beam can be treated as two uniform beams, connected by a torsional spring of local flexibility c at crack location. If constant properties along the beam are considered, from the boundary conditions for the left and right parts of the beam the natural frequency equations for the beams with lumped crack flexibility yield:

1. simply supported beam

$$\begin{aligned} &4\sin\lambda L_0 \sinh\lambda L_0 + \lambda L_0 EIc/L)[\sinh\lambda L_0(\cos\lambda L_0 - \cos\beta\lambda L_0) \\ &+\sin\lambda L_0(\cosh\lambda L_0 - \cosh\beta\lambda L_0)] = 0 \end{aligned} \tag{9.65}$$

   where EIc/L is the dimensionless cracked section flexibility, $\beta = (L - L_0/2)/(L/2)$ a dimensionless crack location measured from mid-point. Equation (9.65) is solved with the aid of *Mathematica* to yield natural frequencies λ_{Ln} as shown in Fig. (9.2).
2. cracked cantilever beam:

$$\begin{bmatrix} \sin\lambda\xi - \sinh\lambda\xi & \cos\lambda\xi - \cosh\lambda\xi & \sin\lambda(1-\xi) + \sinh\lambda(1-\xi) & \cos\lambda(1-\xi) + \cosh\lambda(1-\xi) \\ -\sin\lambda\xi - \sinh\lambda\xi & -\cos\lambda\xi - \cosh\lambda\xi & -\sin\lambda(1-\xi) + \sinh\lambda(1-\xi) & -\cos\lambda(1-\xi) + \cosh\lambda(1-\xi) \\ -\cos\lambda\xi - \cosh\lambda\xi & \sin\lambda\xi - \sinh\lambda\xi & \cos\lambda(1-\xi) - \cosh\lambda(1-\xi) & -\sin\lambda(1-\xi) + \sinh\lambda(1-\xi) \\ \cos\lambda\xi - \cosh\lambda\xi + & -\sin\lambda\xi - \sinh\lambda\xi + & -\cos\lambda(1-\xi) - \cosh\lambda(1-\xi) & -\sin\lambda(1-\xi) - \sinh\lambda(1-\xi) \\ \lambda EIc(-\sin\lambda\xi - \sinh\lambda\xi) & \lambda EIc(-\cos\lambda\xi - \cosh\lambda\xi) & & \end{bmatrix} \tag{9.66}$$

where $\xi = L/L_o$.

3. free–free beam:

$$\begin{pmatrix} 0 & -1 & 0 & 1 & 0 & 0 & 0 & 0 \\ -1 & 0 & 1 & 0 & 0 & 0 & 0 & 0 \\ -\sin\lambda\xi & -\cos\lambda\xi & \sinh\lambda\xi & \cosh\lambda\xi & \sin\lambda\xi & \cos\lambda\xi & -\sinh\lambda\xi & -\cosh\lambda\xi \\ -\cos\lambda\xi & \sin\lambda\xi & \cosh\lambda\xi & \sinh\lambda\xi & \cos\lambda\xi & -\sin\lambda\xi & -\cosh\lambda\xi & -\sinh\lambda\xi \\ \cos\lambda\xi & -\sin\lambda\xi & \cosh\lambda\xi & \sinh\lambda\xi & -\cos\lambda\xi & \sin\lambda\xi & -\cosh\lambda\xi & -\sinh\lambda\xi \\ -\lambda EIc\sin\lambda\xi & -\cos\lambda\xi & +\lambda EIc\sinh\lambda\xi & +\lambda EIc\cosh\lambda\xi & & & & \\ \sin\lambda\xi & \cos\lambda\xi & \sinh\lambda\xi & \cosh\lambda\xi & -\sin\lambda\xi & -\cos\lambda\xi & -\sinh\lambda\xi & -\cosh\lambda\xi \\ 0 & 0 & 0 & 0 & -\sin\lambda L_0 & -\cos\lambda L_0 & \sinh\lambda\xi & \cosh\lambda\xi \\ 0 & 0 & 0 & 0 & -\cos\lambda L_0 & \sin\lambda L_0 & \cosh\lambda\xi & \sinh\lambda\xi \end{pmatrix} \quad (9.67)$$

Equations (9.66) and (9.67) were solved numerically to yield the natural frequencies for the lumped crack flexibility model. Figures (9.3, 9.4, 9.5, and 9.6) show the numerical solutions for the lumped crack flexibility approach and experimental results with aluminum beams.

9.2.5 The Finite Element Method

A parametric Finite Element model is here developed for the numerical prediction of the dynamic response of the cracked beam based on the commercial code ANSYS [44]. The model can be modified accordingly in order to analyse different beam geometrical configurations and varying crack locations and depth. The Finite Element (FE) formulation of an Euler-Bernoulli cracked beam using three-dimensional solid elements, leads to a set of linear algebraic equations of the form [41]:

$$[\mathbf{M}]^s\{\ddot{\mathbf{q}}\}^S + [\mathbf{C}]^s\{\dot{\mathbf{q}}\}^S + [\mathbf{K}]^s\{\mathbf{q}\} = \{\mathbf{f}\}^S \quad (9.68)$$

where, $[\mathbf{M}]^S$, $[\mathbf{C}]^S$ and $[\mathbf{K}]^S$ are mass, damping and stiffness matrices for the vibrating system and $\{\mathbf{q}(t)\}$ the response of a cracked free-free beam in a stationary coordinate system. The damping part of Eq. (9.68) is neglected, i.e. undamped vibration is considered. For the solution of Eq. (9.68), a linearized three-dimensional finite element model of the cracked beam was developed. The FE mesh of the considered crack rod is developed using FE software ANSYS [44] and the non-singular 8-node brick element 'solid 45', which has three degrees of freedom per node, i.e., the displacements in the x, y and z directions. The crack is modelled by assuming the corresponding nodes of the two crack surfaces to deform independently. The crack surfaces are modelled using double nodes identical in location but topologically belong to the two different crack faces.

9.2.6 Experimental Procedure

A fatigue crack growth technique in resonating aluminium cantilever beams was used for the development of a series of cracked specimens for the experimental verification of the proposed method. Homogeneous prismatic straight aluminium

(2024-T351) beams with cross-sectional height $h = 0.0254$ m and cross-sectional width $b = 0.006$ m were prepared. A small notch was introduced to serve as a crack initiation point and the bar was subsequently transversely vibrated at its fundamental lateral natural frequency to force a crack formation and propagation. 30 different specimens were vibrated at different numbers of cycles so that different crack lengths would be obtained. When the desired crack depth was reached, the beam was taken out of the vibrating table and the crack depth was measured to both sides of the beam. Crack depths obtained were varying from 5 to 60 % of the cross-section height.

Each specimen of length $L = 235$ mm was supported at its ends to obtain the appropriate boundary conditions: simply supported, cantilever, or free-free. The crack was positioned at mid-span and facing downwards. A small static load was put opposite the crack to ensure that the crack remains open during vibration. This static load decreased the measured natural frequencies by 1.5 % Vibration measurements were acquired through 1 gr miniature accelerometer put at the opposite side of the crack face. The beam was lightly tapped with a miniature hammer and the resulting vibration signal was recorded. The vibration frequency was calculated by measuring time elapsed for 50 cycles of vibration. Moreover, an FFT transform was performed at the stored signal for an independent measurement of the flexural natural frequencies. The magnitude of the forcing force was kept low to avoid generating higher harmonics caused by geometric and material nonlinearities. However, the transverse excitation produces longitudinal vibration. This coupling does not affect the flexural natural frequencies, although it produced additional peaks on the frequency-response function due to cross-axis sensitivity of the accelerometer. Longitudinal vibration frequencies are well above the flexural vibration frequencies and were easily identified. Experimental results are shown in Figs. (9.2, 9.3, and 9.4) with small circles.

9.3 Torsional Vibration of a Continuous Cracked Rod

9.3.1 The Variational Theorem for a Cracked Rod in Torsion

The first complete statement of the dynamic problem of torsion was made by Saint-Venant who assumed that the displacement field consisted of a rotation of the cross–section along with the warping of the section out of its plane. Only shear stresses in the plane of the sections were considered. Although Saint-Venant takes into account the warping displacement, his theory neglects the longitudinal stress and inertia arising from this stress. Since then, there have been extensive studies in the theory of torsional vibration of shafts with circular and non-circular cross-section. Hu-Washizu-Barr [30–32] variational principle in linear elasticity was used in Refs. [24–29] for the development of a continuous cracked rod vibration theory. The

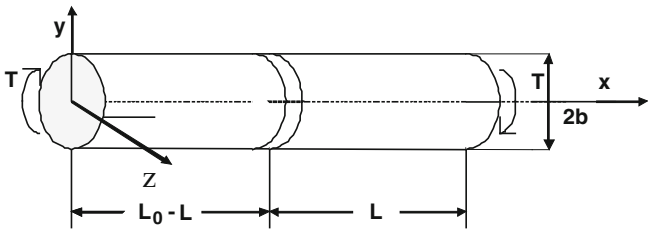

Fig. 9.7 Geometry of a circular cracked rod with a peripheral crack

general variational principle and the independent assumptions about the displacement, the momentum, the strain and the stress fields of the cracked shaft, and the equations of motion for a uniform shaft in torsional vibration, with one or more pairs of transverse symmetrically disposed open edge cracks along its length, were derived. The cracks were modeled as continuous flexibilities using the displacement field in the vicinity of the crack, found with fracture mechanics methods.

A shaft with an open peripheral surface crack is shown in Fig. 9.7. Strain and displacement, stress and strain, and momentum and displacement terms yield in a similar manner to that of Sect. 9.2.1.

To derive the governing equation and applicable boundary conditions for the torsional vibration of a cracked shaft through the variational theorem, Eq. (9.1), the x axis is taken along the center line of the bar, and the yz plane is the plane of the cross-section. Subscripts i, j of the stresses σij take values 1, 2, 3 corresponding to the Cartesian co-ordinates x, y and z, respectively.

Stress and strain fields of the cracked shaft can be obtained by adding the disturbance functions to the stress and strain distributions of the undamaged shaft. Since the distribution of each stress (and the equivalent strain) component is unique, the most general situation will be considered here in which a different disturbance function is added to each component. Thus, the disturbance in the direct components σ_{xx} and γ_{xx} is introduced through a function f_1(x, y, z), the disturbance in the shear components σ_{xy} and γ_{xy} is introduced through a function f_2(x, y, z) and the disturbance in the shear components σ_{xz} and γ_{xz} is introduced through a function f_3(x, y, z). The three crack functions f_1, f_2 and f_3 are all, at present, unknown. As mentioned earlier, Christides and Bar [30] used an empirical exponential function to describe the stress disturbance due to a crack. In this work, the stress disturbance function will be found using fracture mechanics results.

It is further assumed that the presence of the cracks does not alter in any way the displacement fields of the shaft. Finally, the direct strains γ_{yy} and γ_{zz} will be taken as non-zero although the corresponding direct stresses will be assumed zero. For a uniform shaft the following assumptions are made [28–30]:

$$
\begin{aligned}
u &= \Phi(y,z)\theta'(x,t), \upsilon = -z\theta(x,t), w = y\theta(x,t),\\
p_x &= 0, p_y = -zP(x,t), p_z = yP(x,t),\\
\gamma_{xx} &= [\Phi + f_1(x,y,z)]S_1(x,t), \gamma_{yy} = \gamma_{zz} = -v\gamma_{xx},\\
\gamma_{xy} &= \left[\frac{\partial \Phi}{\partial y} - z + f_2(x,y,z)\right] S_2(x,t),\\
\gamma_{xz} &= \left[\frac{\partial \Phi}{\partial z} + y + f_3(x,y,z)\right] S_2(x,t), \gamma_{yz} = 0,
\end{aligned}
\tag{9.69}
$$

$$
\begin{aligned}
\sigma_{xx} &= [\Phi + f_1(x,y,z)]T_1(x,t), \sigma_{yy} = \sigma_{zz} = 0,\\
\sigma_{xy} &= \left[\frac{\partial \Phi}{\partial y} - z + f_2(x,y,z)\right] T_2(x,t),\\
\sigma_{xz} &= \left[\frac{\partial \Phi}{\partial z} + y + f_3(x,y,z)\right] T_2(x,t),\\
\sigma_{yz} &= 0,\\
X_x &= X_y = X_z = 0.
\end{aligned}
$$

In Eqs. (9.69) θ, P, S_1, S_2, T_1 and T_2 are all unknown functions of axial co-ordinate x and time t. The warping function $\Phi(y, z)$ is approximated by that of static torsion and it should satisfy two important conditions [42, 45]:

First, it is a harmonic function, i.e. it satisfies the condition

$$
\frac{\partial^2 \Phi}{\partial y^2} + \frac{\partial^2 \Phi}{\partial z^2} = 0 \tag{9.70}
$$

everywhere in the cross-section. This condition also implies that in case of a doubly symmetrical cross-section, e.g. a circle, an ellipse or a rectangle cross-section, the function $\Phi(y, z)$ is odd in both the y and the z co-ordinates.

Second, the shear stresses σ_{xy} and σ_{xz} of the undamaged shaft (which are functions of Φ) are such that the condition $\sigma_{xy}\, n_y + \sigma_{xz}\, n_z = 0$ is satisfied on the outer surfaces of the shaft, where n_y and n_z are the directional cosines. This condition implies that the resultant shearing stress on the boundary is directed along the tangent to the boundary.

The stress and strain fields in Eq. (9.2) can now be substituted in the general variational Eq. (9.1), and independent variations of the unknowns θ, P, S_1, S_2, T_1 and T_2 can be considered. These independent variations will be considered one by one.

For arbitrary and independent variations δT_1 and δT_2 the strain-displacement term of the general variational Eq. (9.1) becomes

$$\begin{aligned}&\int_v \{[(\phi+f_1)S_1-\phi\theta'']\delta T_1]\\&+\left[\left(\frac{\partial\phi}{\partial y}-z+f_2\right)S_2-\left(\frac{\partial\phi}{\partial y}-z\right)\theta'\right]\left[\left(\frac{\partial\phi}{\partial z}-z+f_2\right)\delta T_2\right]\\&+\left[\left(\frac{\partial\phi}{\partial z}+y+f_3\right)S_2-\left(\frac{\partial\phi}{\partial z}+y\right)\theta'\right]\left[\left(\frac{\partial\phi}{\partial z}+y+f_3\right)\delta T_2\right]\Big\}dV\end{aligned} \tag{9.71}$$

or,

$$\begin{aligned}&\int_v \Big\{\left[\left(\phi^2+2\phi f_1+f_1^2\right)S_1-\left(\phi^2+\phi f_1\right)\theta''\right]\delta T_1\\&+\left[\begin{array}{l}\left\{\begin{array}{c}\left(\frac{\partial\phi}{\partial y}\right)^2+\left(\frac{\partial\phi}{\partial z}\right)^2+(y^2+z^2)+\left(f_2^2+f_3^2\right)\\+2\left(\frac{\partial\phi}{\partial z}y-\frac{\partial\phi}{\partial y}z\right)+2\left(\frac{\partial\phi}{\partial y}f_2+\frac{\partial\phi}{\partial z}f_3\right)+2(yf_3-zf_2)\end{array}\right\}S_2\\-\left\{\left(\frac{\partial\phi}{\partial y}\right)^2+\left(\frac{\partial\phi}{\partial z}\right)^2+(y^2+z^2)+2\left(\frac{\partial\phi}{\partial z}y-\frac{\partial\phi}{\partial y}z\right)+2(yf_3-zf_2)\right\}\\+\left(\frac{\partial\phi}{\partial y}f_2+\frac{\partial\phi}{\partial z}f_3\right)+(yf_3-zf_2)\}\theta'\end{array}\right]\delta T_2\Big\}dV\end{aligned} \tag{9.72}$$

The following integrals are defined over the cross-section A:

$$\begin{aligned}&B(x)=\int_A\left(f_1^2\right)dA, && C(x)=\int_A\left(f_2^2+f_3^2\right)dA,\\&D(x)=\int_A\left(\frac{\partial\phi}{\partial y}f_2+\frac{\partial\phi}{\partial z}f_3\right)dA, && F(x)=\int_A(\phi f_1)dA,\\&M(x)=\int_A(yf_3-zf_2)dA, && J(x)=\int_A(y^2+z^2)dA,\\&K=\int_A\left[\left(\frac{\partial\phi}{\partial y}\right)^2+\left(\frac{\partial\phi}{\partial z}\right)^2\right]dA, && L=\int_A\left(\frac{\partial\phi}{\partial z}y-\frac{\partial\phi}{\partial y}z\right)dA,\\&R=\int_A\left(\phi^2\right)dA\end{aligned} \tag{9.73}$$

In Eq. (9.73), ϕ represents the warping function of static torsion, and $K=-\mathrm{L}$ [30, 45]. Integrating over the cross-section of the shaft, the strain-displacement term (9.72) reduces to

$$\begin{aligned}&\int_x\{[(R+2F+B)S_1-(R+F)\theta'']\delta T_1\\&\quad+[(L+J+C+2D+2M)S_2-(L+J+D+M)\theta']\delta T_2\}dx.\end{aligned} \tag{9.74}$$

9.3.1.1 Stress-Strain and Velocity-Momentum Terms

For the torsion problem the stress-strain term in Eq. (9.1) is given by:

$$\int_V \left\{ \left[\sigma_{xx} - \frac{\partial W}{\partial \tilde{a}_{xx}}\right]\delta\gamma_{xx} - \left(\frac{\partial W}{\partial \gamma_{yy}}\delta\gamma_{yy}\right) - \left(\frac{\partial W}{\partial \tilde{a}_{zz}}\delta\gamma_{zz}\right) + \left[\sigma_{xy} - \frac{\partial W}{\partial \tilde{a}_{xy}}\right]\delta\gamma_{xy} + \left[\sigma_{xz} - \frac{\partial W}{\partial \tilde{a}_{xz}}\right]\delta\gamma_{xz}\right\} \mathrm{d}V \tag{9.75}$$

where

$$W = 1/2\lambda e^2 + G\left(\gamma_{xx}^2 + \gamma_{yy}^2 + \gamma_{zz}^2\right) + 1/2G\left(\gamma_{xy}^2 + \gamma_{yz}^2 + \gamma_{xz}^2\right),$$

$e = \gamma_{xx} + \gamma_{yy} + \gamma_{zz}$, is dilatation, $G = E/(2(1+v))$ shear modulus, and $\lambda = vE/((1+v)(1-2v))$ Lame's constant. Then, the stress-strain term (9.75) simplifies to:

$$\int_V \left\{ [\sigma_{xx} - E\gamma_{xx}]\delta\gamma_{xx} + \left[\sigma_{xy} - G\gamma_{xy}\right]\delta\gamma_{xy} + \left[\sigma_{xz} - G\gamma_{xz}\right]\delta\gamma_{xz}\right\} dV \tag{9.76}$$

Substituting the assumptions (9.69) into stress-strain term (9.76), yields

$$\int_v \left\{ \left[(\phi + f_1)^2 (T_1 - ES_1)\right]\delta S_1 + \left[(T_2 - GS_2)\left\{ \left(\frac{\partial \phi}{\partial y} - z + f_2\right)^2 + \left(\frac{\partial \phi}{\partial z} + y + f_3\right)^2 \right\}\delta S_2\right] dV$$

which, after expanding the squared terms and integrating over the cross-section, the stress-strain term becomes

$$\int_x \left\{ \left[(R + 2F + B)\left(T_1 - ES_1\right)\right]\delta S_1 + \left[(L + J + C + 2D + 2M)\left(T_2 - GS_2\right)\right]\right\} \mathrm{d}x \tag{9.77}$$

In a similar way, the velocity-momentum term becomes

$$\int_x \left\{\rho J\left(\dot{\theta} - p\right)\delta p\right\} dx \tag{9.78}$$

where J is the polar second moment of area of the section.

9.3.1.2 Dynamic Equilibrium Term

The first term of Eq. (9.1) provides the equation of motion. For the torsional problem, and the assumptions of Eq. (9.69) this term becomes

$$\int_V \left\{ \left[\frac{\partial \sigma_{xx}}{\partial x} + \frac{\partial \sigma_{xy}}{\partial y} + \frac{\partial \sigma_{xz}}{\partial z}\right]\delta u + \left[\frac{\partial \sigma_{xy}}{\partial x} - \rho \dot{p}_y\right]\delta \upsilon + \left[\frac{\partial \sigma_{xz}}{\partial x} - \rho \dot{p}_z\right]\delta w \right\} dV \tag{9.79}$$

After proper substitutions, term (9.89) becomes

$$\int_V \left\{ \left[\phi \frac{\partial \sigma_{xx}}{\partial x} - \sigma_{xy}\frac{\partial \phi}{\partial y} - \sigma_{xz}\frac{\partial \phi}{\partial z}\right]\delta\theta' + \left[\frac{\partial \sigma_{xy}}{\partial x} - \rho \dot{p}_y\right]\delta \upsilon + \left[\frac{\partial \sigma_{xz}}{\partial x} - \rho \dot{p}_z\right]\delta w \right\} dV \tag{9.80}$$

Stresses and moments from Eq. (9.69) are substituted in (9.80) yielding the dynamic equilibrium term as

$$\int_V \left\{ \begin{array}{l} \left[\phi\{(\phi + f_1)T_1\}' - \left\{\frac{\partial \phi}{\partial y}\left(\frac{\partial \phi}{\partial y} - z + f_2\right) + \frac{\partial \phi}{\partial z}\left(\frac{\partial \phi}{\partial z} + y + f_3\right)\right\}T_2\right]\delta\theta' \\ + \left[-z\left\{\left(\frac{\partial \phi}{\partial y} - z + f_2\right)T_2\right\}' + \left\{y\left(\frac{\partial \phi}{\partial z} + y + f_3\right)T_2\right\}' - \rho\dot{p}\left(y^2 + z^2\right)\right]\delta\theta \end{array} \right\} dV \tag{9.81}$$

Differentiations with respect to x are performed first, and then the whole term is integrated over the cross–section yielding

$$\int_x \left\{ \left[(R+F)T_1' + F'T_1 - DT_2\right]\delta\theta' + \left[(L+J+M)T_2' + M'T_2 - \rho J\dot{p}\right]\delta\theta \right\} dx \tag{9.82}$$

Noting that $\delta\theta' = \partial(\delta\theta\}/\partial x$, the first term of (9.82) is integrated by parts over x as follows

$$\begin{aligned} &\int_x \left\{ [(R+F)T_1 + F'T_1 - DT_2]\frac{\partial}{\partial x}(\delta\theta)dx \right. \\ &= \left[\left\{F'T_1 + (R+F)T_1' - DT_2\right\}\delta\theta\right]_{x=0}^{x=L} \\ &\left. - \int_x \left\{F''T_1 + 2F'T_1'(R+F)T_1'' - D'T_2 - DT_2'\right\}\delta\theta dx \right. \end{aligned} \tag{9.83}$$

where the shaft length is L_0 with the x origin at one end. Substituting this result into (9.82) the latter provides the equation of motion term

$$\int_x \left\{ -F''T_1 - 2F'T_1' - (R+F)T_1'' + (D'+M')T_2 + (L+J+D+M)T_2' - \rho J\dot{p}\right\}\delta\theta dx \tag{9.84}$$

along with the boundary term

$$\left[\left\{F'T_1 + (R+F)T_1' - DT_2\right\}\delta\theta\right]_{x=0}^{x=L} \tag{9.85}$$

9.3.1.3 Boundary Conditions

The boundary conditions of the problem consist of term (9.85) together with terms obtained from the surface integral over S_g and S_u in Eq. (9.1). In these integrals the surface force is obtained from the stress components as $g_i = \sigma_{ij}\, n_j$ where n_j are the direction cosines of the external normal to the surface with the co-ordinate directions. Following a procedure similar to the one described by Eqs. (9.15–9.20) above, the boundary term for the prescribed forces will be found as [29, 30]:

$$\begin{aligned}&\{[X_A - (R+F)T_1]\delta\theta' + [T_A - (L+J+D+M)T_2 + F'T_1]\\&+ (R+F)T_1'\big]\delta\theta\}_{x=L_0} + \{[X_A + (R+F)T_1]\delta\theta'\\&+ \left[T_A + (L+J+D+M)T_2 - F'T_1 - (R+F)T_1'\right]\delta\theta\}_{x=0}\end{aligned} \tag{9.86}$$

where X_A and T_A correspond to applied force and torque respectively.

On the other hand, for prescribed displacements, the boundary term becomes [29, 30]:

$$\begin{aligned}&\left\{\left[(R+F)\theta' - \int_A (\phi + f_1)\bar{u}dA\right]\delta T_1 + [(L+J+M)\theta\right.\\&\left.- \int_A \left(\frac{\partial\phi}{\partial y} - z + f\right)\bar{v}dA - \int_A \left(\frac{\partial\phi}{\partial z} + y + f_3\right)\bar{w}dA\right]\delta T_2\Big\}_{x=L_0}\\&- \left\{\left[(R+F)\theta' - \int_A (\phi + f_1)\bar{u}dA\right]\delta T_1 + [(L+J+M)\theta\right.\\&\left.- \int_A \left(\frac{\partial\phi}{\partial y} - z + f_2\right)\bar{v}dA - \int_A \left(\frac{\partial\phi}{\partial z} + y + f_3\right)\bar{w}dA\right]\delta T_2\Big\}_{x=0}.\end{aligned} \tag{9.87}$$

9.3.1.4 Governing Equations

The variational statement for the torsional problem can be assembled using Eq. (9.1) and the variational terms (9.74, 9.84, and 9.85) along with the boundary terms (9.86 and 9.87). The variations $\delta\theta$, δp, δS_1, δS_2, δT_1 and δT_2 are regarded as independent so that Eq. (9.1) implies, for arbitrary values of these variations, that each expression multiplied by them in the volume integral must independently be zero. The latter yields the following relations:

The strain-displacement term (9.74) for δT_1 results in

$$S_1 = Q_1'(x)\theta'' \tag{9.88}$$

where

$$Q_1(x) = \frac{(R+F)}{(R+2F+B)} \tag{9.89}$$

and for δT_2,

$$S_2 = Q_2(x)\theta' \tag{9.90}$$

where

$$Q_2(x) = \frac{(L+J+D+M)}{(L+J+C+2D+2M)} \tag{9.91}$$

The stress-strain term (9.74) for δS_1 gives

$$T_1 = ES_1 = EQ_1'(x)\theta'' \tag{9.92}$$

and for δS_2,

$$T_2 = GS_2 = GQ_2(x)\theta'' \tag{9.93}$$

The velocity-momentum term (9.84) for δp yields

$$p = \theta' \tag{9.94}$$

The dynamic equilibrium term (9.85) for $\delta\theta$ yields

$$\begin{aligned} &-F''T_1 - 2F'T_1' - (R+F)T_1'' + (D'+M')T_2 \\ &+ (L+J+D+M)T_2' - \rho J\dot{p} = 0 \end{aligned} \tag{9.95}$$

which is the equation of motion. Substituting for T_1, T_2 and P from Eqs. (9.88–9.95), and denoting

$$\begin{aligned} \eta_1(x) &= (R+F)Q_1(x) \\ \eta_2(x) &= (L+J+D+M)Q_2(x) \end{aligned} \tag{9.96}$$

the equation of motion (9.95) becomes

$$\eta_1 E\theta^{iv} + 2\eta_1' E\theta''' + \left(\eta_1'' E - \eta_2 G\right)\theta'' - \eta_2' G\theta' + \rho J\ddot{\theta} = 0 \tag{9.97}$$

or

$$(\eta_1 E\theta'')'' - (\eta_2 G\theta')' + \rho J\ddot{\theta} = 0 \tag{9.98}$$

The partial differential equation of motion (9.98) is of the fourth order so that two boundary conditions must be satisfied at both ends of the shaft. The solution of the equation of motion with appropriate boundary conditions and application of the Hu-Washizu-Bar variational formulation will be presented in the next Chap. 10.

9.4 Summary and Conclusions

The discrete–continuous models are by far the most commonly used models in dynamic analysis of cracked beams. The basic concept is the introduction of additional boundary conditions at the crack location where two intact beams are connected with a flexibility matrix whose components are determined by linear fracture mechanics. Hence, the most important work by this approach is to determine the local flexibility matrix. The main limitation of the flexibility approach is that it can only be applied to one-dimensional problems and mostly works well for fundamental structural elements.

However, discrete–continuous crack models are advantageous from many aspects. For instance, the intact part of a structure containing no cracks can still be modeled with corresponding partial differential equations; cracks only increase the boundary conditions that require less computational effort, than most finite element methods involving fine meshes around the crack region. While natural frequencies are relatively easier and more accurately measured than other modal parameters, solving an inverse problem for crack detection based only on changes in natural frequencies is not an easy task, considering the fact that natural frequency has a global nature while damage in most cases is a local phenomenon. However, if the crack is the most possible failure mode and no other form of damage exists, detecting the crack by natural frequencies is possible, even if measurement errors occur.

The key issues in developing a proper modeling technique of a cracked beam is to model the crack more accurately, and furthermore identify the variation in the stress field due to the opening and closing of the crack (crack breathing) and the stress-strain field complexity in the region of the developing crack. Also, the modification of the stress field induced by the crack is decaying with the distance from the crack or flaw, and a direct method relating flaw position and size with stiffness change is not easy to develop. Although previous analyses gave comparable results, the analytical methods are always convenient as delivering accurate results, there are more efficient, and provide deep physical insight into the problem. The present methodology gives a more detailed approach to the problem of crack identification in prismatic structural elements and lends itself for further development with applications to breathing cracks, multiple cracks and different crack configurations.

References

1. Irwin, G.R.: Analysis of stresses and strains near the end of a crack traversing a plate. J. Appl. Mech. **24**, 361–364 (1957)
2. Irwin, G.R.: "Fracture", in Handbuch der Physik, 6th edn, pp. 551–590. Springer, Heidelberg (1958)
3. Dimarogonas, A.D.: Vibration for Engineers, 2nd edn. Prentice Hall, Upper Saddle River (1996)
4. Dimarogonas, A.D.: Vibration of cracked structures: a state of the art review. Eng. Fract. Mech. **55**, 831–857 (1996)
5. Chondros, T.: Dynamic Response of Cracked Beams, M.Sc. Thesis, University of Patras, Greece (1977)
6. Chondros, T.G., Dimarogonas, A.D.: Identification of cracks in circular plates welded at the contour, American society of mechanical engineers design engineering technical conference, St. Louis, Paper 79-DET-106, (1979)
7. Chondros, T.G., Dimarogonas, A.D.: Identification of cracks in welded joints of complex structures. J. Sound Vib. **69**, 531–538 (1980)
8. Dimarogonas, A.D., Massouros, G.: Torsional vibration of a shaft with a circumferential crack. Eng. Fract. Mech. **15**, 439–444 (1980)
9. Gudmundson, P.: The dynamic behaviour of slender structures with cross-sectional cracks. J. Mech. Phys Solids **31**, 329–345 (1983)
10. Yuen, M.M.: A numerical study of the Eigen parameters of a damaged Cantilever. J. Sound Vib. **103**(3), 301–310 (1985)
11. Cuntze, R., Hajek, M.: Eigenfrequenzen eines angerissenen Kragträgers, Ingenieur-Archiv, vol. 55, 237–241. Springer, Heidelberg (1985)
12. Chondros, T.G., Dimarogonas, A.D.: Dynamic sensitivity of structures to cracks. J Vib. Acoust. Stress Reliab Des. **111**, 251–256 (1989)
13. Actis, R.I., Dimarogonas, A. D.: Non-linear effects due to closing cracks in vibrating beams 12th ASME Conference on Mechanical Engineering, Vibration and Noise, Montreal, 17–20 Sept 1989
14. Araujo Gomes, A.J.M., Montalvao da Silva.: Theoretical and experimental data on crack depth effects in the dynamic behaviour of free–free beams, J. M. international modal analytical conference IMAC, 9, Union College, Schenectady, 274–283 1991
15. Narkis, Y.: Identification of crack location in vibrating simply supported beams. J. Sound Vib. **172**, 549–558 (1994)
16. Krawczuk, M., Ostachowicz, W.M.: Transverse natural vibrations of a cracked beam loaded with a constant axial force. J. Vib. Acoust. Trans. ASME **115**(4), 524–533 (1995)
17. Boltezar, Strancar, M.B., Kuhelj, A.: Identification of transverse crack location in flexural vibrations of free–free-beams. J. Sound Vib. **211**(5), 729–734 (1998)
18. Ceri, N., Vestroni, F.: Detection of damage in beams subjected to diffuse cracking. J. Sound Vib. **234**(2), 259–276 (2000)
19. Lin, H.P.: Direct and inverse methods on free vibration analysis of simply supported beams with a crack. Eng. Struct. **26**, 427–436 (2004)
20. Mcadams, D.A., Tumer, I.Y.: Toward intelligent fault detection in turbine blades: variational vibration models of damaged pinned–pinned beams. J. Vib. Acoust. **127**, 467–474 (2005)
21. Chondros, T.G., Dimarogonas, A.D.: A consistent cracked bar vibration theory. J. Sound Vib. **200**, 303–313 (1997)
22. Chondros, T.G., Dimarogonas, A.D.: Vibration of a cracked cantilever beam. J. Vib. Acoust. **120**, 742–746 (1998)
23. Chondros, T.G., Dimarogonas, A.D., Yao, J.: A continuous cracked beam vibration theory. J. Sound Vib. **215**(1), 17–34 (1998)
24. Chondros, T.G., Dimarogonas, A.D., Yao, J.: Longitudinal vibration of a bar with a breathing crack. Eng. Fract. Mech. J. **61**, 503–518 (1998)

25. Chondros, T.G., Dimarogonas, A.D., Yao, J.: Longitudinal vibration of a continuous cracked bar. Eng. Fract. Mech. J. **61**, 593–606 (1998)
26. Chondros, T.G.: Vibration of a beam with a breathing crack. J. Sound Vib. **239**(1), 57–67 (2001)
27. Chondros, T.G.: The continuous crack flexibility method for crack identification. Fatigue Fract. Eng. Mater. Struct. **24**, 643–650 (2001)
28. Chondros, T.G.: Variational formulation of a rod under torsional vibration for crack identification. Fatigue Fract. Eng. Mater. Struct. **44**(1), 95–104 (2005)
29. Chondros, T.G., Labeas, G.: Torsional vibration of a cracked rod by variational formulation and numerical analysis. J. Sound Vib. **301**(3–5), 994–1006 (2007)
30. Christides, S., BARR, A.D.S.: One-dimensional theory of cracked Bernoulli-Euler beams. Int. J. Mech. Sci. **26**(11/12), 639–648 (1984)
31. Barr, A.D.S.: An extension of the Hu-Washizu variational principle in linear elasticity for dynamic problems. J. Appl. Mech. Trans. ASME **33**(2), 465 (1966)
32. Hu, H.C.: On some variational principles in the theory of elasticity and plasticity. Sci. Sinica **4**, 33–55 (1955)
33. Shen, M.H.H., Pierre, C.: Natural modes of Bernoulli-Euler beams with symmetric cracks. J. Sound Vib. **138**(1), 115–134 (1990)
34. Shen, M.H.H., Pierre, C.: Free vibrations of beams with a single-edge crack. J. Sound Vib. **170**(2), 237–259 (1994)
35. Timoshenko, S.P.: On the correction for shear of the differential equation for transverse vibrations of prismatic bars. Phil. Mag. **41**, 744–746 (1921)
36. Tada, H., Paris, P., Sih, G.C.: The Stress Analysis of Cracks Handbook, Del Research Corporation, Hellertown (1973, 1985)
37. Benthem, J.P., Koiter, W.T.: Asymptotic approximations to crack problems. In: Sih, G.C. (ed.) Methods of Analysis and Solutions of Crack Problems, Noordhoff, Leyden (1973)
38. Sih, G.C.: Some basic problems in fracture mechanics and new concepts. Eng. Fract. Mech. **5**, 365–377 (1973)
39. Sih, G.C., Mcdonald, B.: Fracture mechanics applied to engineering problems. Strain Energ Density Fract. Criterion Eng. Fract. Mech. **6**, 493–507 (1974)
40. Sih, G.C., Barthelemy, B.M.: Mixed mode fatigue crack growth predictions. Eng. Fract. Mech. **13**, 439–451 (1980)
41. Timoshenko, S., Goodier, J.N.: Theory of Elasticity, McGraw-Hill, Inc., New York (1953)
42. Sokolnikoff, I.S.: Mathematical Theory of Elasticity, 2nd edn. McGraw-Hill, New York (1956)
43. Szabo, I.: Höhere Technische Mechanik. Springer, Heidelberg (1964)
44. ANSYS, Inc., ANSYS ver. 7.1 (2003)
45. Love A.E.H.: The Mathematical Theory of Elasticity 4th edn. Cambridge University Press, Cambridge (1952)

Chapter 10
The Variational Formulation of a Rod in Torsional Vibration for Crack Identification

Abstract In Chap. 10 the Hu-Washizu-Barr variational formulation is used for the development of the differential equation and boundary conditions for a cracked rod. Based on the general variational principle and independent assumptions about displacement, momentum, strain and stress fields of the cracked rod with one or more pairs of transverse symmetrically disposed open edge cracks along its length, the equations of motion in torsional vibration were derived. Crack is introduced as a stress disturbance function, and stress field is determined by fracture mechanics methods. Strain energy density theory has been used for an accurate evaluation of the stress disturbance function. The strain energy density criterion is based on local density of the energy field in the crack tip region, and no special assumptions on the direction in which the energy released by the separating crack surfaces is required.

10.1 Dynamic Behaviour of Cracked Shafts

The assessment of the state of damage of a structural system depends on various factors, among which the identification of existing flaws, their location, type and severity and on damage tolerance. The latter is a measure of the capability of a damaged material or damaged structure to sustain load and/or maintain functional capability. Modern structures, especially in turbomachinery (Fig. 10.1), are designed on the basis of a damage tolerance philosophy, which allows for the presence of sub-critical cracks not growing to critical length between periodic inspections. The damage tolerance concept provides quantitative guidance for the balancing of cost of repair or replacement of damaged components against the possibility that continued service would lead to a catastrophic failure [1, 2].

Despite elements of uncertainty concerning environmental effects such as corrosion, moisture, and temperature effects, a predictive methodology taking into

A. D. Dimarogonas et al., *Analytical Methods in Rotor Dynamics*,
Mechanisms and Machine Science 9, DOI: 10.1007/978-94-007-5905-3_10,

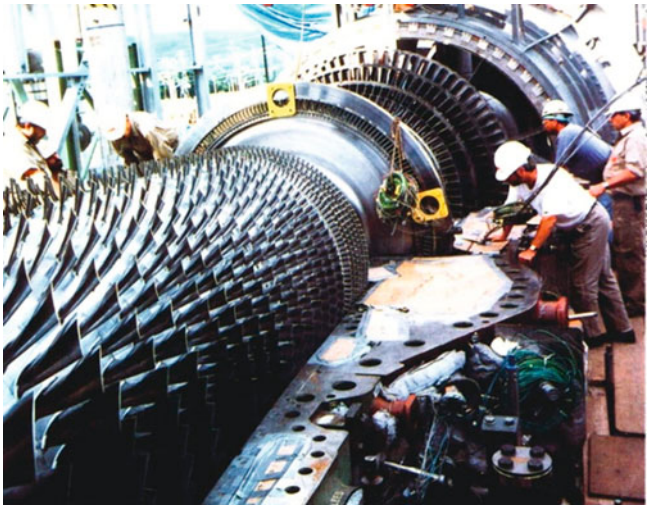

Fig. 10.1 Steam turbine stepped rotor disassembled for scheduled inspection and maintenance

account crack growth mechanisms is valuable in the evaluation procedures. Although, computational technology has provided vast possibilities, the predictive failure analyses tools available in the literature are impractical to implement with complex structural problems. Thus, the extension of current damage tolerance methods to complex structures is not easy [3, 4].

The development of crack detection methods in rotating shafts was initiated in about 1970 [5–8]. Theory and extensive laboratory and field experiments were used to develop methodologies for crack detection based on the second harmonic and the half critical speed sub-harmonic. Further, it was reported that on-line electronic instrument for monitoring and early warning of cracked rotors was developed, to be used as turbine supervisory equipment. This report was widely distributed and, in the sequence, had triggered substantial work in the turbomachinery industry [9–12]. Since the early 1980s there has been substantial academic research on the subject [8–29].

With a stepped rotor, a transfer matrix technique was used to compute the change of critical speed of a shaft due to the crack [9–12]. The results confirmed that for small crack depths the change in critical speed is proportional to $(a/D)2$, where a is the crack depth and D the shaft diameter. For example, an edge crack with depth 54 % of the radius produced a 5.6 % (overestimated) change of the lowest critical speed of the shaft. It was concluded that measurement of the change in critical speed was not an efficient way to monitor rotor cracks.

In order to assist system planners to modify operating practices before large portions of shaft fatigue life have been consumed, it is required that the cumulative fatigue damage associated with various types of system disturbances be determined. This is necessary since cracks initiate at a microscopic level and are not

observable until the shaft has suffered extensive damage. Continued exposure to system disturbances could result in crack growth and subsequent shaft fatigue. In 1973 a long-range program was initiated to determine the torsional fatigue strength of large turbine-generator shafts and to develop analytical techniques to calculate cumulative fatigue damage [12]. The scope of the program was enhanced in servo-hydraulic torsional fatigue and combined axial-torsion fatigue testing machines, the development of torsional extensometry, and the computerization of torsional test equipment to facilitate evaluation of complex torque histories.

A State of the Art review on the vibration of cracked structures provides a detailed description of the papers that followed initial investigations [8]. A wealth of further analytical, numerical and experimental investigations has been reviewed. A broad review of the state of the art in fault diagnosis revealed that mass unbalance, bent shafts and cracked shafts should be given special treatment [13]. The diagnosis of cracks in subcritical and supercritical speed ranges using cross-coupling stiffness terms, for the purpose of online monitoring schemes, was investigated in Ref. [14].

A simple hinge model for small breathing cracks analyzing the transient vibration response of a cracked rotor passing through its critical speed, as an attempt for crack detection and monitoring is considered in Ref. [15]. For deeper cracks the vibrations are violent and there is no definite critical speed but a zone with severe vibrations. A generator rotor case history, where a transverse fatigue crack could grow to a very large extent, for several years, without being detected until its extension reached 60 % of the whole rotor cross-section, is discussed in Ref. [16].

The mathematical foundations for experimental modal analysis of rotating structures are characterized by non-symmetric and time-variant matrices [17]. The equations of motion were solved in Ref. [18] by modal transformation to derive impulse and frequency response functions, which form the basis of modal identification algorithms in time and frequency domains, respectively. The shaft crack detection was formulated as an optimization problem by means of a finite element method and utilizing genetic algorithms to search the solution [18].

A local compliance matrix of different degrees of freedom is used to model the transverse crack in a shaft of circular cross section, based on expressions available of the stress intensity factors and the associated expressions for the strain energy release rates. It is known that when a crack exists in a structure, such as a beam, then the excitation in one-direction causes coupled vibrations in other directions. This property is used in Ref. [19] to identify the crack. The shaft is modeled as a rotating Timoshenko beam including gyroscopic effect and axial vibration due to coupling. The method was applied in rotating cracked shafts to identify depth and location of a transverse surface crack.

The several existing methods for crack detection in rotating shafts are compared in Ref. [20]. Among those methods the lumped crack flexibility is shown to gain wider acceptance by researchers due to the availability of various crack models in the literature. The effect of a notch on a structure is usually simulated by a local bending moment or reduced section, with magnitudes, which were assessed

experimentally or analytically or fine-mesh finite element techniques. Also, an important observation was the recognition of vibration coupling due to cracks as well as parametric vibration and bilinear and non-linear effects characterizing vibration of cracked rotating shafts.

A neural network analyzing cracked rotor's vibration parameters is presented in Ref. [21], while the instantaneous frequency is introduced in Ref. [22] to describe the dependency of frequency components on time for non-stationary signals for machine monitoring and diagnosis. A model-based method for the on-line identification of two cracks in a rotor is studied in Ref. [23]. A finite element model was used for the rotor, while cracks are simulated through local flexibility changes. The continuous wavelet transform (CWT) has been proposed for crack detection and monitoring in a rotor system coasting down through its critical speed [24].

Other methods dealing with the localization of cracks in rotating machinery, based on measured vibrations and the introduction of various techniques are reported in Refs. [24–26], with time domain identification algorithm (the Extended Kalman Filter), or a vector quantity (residue) defined for the non-zero elements corresponding to the nodes encompassing elements carrying cracks.

Although there is an extensive literature on the vibration of cracked shafts attention is restricted to theoretical methods estimating the effect of a crack on overall dynamics. Such estimates were made numerically or by introducing the crack local flexibility concept. Many researchers have used the vibration response to detect cracks in a structure. These detection schemes are based on the fact that the presence of a crack in a structure reduces the stiffness of the structure-hence reducing its natural frequencies. Significant research, both empirical and theoretical, has been conducted to predict the appearance and location of a crack using the vibration signature of the structure. Researchers using the Finite Element Method used beam elements of various dimensions and concentrated masses along the shaft axis to model stepped shafts and turbine discs. However, it is difficult to vary the location of the crack, since every relocation into a shaft segment of different geometry, requires the development of a new cracked beam element. Till present, the greatest difficulty in crack detection and identification remains the quantitative evaluation of the crack parameters and the distinction between a developing crack from other faults such as imbalance, misalignment, shaft bow, bearing failure, etc. [27].

In a rotor, a crack produces vibration of the second and higher harmonics of the rotating frequency [7, 28]. However, the amplitudes of those harmonics can be measured only if the frequency of one of the harmonics closely matches one of the natural frequencies of the shaft. While the signature analysis can easily predict the presence of a crack it is not an easy task to locate the crack using the signature graph.

The key issue in developing a proper modeling technique of cracked rotors is to model the crack more accurately, and furthermore identify the variation in the stress field over one revolution due to the opening and closing of the crack (crack breathing) and the stress-strain field complexity in the region of the developing crack. This situation calls for the application of fracture mechanics methods and continuous cracked rod vibration theory [27–29].

Hu-Washizu theory for the uncracked bar [30–32] was extended to develop a theory for the torsional vibration of the cracked rod based on the general variational principle and independent assumptions about displacement, momentum, strain and stress fields of the cracked rod [27–29]. The equations of motion for a uniform rod in torsional vibration were derived, where the rod had one or more circumferential open edge cracks along its length. This restriction on crack geometry avoided the coupling of torsional and flexural motion, which follows a non-symmetric crack configuration. The cracks were regarded as constantly open to avoid non-linearity associated with compressive stresses over a closing crack face. Furthermore, for the stress field about the crack an exponential decay stress and strain distribution determined experimentally was used.

In this chapter variational formulation is adopted for the study of torsional vibration of cylindrical shafts with circumferential crack. Hu-Washizu-Barr variational formulation is used to develop the differential equation and boundary conditions of the cracked rod [30–32]. The general variational principle and independent assumptions about displacement, momentum, strain and stress fields of the cracked rod, and equations of motion for a uniform rod in torsional vibration are derived, to predict the dynamic response of a cracked shaft considering it in a more fundamental way as a one-dimensional elastic continuum. The crack is modeled as a continuous flexibility using the displacement field in the vicinity of the crack, found with fracture mechanics methods. Rayleigh quotient is used to approximate the natural frequencies of the cracked rod. Independent evaluations of crack identification methods in rotating shafts are compared with the continuous crack flexibility theory [27–32].

10.2 Torsional Vibration of a Continuous Cracked Shaft: Variational Theorem

10.2.1 Cracked Rod-Variational Theorem

A rod with an open peripheral surface crack is shown in Fig. 10.2. Displacement components are denoted by u_i, strain components by γ_{ij} and stress components by σ_{ij}, $i, j = 1, 2, 3$ referring to Cartesian axes x, y, z.

The stress and strain fields of the cracked rod can be obtained by adding the disturbance functions to the stress and strain distributions of the undamaged rod. Here, the most general situation will be considered here by which a different disturbance function is added to each component. Thus, the disturbance in the direct components σ_{xx} and γ_{xx} is introduced through a function $f_1(x,y,z) = f_1$, the disturbance in the shear components σ_{xy} and γ_{xy} is introduced through a function $f_2(x,y,z) = f_2$ and the disturbance in the shear components σ_{xz} and γ_{xz} is introduced through a function $f_3(x,y,z) = f_3$. These functions assume maximum values at the crack tip and decay with distance from the cracked section.

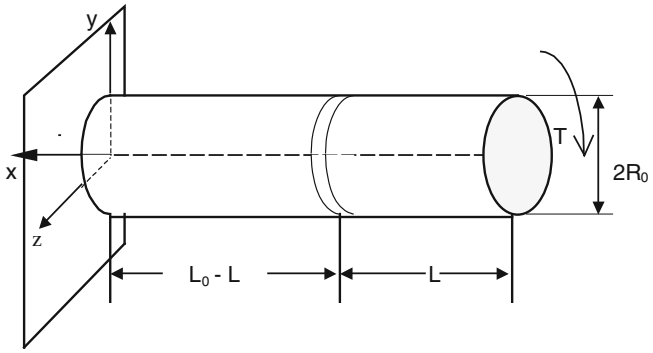

Fig. 10.2 Geometry of a circular cracked rod

The extended Hu-Washizu variational principle extending Barr's theory [30–32] for the uncracked bar, and the general equation for torsional vibration of a cracked rod was formulated in the previous chapter as the fourth order differential Eq. (9.97) [27–30]:

$$\eta_1 E\theta^{iv} + 2\eta_1' E\theta''' + (\eta_1'' E - \eta_2 G)\theta'' - \eta_2 G\theta' + \rho J\ddot{\theta} \tag{10.1}$$

where E is Young's modulus, $G = E/(1 + \nu)$, ν Poisson's ratio, θ angular displacement, ρ material mass density, J polar moment of inertia,

$$\begin{aligned} \eta_1 &= (R + F)\, Q_1(x) \\ \eta_2 &= (L + J + D + M)\, Q_2(x) \\ Q_1(x) &= (R + F)/(R + 2F + B) \\ Q_2(x) &= (L + J + D + M)/(L + J + C + 2D + 2M) \end{aligned} \tag{10.2}$$

R, F, L, J, D, M, B, C are integrals defined over the cross-section A as:

$$\begin{aligned} &B(x) = \int_A (f_1^2)dA \;\; C(x) = \int_A (f_2^2 + f_3^2)dA \;\; D(x) = \int_A \{(\partial\phi/\partial y)f_2 + (\partial\phi/\partial z)f_3\}dA \\ &F(x) = \int_A (\phi f_1)dA \;\; M(x) = \int_A \{yf_3 - zf_2\}dA \;\; J(x) = \int_A \{y^2 + z^2\}dA \\ &K = \int_A \left\{(\partial\phi/\partial y)^2 + (\partial\phi/\partial z)^2\right\}dA \;\; L = \int_A \{(\partial\phi/\partial z)y - (\partial\phi/\partial y)z\}dA \;\; R = \int_A (\phi^2)dA \end{aligned} \tag{10.3}$$

f_1, f_2 and f_3 crack disturbance functions, and ϕ is the warping function.

The three crack disturbance functions f_1, f_2 and f_3 are all, at present, unknown. An empirical exponential function was initially used to describe the stress disturbance due to a crack [30]. In the present, the crack disturbance function will be found by using fracture mechanics results.

10.2.2 The Crack Disturbance Function

Let us consider the free vibration of a circular rod of length L_0 and radius R_0 with a symmetric ring-shaped crack as shown in Fig. 10.2. The depth of the ring-shaped crack is a. This restriction on crack geometry avoids coupling of torsional and flexural vibration which follows a non symmetric crack configuration. For the tearing mode *III* the shear stress distribution is denoted by σ^*_{xz} and σ^*_{yz}.

The stresses σ^*_{xz} and σ^*_{yz} are given as [33]:

$$\begin{bmatrix} \sigma^*_{xz} \\ \sigma^*_{yz} \end{bmatrix} = \frac{K_{III}}{\sqrt{2\pi r}} \cos\frac{\theta}{2} \begin{bmatrix} -\sin\dfrac{\theta}{2} \\ \cos\dfrac{\theta}{2} \end{bmatrix} \tag{10.4}$$

where K_{III} is the stress intensity factor for the tearing mode *III*, and r is the radius at the crack tip [33–36].

For a rod with a circumferential crack under torque T, K_{III} is given as [34]

$$K_{III} = \sigma_{Tn}\sqrt{\pi a} \cdot F_{III}(\alpha) \tag{10.5}$$

where $\sigma_{Tn} = 2T/\pi R_0^3$, a crack depth, R_0 rod radius, $\alpha = a/R_0$, and

$$F_{III}(\alpha) = [\alpha(1-\alpha)]^{1/2}\left[0.3750 + 0.1875(1-\alpha) + (1-\alpha)^2 + 0.1172(1-\alpha)^3 + 0.0732(1-\alpha)^4 + 0.0780(1-\alpha)^5\right]$$

For a cracked rod in pure torsion the stress disturbance function due to the crack is set in the form:

$$f_3(x) = D_0\beta\frac{\sigma^*_{yz}(r = |L-x|, \quad \theta = 0^\circ)}{\sigma_{Tn}}, \ (0 \le x < L) \tag{10.6}$$

where D_0 is a constant and β is a dimension scale factor so that the frequency disturbance function f_3 is dimensionally consistent with Eq. (2) of Ref. [30].

Equations (10.4) and (10.6) yield

$$f_3(x) = \frac{D_0\sqrt{a}F_{III}(a)\beta}{\sqrt{2r}} \tag{10.7}$$

To find the scale factor D_0 in the above equation, a circular rod loaded with a torque T is considered with a ring shaped crack of depth a, as shown in Fig. 10.2. Under general loading, the additional twist angle θ^* along the direction of the initial torque T, due to the presence of a crack, is computed by Castigliano's theorem, and theory of fracture based on field strength of the local energy density [34–37]. D_0 will be computed so that the relative twist of the two ends will be equal to the one computed with fracture mechanics methods for static torque.

If U_T is strain energy per unit volume due to a crack of depth a, Castigliano's theorem demands that additional twist θ^* due to the initial torque T be:

$$\theta^* = \partial U_T / \partial T \tag{10.8}$$

The strain energy per unit volume, of the element located at distance r from the crack tip, has the form [38]

$$U_T = S/r \tag{10.9}$$

where S is the strain energy density factor.

With isotropic and homogeneous materials the strain energy density factor is given as [35–38]

$$S = \alpha_{11} K_I^2 + 2\alpha_{12} K_I K_{II} + \alpha_{22} K_{II}^2 + \alpha_{33} K_{III}^2 \tag{10.10}$$

where K_I, K_{II}, K_{III} are stress intensity factors corresponding to tensile, in-plane shear and out-of-plane shear modes of crack opening respectively, and the coefficients α_{11}, α_{12}, α_{22}, α_{33} are calculated from Eq. (7) of Ref. [30].

From Eqs. (10.5), (10.7), (10.8), (10.9) and (10.10), after the appropriate assumptions for the stress field in the region of the peripheral surface crack are considered, the additional twist is calculated as

$$\theta^* = \frac{4\pi(1 - \nu^2)\sigma_{Tn}}{G}\left[\frac{4a - R_0}{R_0 - a} + \frac{(R_0 - a)^3}{12R_0^3}\right] \tag{10.11}$$

On the other hand, according to the rod deformation analysis theory the general form for the twist angle of the rod in pure torsion is

$$\theta^* = TL_0/GJ \tag{10.12}$$

Assuming that the stress disturbance function $f_3(x)$ in Eq. (10.6) for the torsional vibration of cracked rods acts directly on the torque T, Eq. (10.5), the additional twist due to the crack located at $x = L$ assumes the form:

$$\theta^* = D_0 \frac{\sqrt{a}\sigma_{Tn}\pi L_0(1 - a)^3 R_0^3 F_{III}(\alpha)\beta}{2GJ} \tag{10.13}$$

Equations (10.11) and (10.13), yield the constant D_0 as:

$$D_0 = \frac{4\sqrt{2}\pi(1 - \nu^2)\sqrt{L_0 - L}\beta}{L_0\sqrt{a}F_{III}(\alpha)}\left[\frac{4\alpha - 1}{(1 - \alpha)^4} + \frac{1}{12}\right] \tag{10.14}$$

10.2.3 The Differential Equation of Motion

The variation of the natural frequencies and in particular the fundamental frequency with increasing crack depth is of interest here for the purpose of diagnosing and monitoring cracks. The equation of motion (10.2) for the cracked rod torsional vibration can be solved analytically for the frequency shifting ratios. The frequency

shifting ratio of the fundamental frequency of the torsional vibration of cracked rods will be compared to torsional vibration of uncracked rods.

If the displacement θ is taken in the normal mode form $\theta(x,t) = W(x)\cos\omega^* t$, where $W(x)$ is an assumed shape function and ω^* the fundamental frequency of the cracked rod, Eq. (10.2) will change to:

$$(\eta_1 EW'')'' - (\eta_2 GW')' = \omega^{*2}\rho JW \tag{10.15}$$

The partial differential equation of motion (10.15) is of the fourth order so that two boundary conditions must be satisfied at both ends of the rod. The boundary conditions appropriate to this equation are obtained by equating the boundary terms to zero with prescribed external forces, and prescribed displacements respectively.

10.2.4 Boundary Conditions

A cantilever rod with its fixed end at $x = 0$, (Fig. 10.2) at that point has displacements u, υ and w all prescribed as zero while at the free end $x = L_0$ has the forces prescribed as zero. At $x = 0$, the boundary term, Eq. (19) of Ref. [30], yields $\theta = 0$ and $\theta' = 0$:

At $x = L_0$, the boundary term in Eq. (17) of Ref. [30] yields $\theta''' = 0$ and $(R + F)EQ_1\theta' - (L + J + D + M)GQ_2\theta' = 0$.

If there is no crack in the rod the functions F, B, C, D and M, are all zero. Hence, Q_1(x) and $Q_2(x)$ become unity, η_1 becomes R, and η_2 becomes $L + J$. For the circular rod twisted about its central axis, the warping function will vanish [39], that is

$$\phi = 0 \tag{10.16}$$

The displacement, stress, strain and velocity momentum terms, Eq. (2) of Ref. [30], for the cracked rod will be reduced to:

$$\begin{aligned}
u &= 0,\ \upsilon = -z\theta(x,t), w = y\theta(x,t)\\
p_x &= 0,\ p_y = -zP(x,t),\ p_z = yP(x,t)\\
\gamma_{xx} &= [f_1(x,y,z)]S_1(x,t), \gamma_{yy} = \gamma_{zz} = -v\gamma_{xx}\\
\gamma_{xy} &= [-z + f_2(x,y,z)]S_2(x,t), \gamma_{yz} = 0, \gamma_{xz} = [y + f_3(x,y,z)]S_2(x,t)\\
\sigma_{xx} &= [f_1(x,y,z)]T_1(x,t), \sigma_{yy} = \sigma_{zz} = 0\\
\sigma_{xy} &= [-z + f_2(x,y,z)]T_2(x,t),\ \sigma_{xz} = [y + f_3(x,y,z)]T_2(x,t), \sigma_{yz} = 0\\
X_x &= X_y = X_z = 0
\end{aligned} \tag{10.17}$$

where $P(x,t)$ is the velocity function, $S_1(x,t)$, $S_2(x,t)$ strain functions, $T_1(x,t)$, $T_2(x,t)$ stress functions and X_i body forces.

Now, Eq. (10.3) will change to

$$B(x) = \int_A (f_1^2)dA \quad C(x) = \int_A (f_2^2 + f_3^2)dA \quad D(x) = F(x) = 0 \quad M(x) = \int_A (yf_3 - zf_2)dA$$
$$J = \int_A (y^2 + z^2)dA = (\pi R_0^4)/2$$
$$K = L = R = 0 \tag{10.18}$$

and functions $\eta_1(x)$ and $\eta_2(x)$ become

$$\eta_1(x) = 0$$
$$\eta_2(x) = \frac{(J+M)^2}{(J+C+2M)}. \tag{10.19}$$

10.2.5 Torsional Natural Frequencies of the Cracked Rod-Rayleigh Quotient

Alternatively, an approximate energy method approach, Rayleigh's quotient method as used in Ref. [30], will be employed to estimate the fundamental frequency ω^* of the cracked rod for various crack depths.

In Eq. (10.15) denoting

$$L(W) = (\eta_1 EW'')'' - (\eta_2 GW')'$$

and

$$N(W) = \rho JW. \tag{10.20}$$

Rayleigh quotient, associated with the differential equation of motion takes the form:

$$Q_R(W) = \frac{\int WL(\mathrm{W})\mathrm{d}x}{\int WN(\mathrm{W})\mathrm{d}x} \tag{10.21}$$

where the two integrals are over the length of the rod.

Therefore, $Q_R(W)$ provides an estimate for ω^* from an assumed function W(x) which, for the fundamental mode, will exceed the true value. The numerator of Eq. (10.21) can be integrated by parts resulting in boundary terms which are taken to be zero for an appropriate choice of $W(x)$. The quotient then provides the approximation for the fundamental frequency ω^* of the cracked rod.

$$\omega^{*2} = \frac{\int_0^{L_0} \left\{\eta_1 E(W'')^2 + \eta_2 G(W')^2\right\} dx}{\int_0^{L_0} W^2 dx}. \tag{10.22}$$

Equation (10.22) can now be applied to a prismatic cracked rod for the prediction of the variation of the fundamental frequency for different cross-section geometries and end conditions.

From experimental results available in the literature [13–30], it is conclude that the natural torsional frequencies of the cracked rod are rather insensitive to small depth cracks. Only if total crack depth exceeds 50 % of the depth of the rod, there is an appreciable drop in the value of the natural frequencies. This suggests that the shape function $W(x)$ of the cracked rod might be approximated reasonably well by the shape function of the undamaged rod. With a free-free rod this takes the form $W(x) = \cos(\pi x/L_0)$ [7]. The terms integrated over the length of the rod Eq. (10.22) are symmetric around the rod's mid-span, so only half of the rod ($0 < x < L_0/2$) needs to be considered. The algebra is further simplified if the origin is transferred to the rod mid-span and a new axial co-ordinate given by $s = (L–L_0/2)/(L/2)$ is used. Using the above value of W(x) and new coordinate, s, Eq. (10.22) becomes

$$\omega^{*2} = \frac{4\pi^2}{\rho J L_0^2}\left\{\left(\frac{\pi}{L_0}\right)^2 E \int_{-1}^{1} \eta_1 \sin^2(\pi s)ds + G\int_{-1}^{1} \eta_2 \cos^2(\pi s)ds\right\}. \quad (-1 < s < 1) \tag{10.23}$$

This evaluation can be carried out for a range of crack depths defined by the parameters η_1 and η_2. The frequency shifting ratio of the fundamental frequency for the torsional vibration of the cracked rod, to that of the torsional vibration of the uncracked rod, will be compared with results found from Ref. [40].

For a rod of circular cross section, the function η_1(x) = 0 (Eq. 10.19) and the cracked rod frequency, Eq. (10.23), is reduced to the form

$$\omega^{*2} = \frac{4\pi^2 G}{\rho J L_0^2}\int_{-1}^{1} \eta_2 \cos^2(\pi s)ds. \tag{10.24}$$

If there is no crack, that is $f_2(x) = f_3(x) = 0$, and $C(x) = M(x) = 0$, Eq. (10.18), yield $\eta_1 = 0$, $\eta_2 = J$, Eqs. (10.19) and (10.24) yields the uncracked rod frequency as

$$\omega^2 = \frac{\pi^2 G}{\rho J L_0^2}. \tag{10.25}$$

Thus, from Eqs. (10.24) and (10.25) the frequency ratio becomes

$$\left(\frac{\omega^*}{\omega}\right)^2 = \frac{4}{J}\int_{-1}^{1} \eta_2 \cos^2(\pi s)ds. \tag{10.26}$$

It is worth noting that the function η_2 is not related with the crack disturbance function $f_1(x)$. In other words, the latter $f_1(x)$ does not appear in Eq. (10.26), axial stress σ_{xx} has no effect on the torsional vibration of cracked rods of circular cross-section. Since only torsional vibration is considered here, it is expected that

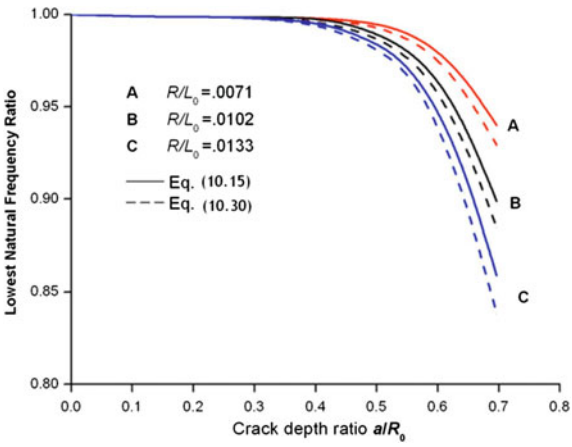

Fig. 10.3 Frequency shifting ratios versus crack depth, Eqs. (10.15) and (10.30) for different ratios R_0/L_0

$$f_2(x) = 0 \text{ and } f_3(x) = D_0 F_{III}(\alpha)\beta \frac{\sqrt{a}}{\sqrt{2r}} \tag{10.27}$$

From Eq. (10.18) substituting with the new axial coordinate s, terms $C(s)$ and $M(x)$ become:

$$C(s) = \frac{\pi D_0^2 F_{III}^2 a \beta^2 (R_0 - a)^2}{L_0 s}, \qquad (-1 < s < 1) \tag{10.28}$$

and

$$M(x) = \int y f_3 dA = 0 \tag{10.29}$$

Hence, the frequency ratio Eq. (10.26) changes to:

$$\Delta\omega^2 = \left(\frac{\omega^*}{\omega}\right)^2 = 4 \int_0^{\frac{1}{2}} \frac{L_0 s \cos^2(\pi s)}{L_0 s + D_0^2 F_{III}^2 a (1-\alpha)^2} ds \tag{10.30}$$

Substituting D_0 from Eq. (10.14) the fundamental frequency shifting ratio Eqs. (10.15) and (10.30) were solved with the aid of Mathematica and results for different R/L_0 ratios are shown in Fig. 10.3. The more slender the rod is, the smaller the frequency shifting ratio drop is.

Furthermore, comparison of the analytical solution of Eq. (10.30) with the analytical solutions from Refs. [40, 41], both with lumped crack flexibility, and experimental results from Ref. [40] are shown in Fig. 10.4. Results agree very well.

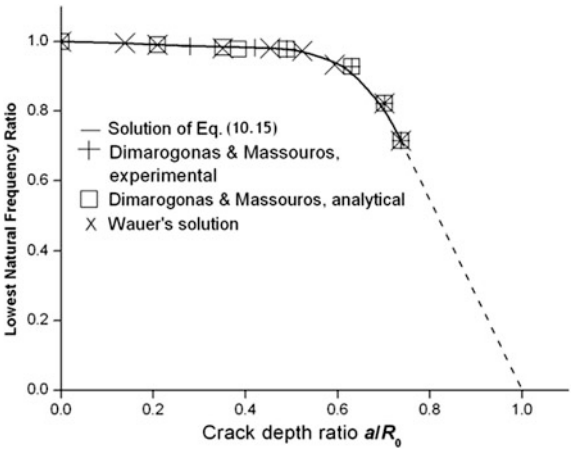

Fig. 10.4 Lowest natural frequency shifting ratio ω/ω^* versus crack depth ratio; comparison of analytical and experimental results. —— solution of Eq. (10.15), + Dimarogonas and Massouros [40], experimental, ❑ Dimarogonas and Massouros [40], analytical, × symbol Wauer's solution [41]

10.3 Finite Element Analysis of a Vibrating Cracked Rod

To compare with analytical results obtained, a Finite Element (FE) formulation of a cracked Euler–Bernoulli beam was investigated. The model adopted is using three-dimensional solid elements, leading to a set of linear algebraic equations of the form:

$$[\mathrm{M}]^{\mathrm{S}}\ \{\ddot{q}\}^{\mathrm{S}} + [\mathrm{C}]^{\mathrm{S}}\ \{\dot{q}\}^{\mathrm{S}} + [\mathrm{K}]^{\mathrm{S}}\ \{q\} = \{f\}^{\mathrm{S}} \tag{10.31}$$

where, $[\mathrm{M}]^{\mathrm{S}}$, $[\mathrm{C}]^{\mathrm{S}}$ and $[\mathrm{K}]^{\mathrm{S}}$ are the mass, damping and stiffness matrices for the vibrating system and $\{q(t)\}$ the response of the vibrating cracked rod in a stationary coordinate system [29]. The damping part of Eq. (10.31) is neglected, since no damping is considered. The FE mesh of the crack rod considered was developed using the FE software ANSYS [42] and the non-singular eight-node brick element 'solid 45', which has three degrees of freedom per node, i.e. the displacements in the x, y and z directions. The circumferential crack is modeled by assuming the corresponding nodes of the two crack surfaces to deform independently.

The crack surfaces are modeled using double nodes which are identical in location but topologically belong to the two different crack faces. Contact elements are not used in the present model, therefore, contact or friction between the crack faces is not taken into account. Element length was reduced in the axial direction towards the crack area.

Solution of the modal eigenvalue problem, using FE model has revealed the extensional, bending and twisting vibration modes, as well as, their interactions. Here, torsional natural frequencies and the sensitivity of the FE mesh with respect to the numerical results for various crack depth ratios are investigated. The FE mesh was refined progressively, from rough to very dense mesh and results of the corresponding frequency drop in close agreement with the analytical solution, Eq. (10.15) are shown in Figs. 10.5, 10.6 and 10.7, for different R_0/L_0 ratios and varying crack depth.

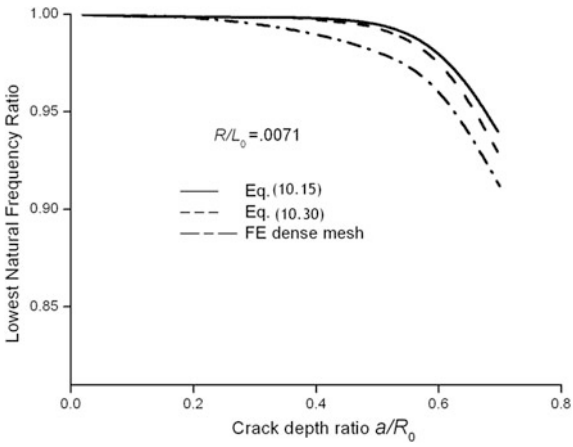

Fig. 10.5 Frequency shifting ratios versus crack depth ratio. $R/L_0 = 0.0071$. Comparison of analytical Eqs. (10.15, 10.30) and FE numerical results Eq. (10.31)

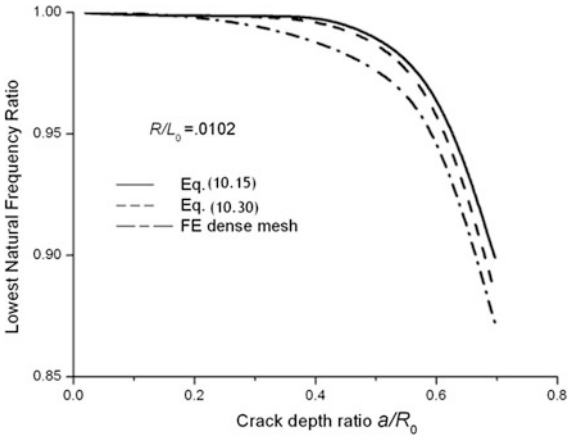

Fig. 10.6 Frequency shifting ratios versus crack depth ratio. $R/L_0 = 0.0102$. Comparison of analytical Eqs. (10.15, 10.30) and FE numerical results Eq. (10.31)

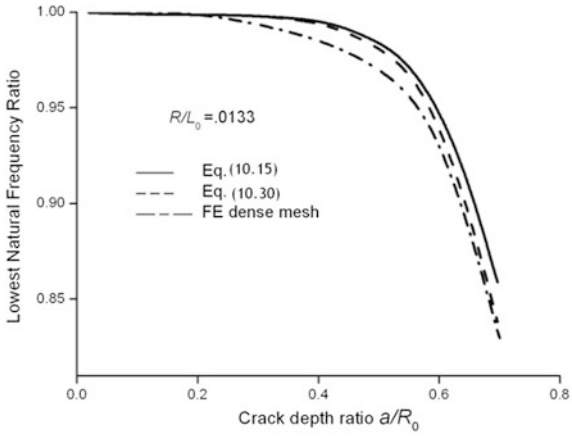

Fig. 10.7 Frequency shifting ratios versus crack depth ratio. $R/L_0 = 0.0133$. Comparison of analytical Eqs. (10.15, 10.30) and FE numerical results Eq. (10.31)

10.4 Summary and Conclusions

From 1971 till present, a wealth of analytical, numerical and experimental results on the dynamic response of cracked rotors has been accumulated. However, many unanswered questions still remain, especially in the area of closing cracks in rotating shafts [5–8, 41, 43].

Here, a differential equation for the torsional vibration of a rod with a circumferential crack was developed. The crack was introduced as a stress disturbance function which needed no *a priori* assumptions (local flexibility formulation [40], a prescribed exponential function formulation [30]) but rather the stress field determined by well-known methods of fracture mechanics [27–29].

Hu-Washizu-Barr variational formulation [30–32] was used to develop the differential equation and the boundary conditions for a cracked rod. The method is based on the general variational principle and the independent assumptions about displacement, momentum, strain and stress fields of a cracked rod, and the equations of motion for a uniform rod in torsional vibration with one or more pairs of transverse symmetrically disposed open edge cracks along its length, were derived. The crack is introduced as a stress disturbance function, the stress field is determined by fracture mechanics methods, and thus one *a priori* assumption for the extent of the stress field due to the crack is not required. The strain energy density theory has been used for an accurate evaluation of the stress disturbance function induced by the crack. Moreover, the strain energy density criterion is based on the local density of the energy field in the crack tip region and requires no special assumptions on the direction in which the energy released by the separating crack surfaces is computed. Thus the strain energy density factor is the only criterion to be used with mixed mode associated with mode *III* and mode *I* and *II* as this is usually the case [35–40]. The crack was regarded as constantly open to avoid non-linearities associated with compressive stresses over a closing crack face.

Although previous analyses produced comparable results [15–26, 40, 41, 43], the method presented provides a more detailed approach to crack identification [27–29]. Multiple cracks can easily be treated by superposition of the crack disturbance functions, if the cracks are not too close. The latter can be also considered using appropriate fracture mechanics solutions for the stress field under static torsional load. The results are almost identical with previous experimental and analytical ones obtained by the lumped local flexibility approach. This method, however, besides its generality, it does not need a priori assumptions for the extent of stress fields due to crack, can be extended to multiple cracks, stepped rods, etc., without adding complexity to the problem, since the same differential equation can be used with different forms of the stress disturbance function.

Finite Elements have been incorporated by many researchers for the derivation of the dynamic behavior of structures with cracks or flaws. It must be mentioned that indiscriminate application of the frequencies calculated by FEM, without consideration of the assumptions under which the crack or flaws models were derived and are valid, might lead to gross errors. However, careful observation of

the behavior of these damage models can lead to extension of their utility for defects of practical engineering importance. There are so many parameters that can be varied in flexural vibration of large-scale composite structures with flaws that it would be very difficult to present and compare results for all cases. Difficulties arising with this type of damaged structure dynamic behavior include for example coupling of flexural and longitudinal vibration. Also, according to the preloading conditions of the structure under investigation, the damage model assumption needs further verification in order to interpret vibration and mode shape measurements.

References

1. Sih, G.C.: Multiple hierarchical scale-dependency on physical mechanisms of material damage: Macromechanical, microstructural and nanochemical, particle and continuum aspects of mesomechanics. In: Sih, G.C., Nait-Abdelaziz, M., Vu-Khanh, T. (eds.) Mesomechanics 2007, ISTE Ltd, London (2007)
2. Donaldson, B.K.: Analysis of Aircraft Structures an Introduction. McGraw-Hill, New York (1993)
3. Sih, G.C., Loeber, J.E.: Torsional vibration of an elastic solid containing a penny-shaped crack. J. Acoust. Soc. Am. **44**(5), 1237–1245 (1968)
4. Loeber, J.E., Sih, G.C.: Torsional wave scattering about a penny-shaped crack on a bimaterial interface. In: Sih, G.C. (eds.) Dynamic Crack Propagation, pp. 513–28. Noordhoff, Leyden (1973)
5. Wauer, J.: On the dynamics of cracked rotors: A literature survey. Appl. Mech. Rev. **43**(1), 13–17 (1990)
6. Gasch, R.: A survey of the dynamic behavior of a simple rotating shaft with a transverse crack. J. Sound Vibr. **160**, 313–332 (1993)
7. Dimarogonas, A.D.: Vibration for engineers, 2nd edn. Prentice-Hall, Upper Saddle River (1996)
8. Dimarogonas, A.D.: Vibration of cracked structures: A state of the art review. Eng. Fract. Mech. **55**(5), 831–857 (1996)
9. Dimarogonas, A.D.: Dynamic response of cracked rotors. General Electric Co., Schenectady, New York (Internal Report) (1970)
10. Dimarogonas, A.D.: Dynamics of cracked shafts. General Electric Co., Schenectady, New York (Internal Report) (1971)
11. Pafelias, T.: Dynamic behaviour of a cracked rotor. General Electric Co., technical information series, no. DF-74-LS-79 (1974)
12. General Electric Co.: A methodology for predicting torsional fatigue life of turbine generator shafts using crack initiation plus propagation, EL-4333 research project 1531-1, Final report (1985)
13. Edwards, S., Lees, A.W., Friswell, M.I.: Fault diagnosis of rotating machinery. Shock Vibr. Digest Shock Vib. Dig. **30**(1), 4–13 (1998)
14. Meng, G., Hahn, E.J.: Dynamic response of a cracked rotor with some comments on crack detection ASME. J. Eng. Gas Turbines Power **119**, 447–455 (1997)
15. Sekhar, A.S., Prabhu, B.S.: Condition monitoring of cracked rotors through transient response. Mech. Mach. Theor. **33**(8), 1167–1175 (1988)
16. Bicego, V., Lucon, E., Rinaldi, C., Crudeli, R.: Failure analysis of a generator rotor with a deep crack detected during operation: Fractographic and fracture mechanics approach. Nucl. Eng. Des. **188**, 173–183 (1999)

17. Irretier, H.: Mathematical foundations of experimental modal analysis in rotor dynamics. Mech. Syst. Sign. Proces. **13**(2), 183–191 (1999)
18. He, Y., Guo, D., Chu, F.: Using genetic algorithms and finite element methods to detect shaft crack for rotor-bearing system. Math. Comput. Simul. **57**, 95–108 (2001)
19. Gounaris, G.D., Papadopoulos, C.A.: Crack identification in rotating shafts by coupled response measurements. Eng. Fract. Mech. **69**, 339–352 (2002)
20. Keiner, H., Gadala, M.S.: Comparison of different modelling techniques to simulate the vibration of a cracked rotor. J. Sound Vibr. **254**(5), 1012–1024 (2002)
21. Kalkat, M., Yildirim, S., Uzmay, I.: Rotor dynamics analysis of rotating machine systems using artificial neural networks. Int. J. Rotating Mach. **9**, 255–262 (2003)
22. Yang, B., Suh, C.S.: Interpretation of crack-induced rotor non-linear response using instantaneous frequency. Mech. Syst. Signal Proces. **18**, 491–513 (2004)
23. Sekhar, A.S.: Model-based identification of two cracks in a rotor system. Mech. Syst. Sig. Proces. **18**, 977–983 (2004)
24. Sekhar, A.S.: Detection and monitoring of crack in a coast-down rotor supported on fluid film bearings. Tribol. Int. **37**, 279–287 (2004)
25. Seibold, S., Weinert, K.: A time domain method for the localization of cracks in rotors. Eur. J. Mech. A/Solids **21**, 793–810 (2002)
26. Andrieux, S., Vare, C.: A 3D cracked beam model with unilateral contact. Application to rotors. J. Sound Vibr. **194**(1), 67–82 (1996)
27. Chondros, T.G.: The continuous crack flexibility method for crack identification. Fatigue Fract. Eng. Mater. Struct. **24**, 643–650 (2001)
28. Chondros, T.G.: Variational formulation of a rod under torsional vibration for crack identification. Fatigue Fract. Eng. Mater. Struct. **44**(1), 95–104 (2005)
29. Chondros, T.G., Labeas, G.: Torsional vibration of a cracked rod by variational formulation and numerical analysis. J. Sound Vibr. **301**(3–5), 994–1006 (2007)
30. Christides, S., Barr, A.D.S.: One-dimensional theory of cracked Bernoulli-Euler beams. Int. J. Mech. Sci. **26**(11/12), 639–648 (1984)
31. Barr, A.D.S.: An extension of the Hu-Washizu variational principle in linear elasticity for dynamic problems. J. Appl. Mech. Trans. ASME **33**(2), 465 (1966)
32. Hu, H.C.: On some variational principles in the theory of elasticity and plasticity. Sci. Sin. **4**, 33–55 (1955)
33. Tada, H., Paris, P., Sih., G.C.: The stress analysis of cracks handbook. Del Research Corporation, Hellertown, Pennsylvania (1973, 1985)
34. Sneddon, I.N.: The distribution of stress in the neighborhood of a crack in an elastic solid. Proc. Roy. Soc. Lond. **A**, 187 (1946)
35. Sih, G.C.: Some basic problems in fracture mechanics and new concepts. Eng. Fract. Mech. **5**, 365–377 (1973)
36. Sih, G.C., Mcdonald, B.: Fracture mechanics applied to engineering problems, strain energy density fracture criterion. Eng. Fract. Mech. **6**, 493–507 (1974)
37. Ismail, A.E., Ariffin, A.K., Abdullah, S., Ghazali, M.J., Daud, R.: Mode III stress intensity factors of surface crack in round bars. Adv. Mater. Res. **214**, 92–96 (2011)
38. Sih, G.C.: Mechanics of fracture initiation and propagation. Kluver, Boston (1991)
39. Love, A.E.H., The mathematical theory of elasticity, 4th edn. Cambridge University Press, Cambridge (1952)
40. Dimarogonas, A.D., Massouros, G.: Torsional vibration of a shaft with a circumferential crack. Eng. Fract. Mech. **15**(3–4), 439–444 (1981)
41. Wauer, J.: Modelling and formulation of equation of motion for cracked rotating shafts. Int. J. Sol. Str. **26**(4), 901–914 (1990)
42. Ansys, Inc. ANSYS ver. 7.1 (2003)
43. Chondros, T.G., Dimarogonas, A.D.: Influence of cracks on the dynamic characteristics of structures. J. Vibr. Acoust. Stress Reliab. Des. **111**, 251–256 (1989)

Index

A. D. Dimarogonas et al., *Analytical Methods in Rotor Dynamics*, Mechanisms and Machine Science 9, DOI: 10.1007/978-94-007-5905-3,